THEORY OF RESISTIVE MIXERS

by

ADEL ABDEL MONEIM SALEH

B.Sc., University of Alexandria, Egypt, U.A.R.
(1963)

M.S., Massachusetts Institute of Technology
(1967)

SUBMITTED IN PARTIAL FULFILLMENT OF THE
REQUIREMENTS FOR THE DEGREE OF
DOCTOR OF PHILOSOPHY

at the

MASSACHUSETTS INSTITUTE OF TECHNOLOGY
January 1970

Signature of Author _____
Department of Electrical Engineering, January 1970

Certified by _____
Thesis Supervisor

Accepted by _____
Chairman, Departmental Committee on Graduate Students

THEORY OF RESISTIVE MIXERS

by

ADEL ABDEL MONEIM SALEH

Submitted to the Department of Electrical Engineering on January 8, 1970 in partial fulfillment of the requirements for the Degree of Doctor of Philosophy.

ABSTRACT

This thesis gives a theoretical study of mixers employing purely resistive devices. The study is divided into two main parts. The first part treats the mixer as a linear periodically time-varying resistance inserted in a passive linear time-invariant imbedding network without paying attention to the method of obtaining the resistance waveform. Different imbedding networks which allow a closed form solution of the mixer equations are identified and classified. A system of nomenclature which introduces names such as Z-, Y-, H- and G-mixers is introduced. These names are derived from the types of network matrices which have to be used for the analysis. The wealth of knowledge of mixer circuits analyzable in a closed form is employed to find the optimum resistance waveforms for various imbedding networks and the optimum imbedding networks for different resistance waveforms; and, in general, to set fundamental limits on the performance of resistive mixers.

The second part of the analysis is concerned with mixers employing diodes with exponential characteristics. In this part the problem of the pumping waveform, pump power and d-c bias parameters is treated. The performance of different mixers is obtained and compared for identical pump power and d-c bias conditions.

Other topics considered in the analysis are the sensitivity of the mixer performance to variations in the source impedance and shape of the resistance waveform, the problem of incomplete terminations of the undesired out-of-band frequencies, and the noise figure and noise temperature ratio in mixers employing purely exponential diodes.

The results of the thesis emphasize the importance of the method of pumping and the proper termination of the out-of-band frequencies on the performance of the mixer.

THESIS SUPERVISOR: Robert P. Rafuse
TITLE: Associate Professor of Electrical Engineering

ACKNOWLEDGEMENT

The author wishes to express his sincere gratitude to his thesis adviser Prof. R.P. Rafuse for his guidance, advice and continued interest through all the phases of the thesis research. Also, thanks are due to Dr. D.H. Steinbrecher for many stimulating and helpful discussions and to Prof. P. Penfield, Jr. for his probing insights and suggestions.

To his colleagues in M.I.T. and to his associates at Sylvania Electric Products in Woburn, Massachusetts goes the author's appreciation for many useful conversations.

Also, the author would like to thank Patricia H. Denton for her help in the editing and typing of the manuscript.

Finally, the author wishes to express his gratitude to the government of the United Arab Republic for providing the opportunity for him to study at M.I.T.

TABLE OF CONTENTS

Page

APPENDIX

CHAPTER 1

INTRODUCTION

"Frequency converters" are used in communication receivers and transmitters, radars, radio and radar astronomy, control systems and many other applications. The frequency converter consists of a "local oscillator" or "pump" and a network containing one or more nonlinear devices and means to couple the local oscillator and the input and output signals. This network is called a "mixer". Inside the mixer the input signal, which is simply called the "signal", and the local oscillator output are "mixed" together in the nonlinear device to produce, among other frequencies, the required output frequency which is separated by filtering. The object is to achieve this with the least possible conversion loss, noise and nonlinear distortion. In hetrodyne receivers, and many other applications, the output signal is called the "intermediate frequency" (i-f). This frequency is usually the difference between the signal and local oscillator frequencies, and in most applications it is much smaller than all the other frequencies involved in the mixer.

The nonlinear device can be a resistance, a reactance or, usually, a combination of both. Traditionally, if the basic mixing process is accomplished by a

nonlinear resistance, which might include some parasitic reactances, the network is simply referred to as a mixer. On the other hand if the mixing is basically accomplished by a nonlinear reactance, possibly containing resistive parasitics, the network is called a "parametric" frequency changer, although generally speaking it is still a mixer.

It is well known that a parametric up converter can produce a power gain which is equal to the ratio between the output and input frequencies;** moreover it is unconditionally stable. This makes parametric up converters very attractive in practice. On the other hand, a parametric down converter is not desirable since, although capable of producing gain, it is potentially unstable. Other examples of mixers having conversion gain are those employing negative resistance devices, such as tunnel diodes.*** However, they too have considerable stability problems. For these reasons, down converters are almost always mixers employing essentially nonlinear positive resistances. This is the type of mixer which will be dealt with throughout this thesis. However, all our results will be applicable to, or can be slightly modified to include up converters; and some of our results can be applied to negative resistance mixers.

** See for example Manley and Rowe (I) or Penfield and Rafuse (I).

*** See for example Chang, Heilmeier and Prager (I); Kim (I); or Pucel (I).

As suggested from the title, the thesis will only be dealing with purely resistive mixers having ideal selective filters. The effect of parasitic reactances, which are bound to exist with any resistive device, will be neglected. It is the belief of the author that this theoretical work is needed and that it is justified with the aforementioned idealizations, even for mixers operating in the microwave frequency region, for the following reasons:

i) Today's semiconductor technology is capable of producing mixer diodes, such as Schottky-barrier diodes,** which exhibit almost purely resistive characteristics even at microwave frequencies.

ii) The mixer imbedding networks which are built at present, together with their methods of pumping, and not the diodes and their parasitic reactances, are responsible for the greatest part of deterioration of their performances.

iii) The treatment of mixers employing purely resistive diodes, although complex enough and contains many unresolved problems as will be seen from this thesis, is considerably simpler than a treatment involving the diode parasitics. This will help us to gain a better understanding of what constitutes

** These are metal-semiconductor junction diodes where current conduction is carried out almost entirely by majority carriers. See for example Sze (I, Chapter 8) for an excellent theoretical treatment.

a good mixer and to establish fundamental limits on its performance.

In Chapter 2, the methods of analysis of different mixers employing linear periodically time-varying resistances are presented. A logical classification system based on the terminations offered to the undesired out-of-band frequencies for the different mixers is given. The system employs names based on the types of network matrices, such as Z-, Y-, H- and G-matrices, which have to be used for the analysis. The analysis given to each mixer is limited to deducing the matrix equation relating the input and output voltages and currents from the resistance waveforms. To find the complete mixer performance one should use Appendix 1, where a complete analysis is given for conversion loss, stability and passivity of two-port networks based on generalized matrix representations. One of the new results in this appendix is the problem of sensitivity of the mixer performance to source impedance variations. Also, Appendix 2 provides the necessary equations for mixers with different image frequency terminations based on the generalized three-port matrices found in Chapter 2.

In Chapter 3, three basic questions concerning fundamental limits on the performance of resistive mixers are given. The questions involve obtaining the optimum

resistance waveforms for the different mixer imbedding networks introduced in Chapter 2, and finding the optimum imbedding networks for different nonnegative resistance waveforms. The parameter to be optimized is the mixer conversion loss. The theme of Chapter 3 can be considered as a search for the world's best mixer.

In both Chapters 2 and 3, the resistance waveform is assumed to be completely arbitrary and independent of the imbedding network. In practice, however, this is not true since the resistance waveform is obtained by pumping a nonlinear device in the imbedding network; and thus it depends on the device used, the method of pumping employed and the imbedding network. This is the purpose of Chapter 4.

In Chapter 4 different mixers employing ideal exponential diodes are analyzed and compared. The analysis given for each mixer consists of two main parts: large-signal and small-signal analysis. The first part includes the calculation of the pumped resistance waveform, the pump power, the resistance offered to the pump and the d-c bias conditions. In the second part of the analysis, the optimum values of the conversion loss and source and output resistance are given for different image frequency terminations. In each case asymptotic approximations are used to obtain simple formulas which are accurate for strongly driven mixers.

A section on conclusions and suggested topics for further research is included at the end of each chapter. The section appearing at the end of Chapter 4 offers practical problems in mixer theory in contrast to the purely theoretical problems at the ends of Chapters 2 and 3.

The eleven Appendices constitute an integral part of the entire thesis. They do not only supplement the chapters but, with the exception of Appendices 4 through 7, they form entities of their own. Appendix 11 in particular gives a complete study of square-wave reversing-switch mixers. Other appendices are concerned with two- and three-port networks, the periodically time-varying resistance, analysis of specific mixer circuits and study of the problem of incomplete termination of the out-of-band frequencies.

Several works in the mixer literature form the starting point and base for this thesis. From these Belevitch (II), Torrey and Whitmer (I) and Tucker (I and IV) provide excellent coverage of the available theory. Other important works are given in the bibliography and are referred to when appropriate.

CHAPTER 2

ANALYSIS AND CLASSIFICATIONS OF MIXER CIRCUITS

In this chapter we give the methods of analysis of different mixers employing linear periodically time-varying resistances. We also represent a logical classification system which depends on the different terminations offered to the undesired out-of-band frequencies. The system employees names based on the types of network matrices which have to be used to analyse the various mixer circuits.

Single-ended as well as balanced mixers will be considered. It will be shown that any single-ended and any balanced mixer circuit employing the same resistance waveform can be made equivalent by using the appropriate imbedding network. This will emphasize the importance of our system of classification.

The analysis given to each mixer is limited to deducing the matrix equation relating the input and output frequency voltages and currents from the resistance waveform. To find the mixer performance Appendices 1 and 2 can be used.

2.1. Notation for Linear Mixers

2.1.1. Frequency notation:

The frequencies resulting from a distortion-free mixer can be put in the form $\omega_n = n\omega_p + \omega_o$; $n = -\infty, \ldots, +\infty$; where $\omega_o = \omega_s - \omega_p$ is the output (i-f) frequency; ω_s and ω_p being the signal and pump frequencies respectively. The above notation will be used instead of $\omega_m = m\omega_p + \omega_s$; $m = -\infty, \ldots, +\infty$; which is often used in the literature. For most mixer applications $\omega_o \ll \omega_p$ and the first notation has the advantage that $|\omega_{-n}| \approx \omega_{+n} \approx n\omega_p$; $n = 0, \ldots, +\infty$; thus the magnitude of the frequency is quickly identifiable by its subscript. Note that $\omega_{-n} < 0$ for $n = +1, \ldots, +\infty$.

In our system of notation the signal frequency $\omega_s = \omega_{+1}$ and the image frequency $\omega_i = -\omega_{-1}$ are <u>odd</u> order frequencies while the i-f frequency $\omega_{if} = \omega_o$, the sum frequency $\omega_u = \omega_{+2}$ and its image $\omega_v = -\omega_{-2}$ are even order frequencies. The frequency notation is shown in Fig. 2.1 for the case $\omega_s > \omega_p$ which will be assumed throughout the thesis.

2.1.2. Voltage and current notation:

For linear mixers pumped with a frequency ω_p, the voltage and current can be written in the $e^{j\omega t}$ representation as

$$v(t) = \sum_{n=-\infty}^{\infty} V_n \, e^{j(n\omega_p + \omega_o)t} \quad , \qquad (2.1)$$

and

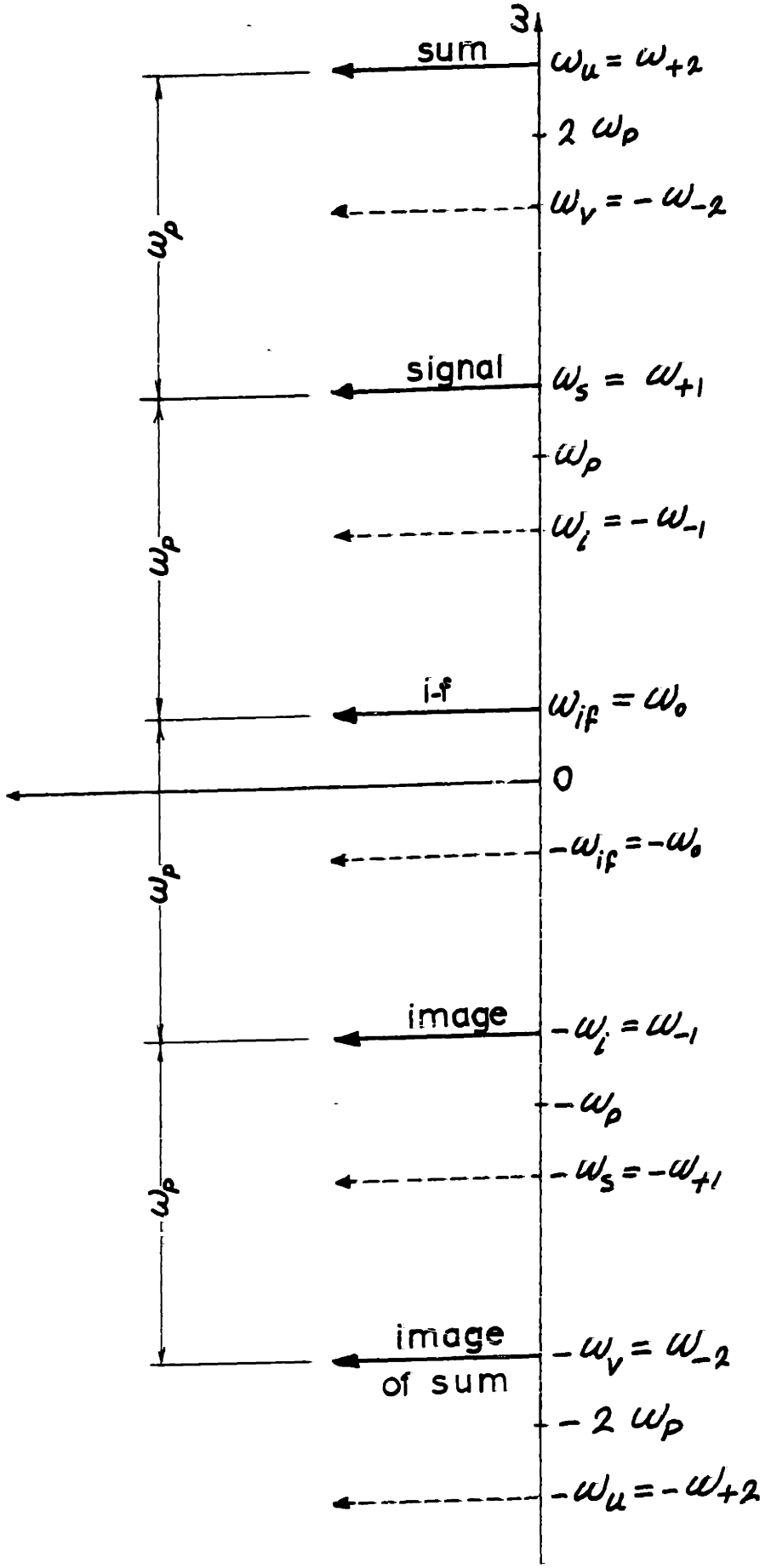

Fig. 2.1. Frequency Notation

$$i(t) = \sum_{n=-\infty}^{\infty} I_n e^{j(n\omega_p + \omega_o)t} \quad . \tag{2.2}$$

We will choose $|V_n|$ and $|I_n|$ to be the root-mean-square values of the voltage and the current at frequency $\omega_n = n\omega_p + \omega_o$. Note that both v(t) and i(t) are complex. They only represent the solid arrows in Fig. 2.1, but they contain all the power in the composite waveform.

The voltages and currents appearing with negative frequencies (V_{-n}, I_{-n}; $n = +1, \ldots, +\infty$) are the complex conjugates of the standard positive frequency representation of these voltages and currents. For example the standard representation of the image is $V_i e^{j\omega_i t}$ and $I_i e^{j\omega_i t}$; $\omega_i > 0$. In our representation it appears as $V_{-1} e^{j\omega_{-1} t}$ and $I_{-1} e^{j\omega_{-1} t}$; $\omega_{-1} = -\omega_i < 0$. Thus it follows that

$$V_{-1} = V_i^* \quad , \tag{2.3}$$

and

$$I_{-1} = I_i^* \quad . \tag{2.4}$$

This has the implication that if the impedance offered to the image frequency is Z_i then the impedance entering our system of equations becomes

$$Z_{-1} = Z_i^* \quad . \tag{2.5}$$

The same is true for all the negative frequency terms.

2.2. The Z- and the Y-Mixers

2.2.1. The basic circuits:

The Z-mixer is a mixer circuit in which all the out-of-band frequencies are open-circuited, Fig. 2.2.

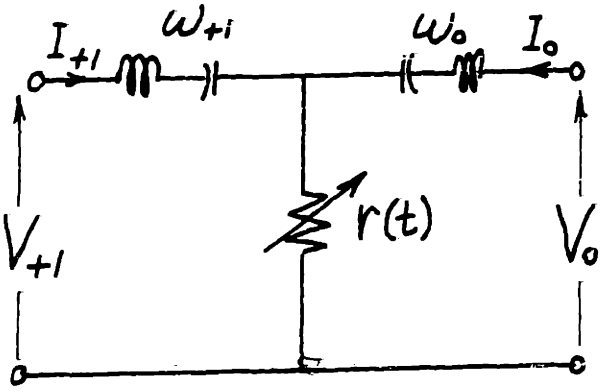

Fig. 2.2. The Z-Mixer

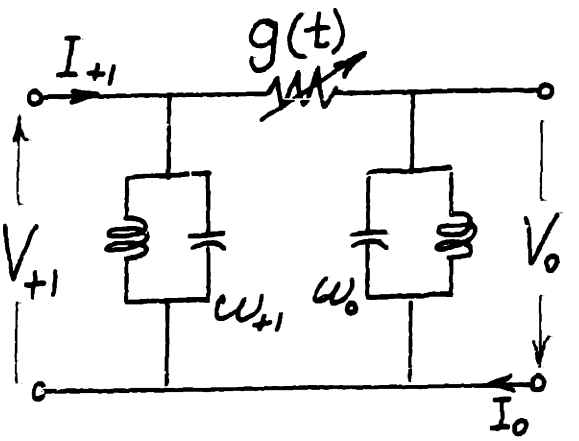

Fig. 2.3. The Y-Mixer

The Y-mixer is a mixer circuit in which all the out-of-band frequencies are short-circuited, Fig. 2.3. In the above figures, and throughout the thesis, the series (parallel) circuit tuned to ω_n is assumed to be a short (open) circuit at ω_n while presenting an open (short) circuit to all other frequencies**. Other equivalent variations of these two types of mixers are given in Figs. 2.9 and 2.10.

The reason behind the names Z and Y will be explained now as we attempt to analyze the circuits. Referring

** This type of circuit is usually referred to, casually, as an infinite-Q circuit. To be more precise, the series (parallel) circuit tuned to ω_n should be defined as a series (parallel) L and C in the limit when $L \to \infty$ ($L \to 0$) with $C=1/(\omega_n^2 L)$.

to Fig. 2.2 (and 2.9) we note that the Z-mixer is characterized by

$$I_n = 0 \qquad \text{all } n,\ n \neq +1 \text{ or } 0 \qquad . \quad (2.6)$$

Thus, only two sinusoidal currents, $I_{+1}\, e^{j\omega_{+1}t}$ and $I_o\, e^{j\omega_o t}$, pass through r(t). The only way to find the voltages V_n; $n = +\infty, \ldots, -\infty$; as explicit functions of I_{+1} and I_o is to use the Z-matrix representation of r(t) as given in Appendix 3, Eqs. (A3.8) ... (A3.10). Further, since we are only interested in V_{+1} and V_o we need only the 2 x 2 submatrix in the middle of the ∞ x ∞ matrix. The Z-mixer equation becomes

$$\begin{bmatrix} V_{+1} \\ V_o \end{bmatrix} = \begin{bmatrix} r_o & r_1 \\ r_1^* & r_o \end{bmatrix} \begin{bmatrix} I_{+1} \\ I_o \end{bmatrix} \qquad . \quad (2.7)$$

It is obvious that we could not have used the Y-matrix representation of Eqs. (A3.12) ... (A3.14) to obtain Eq. (2.7) without inverting the ∞ x ∞ Y-matrix, thus obtaining the Z-matrix again. The fact that the Z-matrix was necessary to obtain the equations for the mixer discussed above suggests the name "Z-mixer".

Once Eq. (2.7) is obtained, Appendix 1 supplies the equations necessary to find the performance of the mixer treating it as a two-port network. If the image frequency ω_{-1} is to be treated differently from the rest of the out-of-band frequencies, one must use the three-port equation

$$\begin{bmatrix} V_{+1} \\ V_o \\ V_{-1} \end{bmatrix} = \begin{bmatrix} r_o & r_1 & r_2 \\ r_1^* & r_o & r_1 \\ r_2^* & r_1^* & r_o \end{bmatrix} \begin{bmatrix} I_{+1} \\ I_o \\ I_{-1} \end{bmatrix} \quad . \qquad (2.8)$$

The performance of the mixer in this case can be found with the help of Appendix 2.

Of course, the Y-mixer of Fig. 2.3 (and 2.10) can be analyzed using the Y-matrix of Eqs. (A3.12) ... (A3.14). The equations so obtained will be the duals of Eqs. (2.6) ... (2.8).

2.2.2. Circuits with idlers:

There are two kinds of idlers: current idlers to allow current to pass through r(t) at frequencies other than ω_{+1} and ω_o in a Z-mixer; and voltage idlers to allow voltages to exist across g(t) at frequencies other than ω_{+1} and ω_o in a Y-mixer. The two kinds are shown in Figs. 2.4 and 2.5.

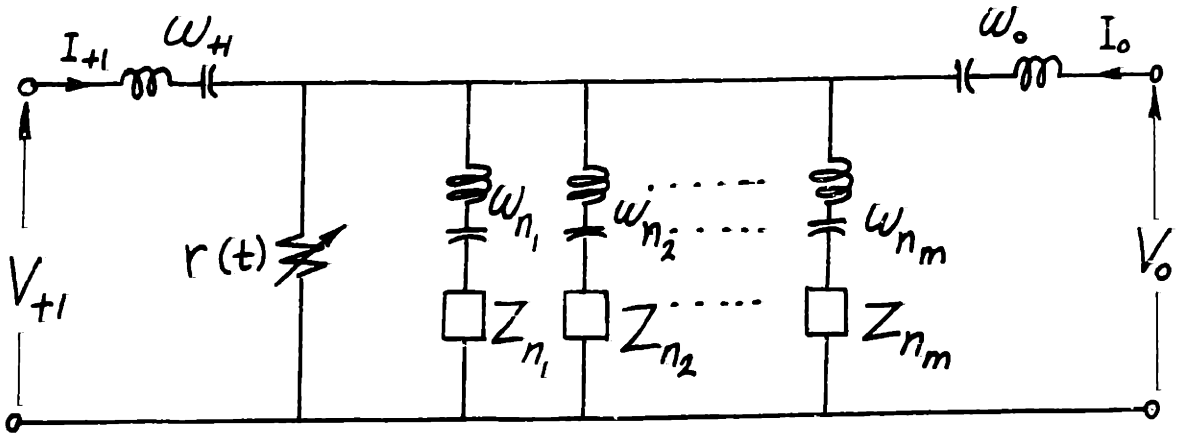

Fig. 2.4. Z-Mixer with m Current-Idler Circuits

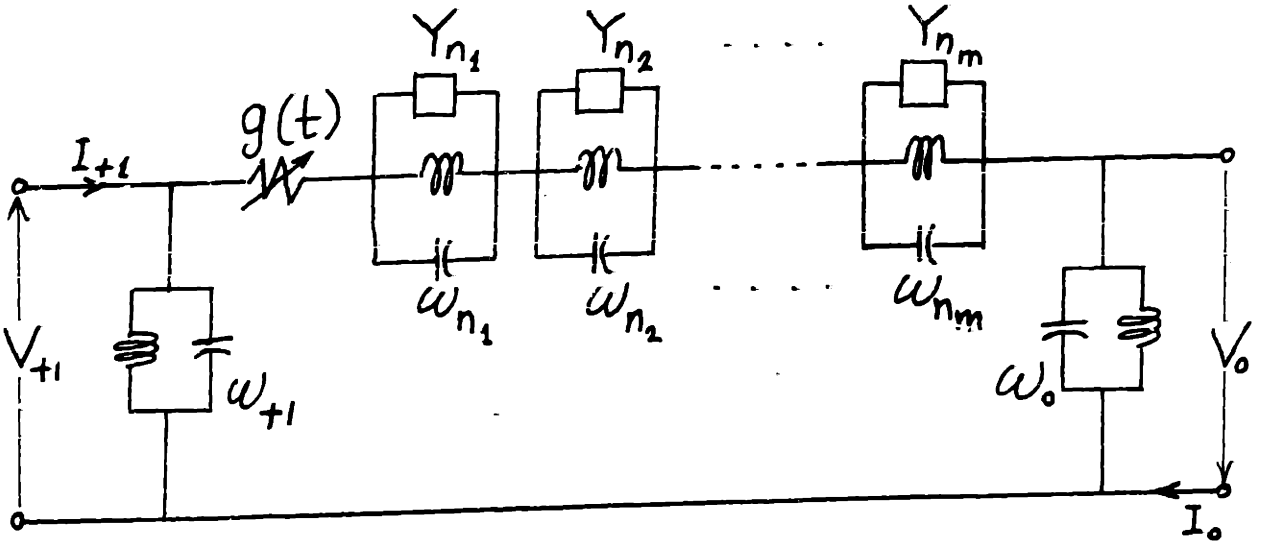

Fig. 2.5. Y-Mixer with m Voltage-Idler Circuits

We now derive the two-port equations for the Z-mixer. The Y-mixer equations can be deduced by duality. Referring to Fig. 2.4 we note that

$$I_n = 0 \quad \text{all } n;\ n \neq 1,\ 0,\ n_1,\ n_2,\ \ldots\ ,\ \text{or } n_m\ . \tag{2.9}$$

We use the Z-matrix of Eqs. (A3.8) ... (A3.10), and eliminate all the rows and the columns that correspond to a zero entry in the $\underline{I}$ vector. Finally we rearrange the remaining rows and columns to put the matrix equation in the form

$$\begin{bmatrix} V_{+1} \\ V_o \\ \hline V_{n_1} \\ V_{n_2} \\ \vdots \\ V_{n_m} \end{bmatrix} = \left[\begin{array}{cc:c} r_o & r_1 & \\ r_1^* & r_o & \underline{Z}_{ab} \\ \hdashline & & \\ \underline{Z}_{ba} & & \underline{Z}_{bb} \end{array}\right] \begin{bmatrix} I_{+1} \\ I_o \\ \hline I_{n_1} \\ I_{n_2} \\ \vdots \\ I_{n_m} \end{bmatrix} \quad . \tag{2.10}$$

The I_n's and the V_n's are the currents and voltages of the corresponding idler frequencies ω_n's. The matrices $\underline{Z}_{ab}$, $\underline{Z}_{ba}$ and $\underline{Z}_{bb}$ are 2 x m, m x 2 and m x m respectively. It can be verified that** $\underline{Z}_{ba} = \underline{Z}_{ab}^{\dagger}$ and $\underline{Z}_{bb} = \underline{Z}_{bb}^{\dagger}$. Using the matrix partitions indicated in Eq. (2.10) it can be rewritten as

$$\begin{bmatrix} \underline{V}_a \\ \underline{V}_b \end{bmatrix} = \begin{bmatrix} \underline{Z}_{aa} & \underline{Z}_{ab} \\ \underline{Z}_{ba} & \underline{Z}_{bb} \end{bmatrix} \begin{bmatrix} \underline{I}_a \\ \underline{I}_b \end{bmatrix} \quad , \qquad (2.11)$$

where the meaning of the symbols is obvious by comparison. The idler frequencies should satisfy the equation

$$\underline{V}_b = -\underline{Z}_L \underline{I}_b \quad , \qquad (2.12)$$

where $\underline{Z}_L$ is the diagonal matrix $\{Z_{n_1}, Z_{n_2}, \ldots, Z_{n_m}\}$ where the Z_n's are the load impedances offered to the different idler frequencies as indicated in Fig. 2.4. Substituting Eq. (2.12) in Eq. (2.11) and eliminating $\underline{I}_b$ we get

$$\underline{V}_a = \underline{Z}_{eq} \underline{I}_a \quad , \qquad (2.13)$$

where

$$\underline{Z}_{eq} = \underline{Z}_{aa} - \underline{Z}_{ab}(\underline{Z}_{bb} + \underline{Z}_L)^{-1}\underline{Z}_{ba} \quad . \qquad (2.14)$$

Given the 2 x 2 matrix $\underline{Z}_{eq}$, the performance of the mixer can be obtained with the help of Appendix 1. Of course, if $\underline{Z}_L = \{\infty, \infty, \ldots, \infty\}$ then $\underline{Z}_{eq} = \underline{Z}_{aa}$ and Eq. (2.13) is identical to Eq. (2.7).

In most applications the current idler is intended

** The superscript † indicates the complex conjugate transposed.

to be a short circuit at the idler frequency, i.e. $\underline{Z}_L = \underline{0}$. Also, the voltage idler in a Y-mixer is intended to open circuit the idler frequency. With this in mind one can think of the Z-mixer as a Y-mixer with an infinite number of open-circuit voltage idlers at all the out-of-band frequencies. Similarly the Y-mixer is a Z-mixer with a short-circuit current idler at every out-of-band frequency. Any arbitrary mixer circuit with specified terminations at all the frequencies involved can be considered as a Z- or a Y-mixer provided with the appropriate idler circuits. However, it should be noted that when the number of idlers is infinite, the technique described in this section will be impractical since one has to invert and multiply infinite matrices. Different techniques will be developed in the remainder of this chapter to handle some important special types of these infinite idler mixers without operating on infinite matrices.

2.3. Separation of the Odd- and Even-Order Frequencies

2.3.1. Single-ended and balanced mixer circuits:

It is well known that the odd- and even-order frequencies produced in a mixer can be separated at different ports by using a four-diode doubly balanced circuit**. In fact a single-ended circuit can be made equivalent to a balanced circuit with the help of ideal selective filters as indicated in Fig. 2.6. In the three circuits given in the figure the voltages, and currents, of all the frequencies involved ($\omega_n = n\omega_p + \omega_o$; $n = -\infty, \ldots, +\infty$) can exist across,

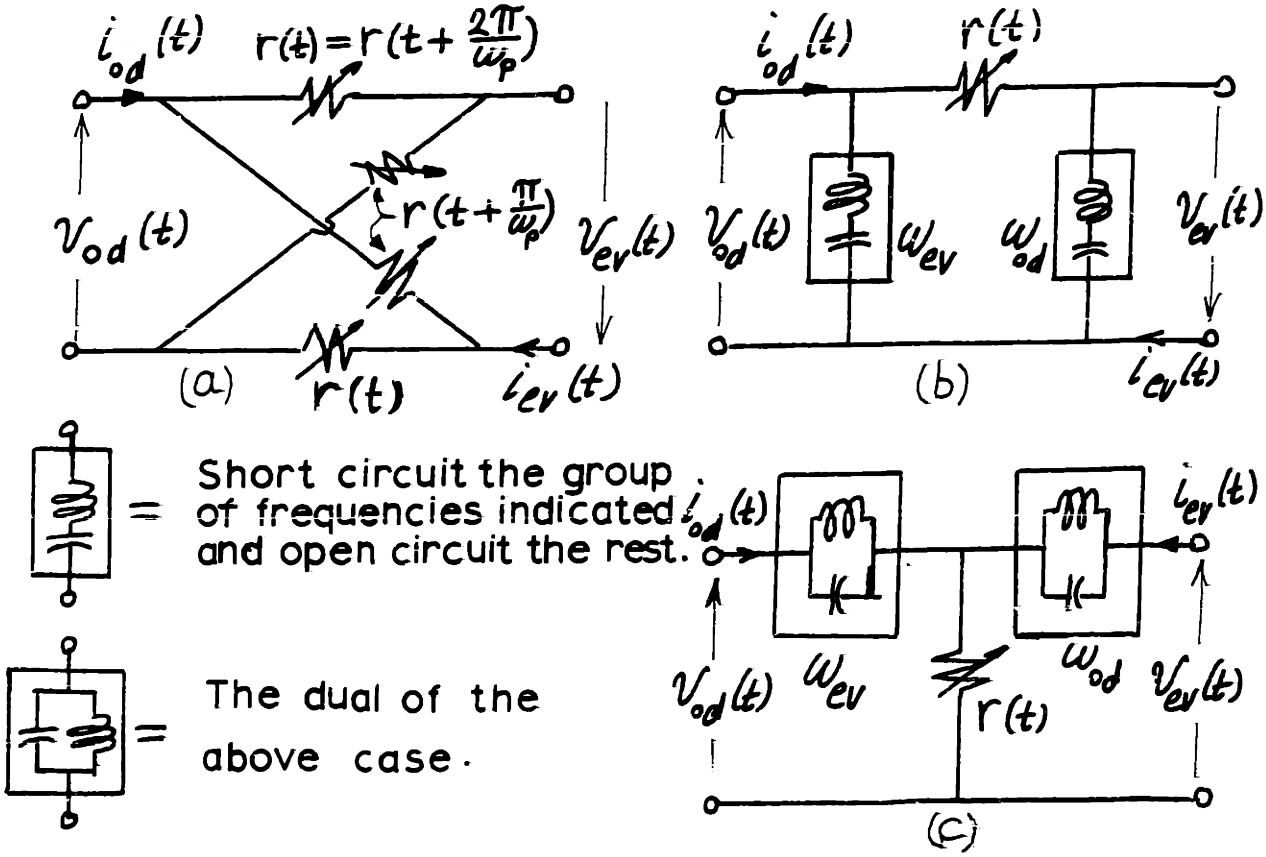

Fig. 2.6. Three Equivalent Basic Mixer Circuits

** Caruthers (I), Tucker (I) and (IV), and Belevitch (II).

and flow through, r(t). While in the balanced circuit (a) symmetry alone separated the odd-order frequencies** ($\omega_{od}=\omega_n$, n odd) and the even-order frequencies ($\omega_{ev}=\omega_n$, n even), selective networks had to be used to achieve the same effect in the single-ended circuits (b) and (c). Actually, the balanced circuit can support another set of odd- and even-order frequencies opposing the set indicated in Fig. 2.6.a. However, these two sets will be independent if no mixing elements are included in the terminations of the circuit.

The ideal selective filters used in Fig. 2.6.b and c can be achieved in practice by using transmission lines provided that $\omega_o \ll \omega_p$. This is shown in Fig. 2.7 where λ_p is the wavelength at the pump frequency ω_p.

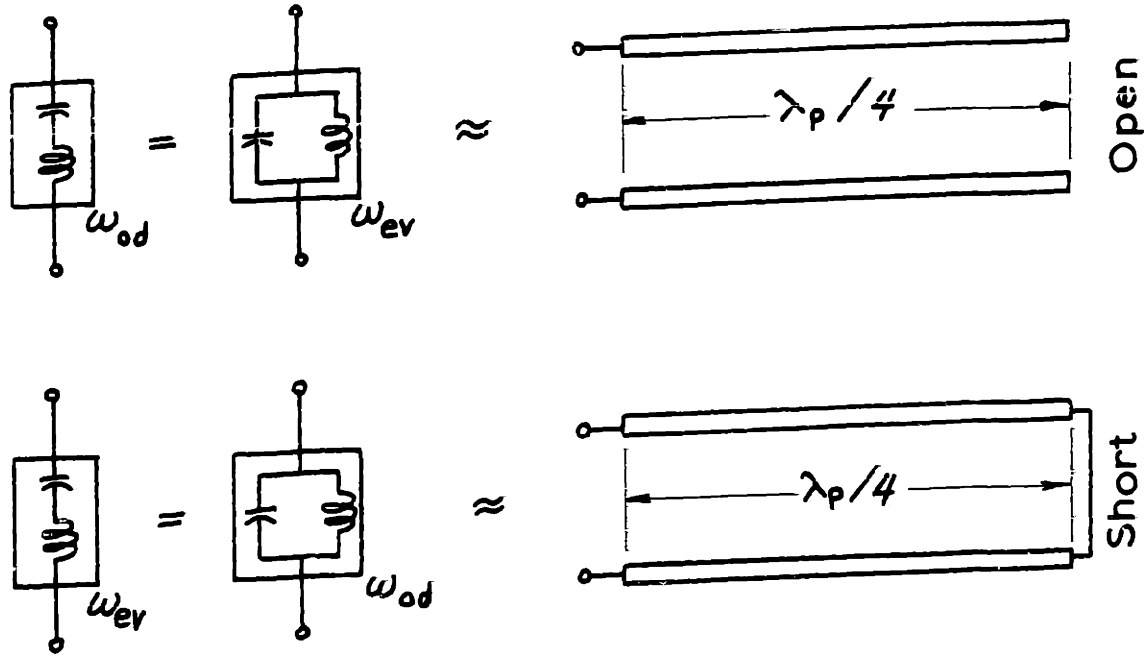

Fig. 2.7. Realization of the Selective Filters if $\omega_o \ll \omega_p$

** Note the frequency notation of Sec. 2.1.1.

We now derive the equations of any of the three circuits in Fig. 2.6. Because of linearity we can write

$$v_{od}(t) = \sum_{n \text{ odd}} V_n e^{j(n\omega_p + \omega_o)t} , \quad (2.15)$$

$$v_{ev}(t) = \sum_{n \text{ even}} V_n e^{j(n\omega_p + \omega_o)t} , \quad (2.16)$$

$$i_{od}(t) = \sum_{n \text{ odd}} I_n e^{j(n\omega_p + \omega_o)t} , \quad (2.17)$$

and

$$i_{ev}(t) = \sum_{n \text{ even}} I_n e^{j(n\omega_p + \omega_o)t} . \quad (2.18)$$

It is clear that

$$v(t) = v_{od}(t) + v_{ev}(t) , \quad (2.19)$$

and

$$i(t) = i_{od}(t) + i_{ev}(t) \quad (2.20)$$

are the voltage across and the current through r(t) respectively**. Thus

$$v(t) = r(t)\, i(t) . \quad (2.21)$$

Further, the Fourier series expansion of r(t)

$$r(t) = \sum_{n=-\infty}^{\infty} r_n e^{jn\omega_p t} \quad (2.22)$$

can be expanded into the odd-harmonic portion

$$r_{od}(t) = \sum_{n \text{ odd}} r_n e^{jn\omega_p t} \quad (2.23a)$$

$$= \tfrac{1}{2}\left[r(t) - r(t+\pi/\omega_p)\right] \quad (2.23b)$$

** There is a trivial factor of a $\frac{1}{2}$ in the right hand sides of Eqs. (2.19) and (2.20) when dealing with the balanced circuit.

and the even-harmonic portion

$$r_{ev}(t) = \sum_{n \text{ even}} r_n e^{jn\omega_p t} \qquad (2.24a)$$

$$= \tfrac{1}{2}\left[r(t) + r(t+\pi/\omega_p)\right] \quad , \qquad (2.24b)$$

We emphasize that <u>neither</u> $r_{od}(t)$ <u>nor</u> $r_{ev}(t)$ are meant to be odd or even functions of time. Substituting the relation

$$r(t) = r_{od}(t) + r_{ev}(t) \qquad (2.25)$$

and Eqs. (2.19) and (2.20) into Eq. (2.21) and separating the even- and odd-order frequency terms we get

$$\begin{bmatrix} v_{od}(t) \\ v_{ev}(t) \end{bmatrix} = \begin{bmatrix} r_{ev}(t) & r_{od}(t) \\ r_{od}(t) & r_{ev}(t) \end{bmatrix} \begin{bmatrix} i_{od}(t) \\ i_{ev}(t) \end{bmatrix} \quad . \qquad (2.26)$$

This is the required equation for <u>any</u> of the three circuits of Fig. 2.6.

2.3.2. Four basic mixer circuits:

There are four basic methods for terminating the odd-order out-of-band frequencies appearing at the input port and the even-order out-of-band frequencies appearing at the output port of any of the circuits of Fig. 2.6. The respective terminations are open-open, short-short, open-short and short-open. The four types of mixers so obtained are given in Fig. 2.8 for the case where ω_{+1} is converted to ω_o. They correspond to the Z- , Y- , H- and G-mixers respectively.

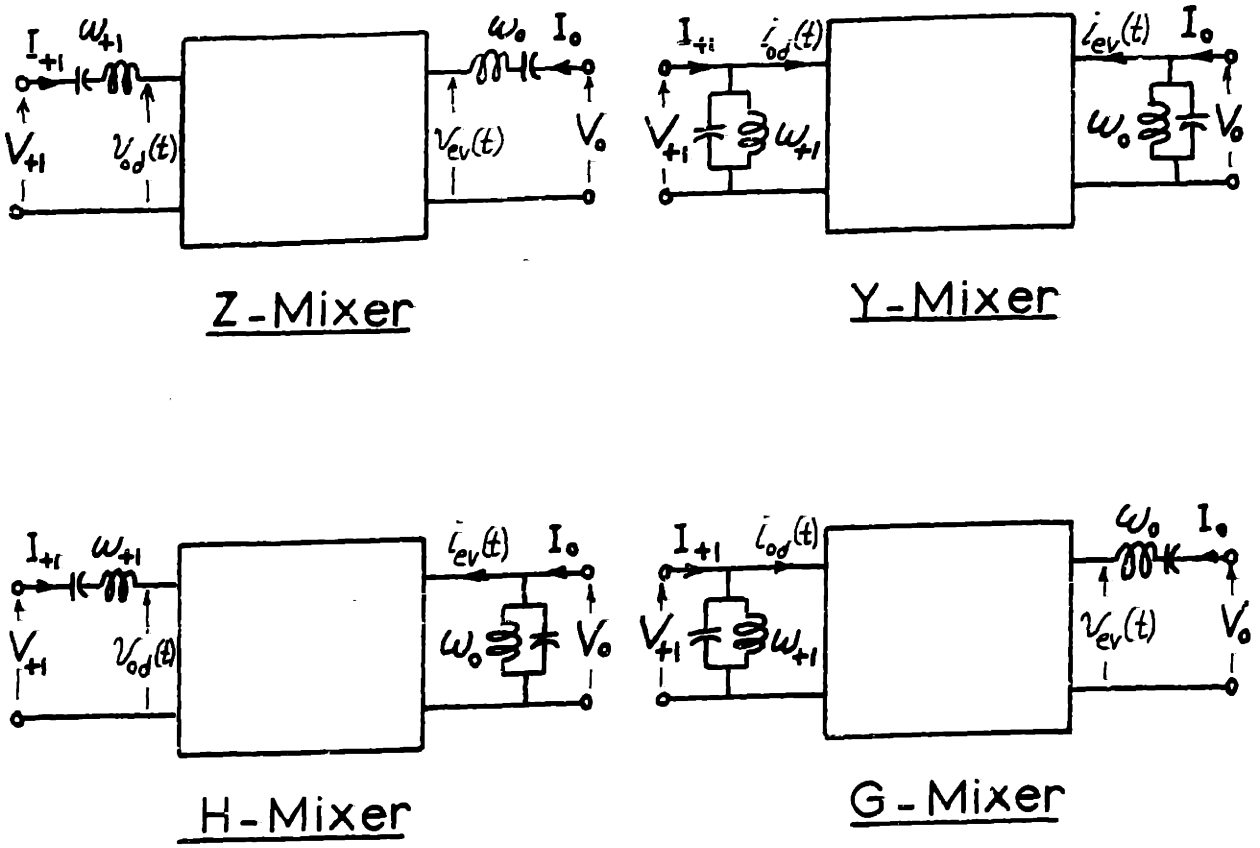

Fig. 2.8. The Four Basic Types of Mixers**

For the Z- or Y-mixers, the separation of the odd- and even-order frequencies does not change the equations given in Sec. 2.2. The details of three equivalent circuits for each of these two types of mixers is given in Figs. 2.9 and 2.10.

The H- and G-mixers are described in detail in the next section. The logical reason behind their names is the type of network matrices that have to be used for their analysis as will be indicated shortly.

** The squares represent any of the three circuits of Fig. 2.6.

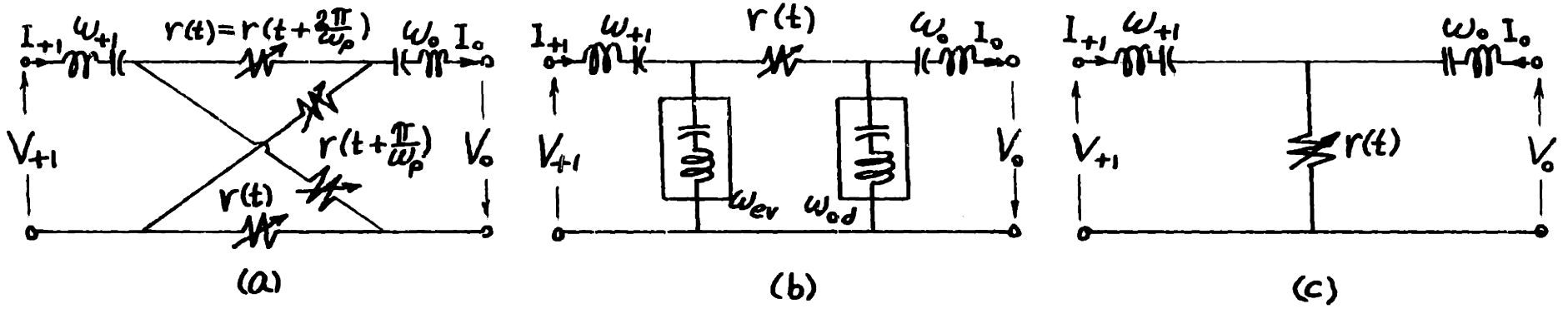

Fig. 2.9. Three Equivalent Z-Mixers

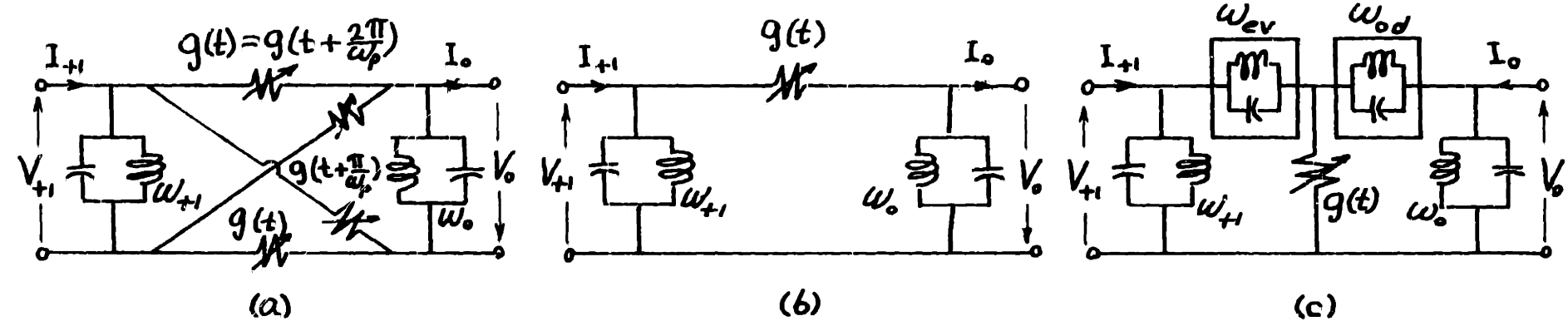

Fig. 2.10. Three Equivalent Y-Mixers

2.4. The H- and G-Mixers

An H-mixer is a mixer circuit in which all the odd-order out-of-band frequencies are open circuited whi all the even-order out-of-band frequencies are short cir cuited**, as shown in Fig. 2.8. It can be thought of as a Z-mixer with infinite short-circuit current idlers at t the even-order out-of-band frequencies; or a Y-mixer witl infinite open-circuit voltage idlers at all the odd-order out-of-band frequencies. The G-mixer is the dual of the H-mixer as given in Fig. 2.8. The details of three equiv circuits for each of these two types of mixers are given Figs. 2.11 and 2.12.

We now give the time-and frequency-domain analy of both the H- and G-mixers.

2.4.1. Time-domain analysis:

Referring to the H-mixer circuit of Fig. 2.8 (or Fig. 2.11) we note that both the input current $i_{od}(t)$ $(= I_{+1} e^{j\omega_{+1}t})$ and the output voltage $v_{ev}(t)$ $(= V_o e^{j\omega_o t})$ are pure tones, while both the input voltage $v_{od}(t)$ and the output current $i_{ev}(t)$ are the sums of many frequencies. Th it is clear that the only way to analyze such a circuit is to find the input voltage and output current as functions of the input current and output voltage. This can be achieved by converting the time-varying Z-matrix Eq. (2.26)

** Note the frequency notation of Sec. 2.1.1.

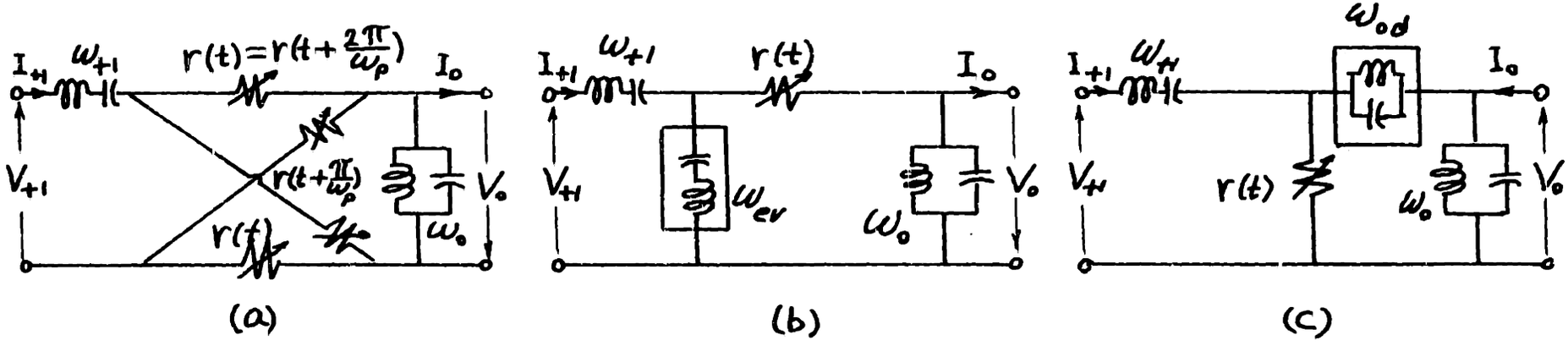

Fig. 2.11. Three Equivalent H-Mixers

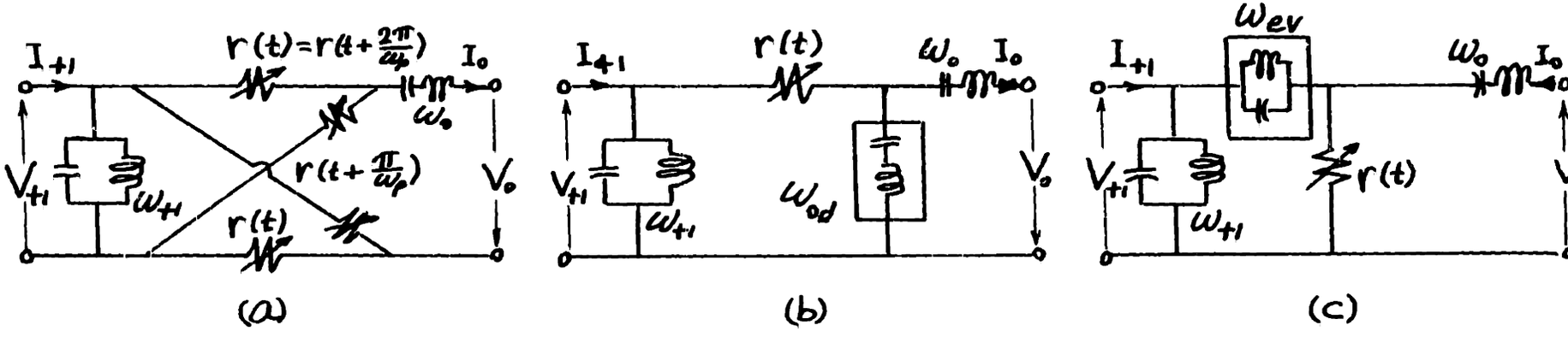

Fig. 2.12. Three Equivalent G-Mixers

to the time-varying H-matrix equation**,

$$\begin{bmatrix} v_{od}(t) \\ \\ i_{ev}(t) \end{bmatrix} = \begin{bmatrix} r_{ev}(t) - \dfrac{r_{od}^2(t)}{r_{ev}(t)} & \dfrac{r_{od}(t)}{r_{ev}(t)} \\ \\ -\dfrac{r_{od}(t)}{r_{ev}(t)} & \dfrac{1}{r_{ev}(t)} \end{bmatrix} \begin{bmatrix} i_{od}(t) \\ \\ v_{ev}(t) \end{bmatrix} \quad , (2.27a)$$

and hence the name "H-mixer".

Similarly the G-mixer can be analyzed by using the time-varying G-matrix equation

$$\begin{bmatrix} i_{od}(t) \\ \\ v_{ev}(t) \end{bmatrix} = \begin{bmatrix} \dfrac{1}{r_{ev}(t)} & -\dfrac{r_{od}(t)}{r_{ev}(t)} \\ \\ \dfrac{r_{od}(t)}{r_{ev}(t)} & r_{ev}(t) - \dfrac{r_{od}^2(t)}{r_{ev}(t)} \end{bmatrix} \begin{bmatrix} v_{od}(t) \\ \\ i_{ev}(t) \end{bmatrix} \quad . (2.28a)$$

If the conductance waveform $g(t) = 1/r(t)$ is known Eqs. (2.27a) and (2.28a) can be written in terms of the odd- and even-harmonic portions of $g(t)$, $g_{od}(t)$ and $g_{ev}(t)$, by using the easy-to-deduce relations

$$g_{ev}(t) = r_{ev}(t) \,/\, [r_{ev}^2(t) - r_{od}^2(t)] \quad , \quad (2.29a)$$

$$g_{od}(t) = -r_{od}(t) \,/\, [r_{ev}^2(t) - r_{od}^2(t)] \quad , \quad (2.29b)$$

$$r_{ev}(t) = g_{ev}(t) \,/\, [g_{ev}^2(t) - g_{od}^2(t)] \quad , \quad (2.30a)$$

and $$r_{od}(t) = -g_{od}(t) \,/\, [g_{ev}^2(t) - g_{od}(t)] \quad . \quad (2.30b)$$

** See Appendix 1, Eq. (A1.3) and Table A1.1.

The time-varying H-mixer equation becomes

$$\begin{bmatrix} v_{od}(t) \\ i_{ev}(t) \end{bmatrix} = \begin{bmatrix} \frac{1}{g_{ev}(t)} & -\frac{g_{od}(t)}{g_{ev}(t)} \\ \frac{g_{od}(t)}{g_{ev}(t)} & g_{ev}(t) - \frac{g_{od}^2(t)}{g_{ev}(t)} \end{bmatrix} \begin{bmatrix} i_{od}(t) \\ v_{ev}(t) \end{bmatrix} \quad ,(2.27b)$$

and the time-varying G-mixer equation becomes

$$\begin{bmatrix} i_{od}(t) \\ v_{ev}(t) \end{bmatrix} = \begin{bmatrix} g_{ev}(t) - \frac{g_{od}^2(t)}{g_{ev}(t)} & \frac{g_{od}(t)}{g_{ev}(t)} \\ -\frac{g_{od}(t)}{g_{ev}(t)} & \frac{1}{g_{ev}(t)} \end{bmatrix} \begin{bmatrix} v_{od}(t) \\ i_{ev}(t) \end{bmatrix} \quad .(2.28b)$$

2.4.2. Frequency-domain analysis:

Using Eqs. (2.15) ... (2.18), the time-domain H-matrix equation of the H-mixer, Eq. (2.27) a or b, can be written in the frequency domain in the infinite H-matrix form

$$\begin{bmatrix} \vdots \\ I_{+2} \\ V_{+1} \\ I_0 \\ V_{-1} \\ I_{-2} \\ \vdots \end{bmatrix} = \begin{bmatrix} \ddots & \ddots & \ddots & \ddots & \ddots & \ddots & \ddots \\ \ddots & H_{+2,+2} & H_{+2,+1} & H_{+2,0} & H_{+2,-1} & H_{+2,-2} & \ddots \\ \ddots & H_{+1,+2} & H_{+1,+1} & H_{+1,0} & H_{+1,-1} & H_{+1,-2} & \ddots \\ \ddots & H_{0,+2} & H_{0,+1} & H_{0,0} & H_{0,-1} & H_{0,-2} & \ddots \\ \ddots & H_{-1,+2} & H_{-1,+1} & H_{-1,0} & H_{-1,-1} & H_{-1,-2} & \ddots \\ \ddots & H_{-2,+2} & H_{-2,+1} & H_{-2,0} & H_{-2,-1} & H_{-2,-2} & \ddots \\ \ddots & \ddots & \ddots & \ddots & \ddots & \ddots & \ddots \end{bmatrix} \begin{bmatrix} \vdots \\ V_{+2} \\ I_{+1} \\ V_0 \\ I_{-1} \\ V_{-2} \\ \vdots \end{bmatrix} \quad ,(2.31)$$

where

$$H_{m,n} = +H^*_{n,m} = \left\langle \left\{ r_{ev}(t) - \frac{r_{od}^2(t)}{r_{ev}(t)} \right\} e^{-j(m-n)\omega_p t} \right\rangle = \left\langle \frac{1}{g_{ev}(t)} e^{-j(m-n)\omega_p t} \right\rangle \quad \left.\begin{array}{l} \\ \\ \end{array}\right\} \text{ m,n odd} \quad , (2.32a)$$

$$H_{m,n} = +H^*_{n,m} = \left\langle \frac{1}{r_{ev}(t)} e^{-j(m-n)\omega_p t} \right\rangle = \left\langle \left\{ g_{ev}(t) - \frac{g_{od}^2(t)}{g_{ev}(t)} \right\} e^{-j(m-n)\omega_p t} \right\rangle \quad \left.\begin{array}{l} \\ \\ \end{array}\right\} \text{ m,n even} \quad , (2.32b)$$

and

$$H_{m,n} = -H^*_{n,m} = \left\langle \frac{r_{od}(t)}{r_{ev}(t)} e^{-j(m-n)\omega_p t} \right\rangle = \left\langle -\frac{g_{od}(t)}{g_{ev}(t)} e^{-j(m-n)\omega_p t} \right\rangle \quad \left.\begin{array}{l} \\ \\ \end{array}\right\} \text{ m odd, n even} \quad . (2.32c)$$

The time averaging $\langle \ldots \rangle = \frac{1}{2\pi} \int_{-\pi}^{\pi} \ldots d\omega_p t$ can be shown to be equivalent to $\frac{1}{\pi} \int_{-\pi/2}^{\pi/2} \ldots d\omega_p t$ for the above equations.

Note that the above infinite H-matrix is <u>neither</u> Hermitian <u>nor</u> skew Hermitian.

The H-mixer is characterized by

$$V_n = 0 \qquad n \text{ even, } n \neq 0 \quad , \qquad (2.33a)$$

and

$$I_n = 0 \qquad n \text{ odd, } n \neq 1 \quad . \qquad (2.33b)$$

Thus, Eq. (2.31) reduces to the two-port H-matrix equation

$$\begin{bmatrix} V_{+1} \\ I_0 \end{bmatrix} = \begin{bmatrix} H_{+1,+1} & H_{+1,0} \\ -H^*_{+1,0} & H_{0,0} \end{bmatrix} \begin{bmatrix} I_{+1} \\ V_0 \end{bmatrix} \quad . \qquad (2.34)$$

The above 2 x 2 H-matrix is skew Hermitian. The performance of the mixer can be calculated from Appendix 1.

If the image frequency ω_{-1} is to be treated differently from the rest of the out-of-band frequencies, one must use the three-port H-matrix equation

$$\begin{bmatrix} V_{+1} \\ I_0 \\ V_{-1} \end{bmatrix} = \begin{bmatrix} H_{+1,+1} & H_{+1,0} & H_{+1,-1} \\ -H^*_{+1,0} & H_{0,0} & H_{0,-1} \\ H^*_{+1,-1} & -H^*_{0,-1} & H_{-1,-1} \end{bmatrix} \begin{bmatrix} I_{+1} \\ V_0 \\ I_{-1} \end{bmatrix} \quad . \qquad (2.35)$$

The performance of the mixer in this case can be found with the help of Appendix 2.

The analysis of the G-mixer is similar to that of the H-mixer, and the resulting equations are the duals of Eqs. (2.31) ... (2.35).

Each of the H- and G-mixers can be modified by adding a finite number of voltage and/or current idlers. The techniques of solving the resulting circuits are identical to those discussed in Sec. 2.2.2 for Z- and Y-mixers with idlers.

2.5. The N-ary Division Schemes

2.5.1. Basic concepts:

We have already considered two types of the N-ary division schemes. The first was the unitary division scheme (N=1) which grouped all the frequencies involved in a mixer into one group. The out-of-band frequencies were either all open-circuited, producing the Z-mixer, or all short-circuited, producing the Y-mixer as shown in Table 2.1.

Table 2.1. The Two Mixers of the Unitary Division Scheme

Number	Out-Of-Band Frequencies ω_n	Assigned Name
1	Open Circuit	Z-mixer
2	Short Circuit	Y-mixer

The second scheme considered was the binary division scheme (N=2) given in Sec. 2.3. The frequencies were divided into two groups, even-order frequencies $\omega_{ev} = \omega_{2n}$ and odd-order frequencies $\omega_{od} = \omega_{2n+1}$. This created the four basic types of mixers indicated in Table 2.2**.

In this system the resistance was divided into the odd-harmonic portion $r_{od}(t) = r_{2n+1}(t)$ and the even-harmonic portion $r_{ev}(t) = r_{2n}(t)$. The former converts currents from either frequency group into voltages in the other frequency

** See also Sec. 2.3.2.

Table 2.2. The Four Mixers of the Binary Division Scheme

Number	Out-Of-Band Frequencies ω_{2n}	ω_{2n+1}	Assigned Name
1	Open	Open	Z-Mixer
2	Short	Open	H-Mixer
3	Short	Short	Y-Mixer
4	Open	Short	G-Mixer

group, while the latter converts either group into itself. This is expressed mathematically in Eq. (2.26) and shown schematically in Fig. 2.13. The H- and G-mixers could not have been analyzed in a closed form without such a binary division scheme.

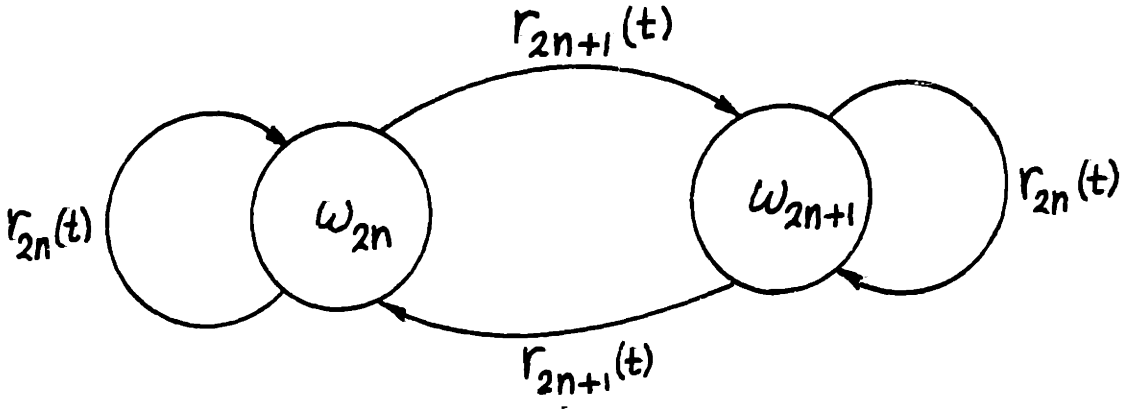

Fig. 2.13. The Binary Division Scheme

It is interesting to note that the binary division scheme described above is unique. That is to say it is not possible to find another scheme in which the frequencies are divided into two groups and the resistance is divided into two harmonic portions such that the frequency conversion can be represented in a manner similar to that given in Fig. 2.13.

The aforementioned division techniques can be extended by dividing the frequencies involved into more than two groups. This will allow us to analyze more mixer circuits in a closed form. For an N-ary division scheme the number of mixer circuits considered is 2^N. This comes about because the out-of-band frequencies in each of the N frequency groups can have two basic states, open circuit or short circuit, resulting in 2^N different circuits. The Z- and Y-mixers will always be included among these circuits. Further, if N= M·L, the 2^N circuits of the N-ary scheme will include the 2^M circuits of the M-ary scheme and the 2^L circuits of the L-ary scheme.

It can be shown that there exists one and only one N-ary division scheme for each value of N. A schematic representation of the unique ternary division scheme (N=3) is given in Fig. 2.14.

There are eight (= 2^3) different mixer circuits that can be analyzed in a closed form using the ternary division scheme. These are given in Table 2.3. The method of analysis of any of the circuits is similar to that given

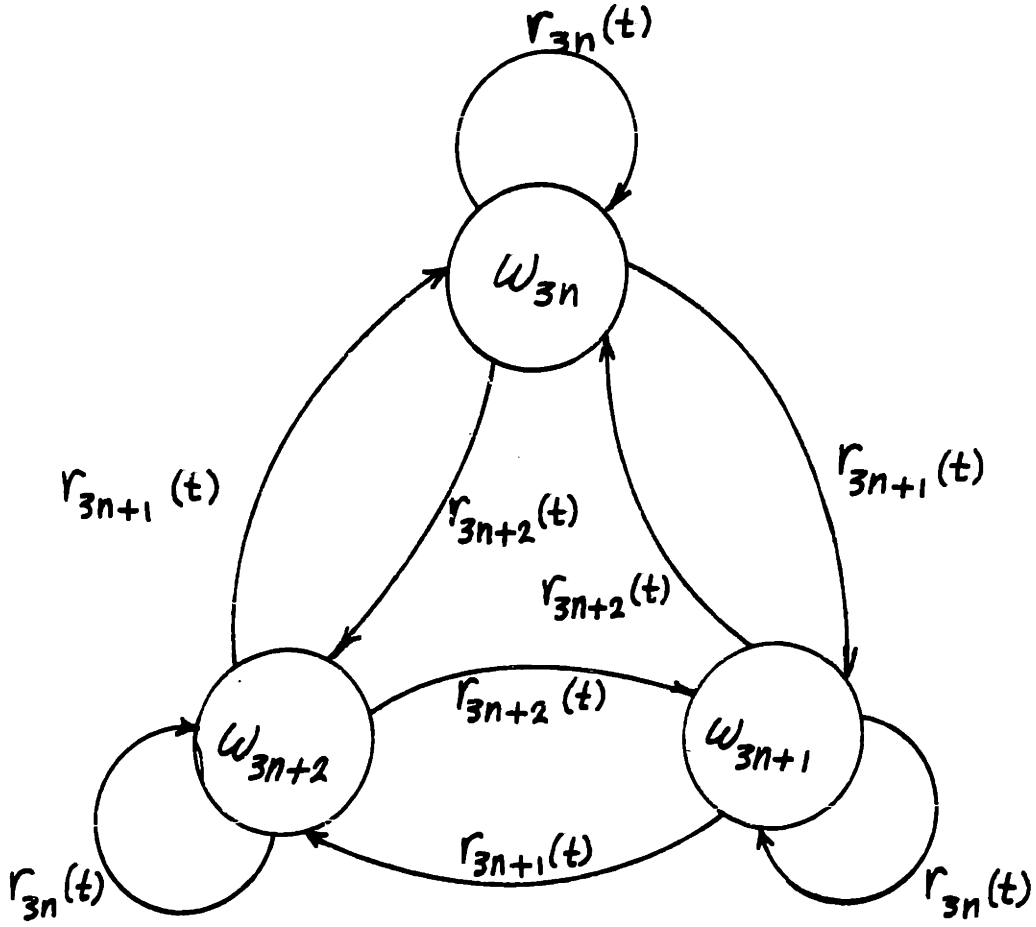

Fig. 2.14. The Ternary Division Scheme

Table 2.3. The Eight Mixers of the Ternary Division Scheme

Number	Out-Of-Band Frequencies ω_{3n}	ω_{3n+1}	ω_{3n+2}	Assigned Name
1	Open	Open	Open	Z-Mixer
2	Short	Open	Open	H_3-Mixer
3	Open	Short	Open	
4	Open	Open	Short	
5	Short	Short	Short	Y-Mixer
6	Open	Short	Short	G_3-Mixer
7	Short	Open	Short	
8	Short	Short	Open	

in Sec. 2.4 for the H- or G-mixers.

If $\omega_o \ll \omega_p$ it is nearly impossible to differentiate the two frequency groups ω_{3n+1} and ω_{3n+2} by simple filtering**. Thus, it is desirable to terminate the out-of-band frequencies falling in both groups with the same terminations. Of course the Z- and Y-mixers appearing as cases 1 and 4 in the table satisfy this requirement, but so do cases 2 and 6 which are assigned the names H_3- and G_3-mixers. These two new mixer circuits will be discussed in detail in the next section as special cases of the H_N- and G_N-mixers.

Following the same procedure as that given in developing Eqs. (2.15) ... (2.26), the time-varying Z-matrix equation for the N-ary divisions scheme can be written as

$$\begin{bmatrix} v_{N\cdot n}(t) \\ v_{N\cdot n+1}(t) \\ \vdots \\ v_{N\cdot n+N-1}(t) \end{bmatrix} = \begin{bmatrix} r_{N\cdot n}(t) & r_{N\cdot n+N-1}(t) & \cdots & r_{N\cdot n+1}(t) \\ r_{N\cdot n+1}(t) & r_{N\cdot n}(t) & \cdots & r_{N\cdot n+2}(t) \\ \vdots & \vdots & & \vdots \\ r_{N\cdot n+N-1}(t) & r_{N\cdot n+N-2}(t) & \cdots & r_{N\cdot n}(t) \end{bmatrix} \begin{bmatrix} i_{N\cdot n}(t) \\ i_{N\cdot n+1}(t) \\ \vdots \\ i_{N\cdot n+N-1}(t) \end{bmatrix} \qquad (2.36)$$

where $v_{N\cdot n}(t)$, $v_{N\cdot n+1}(t)$, ... , $v_{N\cdot n+N-1}(t)$ and $i_{N\cdot n}(t)$,

** This is true because in this case $\omega_{-n} \approx \omega_{+n}$ as indicated in Sec. 2.1.1.

$i_{N\cdot n+1}(t)$, ... , $i_{N\cdot n+N-1}(t)$ are the voltages and currents in the N frequency groups $\omega_{N\cdot n}$, $\omega_{N\cdot n+1}$, ... $\omega_{N\cdot n+N-1}$; and $r_{N\cdot n}(t)$, $r_{N\cdot n+1}(t)$, ... , $r_{N\cdot n+N-1}(t)$ are the N harmonic portions of r(t) and are given by

$$\left.\begin{aligned} r_{N\cdot n+m}(t) &= \sum_{n=-\infty}^{\infty} r_{N\cdot n+m}\, e^{j(N\cdot n+m)\omega_p t} \\ &= \frac{1}{N}\sum_{k=0}^{N-1} r(t+2k\pi/N\omega_p)\, e^{-j2mk\pi/N} \\ &= r^{*}_{N\cdot n+N-m}(t) \end{aligned}\right\} \quad ; \quad (2.37)$$

$$m = 0, 1, \ldots, N-1$$

For N=2 Eq. (2.36) is identical to Eq. (2.26) and Eq. (2.37) is identical to Eqs. (2.23) and (2.24).

2.5.2. The H_N- and G_N- mixers:

The H_N- and G_N-mixers are two of the 2^N possible mixer circuits of the N-ary division scheme. They form an important class of mixers since for N=2 they are the H- and G-mixers; for N=3 they are the H_3- and G_3-mixers; and for N=∞ they are the Z- and Y-mixers respectively.

As a general definition, an H_N-mixer is a mixer circuit in which all the out-of-band frequencies are open circuited except those in the group $\omega_{N\cdot n}$; n= -∞, ... , +∞; which are short circuited. It can be considered as a Z-

mixer with an infinite number of short-circuit current idlers for all the out-of-band frequencies in the group $\omega_{N\cdot n}$; or as a Y-mixer with an infinite number of open-circuit voltage idlers for all the out-of-band frequencies in the N-1 groups $\omega_{N\cdot n+1}, \omega_{N\cdot n+2}, \ldots, \omega_{N\cdot n+N-1}$. The H_N-mixer is shown in Fig. 2.15 for $N \geq 2$.

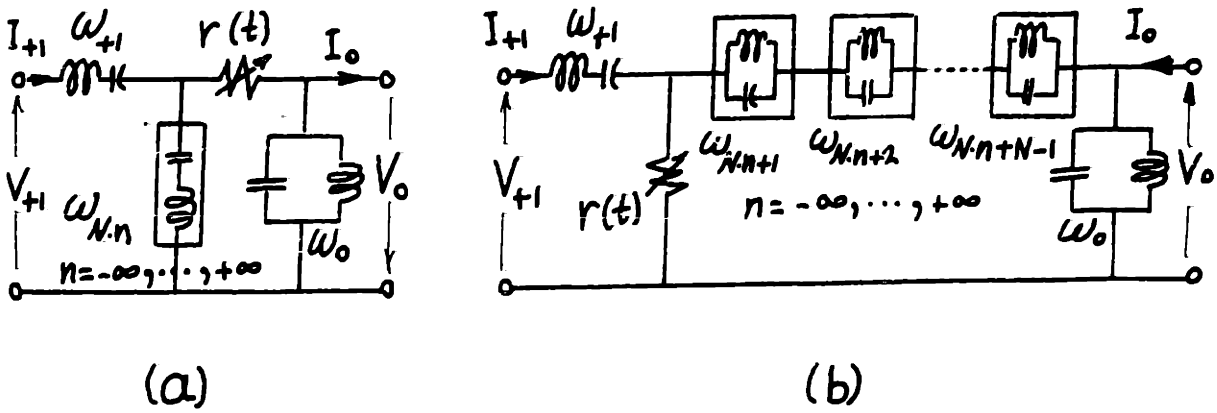

Fig. 2.15. Two Equivalent H_N-Mixers, $N \geq 2$

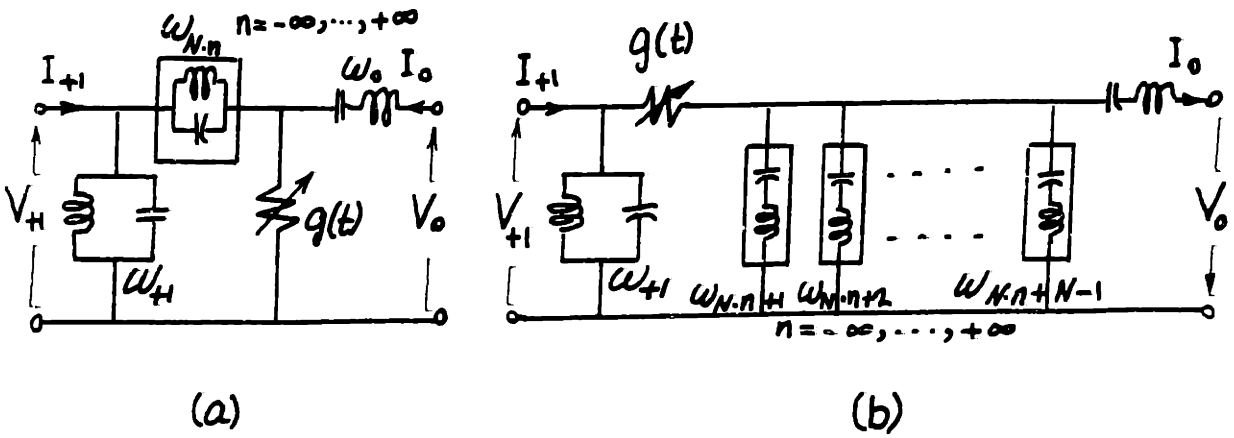

Fig. 2.16. Two Equivalent G_N-Mixers, $N \geq 2$

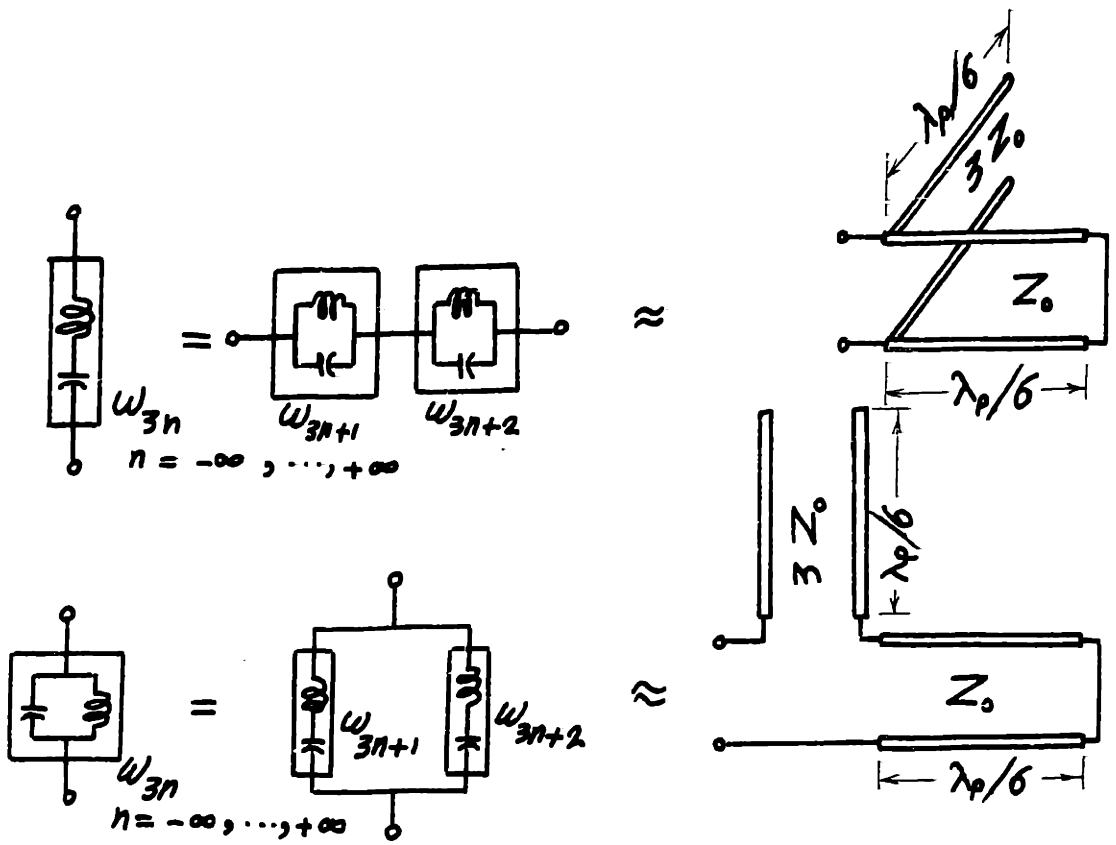

Fig. 2.17. Realization of Filters for the H_3- and G_3-Mixers

The G_N-mixer is the dual of the H_N-mixer. It is shown in Fig. 2.16 for $N \geq 2$.

If $\omega_o \ll \omega_p$ the idler circuits employed in Figs. 2.15 and 2.16 can be realized in practice by using transmission lines. For N=2 the required filters were shown in Fig. 2.7. For N=3 the filters are shown in Fig. 2.17 where λ_p is the wavelength at the pump frequency ω_p.

We now deduce the two-port equations for the H_N- and G_N-mixers. The technique used will be similar to that used in Sec. 2.4 to analyze the H- and G-mixers; of course it will be identical if N=2.

The H_N-mixer is characterized by

$$V_{N\cdot n} = 0 \qquad ; \text{ all } n,\ n\neq 0 \qquad , (2.38a)$$

and

$$I_{N\cdot n+m} = 0 \quad m= 1,2, \ldots ,N-1;\ \text{all } n, (n\neq 0 \text{ if } m=1). \quad (2.38b)$$

Thus in Eq. (2.36)

$$v_{N\cdot n}(t) = V_o\, e^{j\omega_o t} \qquad . (2.39a)$$

$$i_{N\cdot n+1}(t) = I_{+1}\, e^{j\omega_{+1}(t)} \qquad , (2.39b)$$

$$i_{N\cdot n+m}(t) = 0 \quad m= 2,3, \ldots , N-1 \qquad . (2.39c)$$

The time-varying H-matrix equation of the H_N-mixer is deduced from Eqs. (2.36) and (2.37) to be

$$\begin{bmatrix} v_{N\cdot n+1}(t) \\ i_{N\cdot n}(t) \end{bmatrix} = \begin{bmatrix} r_{N\cdot n}(t) - \dfrac{r^2_{N\cdot n+1}(t)}{r_{N\cdot n}(t)} & \dfrac{r_{N\cdot n+1}(t)}{r_{N\cdot n}(t)} \\ -\dfrac{r^*_{N\cdot n+1}(t)}{r_{N\cdot n}(t)} & \dfrac{1}{r_{N\cdot n}(t)} \end{bmatrix} \begin{bmatrix} I_{+1}\, e^{j\omega_{+1}t} \\ V_o\, e^{j\omega_o t} \end{bmatrix} , (2.40)$$

Finally the corresponding two-port H-matrix representation becomes

$$\begin{bmatrix} V_{+1} \\ I_0 \end{bmatrix} = \begin{bmatrix} H_{+1,+1} & H_{+1,0} \\ -H^*_{+1,0} & H_{0,0} \end{bmatrix} \begin{bmatrix} I_{+1} \\ V_0 \end{bmatrix} \qquad , (2.41)$$

where

$$H_{+1,+1} = \left\langle r_{N\cdot n}(t) - \frac{r^2_{N\cdot n+1}(t)}{r_{N\cdot n}(t)} \right\rangle \quad , \quad (2.42a)$$

$$H_{0,0} = \left\langle \frac{1}{r_{N\cdot n}(t)} \right\rangle \quad , \quad (2.42b)$$

and

$$H_{+1,0} = \left\langle \frac{r_{N\cdot n+1}(t)}{r_{N\cdot n}(t)} e^{-j\omega_p t} \right\rangle \quad . \quad (2.42c)$$

The time averaging $\langle \ldots \rangle = \frac{1}{2\pi} \int_{-\pi}^{\pi} \ldots d\omega_p t$ can be shown to be equivalent to $\frac{N}{2\pi} \int_{-\pi/N}^{\pi/N} \ldots d\omega_p t$ for the above equations.

The performance of the mixer can be calculated with the help of Appendix 1.

For the analysis of the G_N-mixer one must use the duals of Eqs. (2.36) ... (2.42).

From the above equations one can verify that H_2-mixer = H-mixer, G_2-mixer = G-mixer, H_∞-mixer = Z-mixer and G_∞-mixer = Y-mixer. The equations are not valid for $N < 2$.

2.6. Conclusions and Topics for Further Research

In this chapter we introduced and gave the methods of analysis of four basic resistive mixers; the Z-, Y-, H- and G-mixers. The names originated from the types of network matrices that had to be used to find the mixer performance. The Z-mixer is obtained by open-circuiting all the out-of-band frequencies and the Y-mixer is obtained by short-circuiting them. For the H- and G-mixers, the out-of-band frequencies were divided into two groups; odd- and even-order frequencies (see the frequency terminology of Sec. 2.1.1). This division was shown to be possible by using the symmetry of four time-varying resistances two of which are 180° out-of-phase with the others, or by using a single resistance with the appropriate filtering. The required filters were simply shown to be quarter wave short and open transmission lines <u>if</u> the i-f frequency, ω_o, is much smaller than the pump frequency, ω_p. The H-mixer is obtained by open-circuiting the odd-order out-of-band frequencies and short-circuiting the even-order ones. The G-mixer is the dual of the H-mixer.

The aforementioned binary frequency division scheme was generalized to the N-ary division scheme for $N \geq 2$. In this scheme the frequencies were divided into N groups; $\omega_{N.n}, \omega_{N.n+1}, \ldots \omega_{N.n+N-1}$ for $n = -\infty, \ldots, +\infty$.

A method of analysis was given to analyze, in a closed form, the circuits obtained when all the out-of-band frequencies in each group are open- or short-circuited. This produced 2^N different mixer circuits analyzable in a closed form for each value of N. Two classes of mixer circuits in the N-ary division scheme were given special attention. These are the H_N- and the G_N- mixers. The former class is obtained by open-circuiting all the out-of-band frequencies except those in the group $\omega_{N.n}$; $n = -\infty, \ldots, +\infty$; which are short circuited. The G_N-mixer has the dual terminations. The importance of the H_N- and G_N-mixers stems from the fact that when N = 2 they are the H- and G-mixers, and when $N = \infty$ they are the Z- and Y-mixers respectively. Also the separation of the frequencies for these mixers in different ports can be achieved by appropriate transmission line filters if $\omega_o \ll \omega_p$. The use of symmetry and more than one resistance for the frequency separation is only possible if constant, or generally linear, phase-shifting networks can be built to operate at <u>all</u> the frequencies involved in the mixer.

In addition to the 2^N basic mixer circuits which can be analyzed in a closed form for any value of N, one can analyze many other modified mixer circuits. These are the ones obtainable from the N-ary division

scheme by providing a finite number of specified out-of-band frequencies with idlers with arbitrary terminations.

An interesting question which deserves more attention is whether or not there exists different frequency division schemes, other than the aforementioned N-ary scheme, for which the resistive mixer circuit obtained can be analyzed in a closed form. There are many frequency division schemes that can be thought of which seem hard, if not impossible, to analyze. For example if all the frequencies ω_n, $n > 1$, are short-circuited while ω_n, $n < 0$, are open-circuited, the resulting analysis requires the inversion of semi-infinite matrices whose inverse is not given in the literature. There are many similar examples.

Another interesting problem which is important in practice is that of parasitic reactances. It can be easily deduced that by adding a fixed or a time-varying reactance in parallel with the resistance in a Y-mixer,** or in series with the resistance in a Z-mixer,*** one can find a closed form solution for the mixer equations. No other configurations seem to exist for the other types of mixers which yield a closed form solution.

** See for example Torrey and Whitmer (I, Sec. 5.13); Edwards (I); and Becker and Ernst (I).

*** See for example Penfield and Rafuse (I, Sec. 4.4 & 4.5) were the resistance is fixed while the series reactance is time-varying.

In practice a capacitance exists across the time-varying resistance and a fixed resistance exists in series with the combination . For example these can be the diode junction capacitance and series resistance. In the literature many authors have dealt with this problem in Y-mixers.** All these authors assumed that the junction capacitance short-circuits all the higher order out-of-band frequencies; ω_n, $|n| > 1$; across the time-varying resistance. Thus only the signal, i-f and image frequency voltages were considered. This assumption reduced the Y-mixer equations to a complex 3 x 3 Y-matrix which can be easily obtained from the values of the diode model parameters. This method of analysis, although approximate, seems to give good results when the junction capacitance is large and the series resistance is small. However, it fails for diodes with small junction capacitance and/or large series resistance.

It seems that one can extend the above mentioned method of analysis to treat <u>all mixer circuits</u> by considering more than three frequencies. For example one can consider that all the higher order out-of-band frequencies; ω_n, $|n| > m$ for some m; are short-circuited across the time-varying resistance and treat the mixer as a Y-mixer

** See for example Peterson and Llewellyn (I), Torrey and Whitmer (I, Sec. 5.12), Macpherson (I) and Bakanowski(II).

whose voltage consists of 2m+1 frequencies; ω_{-m}, ... , ω_{-1}, ω_0, ω_{+1}, ... , ω_{+m}. Such a (2m+1) - frequency Y-mixer can be provided with the appropriate external idlers according to the type of mixer being analyzed. The idler termination should include the junction capacitance and series resistance as well as any external termination. The above procedure is bound to give accurate results as the value of m is increased since the junction capacitance is bound to short-circuit all the higher order out-of-band frequencies: ω_n, $|n| > m$; as m increases.

One last point which has other applications besides mixer theory is a specific problem in broadband filter design. In almost all the available literature on filter theory the object is an optimum amplitude and/or phase transfer characteristics in the filter pass and/or stop bands. The impedances offered to the undesired frequencies are only required to be reactive, or generally to have large reflection coefficients. In mixers, and many other devices such as oscillators, amplifiers and frequency multipliers, one needs a filter which gives specific terminations to the different out-of-band frequencies, for example an open or a short, over a wide frequency band. For example separation of the even- and odd-order frequencies using a single-diode and quarter-wave shorted and opened transmission lines, as described in Sec. 2.3, is desir-

able for microwave frequencies where four-diode symmetrical mixers are hard to achieve, however this technique will certainly produce narrow band mixers. At this point it is desirable to replace the simple transmission lines with broader band selective filters which gives the same effect. This point certainly needs further consideration.

CHAPTER 3

THE OPTIMUM RESISTANCE WAVEFORM AND IMBEDDING NETWORK

3.1. Three Basic Questions

A linear resistive mixer can be represented as a linear, periodically time-varying resistance r(t), imbedded in a passive, linear time-invariant network as shown in Fig. 3.1. The imbedding network provides terminations

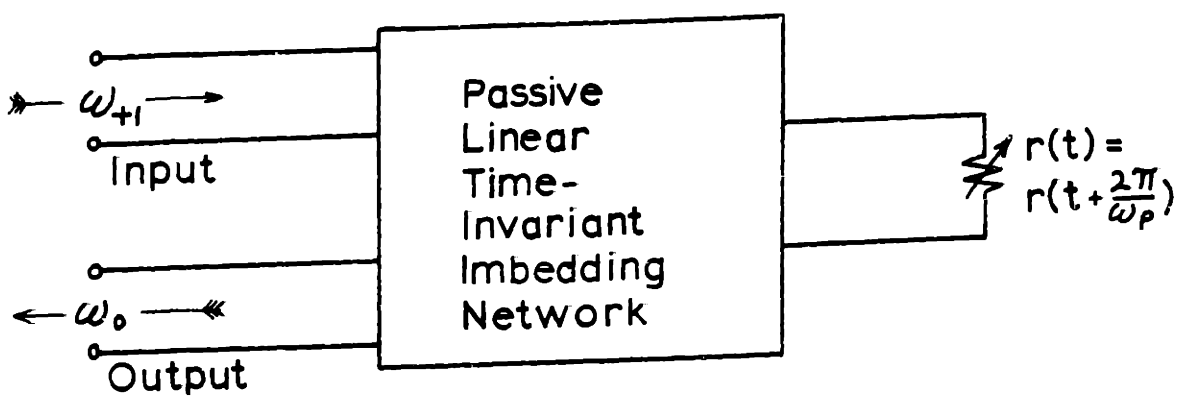

Fig. 3.1. Generalized Representation of a Linear Mixer

and filtering for the undesired out-of-band frequencies. It can be divided into two separate parts as indicated in Fig. 3.2. This is possible since the input and output frequencies are different and they cannot be coupled inside the network**.

** Note that all the mixer circuits discussed in the previous chapter were represented in this manner.

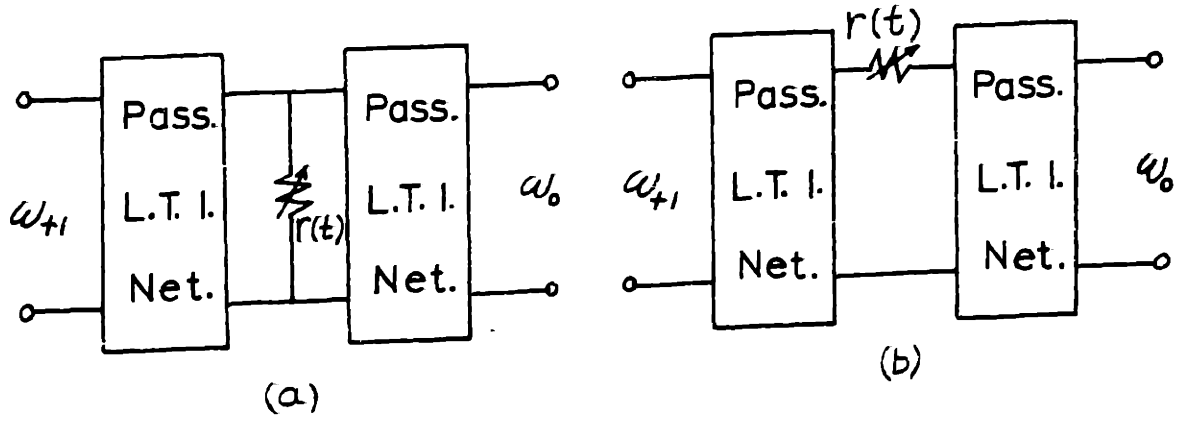

Fig. 3.2. Other Forms of the Generalized Linear Mixer

What resistance waveform should be employed and what imbedding network should be used for the optimum performance of the mixer is not clear. This is the object of this chapter. For this purpose we pose three basic questions and try to answer them in the next sections.

Before posing the questions we note that the only available fundamental limit on the conversion loss of a mixer employing a nonnegative resistance is unity**. One can show that this limit is attainable for a number of mixers; such as a Z-mixer with an impulse-train resistance waveform, a Y-mixer with an impulse-train conductance waveform*** and an H- or a G-mixer with a square-wave-driven ideal switch****.

** See for example Sec. A3.2 in this thesis; or, Page (I), Pantell (I), or Penfield (I).
*** See for example Sec. 3.2.1 or Appendix 8 in this thesis; or, Bakanowski (I), Barber (I), Herold (I), Torrey and Whitmer (I), or Uhlir (I).
**** See for example Sec. 3.2.1 or Appendix 11 in this thesis; or Caruthers (I) or Tucker (I) and (IV).

In all these cases the resistance waveform attains the values of zero and infinity during its cycle. This might not be possible because of device limitations. For this reason we constrain the resistance waveform to fall between prescribed maximum and minimum values in the following three basic questions:

1. Given a mixer imbedding network with certain terminations for the out-of-band frequencies and a resistance that can vary periodically in any desired manner between prescribed nonnegative maximum and minimum values: What is the corresponding optimum resistance waveform that yields the best possible mixer conversion loss?

2. Given a nonnegative resistance that varies periodically in a prescribed waveform: What is the corresponding optimum imbedding network that leads to the best possible mixer conversion loss?

3. Given a resistance that can be varied periodically in any desired fashion bounded by specified maximum and minimum values: What is the corresponding best possible mixer conversion loss?

The fundamental limit on the conversion loss of a mixer employing a resistive device can be found through answering the above questions. We will assume that any imbedding network used is ideal. Thus the fundamental limit will be set by the resistive device. In Appendices 10 and 11 we study the effect of nonideal imbedding networks where the undesired frequencies are not completely terminated.

3.2. Question 1: The Optimum Resistance Waveform

"Given a mixer imbedding network with certain terminations for the out-of-band frequencies and a resistance that can vary periodically in any desired manner between prescribed non-negative maximum and minimum values: What is the corresponding optimum resistance waveform that yields the best possible mixer conversion loss?"

In the following we answer the above question for some important mixer imbedding networks.

3.2.1. The Z- and Y-mixers:

Assume that in the Z-mixer, Figs. 2.2 and 2.9, $0 \leq R_{min} \leq r(t) \leq R_{max} \leq \infty$. The time origin can be chosen to make

$$r(t) = r_o + 2r_1 \cos(\omega_p t) + \ldots\ldots \qquad (3.1)$$

with $r_1 > 0$. Note that $r_o > 0$ from the passivity condition (A3.24a). In this case the Z-matrix of the Z-mixer given in Eq. (2.7) is real symmetric and the optimum conversion loss is given from Eqs. (A1.35) and (A1.38) as

$$L_{opt} = \frac{1 + \sqrt{1 - \epsilon}}{1 - \sqrt{1 - \epsilon}} \qquad , (3.2)$$

with $$\epsilon = (r_1 / r_o)^2 \qquad . (3.3)$$

Note that $0 \leq \epsilon \leq 1$ which follows from the passivity condition (A3.24b) for n= 1. It is clear that to minimize L_{opt} one must maximize ϵ, and hence maximize the ratio

r_1 / r_o. Thus, the optimum resistance waveform can be found by solving the problem:

$$\left.\begin{aligned} &\text{Maximize} \quad \frac{r_1}{r_o} = \frac{\int_{-\pi}^{\pi} r(t)\cos(\omega_p t)\, d\omega_p t}{\int_{-\pi}^{\pi} r(t)\, d\omega_p t} \\ &\text{under the constraint } R_{min} \le r(t) \le R_{max} \end{aligned}\right\} \quad . \quad (3.4)$$

The solution of (3.4) is found in Sec. A4.1 to be

$$\begin{aligned} r(t) &= R_{max} && |t| \le \Delta/2\omega_p \\ &= R_{min} && \Delta/2\omega_p \le |t| \le \pi/\omega_p \end{aligned} \quad , \quad (3.5)$$

where Δ is the solution of the transcendental equation

$$\tan\left(\frac{\Delta}{2}\right) = \frac{\Delta}{2} + \frac{\pi R_{min}}{R_{max} - R_{min}} \quad . \quad (3.6)$$

The above optimum resistance waveform is shown in Fig. 3.3.

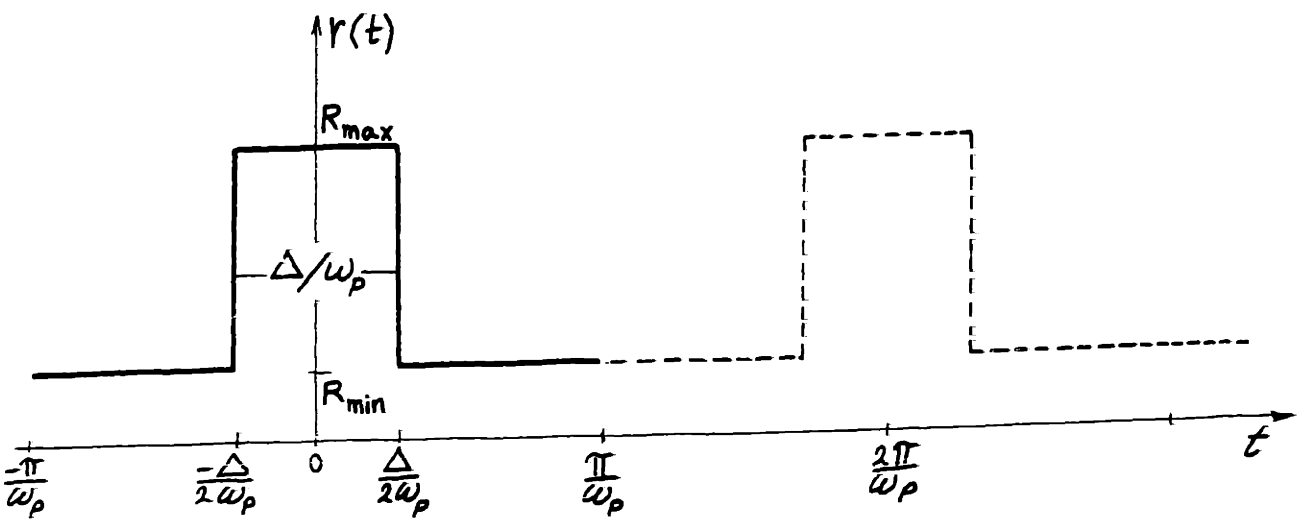

Fig. 3.3. The Optimum Resistance Waveform for a Z-Mixer

The corresponding mixer parameters become

$$\epsilon = \cos^2(\Delta/2) \quad . \quad (3.7)$$

$$L_{opt} = \frac{1 + \sin(\Delta/2)}{1 - \sin(\Delta/2)} \quad . \quad (3.8)$$

$$R_{s,opt} = R_{o,opt} = [R_{min} + (R_{max} - R_{min})\,\Delta/2\pi]\,\sin(\Delta/2) \quad . (3.9)$$

The optimum source and load resistance, $R_{s,opt}$ and $R_{o,opt}$, are calculated from Eqs. (A1.36) and (A1.37). The above equations are plotted in Figs. 3.4 and 3.5 as functions of R_{min}/R_{max}. In Fig. 3.4, the pulse duty ratio

$$P = \Delta / 2\pi \quad (3.10)$$

is plotted instead of Δ. For the Z-mixer, P is defined as the ratio of the time where r(t) attains its maximum value R_{max} to the total period $2\pi/\omega_p$. If $R_{min} \ll R_{max}$ it follows that

$$\Delta \approx 2\,(3\pi\, R_{min}/R_{max})^{1/3} \quad . \quad (3.11)$$

The corresponding mixer parameters become

$$\begin{aligned} L_{opt} &\approx 1 + \Delta \\ &\approx 4.343\ \Delta \quad \text{db} \\ &\approx 18.3\ (R_{min}/R_{max})^{1/3} \quad \text{db} \end{aligned} \quad . \quad (3.12)$$

$$\begin{aligned} R_{s,opt} = R_{o,opt} &= r_o\sqrt{1 - \epsilon} \\ &\approx 3\,(R_{min}^2\, R_{max}/3\pi)^{1/3} \\ &= 1.42\,\sqrt{R_{max}\, R_{min}}\ (R_{min}/R_{max})^{1/6} \end{aligned} \quad . \quad (3.13)$$

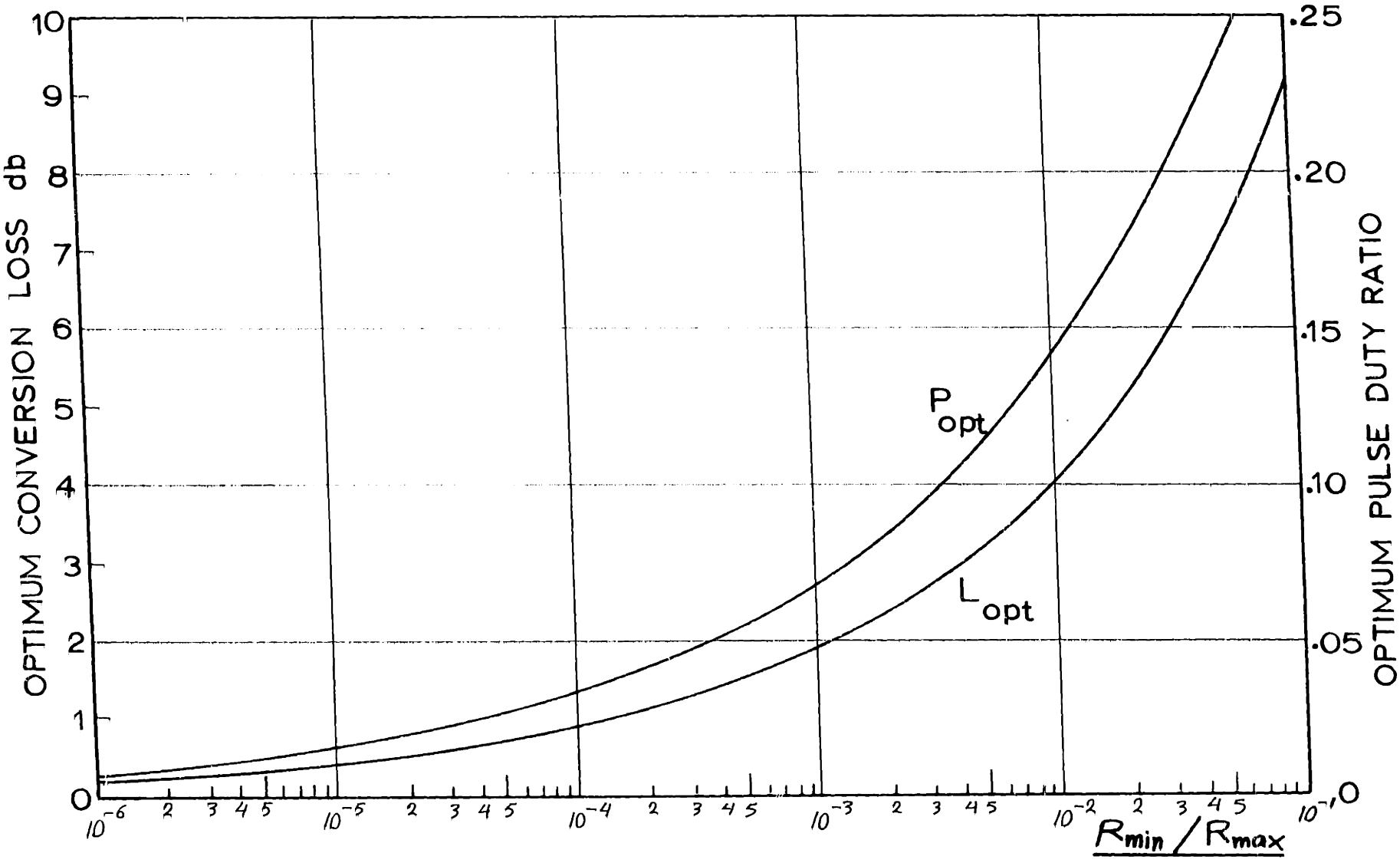

Fig. 3.4. The Fundamental Limit on L_{opt} for the Z- or Y-Mixers and the Corresponding Pulse Duty Ratio of the Optimum Drive Waveform

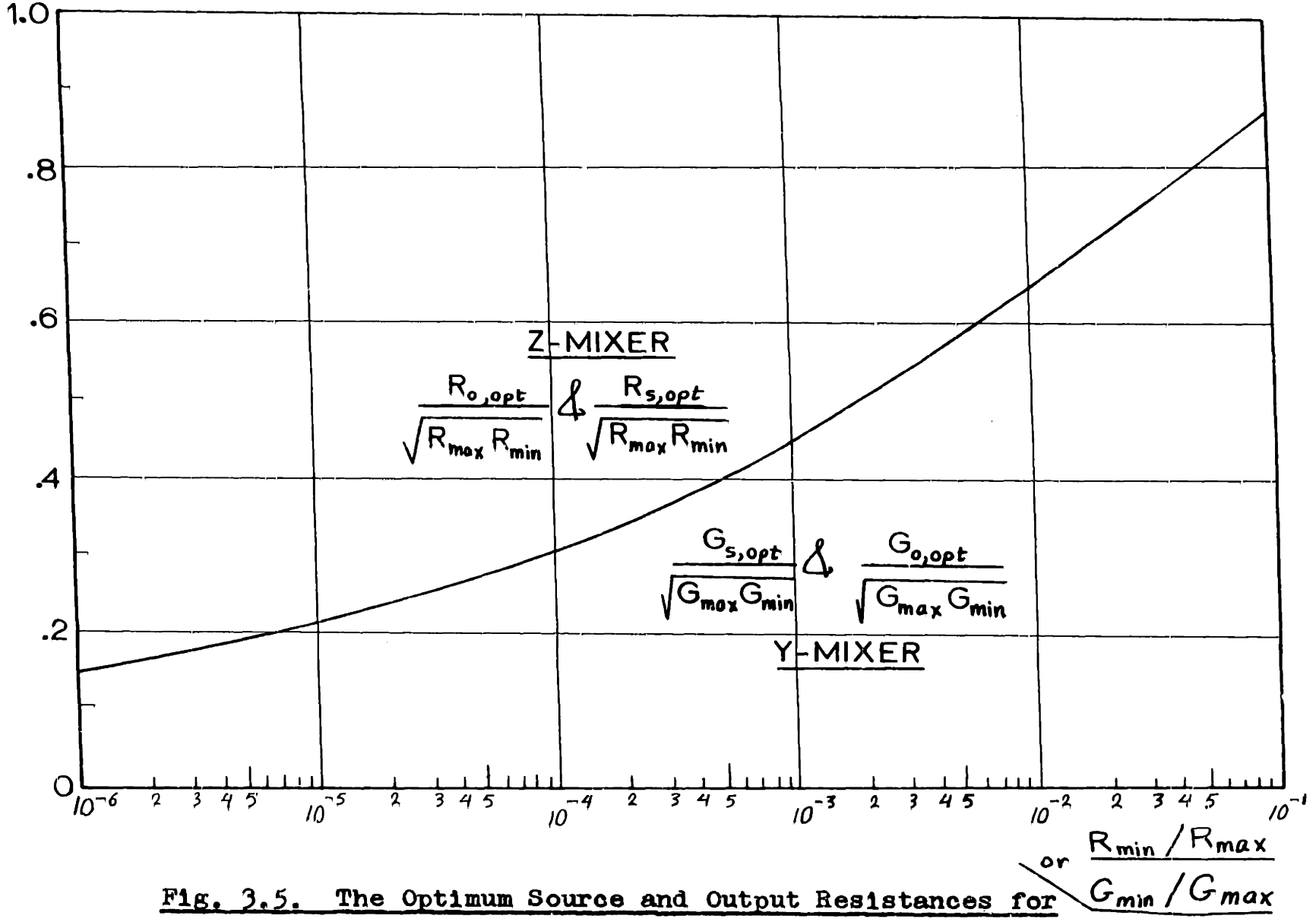

Fig. 3.5. The Optimum Source and Output Resistances for Optimally Driven Z- or Y-Mixers

If $R_{min}/R_{max} = 0$, then $L_{opt} = 1$ (zero db) and r(t) becomes an impulse train (P = zero). In this case $R_{s,opt}$ and $R_{o,opt}$ are both either zero or infinity unless $R_{max} = \infty$ and $R_{min} = 0$, i.e. r(t) is an ideal switch.

The Y-mixer, Figs. 2.3 and 2.10, is analyzed in the same manner. The corresponding equations are the duals of Eqs. (3.1) ... (3.13). The Optimum conductance waveform is shown in Fig. 3.6. The values of L_{opt}, Δ and P are identical to those of the Z-mixer, but P is defined here as the ratio of the time where g(t) attains its maximum value G_{max} $(=1/R_{min})$ to the total period $2\pi/\omega_p$.**

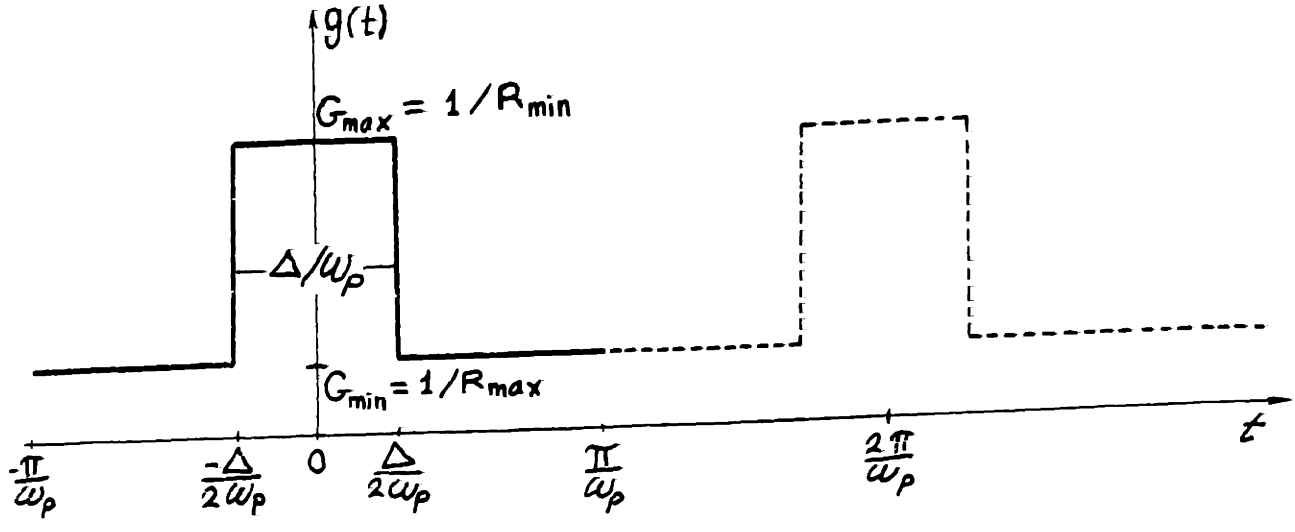

Fig. 3.6. The Optimum Conductance Waveform for a Y-Mixer

** The results concerning rectangular-pulse resistance or conductance waveforms can be applied to other pulsed waveforms. See for example Appendix 8 where we generalize the work of Barber (I) concerning the concept of an equivalent pulse duty ratio.

3.2.2. The H- and G-mixers:

We start by optimizing $r(t)$, $0 \leq R_{min} \leq r(t) \leq R_{max} \leq \infty$, for the H-mixer, Fig. 2.11. The corresponding analysis for the G-mixer, Fig. 2.12, will be deduced by duality.

The entries of the H-matrix equation of the H-mixer, Eq. (2.34), are given in Eqs. (2.32). The time origin can be chosen to make $H_{+1,0}$ real. In this case the H matrix is real skew symmetric and the optimum conversion loss is given from Eqs. (A1.35) and (A1.38) as

$$L_{opt} = \frac{\sqrt{1-\epsilon}+1}{\sqrt{1-\epsilon}-1} \quad , \quad (3.14)$$

with

$$\epsilon = -\frac{H_{+1,0}^2}{H_{+1,+1}\,H_{0,0}} \quad . \quad (3.15)$$

Note that $\epsilon \leq 0$ since both $H_{+1,+1}$, $H_{0,0} \geq 0$ if $r(t) \geq 0$. It is clear that to minimize L_{opt} one must maximize $|\epsilon|$. Writing the H's in terms of $r(t)$ by using Eqs. (2.32) and (2.23) ... (2.25), the optimum $r(t)$ for the H-mixer can be found by solving the problem:

Maximize

$$|\epsilon| = \left.\frac{\left[\int_{-\frac{\pi}{2}}^{\frac{\pi}{2}} \frac{r(t)-r(t+\pi/\omega_p)}{r(t)+r(t+\pi/\omega_p)} \cos(\omega_p t)\, d\omega_p t\right]^2}{\int_{-\frac{\pi}{2}}^{\frac{\pi}{2}} \frac{2}{r(t)+r(t+\pi/\omega_p)}\, d\omega_p t \int_{-\frac{\pi}{2}}^{\frac{\pi}{2}} \frac{2r(t)r(t+\pi/\omega_p)}{r(t)+r(t+\pi/\omega_p)}\, d\omega_p t}\right\} , \quad (3.16)$$

under the constraint $R_{min} \leq r(t) \leq R_{max}$

The solution of (3.16) is found in Sec. A4.2 to be

$$r(t) = R_{max} \qquad |t| \leq \pi/2\omega_p$$

$$= R_{min} \qquad \pi/2\omega_p \leq t \leq 3\pi/2\omega_p \qquad . \quad (3.17)$$

That is to say the optimum r(t) for the H-mixer is a square wave switching between R_{max} and R_{min}. The corresponding r(t) for the G-mixer is obviously identical to that of the H-mixer by duality and symmetry of the r(t) waveform. The optimum r(t) is given in Fig. 3.7. It is interesting to note that the optimum pulse duty ratio of r(t) is $\frac{1}{2}$, independent of the values of R_{max} and R_{min}. This is unlike the optimum pulse duty ratio of r(t) for the Z- or the Y-mixers which is dependent on R_{max} and R_{min}. This is one of the advantages of the H- and G-mixers over the Z- and Y-mixers.

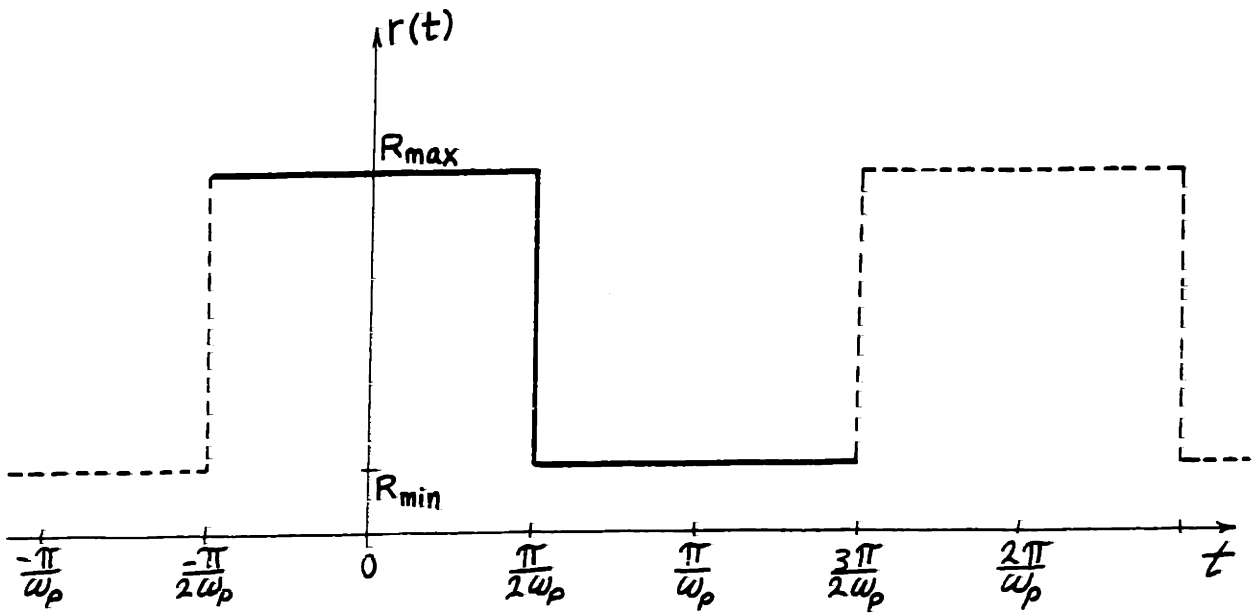

Fig. 3.7. The Optimum Resistance Waveform for an H- or a G-Mixer

The corresponding parameters for the H-mixer become

$$H_{+1,+1} = 2 R_{max} R_{min} / (R_{max} + R_{min}) \quad . \quad (3.18a)$$

$$H_{0,0} = 2 / (R_{max} + R_{min}) \quad . \quad (3.18b)$$

$$H_{+1,0} = \frac{2}{\pi} \frac{R_{max} - R_{min}}{R_{max} + R_{min}} \quad . \quad (3.18c)$$

$$\epsilon = - \frac{(R_{max} - R_{min})^2}{\pi^2 R_{max} R_{min}} \quad . \quad (3.19)$$

$$L_{opt} = \frac{\sqrt{1 - \epsilon} + 1}{\sqrt{1 - \epsilon} - 1} \quad . \quad (3.20)$$

$$R_{s,opt} = H_{+1,+1} \sqrt{1 - \epsilon} \quad . \quad (3.21)$$

$$R_{o,opt} = 1 / (H_{0,0} \sqrt{1 - \epsilon}) \quad . \quad (3.22)$$

The optimum source and output resistances $R_{s,opt}$ and $R_{o,opt}$, are calculated from Eqs. (A1.36) and (A1.37). The above equations are plotted in Figs. 3.8 and 3.9 as functions of R_{min}/R_{max}.

If $R_{min} \ll R_{max}$ it follows that

$$L_{opt} \approx 1 + 2\pi \sqrt{R_{min} / R_{max}}$$

$$\approx 27.3 \sqrt{R_{min} / R_{max}} \text{ db} \quad . \quad (3.23)$$

$$R_{s,opt} \approx \frac{2}{\pi} \sqrt{R_{max} R_{min}} \quad . \quad (3.24)$$

$$R_{o,opt} \approx \frac{\pi}{2} \sqrt{R_{max} R_{min}} \quad . \quad (3.25)$$

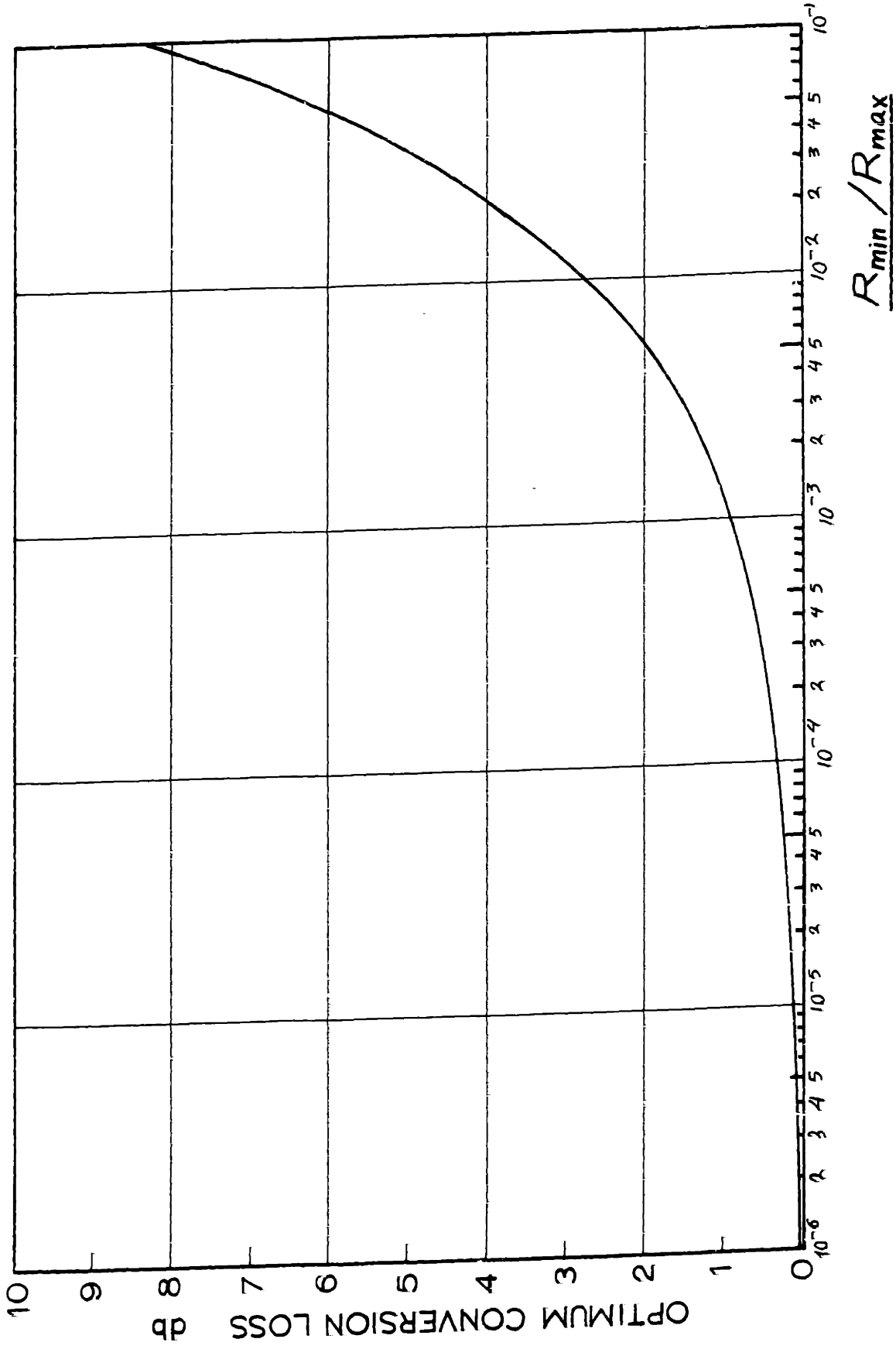

Fig. 3.8. The Fundamental Limit on L_{opt} for the H- or G-Mixers

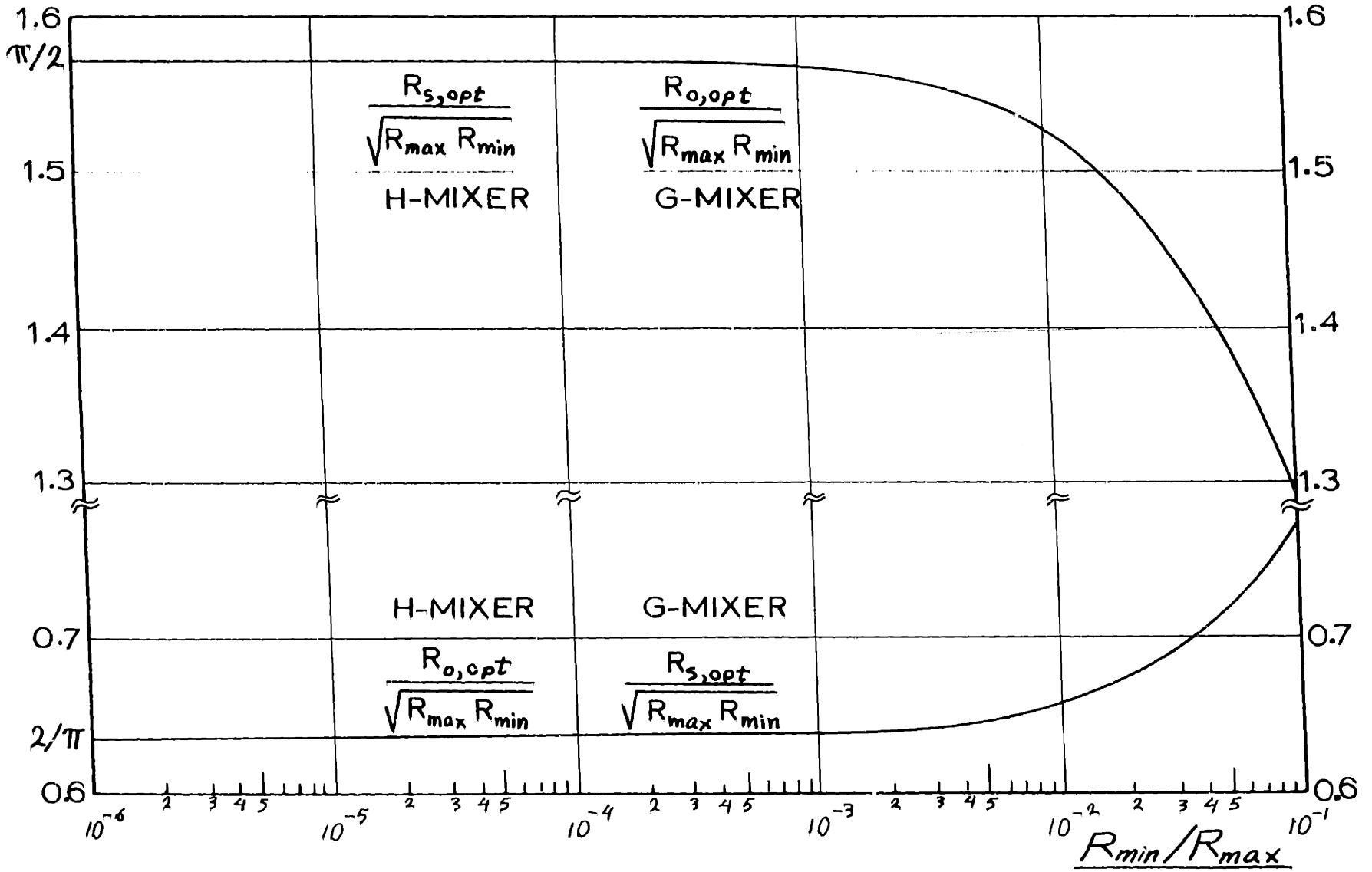

Fig. 3.9. The Optimum Source and Output Resistances for Optimally Driven H- or G-Mixers

If $R_{min} / R_{max} = 0$, then $L_{opt} = 1$ (zero db). In this case the source and output resistances are both either zero or infinity unless $R_{max} = \infty$ and $R_{min} = 0$, i.e. r(t) is an ideal switch**.

For the G-mixer L_{opt} is identical to that of the H-mixer. The rest of the mixer parameters are the duals of the corresponding ones in the H-mixer.

Comparing Figs. 3.4 and 3.8 or Eqs. (3.12) and (3.24) for a given value of R_{min}/R_{max} one notes that L_{opt} for the H- or G-mixers is less than that for the Z- or Y-mixers. Further, with the help of Sec. A1.5 it follows that the conversion loss of the former types of mixers is less sensitive to variations of the source impedance than that of the latter types.

3.2.3. The H_N- and G_N-mixers:

We start by optimizing r(t), $0 \leq R_{min} \leq r(t) \leq R_{max} \leq \infty$, for the H_N-mixer, Figs. 2.15. The corresponding analysis for the G_N-mixer, Fig. 2.16 will be deduced by duality.

Referring to the H-matrix equation of the H_N-mixer, Eq. (2.41), and to Eqs. (A1.32) and (A1.33) the optimum conversion loss can be written as

$$L_{opt} = \frac{\sqrt{1 - \epsilon_N} + 1}{\sqrt{1 - \epsilon_N} - 1} \qquad (3.26)$$

with

$$\epsilon_N = - \frac{|H_{+1,0}|^2}{H_{+1,+1} H_{0,0}} \qquad (\leq 0) \qquad . \quad (3.27)$$

** See for example Appendix 11.

The optimum r(t) to minimize L_{opt} must maximize $|\epsilon_N|$. It is found in Sec. A4.3 that for any value of R_{max}/R_{min}, $N = 2,3$ or 4; or for a sufficiently large value** of R_{max}/R_{min}, $N \geq 5$, the optimum r(t) is given by

$$r(t) = R_{max} \qquad |t| \leq \pi/N\omega_p$$
$$= R_{min} \qquad \pi/N\omega_p \leq t \leq (2 - \tfrac{1}{N})\ \pi/\omega_p \quad . \quad (3.28)$$

That is to say, the optimum r(t) for the H_N-mixer is a rectangular-pulse waveform switching between R_{max} and R_{min} with a pulse duty ratio P = 1/N; where P is defined as the ratio of the time where r(t) attains its maximum value R_{max} to the total period $2\pi/\omega_p$. For the G_N-mixer, the optimum conductance waveform g(t) is given by the dual of Eq. (3.28). In this case P= 1/N still, but P is defined here as the ratio of the time where g(t) attains its maximum value $G_{max}(=1/R_{min})$ to the total period $2\pi/\omega_p$.

The corresponding ϵ_N for the H_N- or G_N-mixers is given by

$$\epsilon_N = - \frac{\sin^2(\pi/N) \cdot (R_{max}/R_{min} - 1) / \pi}{2\pi/N + \pi/(R_{max}/R_{min} - 1)} \quad . \quad (3.29)$$

This is plotted versus N for a given value of R_{max}/R_{min}

** $R_{max}/R_{min} \geq N\,[\cos(2\pi/N)+1]\cos(2\pi/N) + 1$. For $N \to \infty$, H_N-mixer $\to$ Z-mixer, Eq. (3.28) is only valid if $R_{max}/R_{min} \to \infty$. See Sec. A4.3 for more details.

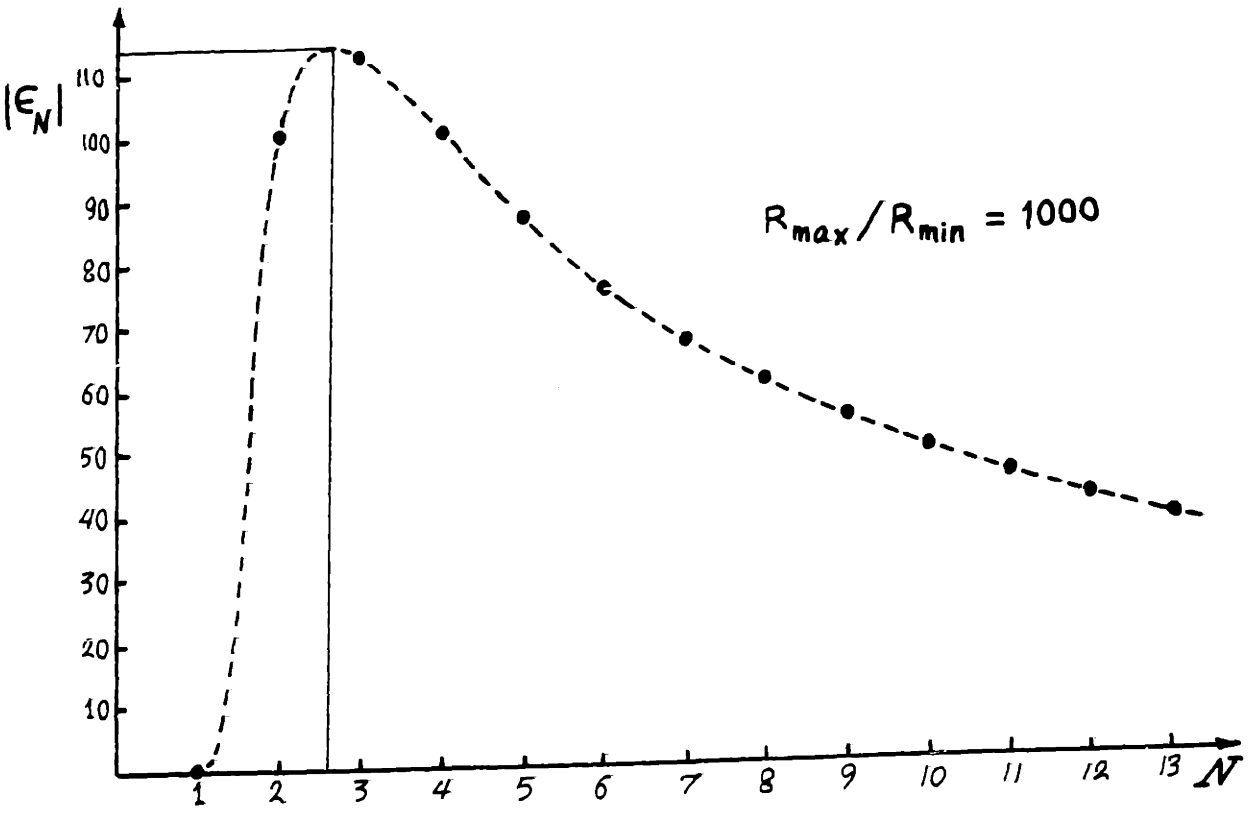

Fig. 3.10. A Typical $|\epsilon_N|$ vs. N Plot

(= 1000) in Fig. 3.10. It is interesting to note that the curve has one peak between N= 2 and 3.** Manipulating Eq. (3.29) shows that if $R_{max}/R_{min} < 4$, then H_2- and G_2-mixers (i.e. the H- and G-mixers) are superior to any other H_N- or G_N-mixer, however, if $R_{max}/R_{min} > 4$, the H_3- and G_3-mixers are the superior ones. The conversion loss is plotted in Fig. 3.11 for several H_N- and G_N-mixers as a function of R_{min}/R_{max}.

If $R_{min} \ll R_{max}$ it follows that

$$\epsilon_N \approx - N \frac{\sin^2(\pi/N)}{2\pi^2} \quad \frac{R_{max}}{R_{min}} \qquad , (3.30)$$

** For $R_{min} \ll R_{max}$ the peak occurs at N ≈ 2.7.

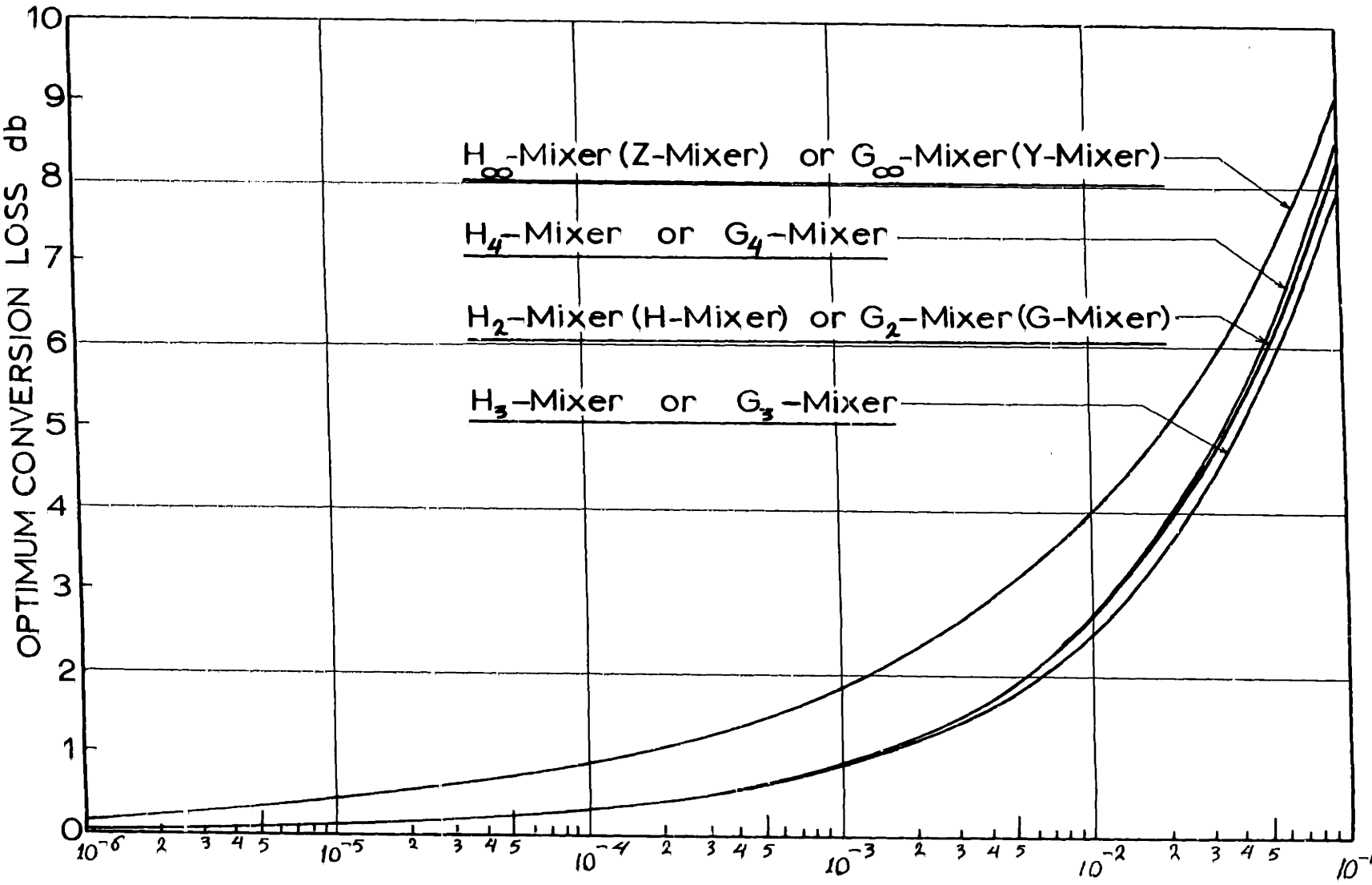

Fig. 3.11. Fundamental Limits on L_{opt} for Different H_N- and G_N-Mixers

and the corresponding conversion loss

$$L_N \approx 1 + \frac{2\sqrt{2}\,\pi}{\sqrt{N}\,\sin(\pi/N)}\sqrt{R_{min}/R_{max}}$$

$$\approx A_N \sqrt{R_{min}/R_{max}} \quad \text{db}, \tag{3.31}$$

where $A_N = 4.343 \times 2\sqrt{2/N}\,\pi/\sin(\pi/N)$ is given in Table 3.1.

Table 3.1. The Value of A_N for Eq. (3.31)

N	A_N	N	A_N
2	27.3	7	33.6
3	25.7	8	35.7
4	27.3	9	37.6
5	29.4	10	39.5
6	31.5	N>>	$\approx 12.3\sqrt{N}$

The corresponding optimum source and output resistances for the H_N-mixer are given by

$$R_{s,opt} \approx \sqrt{2/N}\,\frac{\sin(\pi/N)}{\pi/N}\sqrt{R_{max}\,R_{min}}, \tag{3.32}$$

and

$$R_{o,opt} \approx \sqrt{2/N}\,\frac{\pi/N}{\sin(\pi/N)}\sqrt{R_{max}\,R_{min}}. \tag{3.33}$$

The dual relations hold for the G_N-mixer.

If $R_{min}/R_{max} = 0$, then $L_{opt} = 1$ (zero db). In this case the source and output resistances are both zero or infinity unless $R_{max} = \infty$ and $R_{min} = 0$, i.e. r(t) is an ideal switch.

3.3. Question 2: The Optimum Imbedding Network

> "Given a nonnegative resistance that varies periodically in a prescribed waveform: What is the corresponding optimum imbedding network that leads to the best possible mixer conversion loss?"

Before dealing with this question we give a general discussion of the necessary types of terminations that should be offered to the out-of-band frequencies. Next we find the optimum imbedding network for sinusoidal, square-wave and rectangular-pulse resistance waveforms. No general technique could be developed to deal with a general resistance waveform.**

3.3.1. General properties of the optimum imbedding network:

> Theorem: The optimum passive imbedding network for a mixer with a nonnegative time-varying resistance is lossless; i.e., the out-of-band frequencies should be terminated reactively.

This theorem, as obvious as it might seem, is proven in Sec. A5.1. From the proof it is clear that the theorem is also valid for any unconditionally stable time-varying element (for example a nonnegative time-varying resistance with fixed parasitic reactances). Note that the theorem does not state that any lossless imbedding

** Penfield and Rafuse (I, Secs. 5.6 and 6.4.2) developed a technique to find the fundamental limit on the performance of parametric devices with arbitrary capacitance waveform. However, their technique could not be applied to resistive devices since it produces a nonstationary problem.

network is superior to any lossy one; in fact this is not generally true.

If the time origin can be chosen to make the resistance waveform an even function of time, it seems that a property, much stronger than that given in the above theorem, holds true. We put it here as a hypothesis since it could not be fully proven.

> Hypothesis: The optimum passive imbedding network for a mixer with a nonnegative time-varying resistance should offer either an open-circuit or a short-circuit to each of the out-of-band frequencies if the time origin can be chosen to make the resistance waveform an even function of time.

In Sec. A5.2 we present an argument that supports, but not fully proves, this hypothesis.

3.3.2. Sinusoidal resistance and conductance waveforms:

Here we find the best possible imbedding network for the nonnegative resistance waveform

$$r(t) = r_o + 2r_1 \cos(\omega_p t), \quad \left\{ \begin{matrix} r_o > 0 \text{ and} \\ |r_1| \leq r_o/2 \end{matrix} \right\} \quad , \quad (3.34)$$

and the conductance waveform

$$g(t) = g_o + 2g_1 \cos(\omega_p t), \quad \left\{ \begin{matrix} g_o > 0 \text{ and} \\ |g_1| \leq r_o/2 \end{matrix} \right\} \quad , \quad (3.35)$$

which is the dual case.** Throughout the analysis we assume that the time origin was chosen to make r_1 and g_1 positive.

** The sinusoidal conductance waveform can be obtained in practice by pumping an exponential diode, $i=I_{sat}[\exp(\alpha v)-1]$, by a sinusoidal current waveform.

First assume that we use the sinusoidal resistance waveform, Eq. (3.34), to convert power from the input signal frequency, $\omega_{+1} = \omega_p + \omega_o$, to the output frequency, ω_o. The frequency domain representation** is given in terms of a real symmetric tridiagonal infinite Z-matrix as

$$\begin{bmatrix} \vdots \\ V_{+2} \\ V_{+1} \\ V_o \\ V_{-1} \\ \vdots \end{bmatrix} = \begin{bmatrix} \ddots & \ddots & & & & \\ & r_o & r_1 & & \bigcirc & \\ & r_1 & r_o & r_1 & & \\ & & r_1 & r_o & r_1 & \\ & \bigcirc & & r_1 & r_o & \ddots \\ & & & & \ddots & \ddots \end{bmatrix} \begin{bmatrix} \vdots \\ I_{+2} \\ I_{+1} \\ I_o \\ I_{-1} \\ \vdots \end{bmatrix} \quad (3.36)$$

Since r(t) is an even function of time, it follows from the hypothesis given in Sec. 3.3.1 that the optimum imbedding network must present either a short-circuit or an open-circuit to each of the out-of-band frequencies, ω_n, $n \neq 1$ or 0. Thus, to obtain the optimum network we can start with a Z-mixer, which open circuits all the out-of-band frequencies, and then find the required short circuit current idlers*** to minimize the conversion loss. The only idlers that can affect the mixer operation are those for

** See Sec. A3.1.
*** See Sec. 2.2.2.

frequencies occuring in a <u>continuous sequence</u> next to ω_{+1} and ω_o. This follows because the Z-matrix of Eq.(3.36) is tridiagonal and if any frequency (ω_m say) is open-circuited, (i.e. not provided with an idler) the frequencies lying above it (ω_n, $n > m$) will be decoupled from those lying below it (ω_n, $n < m$). With this in mind, the Z-mixer considered will be equipped with the following short-circuit current idlers:

1. <u>Group of ℓ idlers</u> for frequencies $\omega_{+2}, \omega_{+3}, \ldots, \omega_{\ell+1}$.
2. <u>Group of k idlers</u> of frequencies $\omega_{-1}, \omega_{-2}, \ldots, \omega_{-k}$.
3. <u>No idlers</u> for $\omega_{\ell+2}$ and ω_{-k-1}.
4. <u>Irrelevant idlers</u> for any ω_n, $n > \ell+2$, or $n < -k-1$.

This is shown in Fig. 3.12. The problem now is to find the numbers ℓ and k of the idler circuits to minimize the conversion loss.

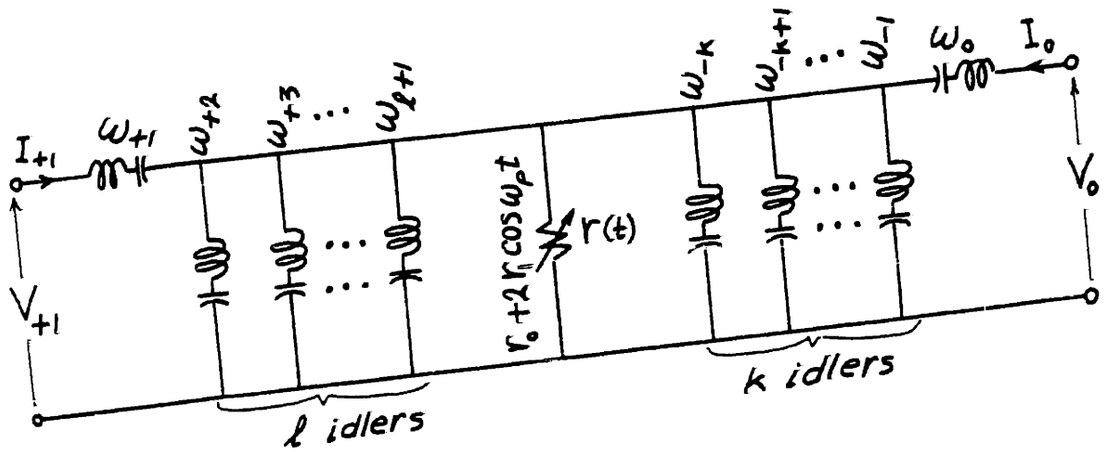

Fig. 3.12. Z-Mixer with Idlers for the Sinusoidal r(t)

It is rigorously shown in Secs. A6.1 and A6.2 that for the passive case, $r_1/r_o \leq 0.5$, the two-port Z-matrix representation of the above mixer is given by

$$\begin{bmatrix} V_{+1} \\ \\ V_o \end{bmatrix} = r_1 \begin{bmatrix} \dfrac{\sinh[(\ell+2)\alpha]}{\sinh[(\ell+1)\alpha]} & 1 \\ \\ 1 & \dfrac{\sinh[(k+2)\alpha]}{\sinh[(k+1)\alpha]} \end{bmatrix} \begin{bmatrix} I_{+1} \\ \\ I_o \end{bmatrix} \quad . (3.37)$$

where

$$\cosh \alpha = r_o/2r_1 \geq 1 \quad . (3.38)$$

The optimum conversion loss of the mixer is given from Eqs. (A1.35) and A1.38) as

$$L_{opt} = \frac{1 + \sqrt{1 - \epsilon}}{1 - \sqrt{1 - \epsilon}} \quad , (3.39)$$

where

$$\epsilon = \frac{\sinh[(\ell+1)\alpha] \sinh[(k+1)\alpha]}{\sinh[(\ell+2)\alpha] \sinh[(k+2)\alpha]} \quad (\leq 1) \ . \ (3.40)$$

Clearly ϵ is a monotonically increasing function of ℓ and k and hence L_{opt} is a monotonically decreasing function of ℓ and k. Thus the optimum imbedding network should have $\ell = k = \infty$. That is to say, the optimum imbedding network is a Z-mixer equipped with an infinite number of short circuit current idlers at all the out-of-band frequencies, which is, of course, a Y-mixer**. The entries of the Z-matrix of the

** See Sec. 2.2.2.

optimum imbedding network can be found from Eqs. (3.37) and (3.38) in the limit when ℓ and k approach infinity. They are given by

$$Z_{11} = Z_{22} = r_1 e^{\alpha}$$

$$= \frac{r_o}{2}\left[1 + \sqrt{1 - \left(\frac{2r_1}{r_o}\right)^2} \right] \quad , (3.41)$$

and

$$Z_{12} = Z_{21} = r_1 \quad . (3.42)$$

Thus

$$\epsilon = \left[\frac{r_o}{2r_1} - \sqrt{\left(\frac{r_o}{2r_1}\right)^2 - 1} \right]^2 \quad . (3.43)$$

The corresponding optimum source and output resistances are given from Eqs. (A1.36) and (A1.37) as

$$R_{s,opt} = R_{o,opt} = Z_{11}\sqrt{1 - \epsilon} \quad . (3.44)$$

The optimum conversion loss and source and output resistances of the optimum imbedding network are plotted in Fig. 3.13 as functions of the ratio $2r_1 / r_o$.

It is interesting to find the asymptotic behavior of the optimum imbedding network as $2 r_1 \approx r_o$. In this case we define the maximum and minimum values of r(t) as

$$R_{max} = r_o + 2r_1 \quad (3.45)$$

and

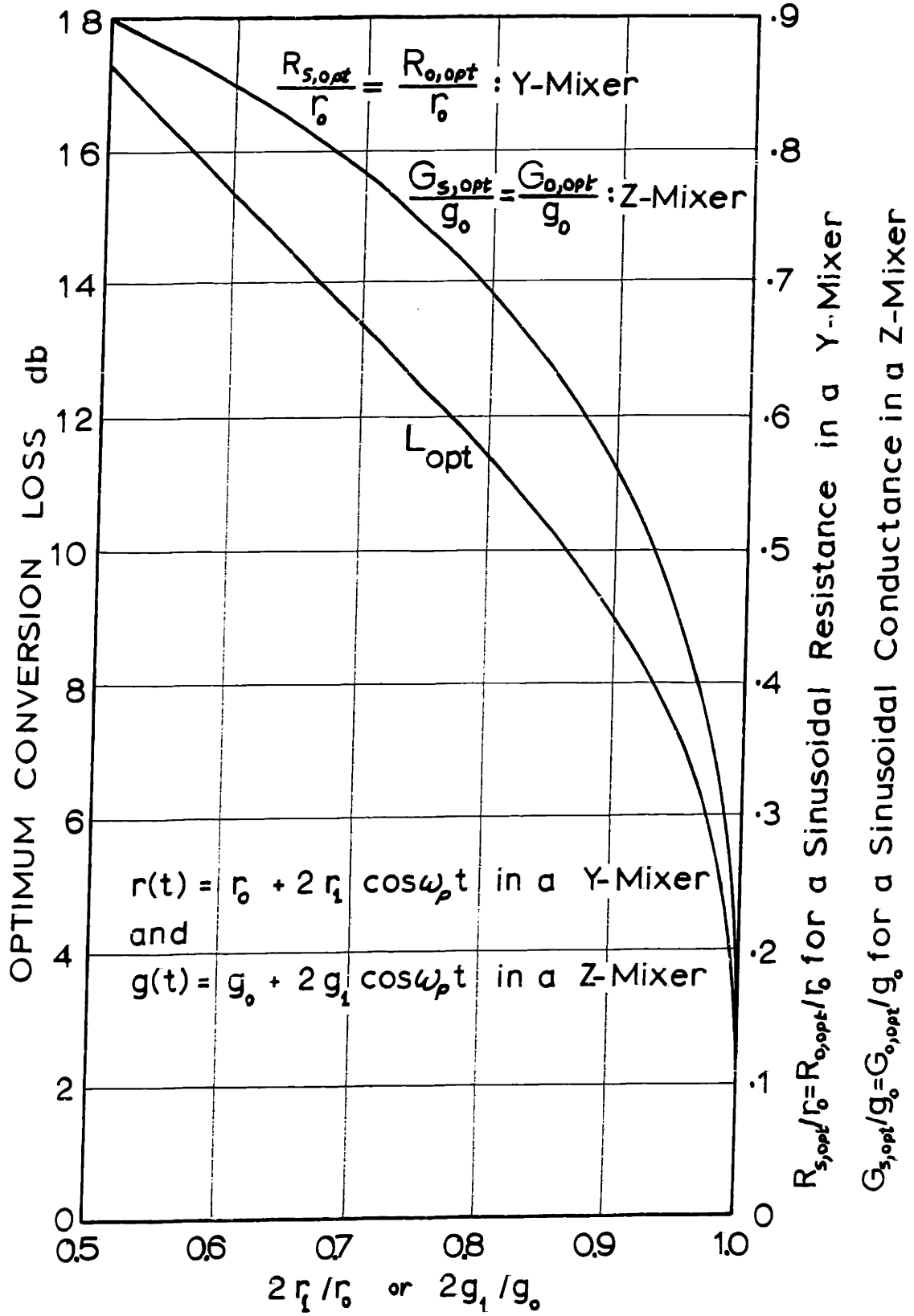

Fig. 3.13. The Performance of the Optimum Imbedding Network for a Sinusoidal Resistance or Conductance Waveform

$$R_{min} = r_o - 2r_1 \quad ; (3.46)$$

note that $R_{min} << R_{max}$. Substituting the above equations in Eqs. (3.43) and (3.39) we get

$$L_{opt} \approx 1 + 4 (R_{min}/ R_{max})^{1/4}$$

$$\approx 17.4 (R_{min}/ R_{max})^{1/4} \quad db \quad . (3.47)$$

By duality, the optimum imbedding network for the sinusoidal conductance waveform of Eq. (3.35) is a Z-mixer. The corresponding mixer parameters are the duals of the above equations and are plotted in Fig. 3.13 as functions of the ratio $2g_1/g_o$.

3.3.3. Square-wave resistance or conductance:

Here we find the best possible imbedding network for the nonnegative square-wave resistance (or conductance).

$$r(t) = r(t + 2\pi/\omega_p) = R_{max} \qquad |t| \leq \pi/2\omega_p$$

$$= R_{min} \quad \pi/2\omega_p \leq t \leq 3\pi/2\omega_p \quad , (3.48)$$

where $R_{max} > R_{min} \geq 0$. This is plotted in Fig. 3.7.

Analyzing this problem in the same manner as that used in the previous section for the sinusoidal resistance waveform does not seem possible. There, the simplicity of the Z-matrix associated with r(t), Eq. (3.36), enabled us

to find the optimum conversion loss of a mixer for any specifications of the open-circuited and short-circuited out-of-band frequencies. This result could not be achieved for any other resistance or conductance waveform and a different technique had to be employed here.

In Sec. 3.2.2 we proved that the optimum resistance waveform for the H- or G-mixers is a square wave. It seems that the converse is also true. That is to say the optimum imbedding network for a square-wave resistance is an H- or a G-mixer. A rigorous proof of this point seems very complicated. Instead, we give an analysis that strongly supports this expectation.

We start with an H-mixer which short-circuits the even-order out-of-band frequencies and open-circuits the odd-order out-of-band frequencies, and then we find the effect of changing the status of any out-of-band frequency from open to short circuit or vice versa.** Two of such modified H-mixers are given in Fig. 3.14. In the first one, Fig. a, we changed the termination of one odd-order out-of-band frequency; ω_k, k odd ($\neq 1$); from an open to a short. It is proven in Sec. A6.3 that the performance of such a mixer is inferior to that of a standard H-mixer for any odd k and for any values of R_{min} and R_{max}. It is also shown there that the optimum

** Each out-of-band frequency is restricted to have one of two states, open or short circuit, because of the hypothesis of Sec. 3.3.1 and the fact that r(t) is an even function of time.

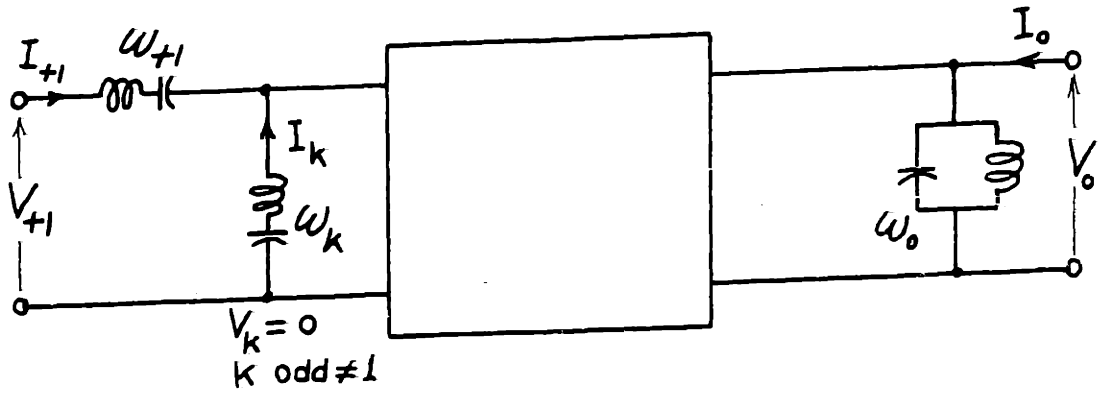

a). Changing the status of one frequency

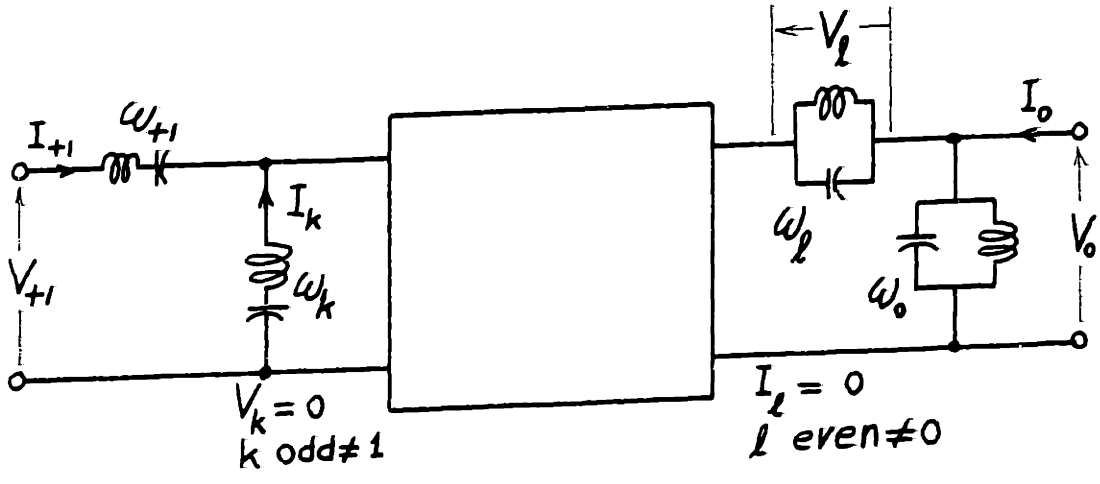

b). Changing the status of two frequencies at opposite sides

Fig. 3.14. Two Modified H-Mixers (The network inside the square represents any circuit in Fig. 2.6)

conversion loss for this mixer does <u>not</u> approach unity as $R_{min}/R_{max} \rightarrow 0$, while, of course, the standard H-mixer does**. By duality and reciprocity it can be shown that we would get exactly the same results obtained for the mixer of Fig. 3.14a for a given odd k if we, instead, changed the status of the even-order out-of-band frequency ω_{1-k}. Thus it appears that changing the status of only one frequency deteriorates the performance of the mixer considerably.

In fact it can be shown generally that if the status of any number of even-order frequencies is changed, then the status of the <u>same</u> number of any odd-order frequencies should be changed otherwise the conversion loss of the mixer will not approach unity as $R_{min}/R_{max} \rightarrow 0$***. This point, of course, does <u>not</u> guarantee rigorously that the standard H-mixer will be superior to that of any modified H-mixer for all values of R_{min} and R_{max} if the above restriction is not met. However, it is clear, at least for $R_{min}/R_{max} \ll 1$, that in finding the optimum imbedding network for the square-wave resistance one should only consider modified H-mixers which obey the aforementioned restriction. The simplest of such modified mixers is the one given in Fig. 3.14b where we changed

** See for example Eqs. (3.23) or Fig. 3.8.

*** See for example Sec. A11.5

the status of one odd-order frequency; ω_k, k odd $\neq 1$; and one even-order frequency; ω_ℓ, ℓ even $\neq 0$. It is shown in Sec. A6.3 that even though the conversion loss of this mixer approaches unity as $R_{min}/R_{max} \rightarrow 0$, it is inferior to the standard H-mixer for any odd k and even ℓ and for all values of R_{min} and R_{max}. It is expected that extending the analysis to modified H-mixers with any finite number of idlers will lead to the same conclusions.

From the above it seems reasonable to conclude that the optimum imbedding network for a square-wave resistance is an H-mixer. Of course, by duality, the G-mixer too will be an optimum imbedding network. The relevant parameters of the two types of mixers with a square-wave resistance were plotted previously in Figs. 3.8 and 3.9.

3.3.4. Rectangular-pulse resistance and conductance waveforms:

Let r(t) be a rectangular-pulse waveform switching between R_{max} and R_{min} with a pulse duty ratio P = 1/N, as given in Eq. 3.28. One can use the same procedure given in the previous section to show that the optimum imbedding network associated with this resistance is an H_N-mixer. Of course, the dual resistance waveform gives a G_N-mixer.

3.4. Question 3: The Optimum Mixer

"Given a resistance that can be varied periodically in any desired fashion bounded by specified maximum and minimum values: What is the corresponding best possible mixer conversion loss?"

In the following we answer the above question and extend the analysis to include parasitic elements.

3.4.1. Fundamental limit on the conversion loss:

Of all the resistance waveforms $R_{min} \leq r(t) \leq R_{max}$, and imbedding networks discussed in Secs. 3.2 and 3.3, the H_3- and G_3-mixers gave the best conversion loss. For $R_{min} \ll R_{max}$ this was approximately given by

$$L_{opt} \approx 1 + 5.92 \sqrt{R_{min}/R_{max}}$$

$$\approx 25.7 \sqrt{R_{min}/R_{max}} \quad \text{db} \qquad . \quad (3.49)$$

This was followed by the H- and G-mixers which gave

$$L_{opt} \approx 1 + 6.28 \sqrt{R_{min}/R_{max}}$$

$$\approx 27.3 \sqrt{R_{min}/R_{max}} \quad \text{db} \qquad . \quad (3.50)$$

We now find a fundamental limit on the conversion loss given $R_{min} \leq r(t) \leq R_{max}$ and show that the above values are very close to this limit.

From the results of Secs. 3.2 and 3.3 we note that the optimum resistance waveforms assumed only their extremum

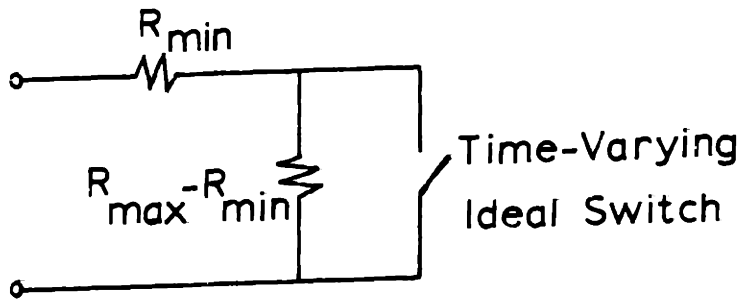

Fig. 3.15. A Model for Optimum Resistance Waveforms

values, R_{min} and R_{max}, during their cycles. A model that yields these types of waveforms is shown in Fig. 3.15. If we apply this model to any mixer and neglect the losses in all the frequencies other than the input signal frequency ω_s and the output (i-f) frequency ω_o, we obtain the circuit of Fig. 3.16. The transformer turns ratio "n" represents the appropriate impedance transformation caused by the ideal-switch mixer.

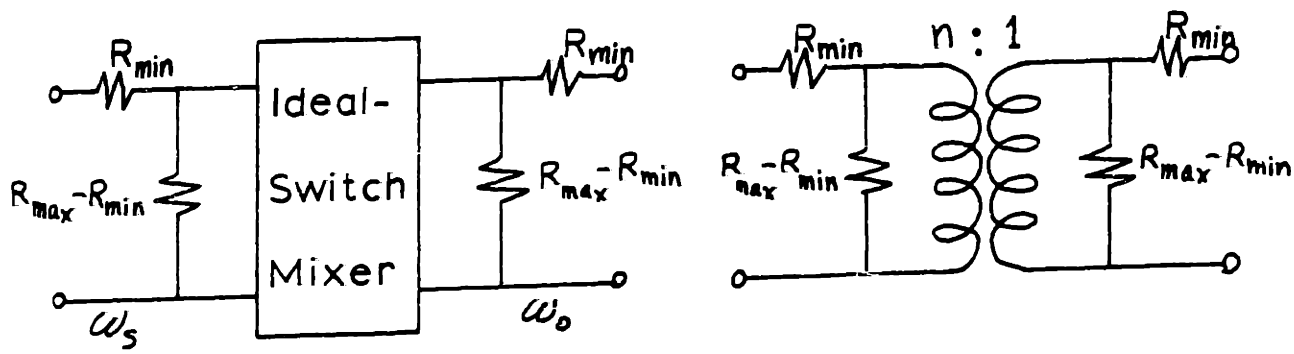

Fig. 3.16. An Optimum Mixer

The optimum conversion loss of the above circuit can be obtained by calculating its Z matrix and using Eqs. (A1.35) and (A1.38) which yields

$$L_{opt} = \frac{1 + \sqrt{1-\epsilon}}{1 - \sqrt{1-\epsilon}} \quad , \quad (3.51)$$

with

$$\epsilon = \frac{n^2 \left[R_{max} - R_{min}\right]^2}{\left[n^2 R_{max} + R_{min}\right]\left[R_{max} + n^2 R_{min}\right]} \quad (\leq 1) \quad . \quad (3.52)$$

Since we are after a fundamental limit we choose the value of n to maximize ϵ and hence minimize L_{opt}. This value is easily found to be n= 1. Substituting in Eqs. (3.52) and (3.51) and assuming $R_{min} \ll R_{max}$ we get the desired fundamental limit

$$L_{opt} \approx 1 + 4\sqrt{R_{min}/R_{max}}$$

$$\approx 17.4\sqrt{R_{min}/R_{max}} \quad \text{db} \quad . \quad (3.53)$$

3.4.2. Effect of junction capacitance and series resistance:

If R_{min}/R_{max} approaches zero the conversion loss in the above equation approaches unity. This can be achieved by a strongly pumped diode. However, in practice, the diode junction capacitance, C, and series resistance, R_s, will prevent the conversion loss from reaching unity. Here we calculate the fundamental limit on the conversion loss set by these parasitic elements.

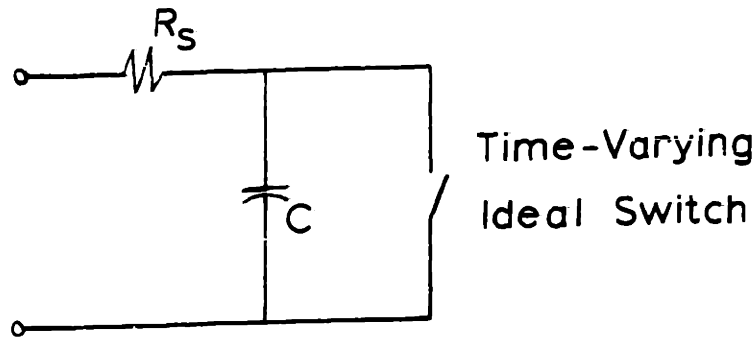

Fig. 3.17. A Strongly Pumped Diode Model

A strongly pumped diode can be represented by the model in Fig. 3.17. This model is applicable for any diode with negligible charge storage in the forward region such as a Schottky-barrier diode. Following the same argument as that in the previous section, the above model gives the mixer circuit of Fig. 3.18 where we assumed that the mixer provides 1:1 impedance transformation. The capacitance on the output (i-f) side was neglected in the final model assuming that $\omega_o \ll \omega_s$. The calculations involved in the model should be performed at the signal frequency ω_s.

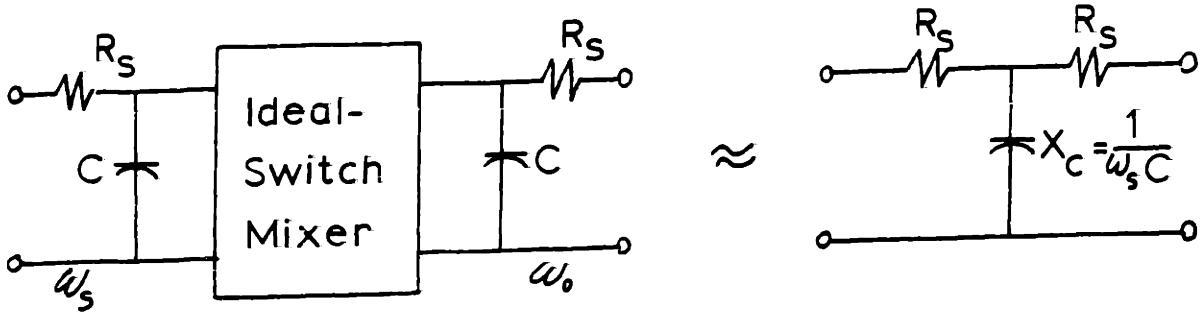

Fig. 3.18. Mixer with Parasitics

The optimum conversion loss of the above circuit can be found to be

$$L_{opt} = 1 + 2\left(\frac{\omega_s}{\omega_c}\right)^2 \left[1 + \sqrt{1 + \left(\frac{\omega_c}{\omega_s}\right)^2}\right] \quad (3.54)$$

where ω_c is the cut-off frequency given by

$$\omega_c = \frac{1}{R_s C} \quad . \quad (3.55)$$

This is the desired fundamental limit. The value of L_{opt} is approximately the same as that obtained by Rafuse**, who analyzed a strongly driven H-mixer with parasitics.

If $\omega_c \ll \omega_s$, Eq. (3.54) is approximated by

$$L_{opt} \approx 1 + 2\,\omega_s/\omega_c$$

$$\approx 8.69\,\omega_s/\omega_c \quad \text{db} \quad . \quad (3.56)$$

** Rafuse (I).

3.5. Conclusions and Topics for Further Research

In this chapter we raised three basic questions concerning fundamental limits on the performance of resistive mixers. 1) What is the optimum r(t) for a given imbedding network if $R_{min} \leq r(t) \leq R_{max}$? 2) What is the optimum imbedding network for a given nonnegative r(t)? 3) Given the maximum and minimum possible values of r(t), what is the optimum r(t) and imbedding network? In other words what is the world's best mixer? In all these questions "optimum" refers to the best possible mixer conversion loss.

In answering Question 1, Sec. 3.2, we showed that the optimum resistance waveforms for all the mixer imbedding networks discussed in Chapter 2 are rectangular-pulse waveforms switching between R_{max} and R_{min} with the appropriate pulse duty ratio. No general proof was given to show whether or not this is true for all imbedding networks. For a Z- and a Y-mixer the optimum pulse duty ratio [Eqs. (3.10) and (3.11)] was dependent on R_{max} and R_{min}. The H- and G-mixers, however, required a pulse duty ratio of $\frac{1}{2}$ independent of R_{max} and R_{min}. Generally, for H_N- (G_N-) mixers the optimum pulse duty ratio of the resistance (conductance) waveform was found to be 1/N. This holds true independent of R_{max} and R_{min}; N = 2,3 or 4. For $N \geq 5$ on the other hand, this requires that $R_{max} >> R_{min}$,

in particular the ratio R_{max}/R_{min} should satisfy condition (A4.23).

Comparing the Z- or Y-mixer with the H- or G-mixer for any R_{max} and R_{min}, the above mentioned analysis showed that the latter type of mixers are superior to the former ones for the following reasons:

i) For $R_{max} >> R_{min}$, the optimum conversion loss for the Z- or Y-mixer is given by $L_{opt} \approx 18.3(R_{min}/R_{max})^{1/3}$ db, while that of the H- or G-mixer is $L_{opt} \approx 27.3\ (R_{min}/R_{max})^{\frac{1}{2}}$ db.

ii) The optimum pulse duty ratio for the Z- or Y-mixer is dependent on the values of R_{max} and R_{min} while that for the H- or G-mixer is $\frac{1}{2}$ for any R_{max} and R_{min}.

iii) For $R_{max} >> R_{min}$, the optimum resistance waveform for the Z- or Y-mixer consists of very narrow pulses and hence requires a very broadband pumping circuit which is hard, if not impossible, to realize in practice; on the other hand that for the H- or G-mixer is a square-wave which can be achieved much easier.

Also, of all the Z-, Y-, H-, G-, H_N- and G_N-mixers; the H_3- and G_3-mixers gave the best conversion loss [$L_{opt} \approx 25.7\ (R_{max}/R_{min})^{\frac{1}{2}}$ db, if $R_{max} >> R_{min}$]. This, of course, does not differ much from the optimum conversion loss of the H- and G-mixers. Thus, because of the complexity of the H_3- and G_3-mixers, the H- and G-mixers seem to

be very attractive.

An extremely interesting result, that might have a direct application for Question 1, was observed from some of the results of Chapter 4 (See Secs. 4.2.1 and 4.2.3) and Appendix 10 (See Sec. A10.4). In many single-diode mixers with idealized diode characteristics, the pumped diode resistance waveform was found to be identical to the required optimum resistance waveform deduced in the present chapter, or to approach it as the pumping level increases without limits. Whether or not a general theorem concerning this property can be proven is not clear.

In answering Question 2, Sec. 3.3, we proved that for any nonnegative r(t), the optimum imbedding network is lossless, i.e. the out-of-band frequency should be terminated reactively. Further we stated in an unproven hypothesis that if the time origin can be chosen to make r(t) an even function of time, the optimum imbedding network should offer an open- or a short-circuit to each of the out-of-band frequencies. The hypothesis and possible procedures that might lead to its proof or disproof are discussed in Appendix 5. This problem requires further investigation.

Considering specific resistance waveforms and assuming that the aforementioned hypothesis is true we obtained several interesting results. For a sinusoidal

resistance (conductance) waveform, the optimum imbedding network was found to be a Y- (Z-) mixer. For a square-wave resistance it was shown by starting with an H- or a G-mixer and perturbing the status of one or two frequencies from open to short or vice versa that the standard H- and G-mixers gave the best conversion loss. Thus it seems that both of these two mixers are optimum imbedding networks for the square-wave resistance. More general analysis is needed to make this result more rigorous. Further, employing the same technique, it was deduced that the optimum imbedding network for a rectangular-pulse resistance (conductance) waveform with a pulse duty ratio 1/N is the H_N- (G_N) mixer.

Question 2 leaves us with many interesting unanswered problems which need further attention. Beside the ones discussed above we mention the following:

i) Given any r(t), is there a general procedure to deduce **the** optimum imbedding network, or at least to find a tight bound for the optimum mixer conversion loss?

ii) Perhaps it can be proven that if r(t) does not attain the values of zero and/or infinity during its cycle, then the optimum conversion loss does not reach unity (zero db). However, if any r(t) attains either or both of these limits, does there always exist an associated imbedding network which produces a mixer with a conversion loss of

unity?

In attempting to answer Question 3, Sec. 3.4, we showed by a heuristic argument that if the resistance waveform is restricted to lie between two given nonnegative values, R_{max} and R_{min}, then the best possible mixer conversion loss is $L_{opt} \approx 17.4\ (R_{min}/R_{max})^{\frac{1}{2}}$ db. However, we did not show whether or not this limit can indeed be attained by any combination of r(t) and imbedding network. As mentioned above, the analysis of Sec. 3.2 showed that the best mixer which comes close to the above limit is the H_3- (G_3-) mixer with a rectangular-pulse resistance (conductance) waveform with pulse duty ratio = 1/3. Of course whether or not the H_3- and G_3- mixers are the world's best mixers is still an open question.

There are many problems based on imperfections in trying to realize the optimum mixer which are answered in the appendices.

i) In Appendix 1, where a general analysis of two-port networks is given, the problem of not providing the mixer with its optimum source impedance was treated, Sec. A1.5. It was shown that by the knowledge of L_{opt} and $Z_{s,opt}$ only, one can find the mixer performance for any source impedance. Further, it was deduced that the nearer L_{opt} is to unity, the less sensitive the conversion loss is to source impedance variations.

ii) In Appendix 8 a general study of Y-mixers with narrow-pulse conductance waveforms is given. The results can, of course, be applied to Z-mixers by duality. The study gave a procedure to find the sensitivity of the conversion loss to the exact shape of the conductance waveform.

iii) In Appendix 10 the problem of incomplete termination of the out-of-band frequencies in a Y-mixer was studied. One can use duality to apply the results to Z-mixers. Further, in Appendix 11, Sec. A11.6 the same problem in square-wave driven H- and G-mixers was analyzed.

In practice, especially at high frequencies, a pure resistive waveform cannot be achieved. For example the values of the junction capacitance, C, and series resistance, R_s, of a mixer diode are finite and should be taken into account. In Sec. 3.4.2 is given a heuristic analysis to show that the best possible mixer conversion loss with these parasitics is $L_{opt} \approx 8.69\ \omega_s/\omega_c$ db where $\omega_c = 1/(R_s C)$ is the diode cut-off frequency and ω_s is the signal frequency. A more general and rigorous analysis of this problem is needed. For example it is desirable to answer the aforementioned three basic questions for a mixer diode with parasitics.

CHAPTER 4

MIXERS WITH EXPONENTIAL DIODES

4.1. Introduction

In the previous chapters we considered the mixer to consist of one or more linear, positive, periodically-time-varying resistances imbedded in a passive, linear, time-invariant network. The resistance waveforms were assumed to be arbitrary and independent of the imbedding network. In practice, the time-varying resistance is obtained by pumping a nonlinear resistive device with a local oscillator. If the level of the local oscillator is much higher than that of the signal, the signal sees the device as linear, periodically-time-varying resistance.** It is obvious that the resistance waveform will depend on the particular device used, the imbedding network, and the shape and power of the pumping waveform. In this Chapter we obtain the pumped resistance waveforms and find and compare the performances of different important mixers.

The particular nonlinear device which will be dealt with here is the exponential diode since it is one of the most

** This will be assumed to hold in our analysis. Of course, this assumption is only approximate and nonlinear distortion, however small, will exist in the mixer. This problem will not be discussed in this thesis. Numerous studies of the subject in the literature include, Agrowal and Hanson (I), Gretsch (I), Lepoff and Cowley (I), Orloff (I), Rafuse (II), Snyder (I) and Stoodley (I).

important devices used in mixers. The v-i characteristics of an ideal exponential diode assumes the form

$$i = I_{sat}\,(e^{\alpha v} - 1) \qquad . \quad (4.1)$$

The small signal conductance for this diode is given by

$$g = \frac{di}{dv} = \alpha(i + I_{sat}) \approx \alpha i \qquad . \quad (4.2)$$

In the above equations I_{sat} is the diode saturation current and $\alpha = q/kT \approx 40$ volt^{-1} at room temperature. A Schottky-barrier diode is the best known device to exhibit this characteristics over several current decades even at microwave frequencies.** The effects of the diode series resistance, reverse breakdown region and junction capacitance will be neglected in our analysis.

The procedure employed in this chapter for analyzing any mixer circuit consists of two main parts: 1) the large signal analysis, and 2) the small signal analysis. The first part is concerned with the pumping waveform, the pump power, the impedance offered to the pump, and the d-c bias conditions. The second part is concerned with the mixer performance for three image terminations; short-circuit, broadband input*** and open-circuit. This is obtained by calculating the diode resistance, or conductance, waveform and deducing the mixer matrix equation with the help of Chapter 2, then using Appendix 2 to find the performance.

The symbols which will be used throughout this

** See Sze (I, Chapter 8).
*** i.e., Equal termination for both signal and image frequencies.

chapter are listed below:

1. Large Signal Parameters:

v_d: Large signal diode voltage.

i_d: Large signal diode current.

V_{dc}: Diode d-c bias voltage. } Under pump conditions

I_{dc}: Diode d-c bias current. }

V_p: Fundamental component of pump voltage. It will be assumed nonnegative.

I_p: Fundamental component of pump current. It will be assumed nonnegative

$R_p = V_p/I_p$: Resistance offered to the pump.

$G_p = 1/R_p$: Conductance offered to the pump.

$P_p = \frac{1}{2}V_pI_p$: Pump power.

$$x_1 = I_{dc} / \{I_{sat} e^{\alpha V_{dc}}\} ,$$

$$x_2 = \alpha P_p / \{I_{sat} e^{\alpha V_{dc}}\} ,$$

$$x_3 = \alpha P_p / I_{dc} = x_2/x_1 ,$$

} Dimensionless d-c and pump parameters.

2. Small Signal Parameters:

L_n: Optimum conversion loss for case n.

$R_{s,n}$: Optimum source resistance for case n.

$G_{s,n} = 1/R_{s,n}$.

$R_{o,n}$: Optimum output resistance for case n.

$G_{o,n} = 1/R_{o,n}$.

n= 1: Standard image termination for the particular mixer used. Corresponds to short image for a Y- or a G-mixer and to open image for a Z- or an H-mixer.

n= 2: Broadband input termination; both signal and image are having the same termination.

n= 3: Modified image termination for the particular mixer used. Corresponds to open image for a Y- or a G-mixer and to short image for a Z- or an H-mixer.

The terminology used in Appendix 2 for the signal, i-f and image voltages and currents will be used.

4.2. Single-Diode Mixers

In a single-diode mixer, the terminations offered by the imbedding network to the undesired frequencies will affect the local oscillator pumping waveforms. For example, using the frequency notation of Sec. 2.1.1, if $\omega_o \ll \omega_p$, then the n'th harmonic of the pump, $n\omega_p$, will see the same termination offered to the frequencies $\omega_n (= n\omega_p + \omega_o)$ and $\omega_{-n} (= -n\omega_p + \omega_o)$. Of course the same is also true for a multi-diode mixer in which each diode is individually terminated since in this case each diode by itself acts as a single-diode mixer.

A single-diode mixer is suitable for microwave frequencies since in this case it is desirable to place the r-f terminations right next to the diode. In practice, one connects two single-diode circuits through a 'magic tee' junction to form a balanced mixer. This resulting mixer has the advantages of isolating the local oscillator (pump) and signal ports as well as supressing the local oscillator noise.** However its performance is identical to that of a single diode mixer driven from a noiseless local oscillator.

We now consider the single diode realizations of the four basic mixer circuits discussed in Chapter 2. Next, in Sec. 4.2.5, we compare their performance for identical conditions of d-c bias and pump power.

** See for example Pound (I, Sec. 6.5).

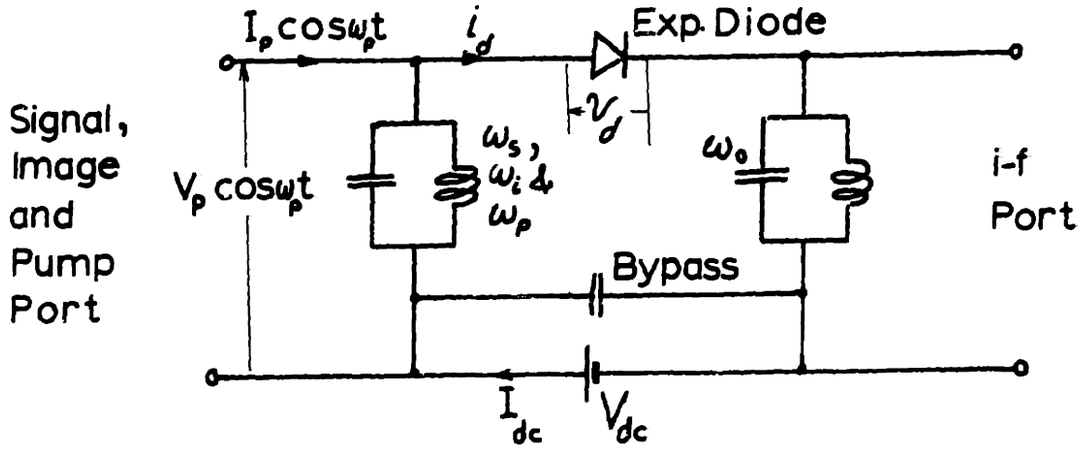

Fig. 4.1. Pumping a Single-Diode Y-Mixer

4.2.1. The Y-mixer:**

The single-diode Y-mixer is shown in Fig. 4.1., where only the pumping and bias signals are shown. The pumping voltage across the diode, v_d, is constrained to be sinusoidal while i_d can have all the possible harmonics since the imbedding network short-circuits all the pump harmonics, Thus,

$$v_d = V_{dc} + V_p \cos\omega_p t \quad , \quad (4.3)$$

Hence, Eq. (4.1) gives

$$i_d = I_{sat} \left[e^{\alpha(V_{dc} + V_p \cos\omega_p t)} - 1 \right] \quad , \quad (4.4)$$

Using the integral

$$\frac{1}{2\pi} \int_0^{2\pi} e^{A\cos x} \cos(nx)dx = \mathcal{I}_n(A) \quad , \quad (4.5)$$

** Many authors have dealt with this mixer such as Torrey and Whitmer (I, Sec. 5.11) and Barber (I).

where $\mathcal{I}_n$ is the modified Bessel function of the first kind of order n, Eq. (4.4) gives

$$i_d = I_{sat}\, e^{\alpha V_{dc}} [\, \mathcal{I}_o(\alpha V_p) + 2\mathcal{I}_1(\alpha V_p) \cos \omega_p t + 2\mathcal{I}_2(\alpha V_p) \cos(2\omega_p t) + \ldots \,] - I_{sat} \,. \quad (4.6)$$

From the above, if the reverse saturation current is neglected, it follows that

$$I_{dc} = I_{sat}\, e^{\alpha V_{dc}}\, \mathcal{I}_o(\alpha V_p) \quad (4.7a)$$

$$\approx I_{sat}\, \frac{e^{\alpha(V_p+V_{dc})}}{\sqrt{2\pi\alpha V_p}} \quad , \alpha V_p >> 1 \quad ; \quad (4.7b)$$

$$I_p = 2\, I_{sat}\, e^{\alpha V_{dc}}\, \mathcal{I}_1(\alpha V_p) \quad (4.8a)$$

$$\approx 2\, I_{dc} \quad , \alpha V_p >> 1 \quad ; \quad (4.8b)$$

$$P_p = \frac{I_{sat}}{\alpha}\, e^{\alpha V_{dc}}\, \alpha V_p\, \mathcal{I}_1(\alpha V_p) \quad (4.9a)$$

$$\approx I_{dc}\, V_p \quad , \alpha V_p >> 1 \quad ; \quad (4.9b)$$

and

$$G_p \approx 2\alpha I_{sat}\, e^{\alpha V_{dc}}\, \frac{\mathcal{I}_1(\alpha V_p)}{\alpha V_p} \quad (4.10a)$$

$$\approx 2I_{dc}/V_p \quad , \alpha V_p >> 1 \quad . \quad (4.10b)$$

** See for example Abramowitz and Stegun (I, Eq. 9.7.1) for the assymptotic expansions of the modified Bessel functions for a large argument.

The above d-c and pump parameters, normalized in terms of appropriate quantities, are plotted in Fig. 4.2 as functions of $1/\sqrt{\alpha V_p}$.

The small signal conductance waveform can be calculated from Eqs. (4.2), (4.4) and (4.6) to be

$$g(t) = \alpha I_{sat} e^{\alpha(V_{dc} + V_p \cos \omega_p t)} \qquad (4.11a)$$

$$= y_o + 2 y_1 \cos \omega_p t + 2 y_2 \cos(2\omega_p t) + \ldots \quad , \qquad (4.11b)$$

where

$$y_n = \alpha I_{sat} e^{\alpha V_{dc}} \mathcal{I}_n(\alpha V_p) \quad . \qquad (4.11c)$$

It is interesting to note that g(t) approaches an impulse train as $\alpha V_p \longrightarrow \infty$. This limiting g(t) is known to be the ideal conductance waveform for the Y-mixer as given in Sec. 3.2.1.

Referring to Sec. 2.2.1, the mixer equations can be put in the Y-matrix form

$$\begin{bmatrix} I_s \\ I_o \\ I_i^* \end{bmatrix} = \begin{bmatrix} y_o & y_1 & y_2 \\ y_1 & y_o & y_1 \\ y_2 & y_1 & y_o \end{bmatrix} \begin{bmatrix} V_s \\ V_o \\ V_i^* \end{bmatrix} \quad . \qquad (4.12)$$

With the help of Appendix 2 one can calculate the optimum conversion loss, and source and output conductances for the three image terminations considered.

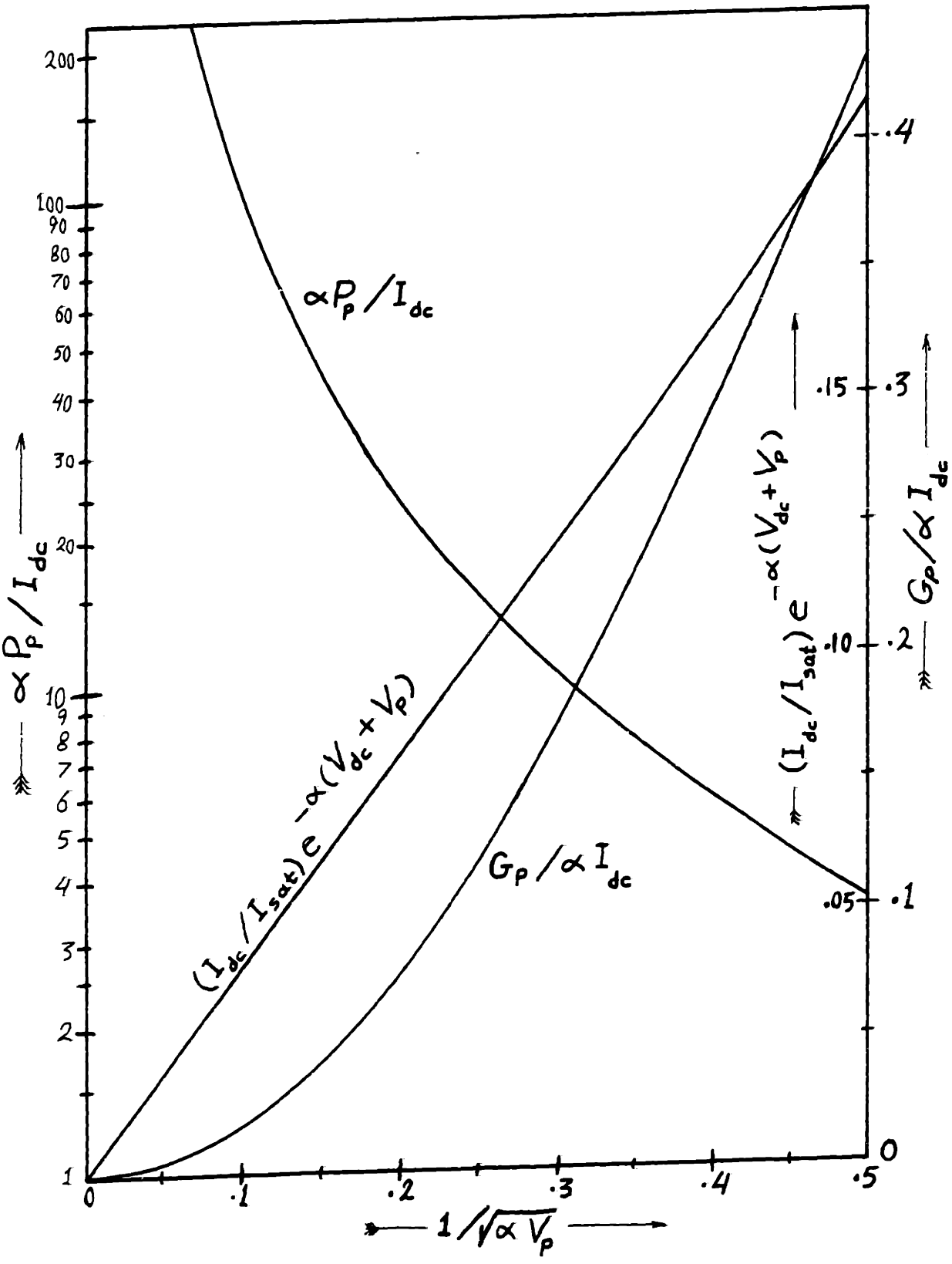

Fig. 4.2. Bias and Pump Parameters for a Single-Diode Y-Mixer

The results are plotted in Figs. 4.3 and 4.4 as functions of $1/\sqrt{\alpha V_p}$.

For $\alpha V_p \gg 1$, the above mentioned mixer parameters can be approximated with the help of the asymptotic expansions of the modified Bessel functions. In this case, Appendix 2 gives the following results:**

$$\epsilon_1 = \left\{\frac{y_1}{y_o}\right\}^2 = \left\{\frac{\mathfrak{I}_1(\alpha V_p)}{\mathfrak{I}_o(\alpha V_p)}\right\}^2 \approx 1 - \frac{1}{\alpha V_p} + O\left[\frac{1}{(\alpha V_p)^3}\right] \quad , \quad (4.13)$$

$$\theta = \frac{y_2}{y_o} = \frac{\mathfrak{I}_2(\alpha V_p)}{\mathfrak{I}_o(\alpha V_p)} \approx 1 - \frac{2}{\alpha V_p} + \frac{1}{(\alpha V_p)^2} \quad , \quad (4.14)$$

$$\epsilon_2 = \frac{2\epsilon_1}{1+\theta} \approx 1 - \frac{1}{2}\frac{1}{(\alpha V_p)^2} \quad , \quad (4.15)$$

and

$$\epsilon_3 = \frac{\epsilon_1}{1-\epsilon_1}\frac{1-\theta}{1+\theta} \approx 1 - \frac{1}{2}\frac{1}{\alpha V_p} \quad , \quad (4.16)$$

The performance of the Y-mixer becomes:

1. Short Image

$$L_1 \approx 1 + 2/\sqrt{\alpha V_p} \quad (4.17a)$$

$$\approx 8.686 / \sqrt{\alpha V_p} \quad \text{db} \quad , \quad (4.17b)$$

$$G_{s,1} = G_{o,1} \approx \alpha I_{dc} / \sqrt{\alpha V_p} \quad , \quad (4.18)$$

** These approximate results can be considered as a part of a more general analysis of Y-mixers with arbitrary pulsed conductance waveforms. This analysis is given in Appendix 8 and is a generalization of the work of Barber (I).

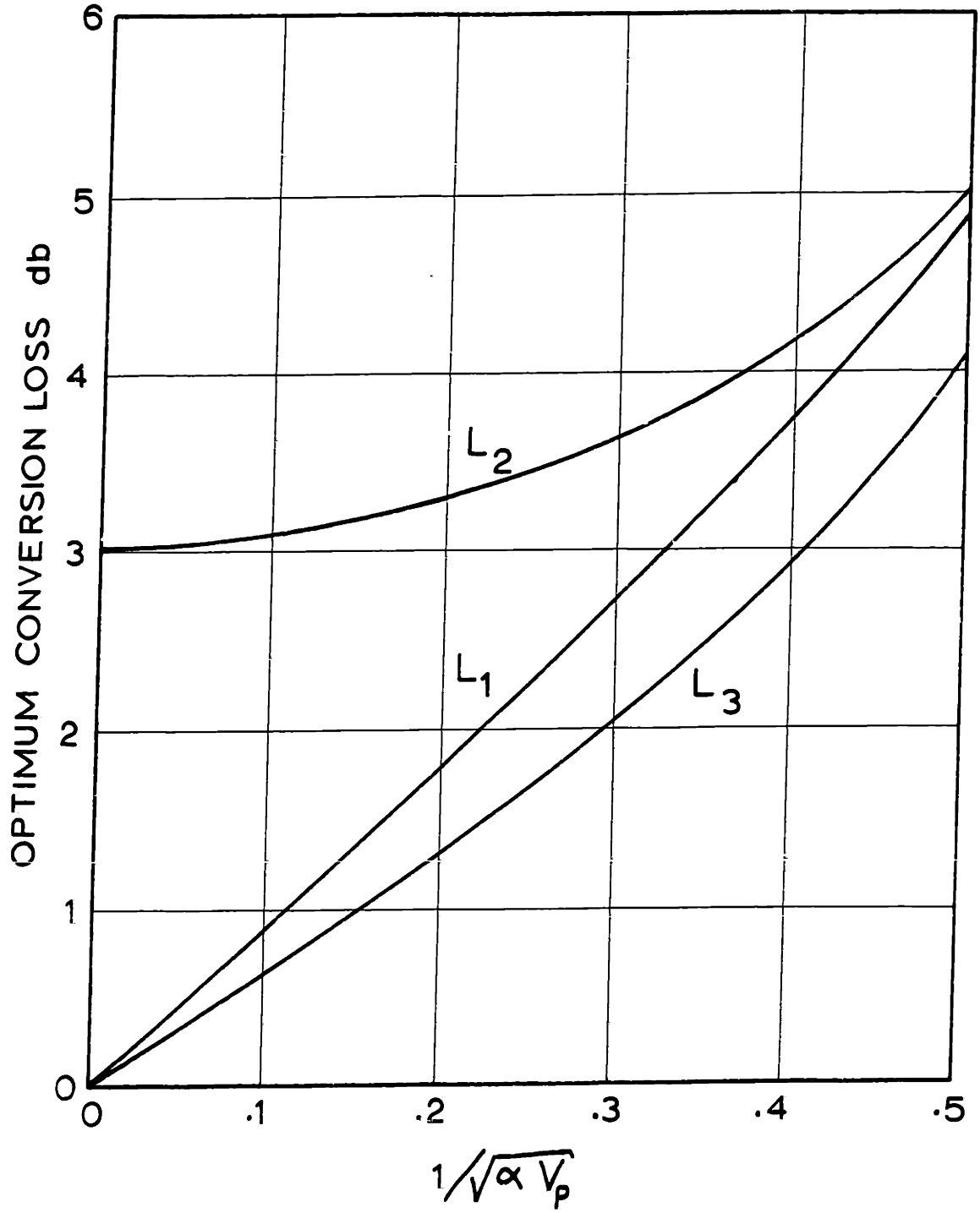

Fig. 4.3. The Optimum Conversion Loss for a Single-Diode Y-Mixer (1. Short Image, 2. Broadband Input, 3. Open Image)

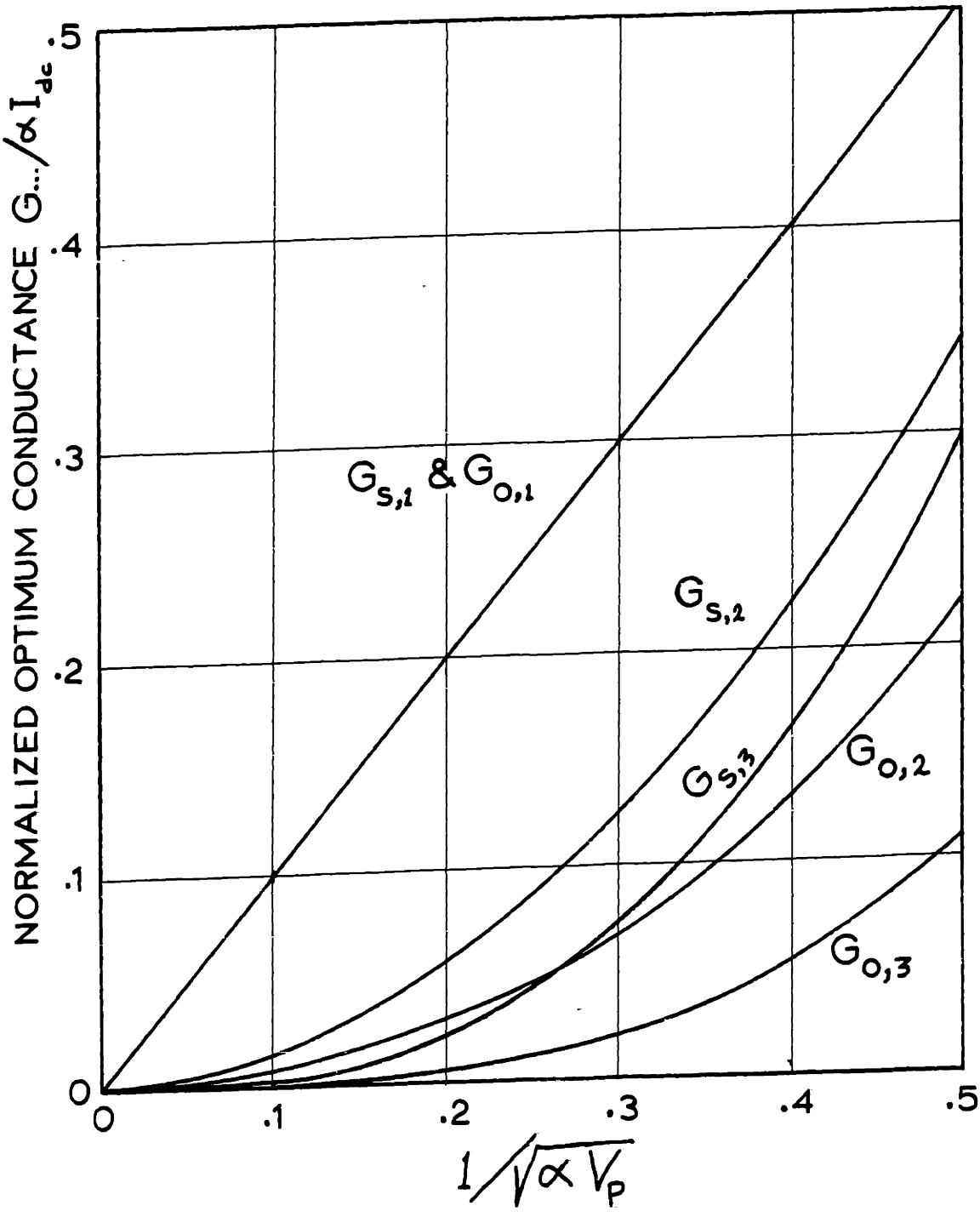

Fig. 4.4. The Optimum Source and Output Conductances for a Single-Diode Y-Mixer
1. Short Image, 2. Broadband Input, 3. Open Image

2. Broadband Input

$$L_2 \approx 2\,(1 + \sqrt{2} / \alpha V_p) \qquad (4.19a)$$

$$\approx 3 + 4.343\,\sqrt{2} / \alpha V_p \quad \text{db} \qquad (4.19b)$$

$$G_{s,2} \approx \sqrt{2}\,\alpha\, I_{dc} / \alpha\, V_p \qquad (4.20)$$

$$G_{o,2} \approx G_{s,2} / 2 \qquad (4.21)$$

3. Open Image

$$L_3 \approx 1 + \sqrt{2} / \sqrt{\alpha V_p} \qquad (4.22a)$$

$$\approx 4.343\,\sqrt{2} / \sqrt{\alpha V_p} \quad \text{db} \qquad (4.22b)$$

$$G_{s,3} \approx 2\sqrt{2}\,\alpha\, I_{dc} / (\alpha V_p)^{3/2} \qquad (4.23)$$

$$G_{o,3} \approx G_{s,3} / 4 \qquad (4.24)$$

It is shown in Appendix 8, where a general study of Y-mixers with arbitrary pulsed conductance waveforms is given, that the performance of the mixer for cases 2 and 3 is much more sensitive to the exact shape of the conductance waveform than that of case 1.

In realizing a Y-mixer in practice, one might not be able to short-circuit all the undesired frequencies, and hence the performance of the mixer will be degraded. In Appendix 10 we study the effects of the incomplete terminations on the performance of the mixer. To make the calculations possible, the diode was modeled as an ideal switch driven with the appropriate pulse duty ratio.

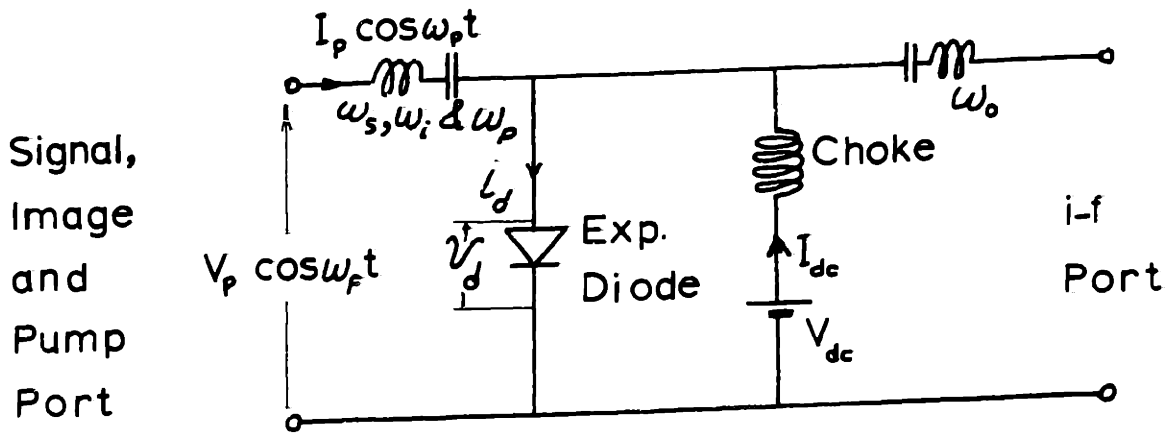

Fig. 4.5. Pumping a Single-Diode Z-Mixer

4.2.2. The Z-mixer:

The single-diode Z-mixer is shown in Fig. 4.5. The pump current through the diode, i_d, is constrained to be sinusoidal while v_d can have all the possible harmonics since the imbedding network open-circuits all the pump harmonics. Thus,

$$i_d = I_{dc} + I_p \cos \omega_p t \quad , \quad (4.25)$$

Clearly, I_p must satisfy the inequality $I_p \leq I_{dc} + I_{sat}$ since $i_d \geq - I_{sat}$. If we define

$$a = \frac{I_p}{I_{dc} + I_{sat}} \quad , \; a \leq 1 \quad , \quad (4.26)$$

Eq. (4.1) gives

$$\alpha v_d = \log_e \frac{I_{dc} + I_{sat}}{I_{sat}} + \log_e (1 + a \cos \omega_p t) \quad . \quad (4.27)$$

Using the integrals

$$\frac{1}{2\pi}\int_0^{2\pi} \log_e(1 + a\cos x)\,dx = \log_e \frac{1+\sqrt{1-a^2}}{2} \quad , \quad (4.28a)$$

and

$$\frac{1}{2\pi}\int_0^{2\pi} \cos x \log_e(1 + a\cos x)\,dx = \frac{a}{1+\sqrt{1-a^2}} \quad , \quad (4.28b)$$

for $|a| \leq 1$, and neglecting the reverse saturation current, one obtains

$$e^{\alpha V_{dc}} = \frac{I_{dc}}{I_{sat}} \frac{1+\sqrt{1-a^2}}{2} \quad , \quad (4.29)$$

$$\alpha V_p = \frac{2a}{1+\sqrt{1-a^2}} \quad , \quad (4.30)$$

$$P_p = \frac{I_{dc}}{\alpha}\left[1 - \sqrt{1-a^2}\right] \quad , \quad (4.31)$$

and

$$R_p = \frac{1}{\alpha I_{dc}} \frac{2}{1+\sqrt{1-a^2}} \quad . \quad (4.32)$$

The above bias and pump parameters normalized, in terms of appropriate quantities, are plotted in Fig. 4.6 as functions of a quantity "b" defined by

$$b^2 = \sqrt{1 - a^2} \quad . \quad (4.33)$$

It is interesting to note that from Eqs. (4.29) and (4.32) one obtains the relation

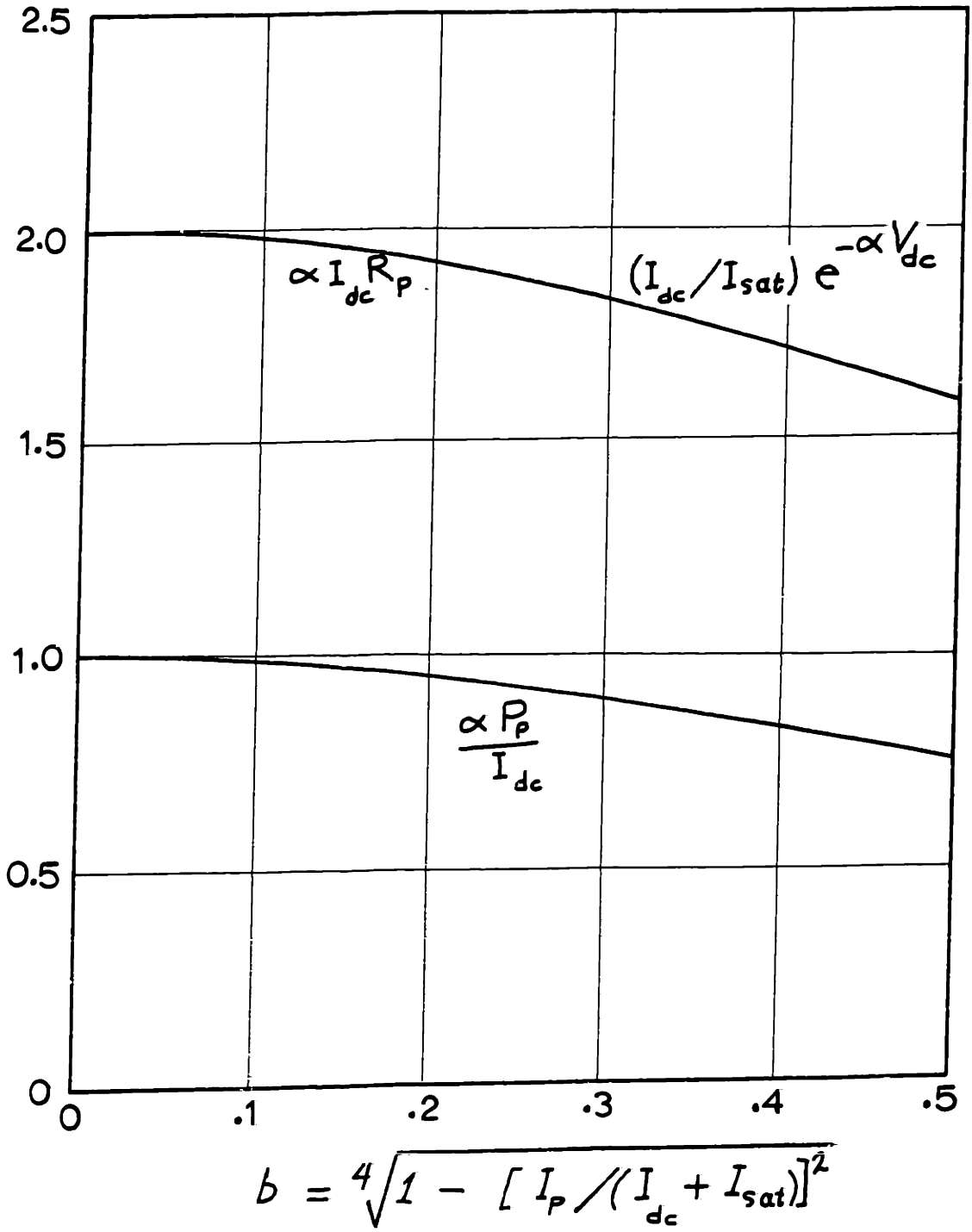

Fig. 4.6. Bias and Pump Parameters for a Single-Diode Z-Mixer

$$R_p = \frac{1}{\alpha\, I_{sat}\, e^{\alpha V_{dc}}} \quad , \quad (4.34)$$

which states that the pump sees the diode as a linear resistance, independent of I_p, <u>if</u> the diode is biased by a constant d-c voltage.

The above equations present the following paradox: If the diode is biased by a constant d-c current source, I_{dc}, then $I_p \leq I_{dc} + I_{sat}$ from Eq. (4.26) and if it is biased by a constant d-c voltage, V_{dc}, then $I_p \leq 2\, I_{sat}\, e^{\alpha V_{dc}}$ from Eqs. (4.26) and (4.29). At the same time $V_p \leq 2/\alpha$ ($\approx$ 50 m.v.) from Eqs. (4.26) and (4.30). Thus, it seems that both the voltage and current at the pump port of Fig. 4.5 are limited!! This is clearly impossible**.

The paradox can be resolved however by noting that as I_p attains its maximum possible value, i.e. a = 1, the diode voltage waveform, v_d, assumes the value of $-\infty$ at the points $\omega_p t = (2n+1)\pi$. If a train of negative impulses is added to the voltage waveforms at these points, the value of V_p will certainly increase,

** To demonstrate this, assume that the signals in the pump port are limited by $I_p \leq I_{p,max}$ and $V_p \leq V_{p,max}$. If one drives this port by a generator with an internal resistance R and an e.m.f. $E\cos\omega_p t$ such that $E > V_{p,max} + R\, I_{p,max}$, no values for I_p and V_p that satisfy the above constraints can be found.

while the current waveform will not be affected. Thus, one concludes that the train of impulses will exist if $\alpha V_p > 2$. In this case I_p will still be limited while V_p will be allowed to assume any value. This resolves the paradox.

One should note that in practice the above status will never be attained since the diode reverse breakdown is bound to occur before a = 1. This makes it meaningless to try to find the bias and pump equations analogous to Eqs. (4.29) ... (4.34) when $\alpha V_p \geq 2$ without specifying the characteristics of the diode in the breakdown region. This problem will not be considered here and our analysis will be limited to $\alpha V_p < 2$, i.e. $V_p < 50$ m.v. approximately.**

With the above restriction in mind, and if the reverse saturation current is neglected, the small signal conductance waveform is found from Eqs. (4.2), (4.25) and (4.26) to be sinusoidal given by

$$g(t) = \alpha I_{dc} (1 + a \cos \omega_p t) \quad . \quad (4.35)$$

It is interesting to note that the optimum imbedding network for a sinusoidal conductance waveform is found from Sec. 3.3.2 to be the Z-mixer. Thus, the results of Sec. 3.3.2 can be applied here. However, we will go

** This limitation is equivalent to $P_p < I_{dc}/\alpha$ as can be deduced from Eq. (4.31)

through the analysis independantly since we need to consider three possible image terminations.

Since we are analyzing a Z-mixer one needs the resistance waveform given by

$$r(t) = \frac{1}{\alpha I_{dc}} \frac{1}{1 + a \cos \omega_p t} \qquad (4.36a)$$

$$= z_o + 2z_1 \cos \omega_p t + 2z_2 \cos(2\omega_p t) + \ldots \quad , \qquad (4.36b)$$

where

$$z_n = \frac{1}{\alpha I_{dc}} \frac{1}{\sqrt{1-a^2}} \left\{ \frac{a}{1 + \sqrt{1-a^2}} \right\}^n \quad . \qquad (4.36c)$$

In developing Eq. (4.36c) we made use of the integral

$$\frac{1}{2\pi} \int_o^{2\pi} \frac{\cos(nx)}{1 + a \cos x} dx = \frac{1}{\sqrt{1-a^2}} \left\{ \frac{a}{1+\sqrt{1-a^2}} \right\}^n \quad ,$$

$$|a| \leq 1 \quad . \qquad (4.37)$$

Referring to Sec. 2.2.1, the mixer equations can be put in the Z-matrix form

$$\begin{bmatrix} V_s \\ V_o \\ V_i^* \end{bmatrix} = \begin{bmatrix} z_o & z_1 & z_2 \\ z_1 & z_o & z_1 \\ z_2 & z_1 & z_o \end{bmatrix} \begin{bmatrix} I_s \\ I_o \\ I_i^* \end{bmatrix} \quad . \qquad (4.38)$$

With the help of Appendix 2 one can calculate the optimum conversion loss, and source and output resistances for the three image terminations considered. The results are plotted in Figs. 4.7 and 4.8 as functions of the quantity "b" defined in Eq. (4.33). Note that in case 3, short image, the optimum conversion loss does not attain the theoretical minimum value of zero db.

For $I_p \approx I_{dc} + I_{sat}$, i.e. $a \approx 1$, the mixer parameters can be approximated to simple expressions. For this purpose let "b" of Eq. (4.33) be $<< 1$. Appendix 2 gives

$$\epsilon_1 = \left\{\frac{z_1}{z_o}\right\}^2 = \left\{\frac{a}{1 + \sqrt{1-a^2}}\right\}^2 \approx 1 - 2\,b^2 \quad , \quad (4.39)$$

$$\theta = \frac{z_2}{z_o} = \epsilon_1 \quad , \quad (4.40)$$

$$\epsilon_2 = \frac{2\,\epsilon_1}{1 + \theta} \approx 1 - b^2 \quad , \quad (4.41)$$

and

$$\epsilon_3 = \frac{\epsilon_1}{1 - \epsilon_1} \frac{1 - \theta}{1 + \theta} \approx \frac{1}{2}\,(1 - b^2) \quad . \quad (4.42)$$

The performance of the Z-mixer becomes:

1. Open Image

$$L_1 \approx 1 + 2\sqrt{2}\,b \quad (4.43a)$$

$$\approx 8.686\,\sqrt{2}\,b \quad \text{db} \quad . \quad (4.43b)$$

$$R_{s,1} = R_{o,1} \approx \frac{1}{\alpha I_{dc}} \frac{\sqrt{2}}{b} \quad . \quad (4.44)$$

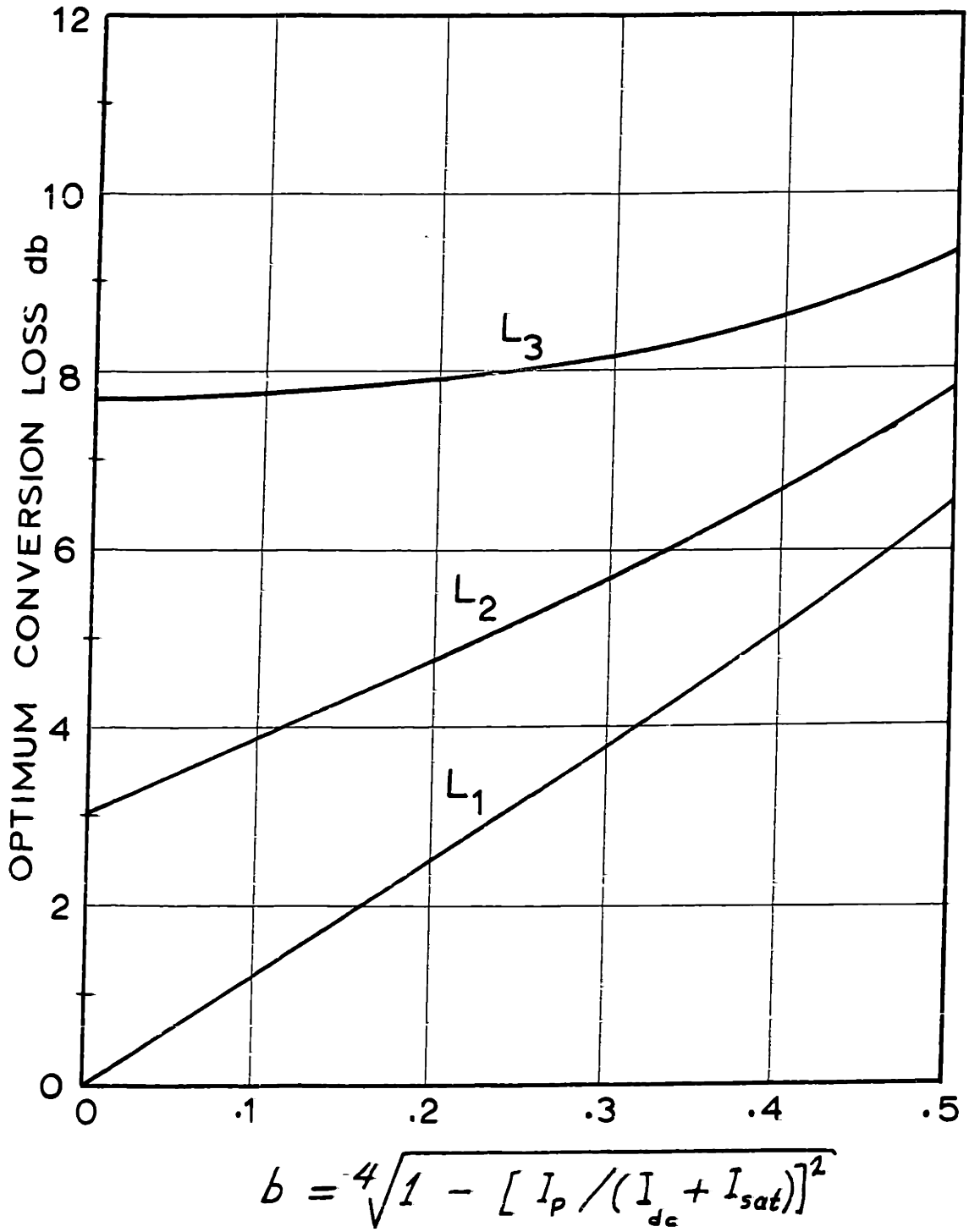

Fig. 4.7. The Optimum Conversion Loss for a Single-Diode Z-Mixer (1. Open Image, 2. Broadband Input, 3. Short Image)

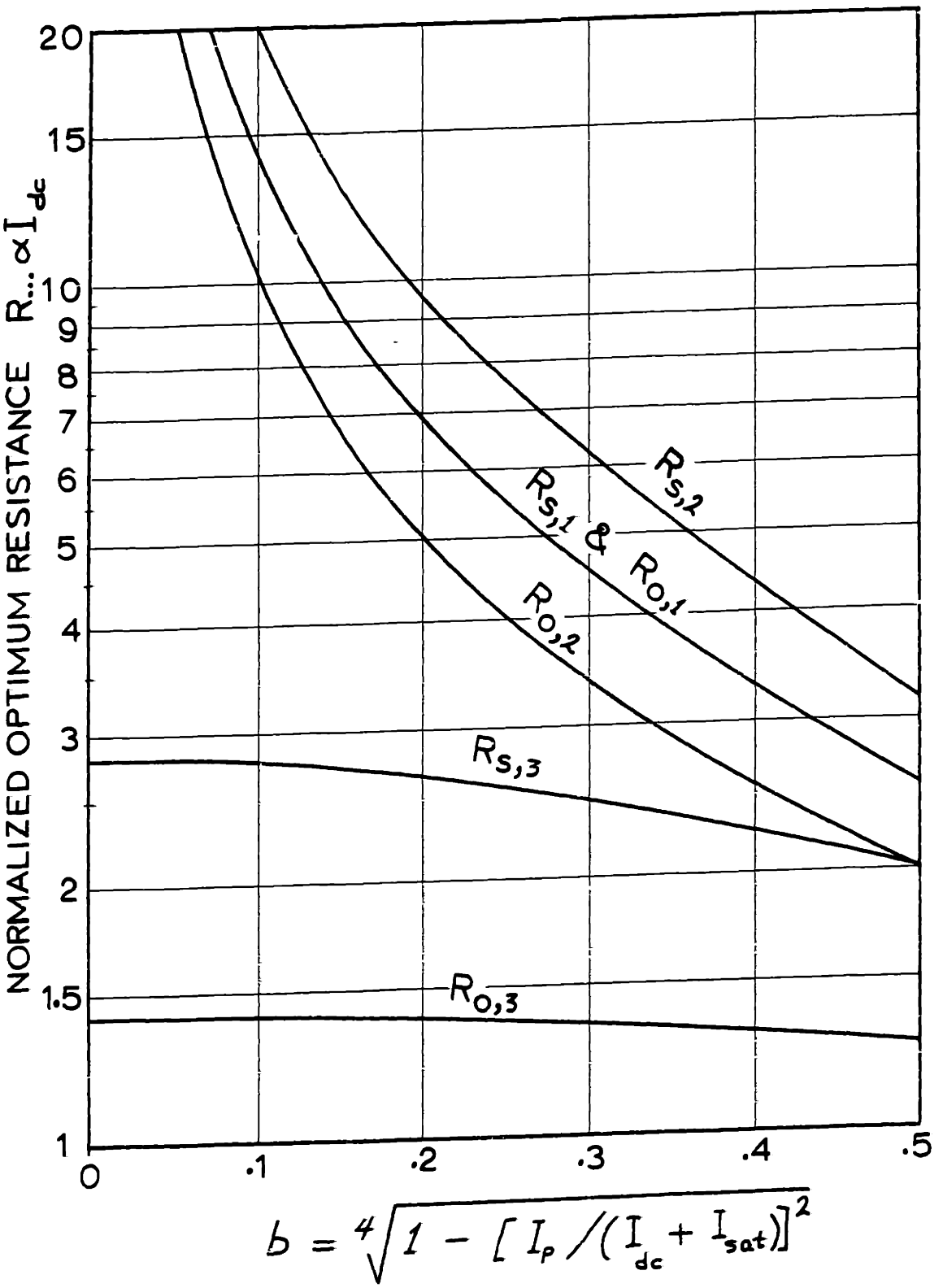

Fig. 4.8. The Optimum Source and Output Resistances for a Single-Diode Z-Mixer 1. Open Image, 2. Broadband Input, 3. Short Image

2. Broadband Input

$$L_2 \approx 2\,(1 + 2b) \tag{4.45a}$$

$$\approx 3 + 8.686\,b \quad \text{db} \tag{4.45b}$$

$$R_{s,2} \approx \frac{1}{\alpha\, I_{dc}}\,\frac{2}{b} \tag{4.46}$$

$$R_{o,2} \approx R_{s,2}/2 \tag{4.47}$$

3. Short Image

$$L_3 \approx \frac{\sqrt{2}+1}{\sqrt{2}-1}\,(1 + \sqrt{2}\,b^2) \tag{4.48a}$$

$$\approx 7.66 + 4.343\,\sqrt{2}\,b^2 \quad \text{db} \tag{4.48b}$$

$$R_{s,3} \approx \frac{2\sqrt{2}}{\alpha\, I_{dc}} \tag{4.49}$$

$$R_{o,3} \approx R_{s,3}/4 \tag{4.50}$$

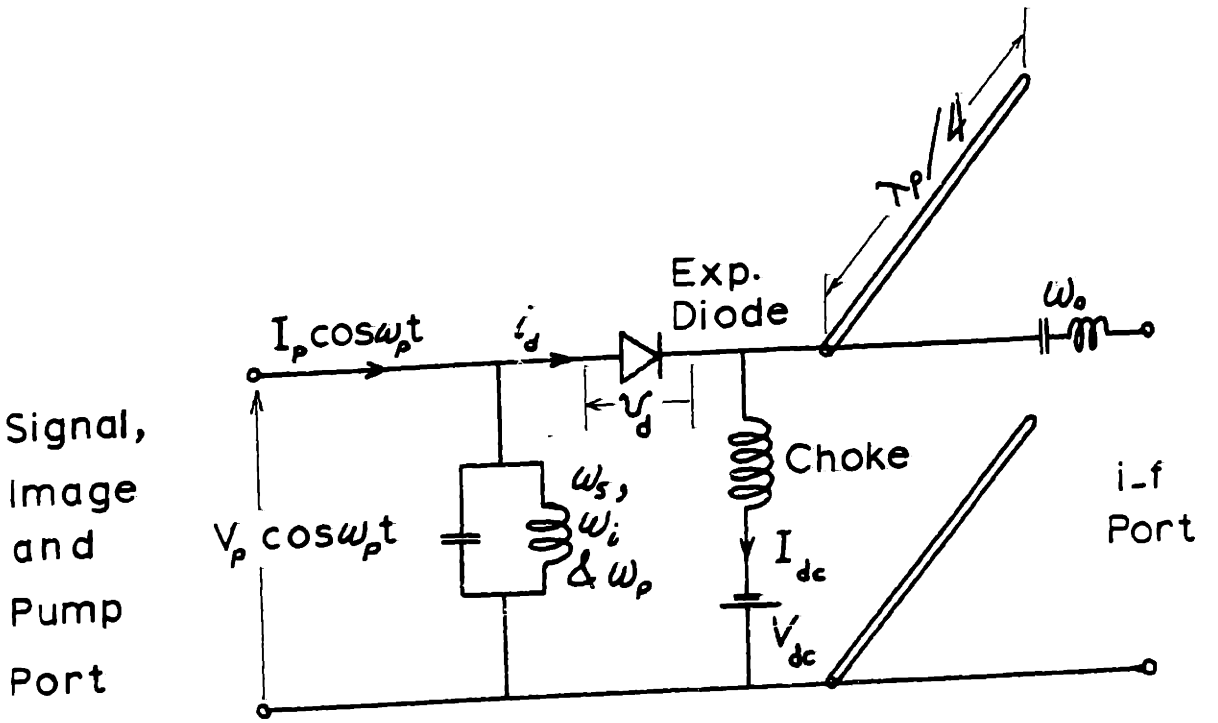

Fig. 4.9. Pumping a Single-Diode G-Mixer

4.2.3. The G-mixer:

The single-diode G-mixer is shown in Fig. 4.9 where the open-circuit quarter-wave line is intended to short-circuit all the odd-order frequencies as suggested in Fig. 2.7. Beside the d-c and fundamental components of current and voltage, the circuit of Fig. 4.9 only allows current with odd harmonics; $i_{od}(t)$: $n\omega_p$, $|n|$ odd ≥ 3; and voltage with even harmonics; $v_{ev}(t)$: $n\omega_p$, $|n|$ even ≥ 2. Thus

$$i_d = I_{dc} + I_p \cos\omega_p t + i_{od}(t) \quad , \quad (4.51)$$

and

$$v_d = V_{dc} + V_p \cos\omega_p t + v_{ev}(t) \quad . \quad (4.52)$$

Substituting the above equations in Eq. (4.1) we get

$$I_{dc} + I_{sat} + I_p \cos \omega_p t + i_{od}(t)$$

$$= I_{sat}\, e^{\alpha[V_{dc} + V_p \cos \omega_p t + v_{ev}(t)]} \quad . \quad (4.53a)$$

Substituting $\omega_p t + \pi$ for $\omega_p t$, Eq. (4.53a) gives

$$I_{dc} + I_{sat} - I_p \cos \omega_p t - i_{od}(t)$$

$$= I_{sat}\, e^{\alpha[V_{dc} - V_p \cos \omega_p t + v_{ev}(t)]} \quad . \quad (4.53b)$$

Dividing Eqs. (4.53) a and b and solving for i_d, one obtains**

$$i_d = I_{dc} + (I_{dc} + I_{sat}) \tanh(\alpha V_p \cos \omega_p t) \quad . \quad (4.54)$$

Adding Eqs. (4.53) a and b, one obtains**

$$\alpha[v_{ev}(t) + V_{dc}] = \log_e \frac{I_{dc} + I_{sat}}{I_{sat}} + \log_e \operatorname{sech}(\alpha V_p \cos \omega_p t). \quad (4.55)$$

Presumably, for given values of V_p and V_{dc}, equating the d-c coefficients of both sides of Eq. (4.55) gives an equation for I_{dc}. Substituting this value in Eq. (4.54), one can calculate I_p and hence, P_p and R_p. Unfortunately, the results of the Fourier integrals necessary for the analysis cannot be written in a closed form. However, for $\alpha V_p \gg 1$, one can obtain asymptotic approximations for the integrals. It is shown in Secs. A7.1

** This technique works only for exponential diodes.

and A7.2 that for A >> 1

$$f_1(A) = \frac{1}{2\pi} \int_o^{2\pi} \cos x \tanh(A \cos x) \approx \frac{2}{\pi} \quad . \quad (4.56)$$

$$f_2(A) = \frac{1}{2\pi} \int_o^{2\pi} \log_e \operatorname{sech}(A \cos x)\, dx \approx \log_e 2 - \frac{2}{\pi} A \quad . \quad (4.57)$$

Using these approximations and neglecting the reverse saturation current, Eq. (4.55) gives

$$I_{dc} \approx \frac{1}{2} I_{sat}\, e^{\alpha(V_{dc} + \frac{2}{\pi} V_p)} \quad , \quad (4.58)$$

and Eq. (4.54) gives

$$I_p \approx \frac{4}{\pi} I_{dc} \quad . \quad (4.59)$$

Thus,

$$P_p \approx \frac{2}{\pi} I_{dc}\, V_p \quad , \quad (4.60)$$

and

$$G_p \approx \frac{4}{\pi} I_{dc}/V_p \quad . \quad (4.61)$$

The above bias and pump parameters, normalized in terms of appropriate quantities, are plotted in Fig. 4.10 as functions of $1/\sqrt{2\alpha V_p/\pi}$. Exact calculations based on numerical integration of Eqs. (4.54) and (4.55) were used.

The small signal conductance waveform is calculated from Eqs. (4.2) and (4.54) to be

$$g(t) = \alpha I_{dc} [1 + \tanh(\alpha V_p \cos \omega_p t)] \quad , \quad (4.62)$$

where we neglected the reverse saturation current.

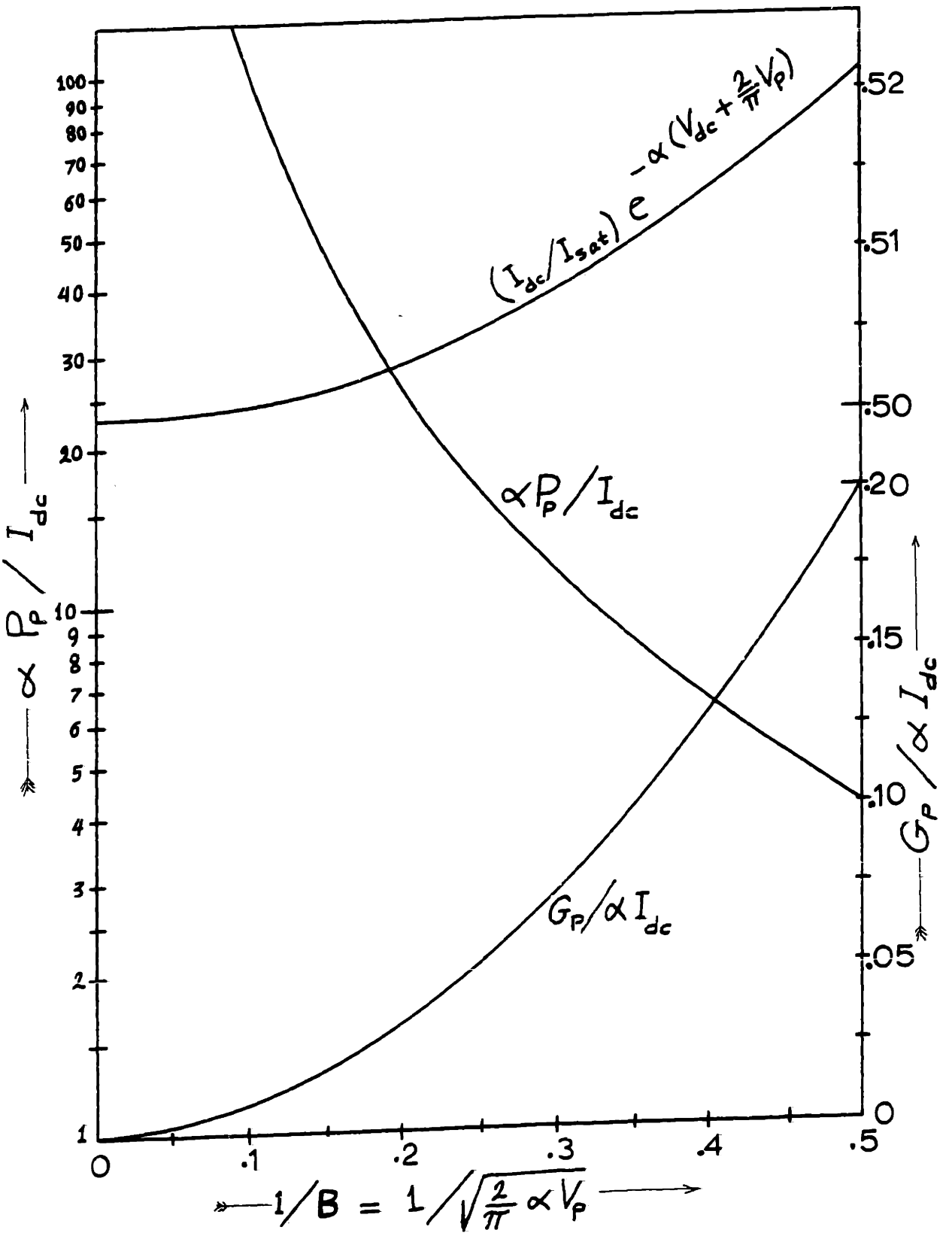

Fig. 4.10. Bias and Pump Parameters for a Single-Diode G-Mixer

It is interesting to note that as $\alpha V_p \rightarrow \infty$, $g(t)$ approaches a square-wave. This conductance waveform and the G-mixer were shown be be optimum for one another in Secs. 3.2.2 and 3.3.3.**

To analyze the G-mixer, one needs to know the even- and odd-harmonic portions of $g(t)$. These are given by

$$g_{ev}(t) = \alpha I_{dc} \quad , \quad (4.63)$$

and

$$g_{od}(t) = \alpha I_{dc} \tanh(\alpha V_p \cos\omega_p t) \quad . \quad (4.64)$$

The equation of the mixer can now be put in the G-matrix form

$$\begin{bmatrix} I_s \\ V_o \\ I_i^* \end{bmatrix} = \begin{bmatrix} G_{11} & G_{12} & G_{13} \\ -G_{12} & G_{22} & -G_{12} \\ G_{13} & G_{12} & G_{11} \end{bmatrix} \begin{bmatrix} V_s \\ I_o \\ V_i^* \end{bmatrix} \quad , \quad (4.65)$$

where the G's are calculated from the duals of the relations given in Sec. 2.4.2. The results are given by

$$G_{11} = \alpha I_{dc} \left\langle \operatorname{sech}^2(\alpha V_p \cos\omega_p t) \right\rangle \quad , \quad (4.66a)$$

** Generally, it can be shown that for a single-diode G_N-mixer, as $\alpha V_p \rightarrow \infty$, the pumped conductance waveform approaches a rectangular-wave with pulse duty ratio $1/N$. This conductance waveform and the G_N-mixer are optimum for one another as shown in Secs. 3.2.3 and 3.3.4.

$$G_{12} = \left\langle \cos\omega_p t \, \tanh(\alpha V_p \cos\omega_p t) \right\rangle \quad , \quad (4.66b)$$

$$G_{13} = \alpha I_{dc} \left\langle \cos(2\omega_p t) \, \mathrm{sech}^2(\alpha V_p \cos\omega_p t) \right\rangle , \quad (4.66c)$$

and

$$G_{22} = \frac{1}{\alpha I_{dc}} \quad , \quad (4.66d)$$

where $\left\langle \ldots \right\rangle = \frac{1}{2\pi} \int_0^{2\pi} \ldots \, d\omega_p t$.

With the help of Appendix 2 one can calculate the optimum conversion loss, and source and output conductances for the three image terminations considered. The results are plotted in Figs. 4.11 and 4.12 as functions of $1/\sqrt{2\alpha V_p/\pi}$. Since the results of the Fourier integrals in Eqs. (4.66) a ... c cannot be written in a closed form, numerical integrations were employed.

The aforementioned results can be approximated by using asymptotic expansions for the integrals when $\alpha V_p \gg 1$. The integral required for G_{12} was given previously in Eq. (4.56). The remaining integrals are found from Secs. A7.3 and A7.4 to be

$$f_3(A) = \frac{1}{2\pi} \int_0^{2\pi} \mathrm{sech}^2(A \cos x) \, dx \approx \frac{2}{\pi} \frac{1}{A} \quad , \quad (4.67)$$

and

$$f_4(A) = \frac{1}{2\pi} \int_0^{2\pi} \cos(2x) \, \mathrm{sech}^2(A \cos x) \, dx \approx \frac{\pi}{3} \frac{1}{A^3} - f_3(A), \quad (4.68)$$

for $A \gg 1$. Substituting these results in Eqs. (4.66) a...c, one obtains

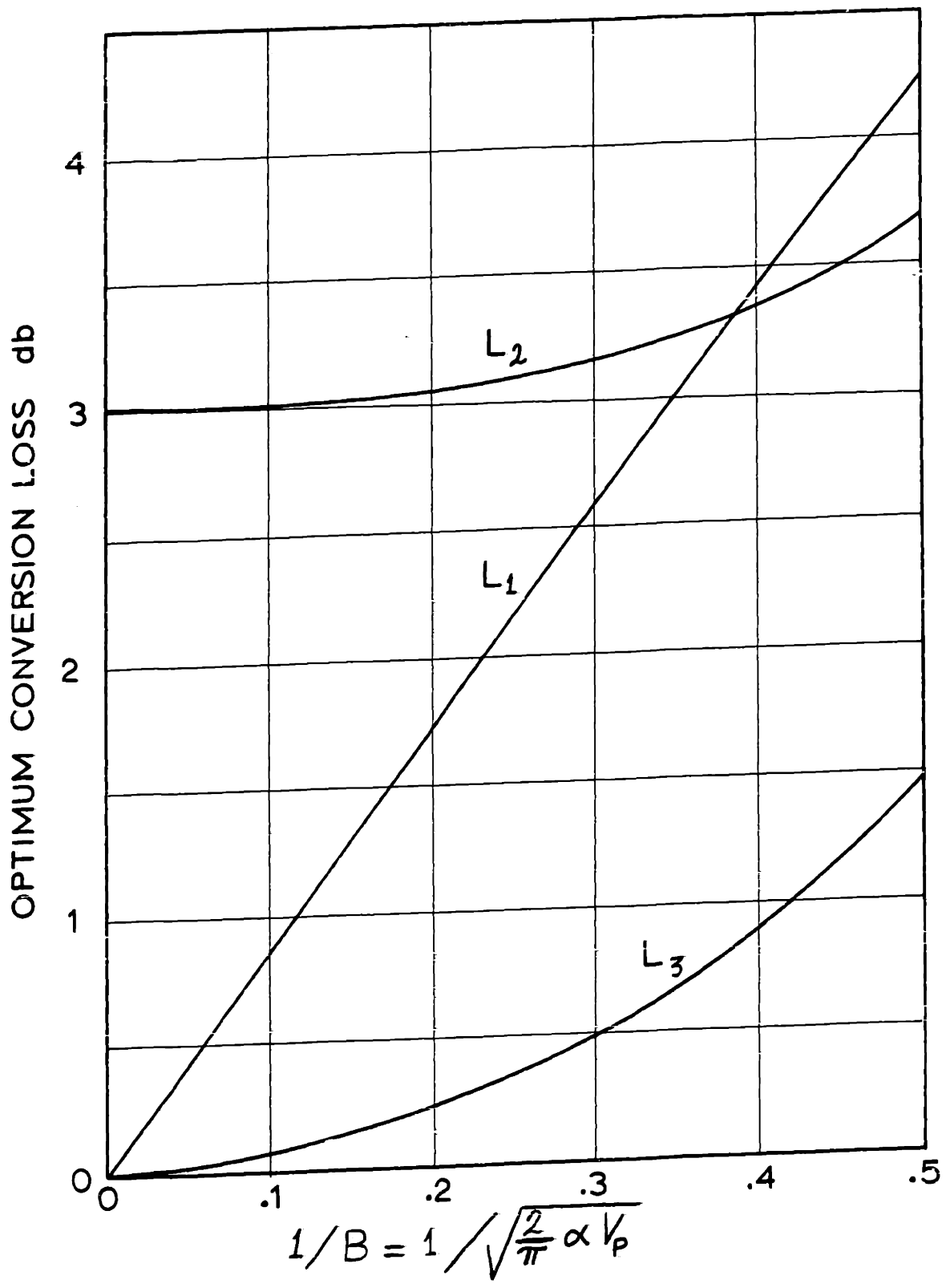

Fig. 4.11. The Optimum Conversion Loss for a Single-Diode G-Mixer (1. Short Image, 2. Broadband Input, 3. Open Image

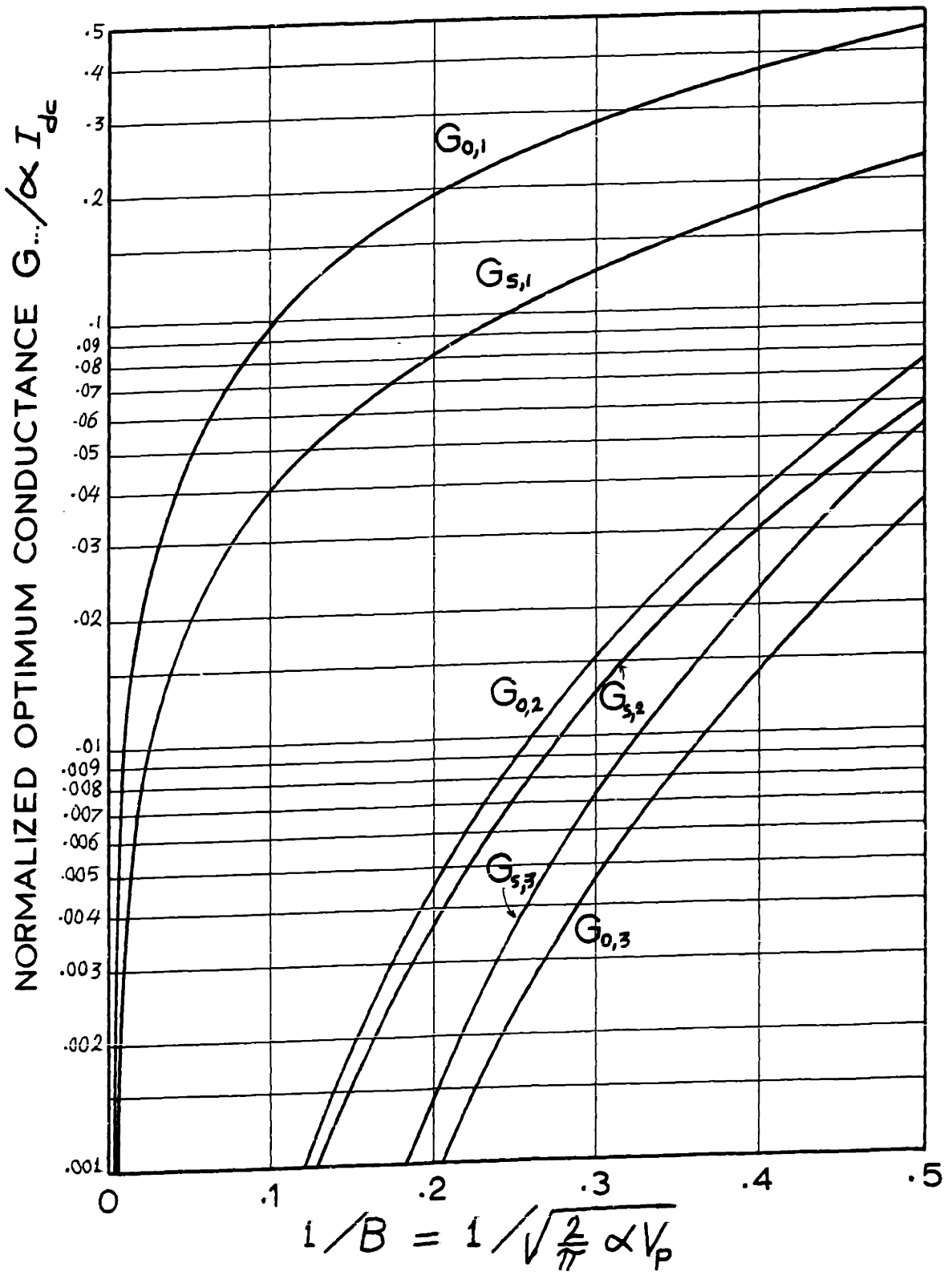

Fig. 4.12. The Optimum Source and Output Conductances for a Single-Diode G-Mixer

1. Short Image 2. Broadband Input 3. Open Image

$$G_{11} \approx \alpha I_{dc} \frac{2}{\pi} \frac{1}{V_p} \quad , \quad (4.69a)$$

$$G_{12} \approx \frac{2}{\pi} \quad , \quad (4.69b)$$

and

$$G_{13} \approx \alpha I_{dc} \frac{\pi}{3} \frac{1}{(\alpha V_p)^3} - G_{11} \quad . \quad (4.69c)$$

From Appendix 2 we get

$$\epsilon_1 = - \frac{G_{12}^2}{G_{11} G_{22}} \approx - B^2 \quad , \quad (4.70)$$

$$\theta = \frac{G_{13}}{G_{11}} \approx \frac{2}{3 B^4} - 1 \quad , \quad (4.71)$$

$$\epsilon_2 = \frac{2 \epsilon_1}{1 + \theta} \approx - 3 B^6 \quad , \quad (4.72)$$

and

$$\epsilon_3 = \frac{\epsilon_1}{1 - \epsilon_1} \frac{1 - \theta}{1 + \theta} \approx - 3 B^4 \quad , \quad (4.73)$$

where

$$B = \sqrt{\frac{2}{\pi} \alpha V_p} \qquad (>> 1) \qquad (4.74)$$

The performance of the G-mixer becomes:

1. Short Image

$$L_1 \approx 1 + 2/B \qquad (4.75a)$$

$$\approx 8.686/B \quad \text{db} \quad . \quad (4.75b)$$

$$G_{s,1} \approx \frac{4}{\pi^2} \alpha I_{dc}/B \qquad (4.76)$$

$$G_{o,1} \approx \frac{\pi^2}{4} G_{s,1} \qquad (4.77)$$

2. Broadband Input

$$L_2 \approx 2\left[1 + 2/(\sqrt{3}\,B^3)\right] \tag{4.78a}$$

$$\approx 3 + 8.686/(\sqrt{3}\,B^3) \tag{4.78b}$$

$$G_{s,2} \approx \frac{8}{\pi^2}\,\alpha\, I_{dc}/(\sqrt{3}\,B^3) \tag{4.79}$$

$$G_{o,2} \approx \frac{\pi^2}{8}\,G_{s,2} \tag{4.80}$$

3. Open Image

$$L_3 \approx 1 + 2/(\sqrt{3}\,B^2) \tag{4.81a}$$

$$\approx 8.686/(\sqrt{3}\,B^2) \tag{4.81b}$$

$$G_{s,3} \approx \frac{16}{\pi^2}\,\alpha\, I_{dc}/(\sqrt{3}\,B^4) \tag{4.82}$$

$$G_{o,3} \approx \frac{\pi^2}{16}\,G_{s,3} \tag{4.83}$$

Since the conductance waveform of the mixer, Eq. (4.62), approaches a square-wave for B >> 1, one would expect to obtain the above approximations with a square-wave resistance switching between two appropriate levels, say R_f and R_b. From Appendix 11, where an extensive analysis of square-wave mixers is given, one can show that the above expectation is true in some sense. It can be shown by comparison that the results of case 1 (short image) can be obtained if $R_f \approx 1/(2\alpha I_{dc})$ and $R_b \approx \pi^2 B^2/(2\alpha I_{dc})$ and that of case 2 (broadband input)

is obtained for the same R_f but with $R_b \approx 3\pi^2 B^6/(4\alpha I_{dc})$. The analysis in Appendix 11 predicts that the conversion loss of a G-mixer with an open image never attains unity for any square-wave resistance. On the other hand Eq. (4.81) for case 3 above shows that $L_3 \longrightarrow 1$ as $B \longrightarrow \infty$. This large discrepancy between the two results means that the performance of case 3 is very sensitive to the exact shape of the resistance waveform.

In Appendix 11, we also studied the degradations of the performance of a G- (or an H-) mixer due to incomplete terminations of the undesired frequencies. To make the calculations possible, the diode was modeled as an ideal switch driven in a square-wave fashion. The results apply only for cases 1 and 2 since case 3 cannot be represented by a square-wave resistance model as mentioned above.

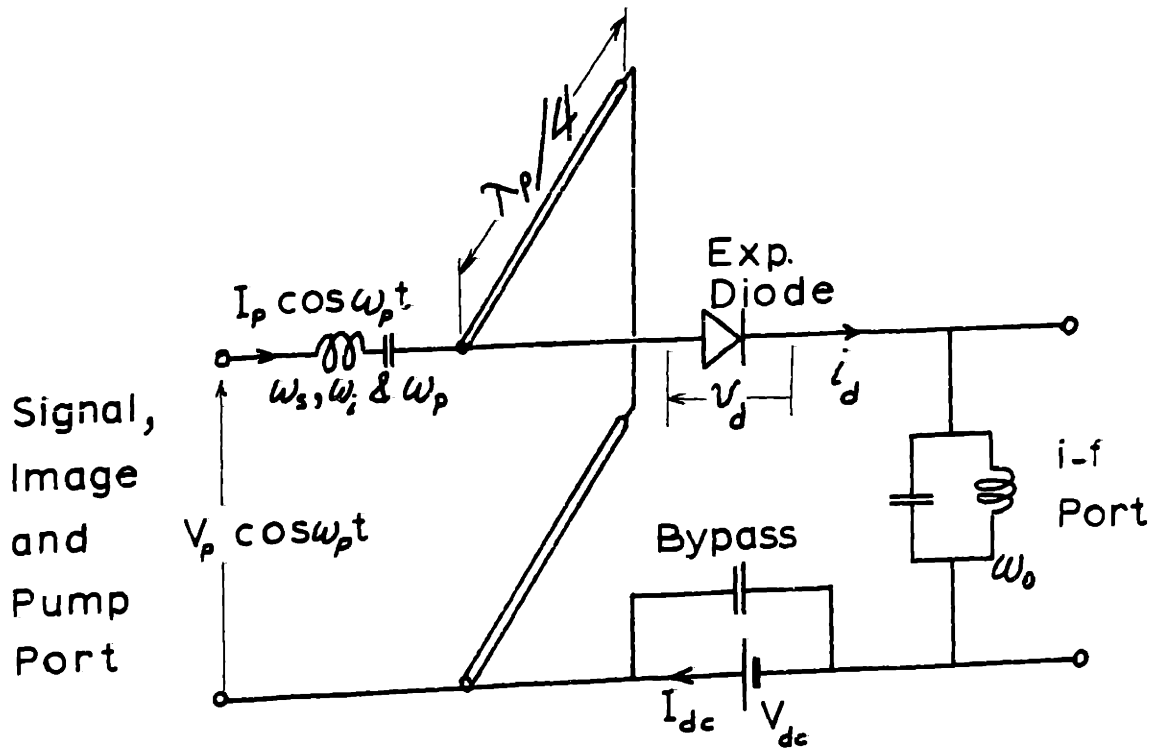

Fig. 4.13. Pumping a Single-Diode H-Mixer

4.2.4. The H-mixer:

The single-diode H-mixer is shown in Fig. 4.13 where the short-circuit quarter-wave line is intended to short-circuit all the even-order frequencies as suggested in Fig. 2.7. Beside the d-c and fundamental components of current and voltage, the circuit of Fig. 4.13 only allows current with even harmonics: $i_{ev}(t)$: $n\omega_p$, $|n|$ even ≥ 2; and voltage with odd harmonics: $v_{od}(t)$: $n\omega_p$, $|n|$ odd ≥ 3. Thus

$$i_d = I_{dc} + I_p \cos\omega_p t + i_{ev}(t) \quad , \quad (4.84)$$

and

$$v_d = V_{dc} + V_p \cos\omega_p t + v_{od}(t) \quad . \quad (4.85)$$

Substituting the above equations in Eq. (4.1) and employing the technique used to derive Eqs. (4.54) and (4.55) in the previous section, one obtains

$$i_d = - I_{sat} + I_{sat}\, e^{\alpha V_{dc}} \left[A \cos\omega_p t + \sqrt{1 + A^2 \cos^2(\omega_p t)}\right] \quad , \quad (4.86)$$

and

$$\alpha\left[V_p \cos\omega_p t + v_{od}(t)\right] = \sinh^{-1}(A \cos\omega_p t) \quad , \quad (4.87)$$

where

$$A = \frac{I_p}{I_{sat}\, e^{\alpha V_{dc}}} \quad . \quad (4.88)$$

Presumably, for given values of I_p and V_{dc}, one can calculate I_{dc} from Eq. (4.86) and V_p, and hence P_p and R_p, from Eq. (4.87). Unfortunately, the results of the Fourier integrals necessary for the analysis cannot be written in a closed form. However, for $I_p >> I_{sat}\, e^{\alpha V_{dc}}$, i.e. for $A >> 1$, one can obtain asymptotic approximations from the integrals. It is shown in Secs. A7.7 and A7.8 that for $A >> 1$

$$f_7(A) = \frac{1}{2\pi}\int_0^{2\pi} \sqrt{1 + A^2 \cos^2 x}\; dx \approx \frac{2}{\pi} A \quad , \quad (4.89)$$

and

$$f_8(A) = \frac{1}{2\pi}\int_0^{2\pi} \cos x \sinh^{-1}(A \cos x)\, dx \approx \frac{2}{\pi}\left[\log_e(4A) - 1\right] \quad . \quad (4.90)$$

Using these approximations and neglecting the reverse saturation current, Eq. (4.86) gives**

$$I_{dc} \approx \frac{2}{\pi} A\, I_{sat}\, e^{\alpha V_{dc}} \qquad (4.91a)$$

$$= \frac{2}{\pi} I_p \quad , \qquad (4.91b)$$

and Eq. (4.87) gives

$$\alpha V_p = \frac{4}{\pi} [\log_e(4A) - 1] \quad . \qquad (4.92)$$

Thus

$$P_p \approx \frac{I_{dc}}{\alpha} [\log_e(4A) - 1] \quad , \qquad (4.93)$$

and

$$R_p \approx \frac{8}{\pi^2} \frac{1}{\alpha I_{dc}} [\log_e(4A) - 1] \quad . \qquad (4.94)$$

The above bias and pump parameters, normalized in terms of appropriate quantities, are plotted in Fig. 4.14 as functions of 1/A. Exact calculations based on numerical integration of Eqs. (4.86) and (4.87) were used. Note that the value of A can be extremely high, especially if $V_{dc} \leq 0$.

The small signal conductance waveform is given from Eqs. (4.2) and 4.86) as

$$g(t) = \alpha\, I_{sat}\, e^{\alpha V_{dc}} [A \cos\omega_p t + \sqrt{1 + A^2 \cos^2\omega_p t}\,] \quad . \qquad (4.95)$$

** It is interesting to note that i_d approaches a half wave rectified sinusoidal current with amplitude = $2I_p$. This explains the $2/\pi$ factor in Eq. (4.91b).

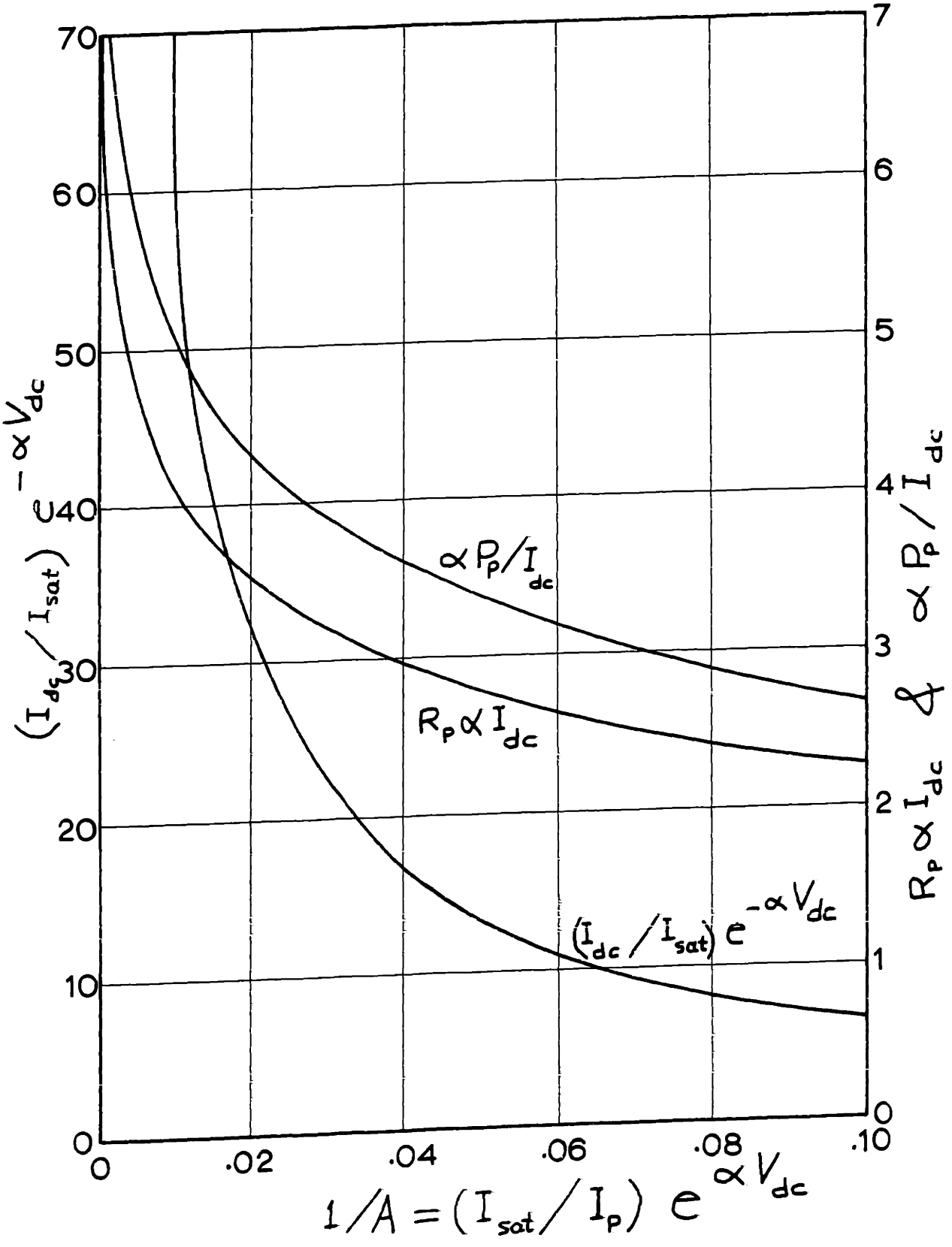

Fig. 4.14. Bias and Pump Parameters for a Single-Diode H-Mixer

The odd- and even-harmonic portions of g(t) are given by

$$g_{od}(t) = \alpha\, I_{sat}\, e^{\alpha V_{dc}}\, A \cos \omega_p t \qquad (4.96)$$

and

$$g_{ev}(t) = \alpha\, I_{sat}\, e^{\alpha V_{dc}} \sqrt{1 + A^2 \cos^2 \omega_p t} \quad . \qquad (4.97)$$

From Sec. 2.4.2, the mixer equations can be put in the H-matrix form

$$\begin{bmatrix} V_s \\ I_o \\ V_i^* \end{bmatrix} = \begin{bmatrix} H_{11} & H_{12} & H_{13} \\ -H_{12} & H_{22} & -H_{12} \\ H_{13} & H_{12} & H_{11} \end{bmatrix} \begin{bmatrix} I_s \\ V_o \\ I_i^* \end{bmatrix} \quad , \qquad (4.98)$$

where the H's are given by

$$H_{11} = \frac{e^{-\alpha V_{dc}}}{\alpha\, I_{sat}} \left\langle \frac{1}{\sqrt{1 + A^2 \cos^2 \omega_p t}} \right\rangle \quad , \qquad (4.99a)$$

$$H_{12} = - \left\langle \frac{A \cos \omega_p t}{\sqrt{1 + A^2 \cos^2 \omega_p t}} \cos \omega_p t \right\rangle \quad , \qquad (4.99b)$$

$$H_{13} = \frac{e^{-\alpha V_{dc}}}{\alpha\, I_{sat}} \left\langle \frac{\cos(2\omega_p t)}{\sqrt{1 + A^2 \cos^2 \omega_p t}} \right\rangle \quad , \qquad (4.99c)$$

and

$$H_{22} = \alpha\, I_{sat}\, e^{\alpha V_{dc}} \left\langle \frac{1}{\sqrt{1 + A^2 \cos^2 \omega_p t}} \right\rangle \quad , \qquad (4.99c)$$

where $\langle \ldots \rangle = \frac{1}{2\pi} \int_0^{2\pi} \ldots d\omega_p t.$

Using numerical integration of Eqs. (4.99), the optimum conversion loss, and source and output resistances for the three image terminations considered were calculated with the help of Appendix 2. The results are plotted in Figs. 4.15 and 4.16 as functions of 1/A.

The aforementioned results can be approximated using asymptotic expansions for the integrals when $A >> 1$, i.e. $I_p >> I_s e^{\alpha V_{dc}}$. It is shown in Secs. A7.9 and A7.10 that for $A >> 1$

$$f_9(A) = \frac{1}{2\pi} \int_0^{2\pi} \frac{1}{\sqrt{1 + A^2 \cos^2 x}} dx \approx \frac{2}{\pi} \frac{1}{A} \log_e(4A), \quad (4.100)$$

and

$$f_{10}(A) = \frac{1}{2\pi} \int_0^{2\pi} \frac{\cos x}{\sqrt{1 + A^2 \cos^2 x}} dx \approx \frac{2}{\pi} \frac{1}{A} . \quad (4.101)$$

Substituting these results in Eqs. (4.99)** and using Eqs. (4.88) and (4.91) we get

$$H_{11} \approx \frac{4}{\pi^2} \frac{1}{\alpha I_{dc}} \log_e(4A) , \quad (4.102a)$$

$$H_{12} \approx -\frac{2}{\pi} , \quad (4.102b)$$

** The integral needed for H_{13} can be obtained from $f_9(A)$ and $f_{10}(A)$ be expanding $\cos(2\omega_p t) = 2\cos^2(\omega_p t) - 1$.

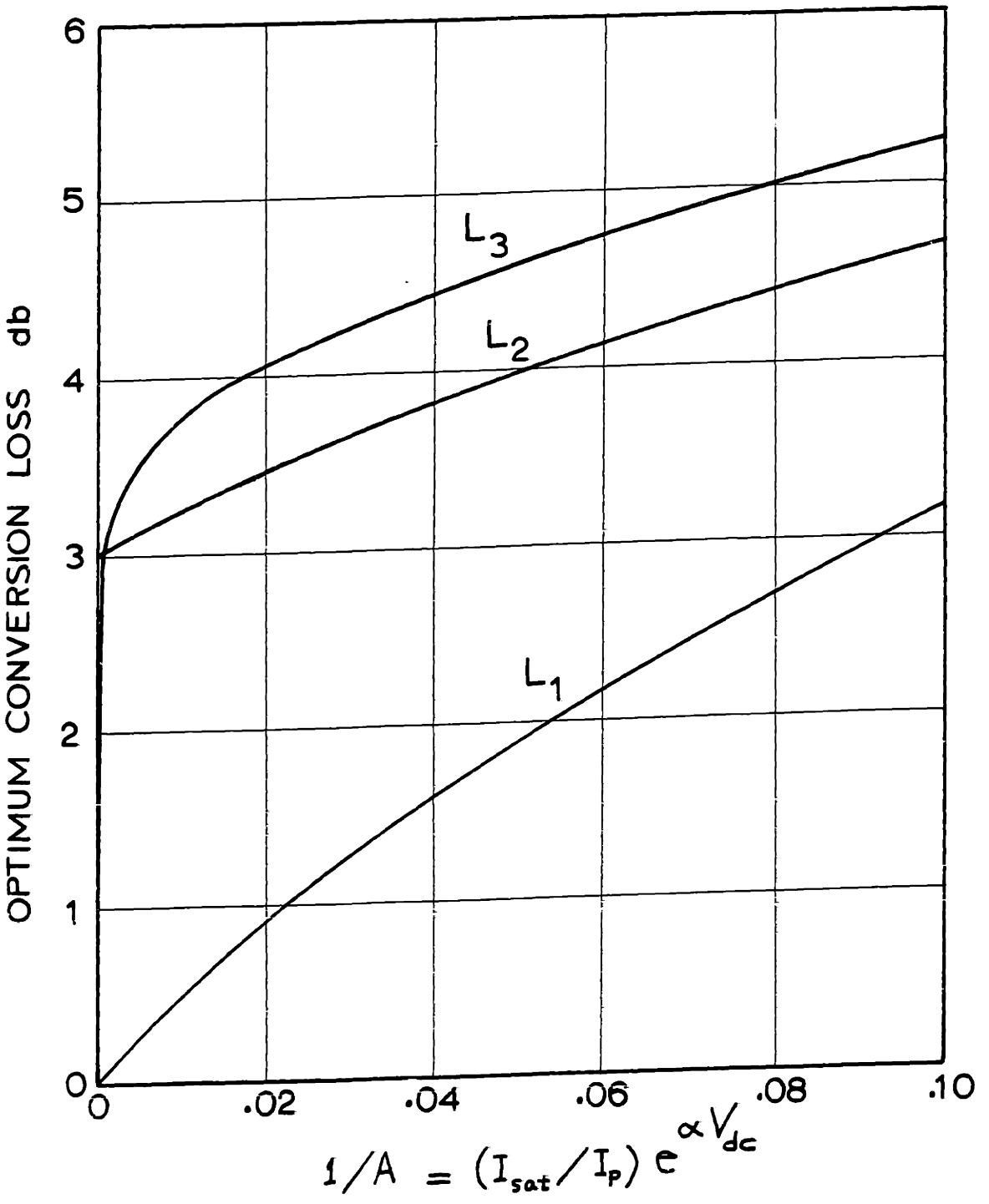

Fig. 4.15. The Optimum Conversion Loss of a Single-Diode H-Mixer (1. Open Image, 2. Broadband Input, 3. Short Image)

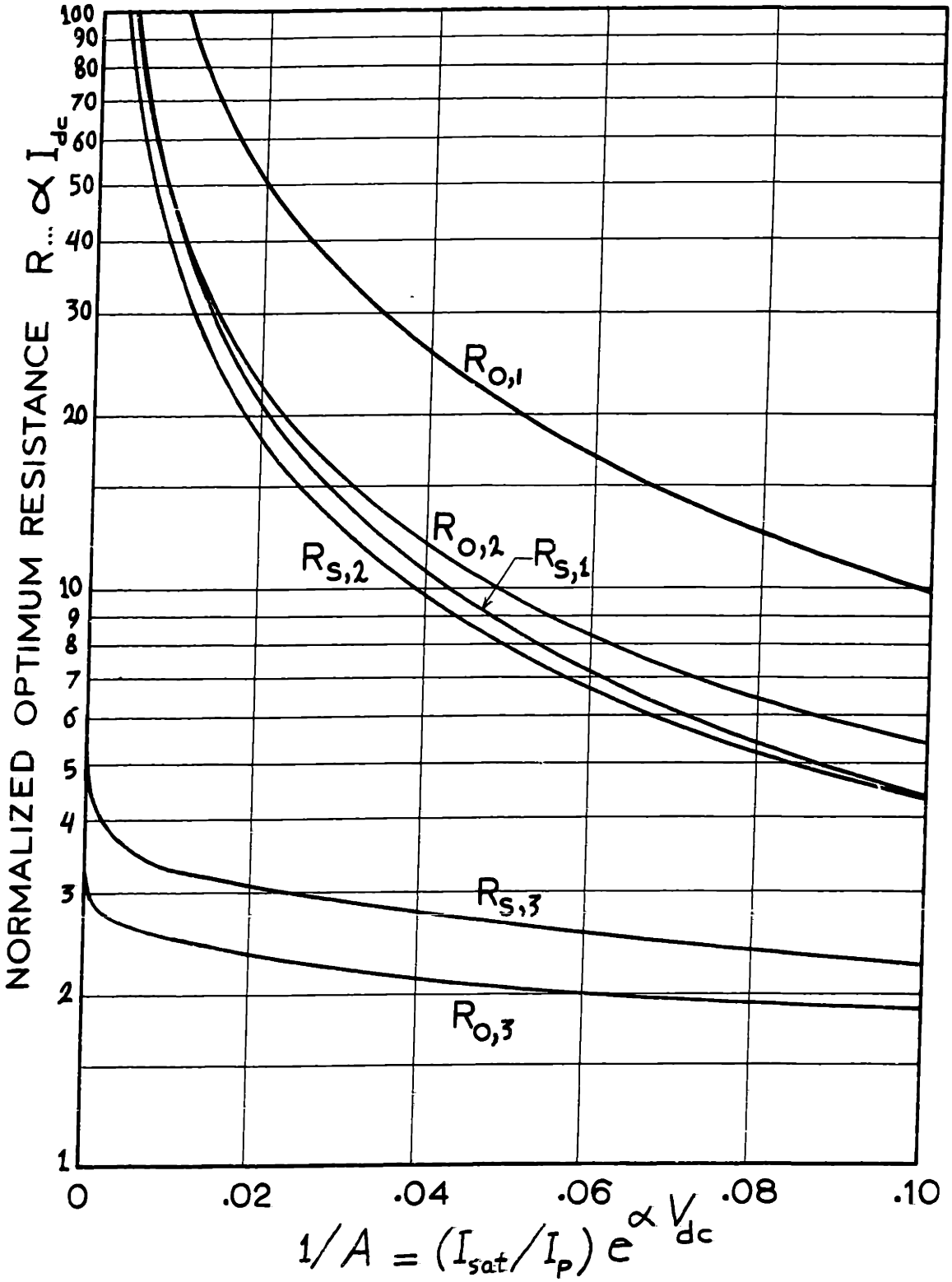

Fig. 4.16. The Optimum Source and Output Resistances for a Single-Diode H-Mixer
1. Open Image, 2. Broadband Input, 3. Short Image

$$H_{13} \approx \frac{8}{\pi^2} \frac{1}{\alpha I_{dc}} - H_{11} \quad , \quad (4.102c)$$

and

$$H_{22} \approx \frac{\alpha I_{dc}}{A^2} \log_e(4A) \quad . \quad (4.102d)$$

Appendix 2 gives

$$\epsilon_1 = \frac{-H_{12}^2}{H_{11} H_{12}} \approx - [A/\log_e(4A)]^2 \quad (4.103)$$

$$\theta = \frac{H_{13}}{H_{11}} \approx - 1 + 2/\log_e(4A) \quad (4.104)$$

$$\epsilon_2 = \frac{2\epsilon_1}{1 + \theta} \approx - A^2/\log_e(4A) \quad (4.105)$$

$$\epsilon_3 = \frac{\epsilon_1}{1 - \epsilon_1} \frac{1 - \theta}{1 + \theta} \approx - \log_e(4A) \quad . \quad (4.106)$$

The performance of the H-mixer becomes:

1. Open Image

$$L_1 \approx 1 + \frac{2}{A} \log_e(4A) \quad (4.107a)$$

$$\approx \frac{8.686}{A} \log_e(4A) \quad \text{db} \quad . \quad (4.107b)$$

$$R_{s,1} \approx \frac{4}{\pi^2} \frac{1}{\alpha I_{dc}} A \quad . \quad (4.108)$$

$$R_{o,1} \approx \frac{\pi^2}{4} R_{s,1} \quad . \quad (4.109)$$

2. Broadband Input

$$L_2 \approx 2\left[1 + \frac{2}{A}\sqrt{\log_e(4A)}\right] \qquad (4.110a)$$

$$\approx 3 + \frac{8.686}{A}\sqrt{\log_e(4A)} \quad \text{db} \quad . \qquad (4.110b)$$

$$R_{s,2} \approx \frac{8}{\pi^2}\frac{1}{\alpha I_{dc}} A/\sqrt{\log_e(4A)} \quad . \qquad (4.111)$$

$$R_{o,2} \approx \frac{\pi^2}{8} R_{s,2} \quad . \qquad (4.112)$$

3. Short Image**

$$L_3 \approx 1 + 2/\sqrt{\log_e(4A)} \qquad (4.113a)$$

$$\approx 8.686 / \sqrt{\log_e(4A)} \quad \text{db} \qquad (4.113b)$$

$$R_{s,3} \approx \frac{16}{\pi^2}\frac{1}{\alpha I_{dc}}\sqrt{\log_e(4A)} \quad . \qquad (4.114)$$

$$R_{o,3} \approx \frac{\pi^2}{16} R_{s,3} \quad . \qquad (4.115)$$

It can be shown from Appendix 11, where an extensive analysis of square-wave mixers is given, that a square-wave resistance switching between two appropriate levels, say R_f and R_b, can yield the same results as cases 1 (open image) and 2 (broadband input) above. For case 1, $R_f \approx 2\log_e(4A)/(\pi^2\alpha I_{dc})$ and $R_b \approx 2A^2/[\alpha I_{dc}\log_e(4A)]$; and for case 2, R_b has the same value

** The approximations here are valid for extremely large values of A since $\epsilon_3 \sim \log_e(A)$.

but $R_f \approx 4/(\pi^2 \alpha I_{dc})$. On the other hand no square-wave resistance can give the results of case 3 (an H-mixer with short image) since in this case the analysis of Appendix 11 predicts that the conversion loss never attains unity while Eq. (4.113) shows that $L_3 \longrightarrow 1$ as $A \longrightarrow \infty$.

In Appendix 11, we also studied the effect of the incomplete terminations on the performance of an H- (or a G-) mixer. A square-wave driven ideal-switch diode was used in the analysis to make the calculations possible. The results would only apply for cases 1 and 2 since case 3 cannot be represented by a square-wave resistance model as mentioned above.

4.2.5. Comparison

Here we compare the performance of the four mixers discussed above for identical d-c bias and pump conditions. Inspection of the small and large signal equations and/or figures for any of the mixers shows that the conversion loss can be determined with the knowledge of any of the following dimensionless quantities:**

$$X_1 = \frac{I_{dc}}{I_{sat}\, e^{\alpha V_{dc}}} \quad , \quad (4.118)$$

$$X_2 = \frac{\alpha\, P_p}{I_{sat}\, e^{\alpha V_{dc}}} \quad , \quad (4.119)$$

or

$$X_3 = \frac{\alpha\, P_p}{I_{dc}} = \frac{X_2}{X_1} \quad , \quad (4.120)$$

These three quantities will form our basis for the comparison.

The pump power that should be applied in practice to achieve a certain mixer performance is higher than P_p discussed above to compensate for circuit loss at the pump frequency. In fact P_p can be interpreted as the pump power applied to the diode junction only. Thus the quantities X_2 and X_3 will be less than those

** Note that α ($= q/kT \approx 40$ at room temperature) has the dimension of volt^{-1}.

obtained from measured data. However, X_1 should agree with practically measured data since it is only a function of d-c parameters.

From the previous analysis of the Y-, G- and H-mixers, it is shown that X_1, X_2 and X_3 approach infinity as the conversion loss approaches zero db. That is to say one needs infinite pump power and/or d-c bias to obtain an ideal Y-, G- or H-mixer. However, the Z-mixer is quite different since one can obtain a conversion loss of zero db with finite pump power and d-c bias, because in this case $X_1 = 2$, $X_2 = 2$ and $X_3 = 1$. Thus it seems that the Z-mixer is by far superior to any of the other three mixers.**

At this point it is appropriate to mention a possible disadvantage of the Z-mixer. The analysis given in Sec. 4.22 shows that the amount of pump power that can be applied to the diode is limited to $P_p < I_{dc}/\alpha$ (since $I_p < I_{dc}$ and $V_p < 2/\alpha$; also $X_1 < 2$, $X_2 < 2$ and $X_3 < 1$) otherwise the diode will be driven in the noisy breakdown region. This limit is very small (of the order of microwatts***) and hence, a large amount of nonlinear distortion could exist in the mixer except for extremely small power at the signal frequency or for large d-c

** See also Dragone (II, Sec. 9.3) where he showed that a Z-mixer is much better than a Y-mixer for the same amount of pump voltage swing across the diode.

*** For example for I_{dc} = 1 milliampere, $P_p < 25$ microwatt.

current bias. This problem seems not to exist for the Y-, G- and H-mixers.

The conversion losses of different configurations of the Y-, G- and H-mixers are plotted as functions of X_1, X_2 and X_3 in Figs. 4.17, 4.18 and 4.19 for X_1 ranging from 1 to 10^6, X_2 from 1 to 10^6 and X_3 from zero to 30. The performance of the Z-mixer was not plotted since its analysis is only valid for $X_1 < 2$, $X_2 < 2$ and $X_3 < 1$. From the nine curves given in each figure and from the previous discussion of the Z-mixer it appears that the ranking of the mixers is**

a). Image short or open ($L \geq 0$ db)

1. Z-mixer with open image.
2. H-mixer with open image.
3. G-mixer with open image.
4. Y-mixer with open image.
5. Y-, G- or H-mixer with short image.

b). Broadband input ($L \geq 3$ db)

6. Z-mixer.
7. H-mixer.
8. G-mixer.
9. Y-mixer.

The asymptotic approximations for the conversion losses of the aforementioned Y-, G- or H-mixer configurations for $\log_e X_1$, $\log_e X_2$ and $X_3 >> 1$, can be calculated with the help of the approximations given at the ends of Secs.

** A Z-mixer with short image was not considered since its minimum possible conversion loss is 7.66 db as can be seen from Fig. 4.7 or Eq. (4.48b).

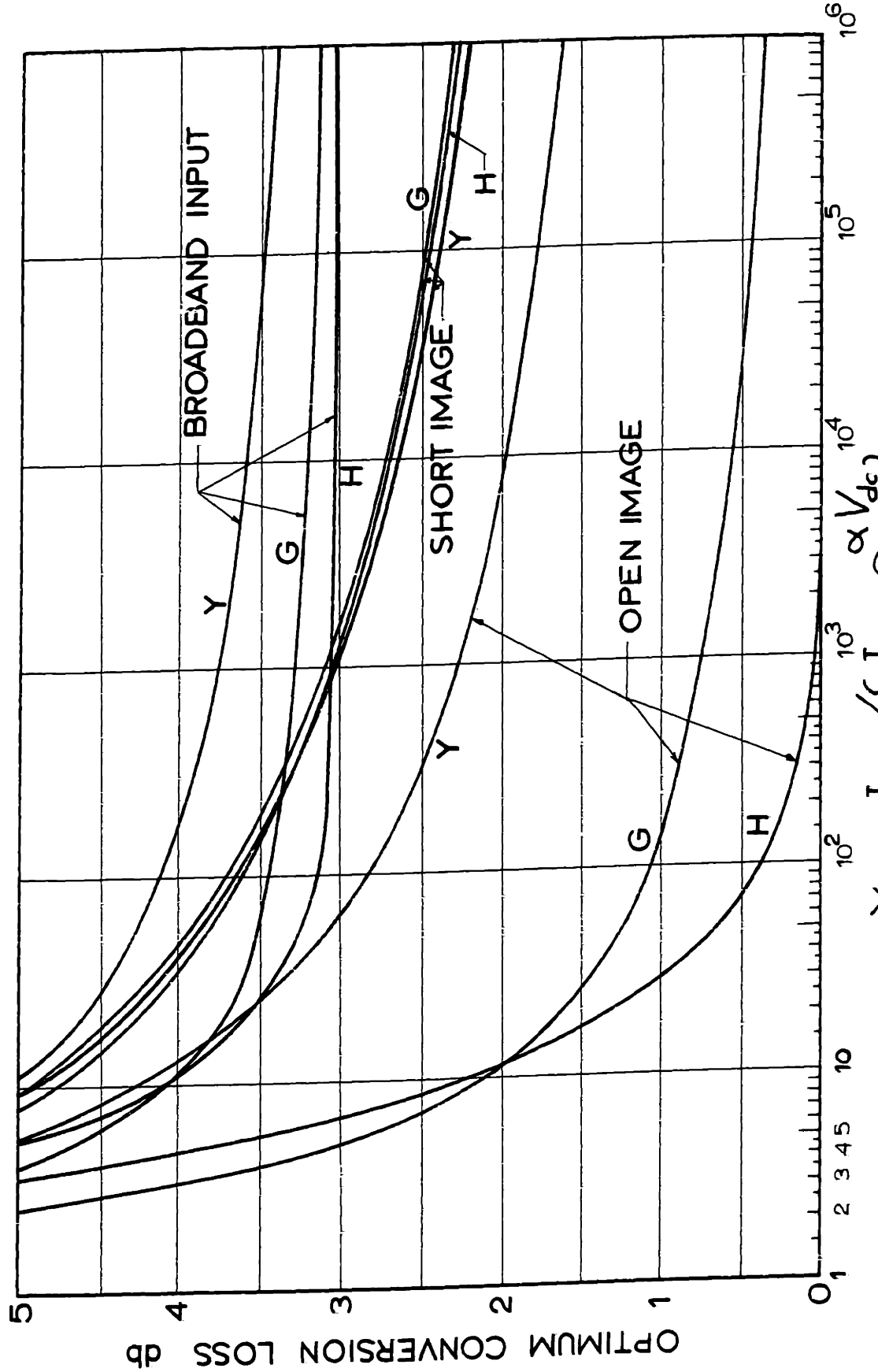

Fig. 4.17. The Optimum Conversion Losses of Y-, G- and H-Mixers as Functions of X_1

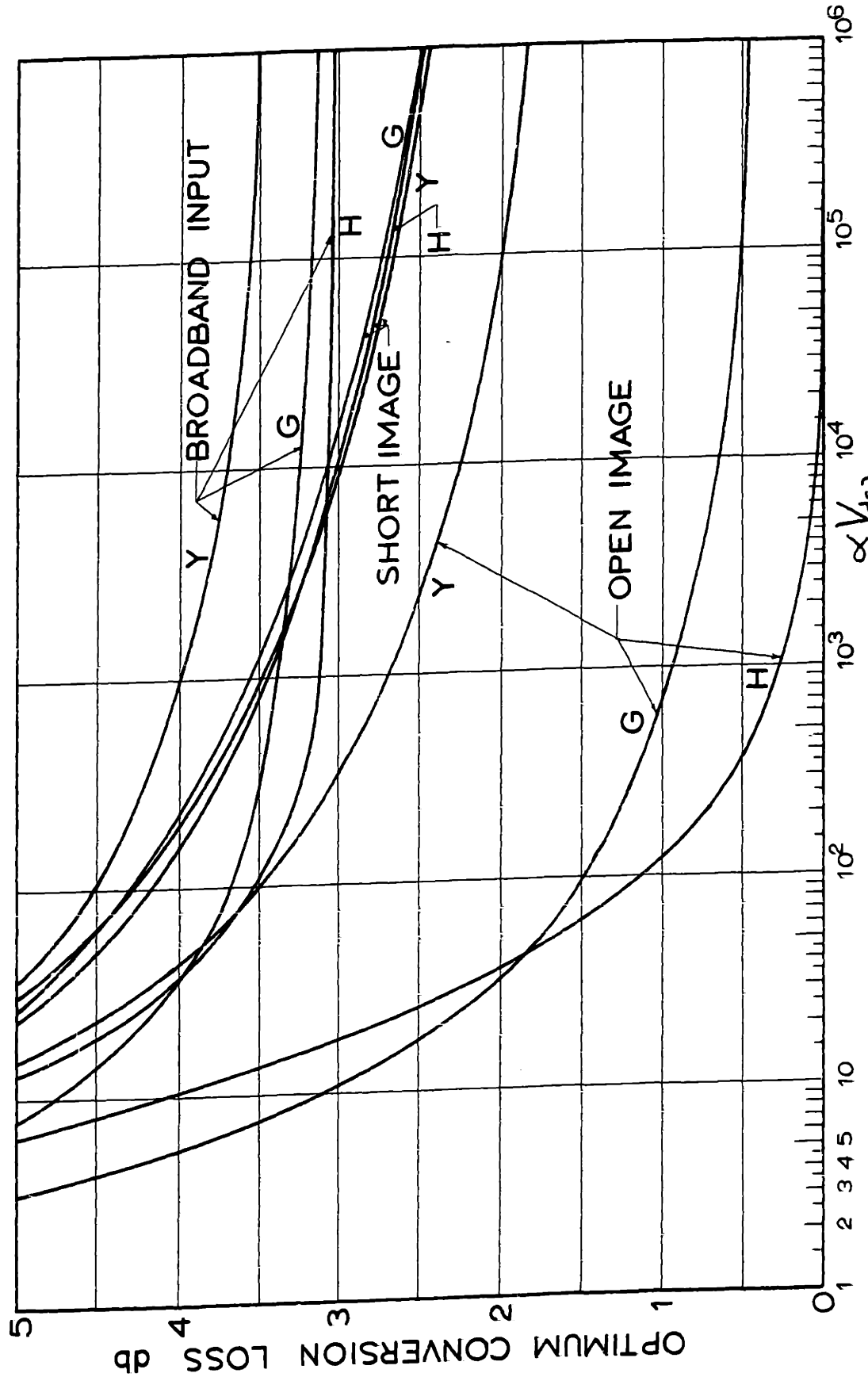

Fig. 4.18. The Optimum Conversion Losses of Y-, G- and H-Mixers as Functions of X_2

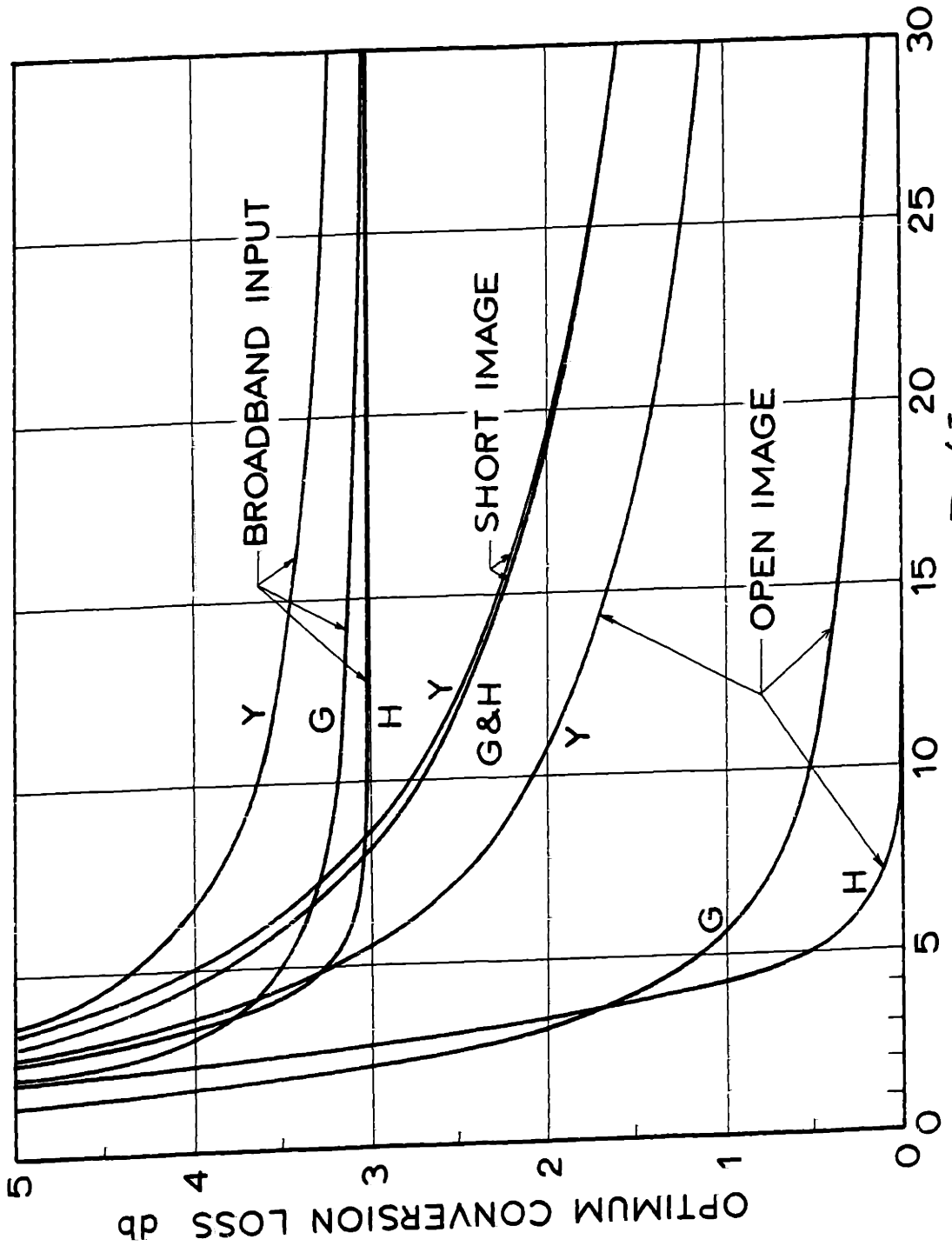

Fig. 4.19. The Optimum Conversion Losses of Y-, G- and H-Mixers as Functions of X_3

Table 4.1. Asymptotic Approximations of the Optimum Conversion Losses for Different Mixers with Short or Open Image for $\log X_1$, $\log X_2$ and $X_3 \gg 1$

MIXER TYPE	Image Termination	Conversion Loss in db		
		$X_1 = \frac{I_{dc}}{I_{sat} e^{\alpha V_{dc}}}$	$X_2 = \frac{\alpha P_p}{I_{sat} e^{\alpha V_{dc}}}$	$X_3 = \frac{\alpha P_p}{I_{dc}}$
Y-MIXER	Short	$\frac{8.686}{\sqrt{\log X_1}}$	$\frac{8.686}{\sqrt{\log X_2}}$	$\frac{8.686}{\sqrt{X_3}}$
	Open	$\frac{4.343\sqrt{2}}{\sqrt{\log X_1}}$	$\frac{4.343\sqrt{2}}{\sqrt{\log X_2}}$	$\frac{4.343\sqrt{2}}{\sqrt{X_3}}$
G-MIXER	Short	$\frac{8.686}{\sqrt{\log X_1}}$	$\frac{8.686}{\sqrt{\log X_2}}$	$\frac{8.686}{\sqrt{X_3}}$
	Open	$\frac{8.686/\sqrt{3}}{\log X_1}$	$\frac{8.686/\sqrt{3}}{\log X_2}$	$\frac{8.686/\sqrt{3}}{X_3}$
H-MIXER	Open	$\frac{8.686}{\pi/2}\frac{\log X_1}{X_1}$	$\frac{8.686}{\pi/2}\frac{[\log X_2]^2}{X_2}$	$\frac{8.686}{e/4} X_3 e^{-X_3}$
	Short	$\frac{8.686}{\sqrt{\log X_1}}$	$\frac{8.686}{\sqrt{\log X_2}}$	$\frac{8.686}{\sqrt{X_3}}$
Square-Wave H-mixer, Open Image or G-Mixer, Short Image		$\frac{4.343\pi}{X_1}$	$4.343\pi\frac{\log X_2}{X_2}$	$8.686\pi e^{-X_3}$

NOTE: Throughout the Table, $\log = \log_e$.

Table 4.2. Asymptotic Approximations of the Optimum Conversion Losses for Different Mixers with Broadband Input for $\log X_1$, $\log X_2$ and $X_3 >> 1$

Mixer Type	Conversion Loss in db		
	$X_1 = \frac{I_{dc}}{I_{sat} e^{\alpha V_{dc}}}$	$X_2 = \frac{\alpha P_p}{I_{sat} e^{\alpha V_{dc}}}$	$X_3 = \frac{\alpha P_p}{I_{dc}}$
Y-Mixer Broadband Input	$3 + \frac{4.343}{\log X_1}$	$3 + \frac{4.343}{\log X_2}$	$3 + \frac{4.343}{X_3}$
G-Mixer Broadband Input	$3 + \frac{8.686/\sqrt{3}}{[\log X_1]^{3/2}}$	$3 + \frac{8.686/\sqrt{3}}{[\log X_2]^{3/2}}$	$3 + \frac{8.686/\sqrt{3}}{X_3^{3/2}}$
H-Mixer Broadband Input	$3 + \frac{8.686}{\pi/2} \frac{\sqrt{\log X_1}}{X_1}$	$3 + \frac{8.686}{\pi/2} \frac{[\log X_2]^{3/2}}{X_2}$	$3 + \frac{8.686}{e/4} \sqrt{X_3}\, e^{-X_3}$
Square-Wave G- or H-Mixer, Broadband Input	$3 + \frac{4.343}{\sqrt{2}} \frac{\pi}{X_1}$	$3 + \frac{4.343\pi}{\sqrt{2}} \frac{\log X_2}{X_2}$	$3 + 4.343\sqrt{2}\, \pi\, e^{-X_3}$

NOTE: Throughout the Table, log = $\log_e$.

4.2.1, 4.2.3 and 4.2.4. The results are given in Tables 4.1 and 4.2. We also added the case of a square-wave driven exponential-diode G- or H-mixer for comparison.**

Although it seems from the above comparisons that the Y-mixer is the most inferior mixer, it is very important for high frequency applications. The reason being the finite diode junction capacitance which tends to short-circuit the high-order out-of-band frequencies. Thus, the realization of a Z-, G- or H-mixer will not be possible since, in each, one needs to open-circuit an infinite sequence of frequencies. On the other hand, if the diode series resistance is neglected, the Y-mixer can be easily realized.

Let us assume that the operating frequency is high enough such that the frequencies $\omega_n (= n\omega_p + \omega_o)$ are short-circuited by the junction capacitance for $|n| \geq 3$. That is to say in addition to the signal, i-f and image frequencies, voltage will exist across the diode at the sum frequency, ω_{+2}, and its image, ω_{-2}, only. Of course if these two frequencies are shorted, one obtains a stan-

** The results for this case are calculated as follows: It can be shown that if the exponential diode is driven by a large signal square-wave pump then its resistance will switch between R_f and R_b where $\delta = \sqrt{R_f/R_b} \approx 1/(2X_1) \approx [\log X_2]/(2X_2) \approx \exp(-X_3) \ll 1$. From Appendix 11, the conversion loss for a G-mixer with short image or an H-mixer with open image is $L \approx 1 + 2\pi\delta \approx 8.686\pi\delta$ db and for either mixer with broadband input is $L \approx 2\ (1 + \sqrt{2}\ \pi\delta)$ $\approx 3 + 4.343\ \sqrt{2}\ \pi\delta$ db.

dard Y-mixer. On the other hand, if they are open-circuited one will obtain a first order realization of a Z- or G-mixer. In this case it seems that the performance of the mixer will be superior to the standard Y-mixer. However, It is shown in Appendix 9, where we studied the asymptotic behaviour of a Y-mixer with open-circuited ω_{+2} and ω_{-2}, that the standard Y-mixer is better.** Thus, it seems that one needs to open-circuit frequencies of higher order than $\omega_{\pm 2}$ to improve the performance of the Y-mixer. It is not clear how many and which frequencies should be opened to improve the mixer performance since the analysis gets to be very complex.

Clearly, the value of the optimum conversion loss for any of the mixers can be decreased by increasing the values of X_1, X_2 and X_3. This, of course, can be done by increasing the pump power. However, it is interesting to note that the same effect can be acheived by increasing the diode d-c bias voltage in the negative direction while keeping the pump power fixed as can be observed from Eq. (4.119). This, however, has two main limitations: 1. The diode might be driven in its noisy breakdown region; 2. The value of the d-c current may

** Note that open-circuiting ω_{+2} and ω_{-2} implies that the second harmonic of the pump will also be open-circuited. Thus, one has to calculate the new diode conductance waveform which complicates the analysis considerably.

be very small such that the value of the optimum source resistance will be too large to be achieved in practice, since $R_{s,opt} \sim 1/(\alpha I_{dc})$. This last point is very serious and seems to form an important limit on the mixer performance in practice. For this purpose it appears desirable to calculate and compare the actual conversion losses of the different mixers when a source resistance much less than the optimum source resistance is used.

It is shown in Sec. A1.5 that the conversion loss, L, associated with a given source resistance, R_s, can be calculated from the values of the optimum conversion loss, L_{opt}, and the optimum source resistance, $R_{s,opt}$, by using Eq. (A1.44) which is rewritten here as

$$L = L_{opt} \frac{1 + \frac{1}{2} \frac{L_{opt}^2 - 1}{L_{opt}^2 + 1} \left\{ \frac{R_s}{R_{s,opt}} + \frac{R_{s,opt}}{R_s} \right\}}{1 + \frac{L_{opt}^2 - 1}{L_{opt}^2 + 1}} \quad . \quad (4.121)$$

This equation is valid only for reciprocal (at least in the magnitude sense, i.e., $|z_{12}| = |z_{21}|$) two-port networks. Thus, for our case, it can be applied only to mixers with open or short image. On the other hand, it can be shown that it also applies to mixers with broadband input if L and L_{opt}, in Eq. (4.121), are replaced by L/2 and $L_{opt}/2$.

Let L_{opt} and $R_{s,opt}$ be represented by the approximate relations

$$L_{opt} \approx 1 + a\,\delta_1 \quad , \quad (4.122)$$

and

$$R_{s,opt} \approx \frac{b}{\alpha I_{dc}} \frac{1}{\delta_2} \quad , \quad (4.123)$$

where "a" and "b" are constants of the order of unity and δ_1 and δ_2 are small parameters which depend on the d-c bias and pump power. Inspection of the approximations at the ends of Secs. 4.2.1 ... 4.2.4 show that the above two equations are general representations for any strongly pumped mixer.** Now let the actual source resistance, R_s, satisfy the condition

$$R_s \ll R_{s,opt} \quad , \quad (4.124)$$

which is usually the case as discussed above. Substitution in Eq. (4.121) gives

$$L \approx 1 + \frac{1}{2} \frac{ab}{\alpha I_{dc} R_s} \frac{\delta_1}{\delta_2} \quad . \quad (4.125)$$

For the purpose of clarity, we give in Fig. 4.20 typical

** For example for a Y-mixer with short image, Eqs. (4.17) and (4.18) give a = 2, b = 1 and $\delta_1 = \delta_2 = 1/\sqrt{\alpha V_p}$; for a Y-mixer with broadband input, Eqs. (4.19) and (4.20) give a = $\sqrt{2}$, b = $1/\sqrt{2}$ and $\delta_1 = \delta_2 = 1/\alpha V_p$; and for a Y-mixer with open image, Eqs. (4.22) and (4.23) give a = $\sqrt{2}$, b = $1/2\sqrt{2}$, $\delta_1 = 1/\sqrt{\alpha V_p}$ and $\delta_2 = (\alpha V_p)^{-3/2}$. Note that in the second case, Eq. (4.122) represented $L_{opt/2}$ rather than L_{opt}.

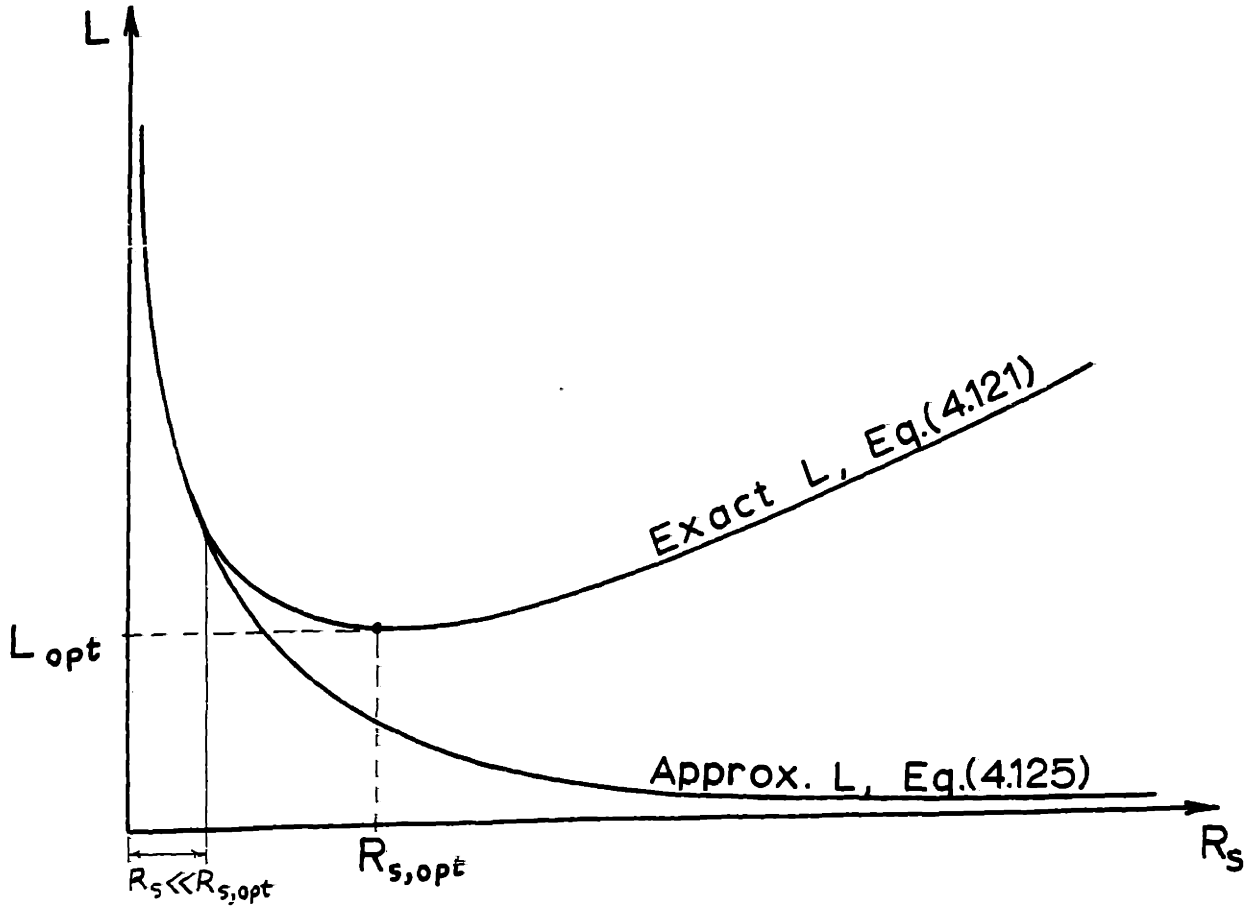

Fig. 4.20. Typical Plots of Eqs. (4.121) and (4.25)

plots of the approximate value of L as given from the above equation and the exact value of L as given from Eq. (4.121) as functions of R_s.

The approximate value of L, Eq. (4.125), for different strongly pumped mixers is given in Table 4.3 as a function of I_{dc}, $R_s (\ll R_{s,opt})$ and X_3 $(=\alpha P_p/I_{dc} \gg 1)$ which is used to represent the diode bias and pump conditions. It is observed that most of the entries of the tables are independent of X_3. This comes about since for most mixers $\delta_1 = \delta_2$. However, for the three cases, Y-, G- and H-mixers with open image it seems that L increases

Table 4.3. The Conversion Losses for Different Mixers for $R_s << R_{s,opt}$ and $X_3 = \alpha P_p / I_{dc} >> 1$

MIXER TYPE	IMAGE TERMINATION	CONVERSION LOSS (RATIO)
Y-MIXER	Short Image	$1 + \frac{1}{\alpha I_{dc} R_s}$
	Broadband Input	$2\left(1 + \frac{1}{2}\frac{1}{\alpha I_{dc} R_s}\right)$
	Open Image	$1 + \frac{1}{4}\frac{1}{\alpha I_{dc} R_s} X_3$
Z-MIXER	Open Image	$1 + \frac{2}{\alpha I_{dc} R_s}$
	Broadband Input	$2\left(1 + \frac{2}{\alpha I_{dc} R_s}\right)$
G-MIXER	Short Image	$1 + \frac{\pi^2}{4}\frac{1}{\alpha I_{dc} R_s}$
	Broadband Input	$2\left(1 + \frac{\pi^2}{8}\frac{1}{\alpha I_{dc} R_s}\right)$
	Open Image	$1 + \frac{\pi^2}{16}\frac{1}{\alpha I_{dc} R_s} X_3$
H-MIXER	Open Image	$1 + \frac{4}{\pi^2}\frac{1}{\alpha I_{dc} R_s} X_3$
	Broadband Input	$2\left(1 + \frac{8}{\pi^2}\frac{1}{\alpha I_{dc} R_s}\right)$
	Short Image	$1 + \frac{16}{\pi^2}\frac{1}{\alpha I_{dc} R_s}$

as X_3 increases. Actually this means that there is an optimum value for X_3 because it is obvious that the exact value of L will increase as X_3 decreases since in this case L_{opt} will increase. Thus to find the optimum value of X_3 one needs to use at least second order approximations for L_{opt}, $R_{s,opt}$ and L instead of the first order approximations given in Eqs. (4.122) ... (4.125). However, without going through this complicated analysis, since the value of X_3 should be large if L_{opt} is to be small, it appears that these three mixers (Y-, G- and H-mixers with open image) will have conversion losses higher than or comparable to those of the other mixers.

It is interesting to note that the same three mixers, when supplied with their optimum source resistances, gave better performance than the Y-, G- and H-mixers with short image as can be seen from Figs. 4.17, 4.18 and 4.19 or Table 4.1. However, their optimum source resistances are extremely high. Thus it seems that while one mixer can be superior under certain conditions it can be inferior under other conditions. Hence, no general statement can be made as to which mixer is best.

4.3. Multi-diode Mixers

Unlike a single-diode mixer, a multi-diode mixer can be pumped by an arbitrary waveform independent of the terminations offered by the imbedding network to the undesired frequencies. This is true provided that these terminations are applied to the diodes as a whole and not to each diode by itself. As mentioned earlier, the latter case produces results identical to those of a single-diode mixer since each diode by itself acts as a single-diode mixer.

The particular prototype multi-diode mixer considered will be the four-diode doubly balanced ring mixer.** This will be terminated to form a Z-, Y-, H- or G-mixer as shown in Figs. 2.9a, 2.10a, 2.11a or 2.12a respectively. Two kinds of pumping will be discussed; sinusoidal voltage pumping and sinusoidal current pumping.

4.3.1. Duality in ring mixers with exponential diodes:

Before proceeding with the analysis of any particular method of pumping, we derive general equations and duality relations for the ring mixer. Referring to Fig. 4.21, the diode voltage is given by

$$v_d = V_{dc} + v_p(t) \quad , \quad (4.126)$$

** See Chapter 2, or Caruthers (I), Tucker (I) and (IV), or Belevitch (II).

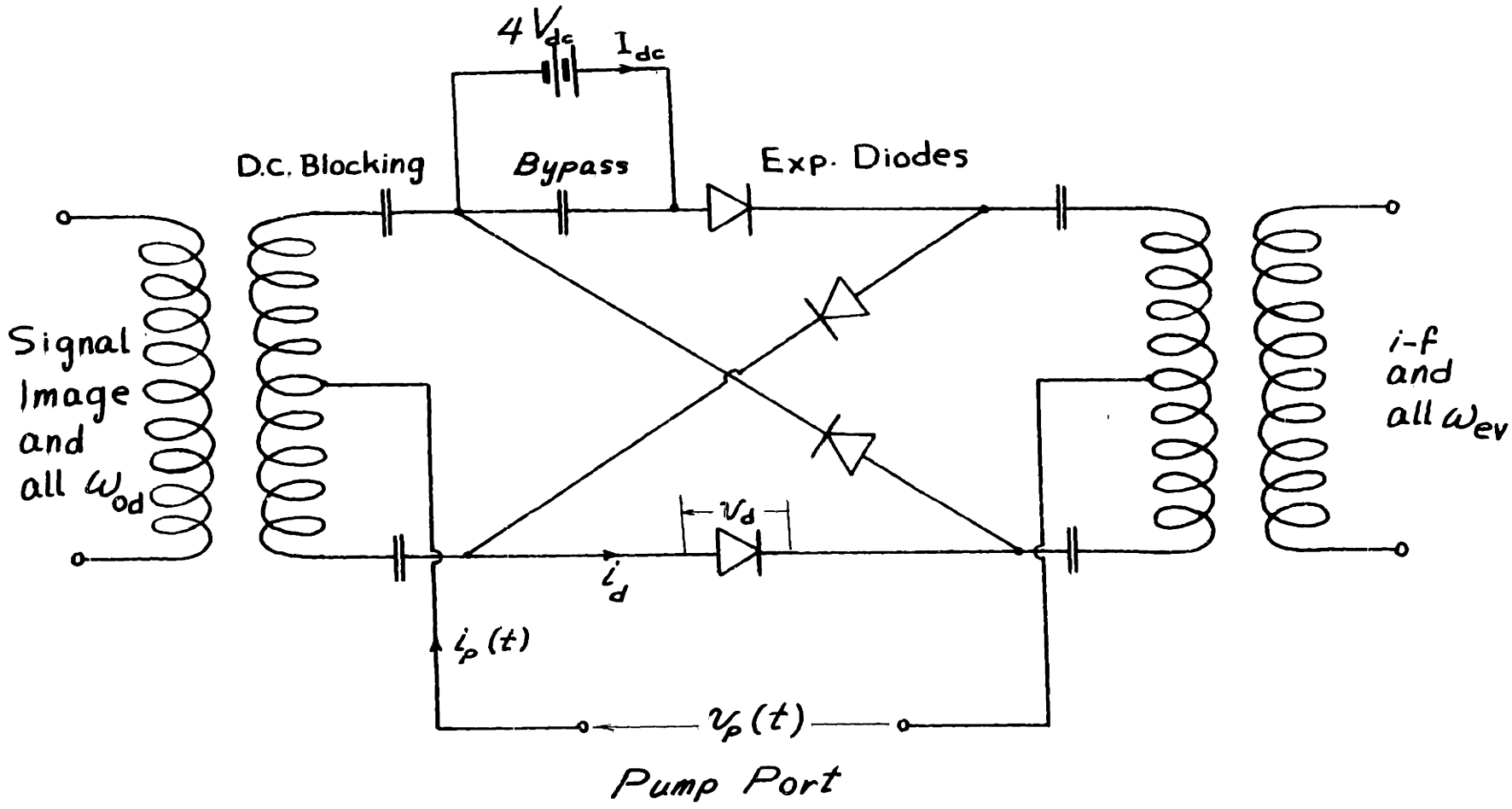

Fig. 4.21. Pumping the Four-Diode Doubly Balanced Ring Mixer

where $v_p(t)$ is the voltage waveform in the pump port. Thus, for exponential diodes, the diode current is given by

$$i_d = I_{sat}\, e^{\alpha V_{dc}}\, e^{\alpha v_p(t)} - I_{sat} \quad , \quad (4.127)$$

and hence its conductance waveform is

$$g(t) = \alpha I_{sat}\, e^{\alpha V_{dc}}\, e^{\alpha v_p(t)} \quad , \quad (4.128)$$

and its resistance waveform is

$$r(t) = \frac{1}{g(t)} = \frac{1}{\alpha I_{sat}\, e^{\alpha V_{dc}}}\, e^{-\alpha v_p(t)} \quad (4.129)$$

Adding the currents in the four diodes with the proper sign, Eq. (4.127) gives the pump current as

$$i_p(t) = 4\, I_{sat}\, e^{\alpha V_{dc}} \sinh[\alpha v_p(t)] \quad . \quad (4.130)$$

The property of the ring mixer to separate the even- and odd-order frequencies is only true if $v_p(t)$ contains only odd harmonics of the pump frequency ω_p, i.e.

$$v_p(t) = - v_p\,(t + \pi/\omega_p) \quad . \quad (4.131)$$

It follows from Eq. (4.130) that $i_p(t)$ also must have only odd harmonics of ω_p. If this is assumed, an interesting duality relation exists for the ring mixer. This is given from Eqs. (4.128), (4.129) and (4.131) by

$$\frac{g(t)}{\alpha I_{sat}\, e^{\alpha V_{dc}}} = r(t + \pi/\omega_p)\ \alpha\ I_{sat}\, e^{\alpha V_{dc}} \quad , \quad (4.132)$$

which is only true for exponential diodes. This duality relation** is very important since it tells us that the performance of a ring Y-mixer is identically the dual of that of a ring Z-mixer. Thus, for the same $v_p(t)$, the optimum conversion loss of a Y-mixer with short image, broadband input or open image is equal to that of a Z-mixer with open image, broadband input or short image respectively. Also, because of the "$\alpha I_{sat}\ \exp(\alpha V_{dc})$" factors in Eq. (4.132), if G_s and G_o are the optimum source and output conductances for a Y-mixer, and R_s and R_o are the optimum source and output resistances for the dual Z-mixer, Then

$$\frac{[G_s \text{ or } G_o]}{\alpha I_{sat}\, e^{\alpha V_{dc}}} = [R_s \text{ or } R_o]\ \alpha I_{sat}\, e^{\alpha V_{dc}} \quad . \quad (4.133)$$

Of course, all the above duality relations will also hold between the ring G- and H-mixers.

4.3.2. Sinusoidal voltage pumping:

If the ring mixer of Fig. 4.21 is pumped by a sinusoidal voltage as indicated in Fig. 4.22, it follows

** The constant phase shift π/ω_p is, of course, not important.

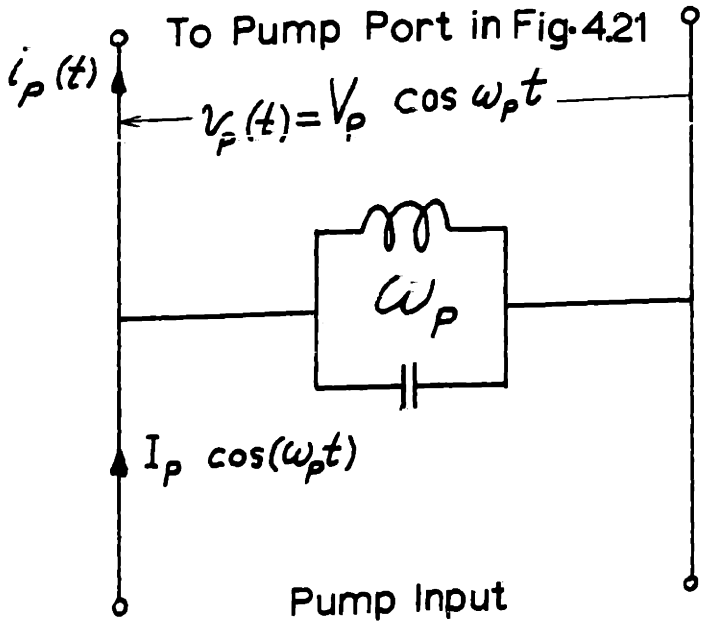

Fig. 4.22. Sinusoidal Voltage Pumping

that

$$v_p(t) = V_p \cos \omega_p t \quad , \quad (4.134)$$

and hence the diode voltage is given by

$$v_d = V_{dc} + V_p \cos \omega_p t \quad , \quad (4.135)$$

which is identical to that of a single-diode Y-mixer. Thus, the analysis given for the bias and pump conditions discussed in Sec. 4.2.1 applies here. Of course, the parameters I_p, P_p and G_p for the ring mixer are four times those appearing in Eqs. (4.8) ... (4.10) for the same V_p. The small signal conductance waveform for each diode is identical to that given in Eqs. (4.11). We

rewrite it here as

$$g(t) = \alpha I_{sat} e^{\alpha(V_{dc} + V_p \cos\omega_p t)} \quad . \quad (4.136)$$

According to Sec. 2.3, the performance of the Y-mixer connected in a ring configuration will be identical to that of the single-diode Y-mixer. Thus, all the results of Sec. 4.2.1 apply for the ring Y-mixer.

According to the duality relation discussed in the previous section, it follows that the performance of the Z-mixer in this case is identically the dual to that of the Y-mixer. The performance curves of the ring Y- and Z-mixers are plotted in Figs. 4.23 and 4.24 as functions of $1/\sqrt{\alpha V_p}$. These curves present the same results as Figs. 4.3 and 4.4 of the single-diode Y-mixer.

To analyze the G-mixer, one needs the even- and odd- harmonic portions of g(t). These are given from Eq. (4.131) as

$$g_{ev}(t) = \alpha I_{sat} e^{\alpha V_{dc}} \cosh(\alpha V_p \cos\omega_p t) \quad . \quad (4.137)$$

and

$$g_{od}(t) = \alpha I_{sat} e^{\alpha V_{dc}} \sinh(\alpha V_p \cos\omega_p t) \quad . \quad (4.138)$$

The equations of the mixer can now be put in the G-matrix form of Eq. (4.65), where the G's are given, from Sec. 2.42 and the above equations by

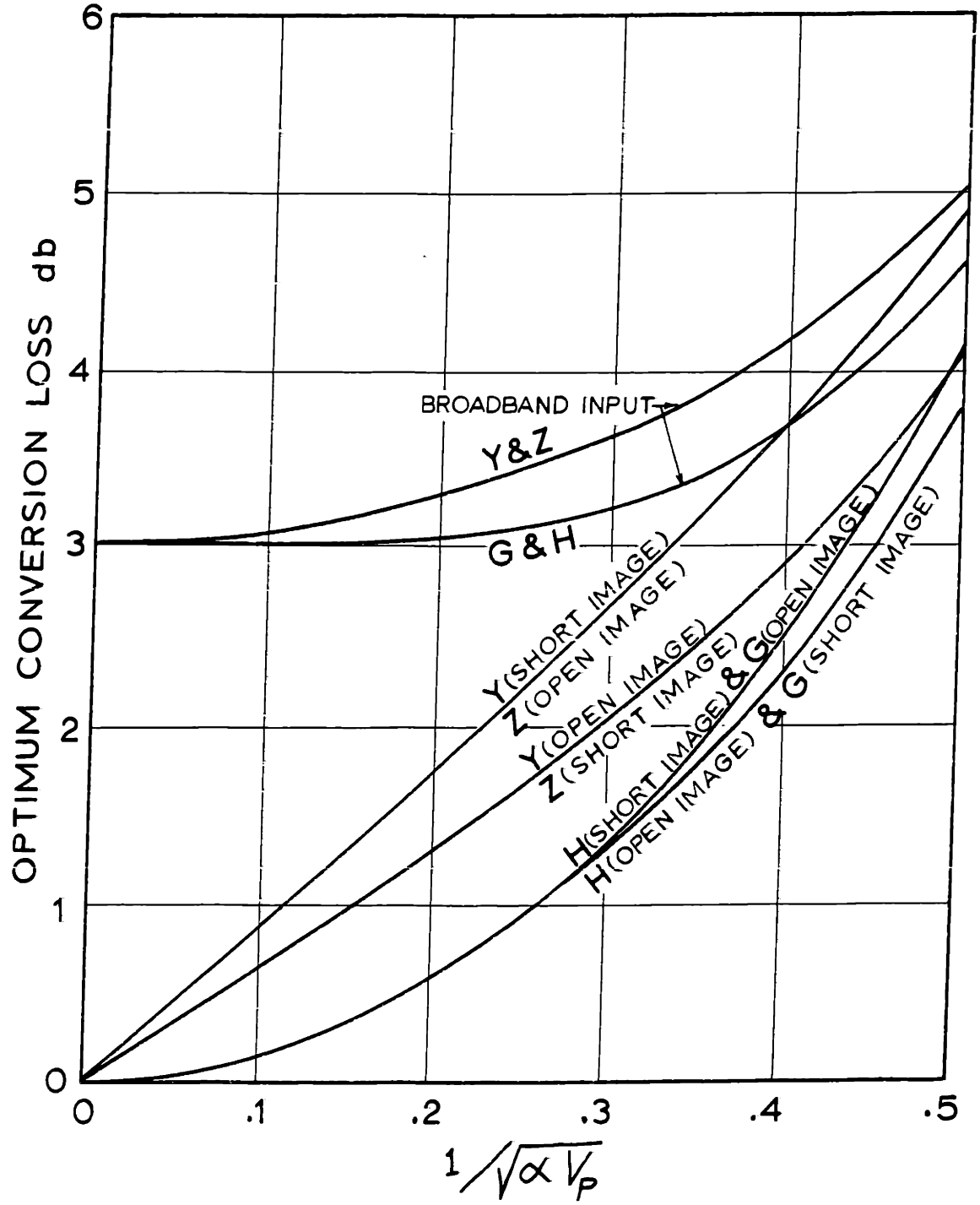

Fig. 4.23. The Optimum Conversion Losses for Different Configurations of Ring Y-, Z-, G- and H-Mixers with Sinusoidal Voltage Pumping

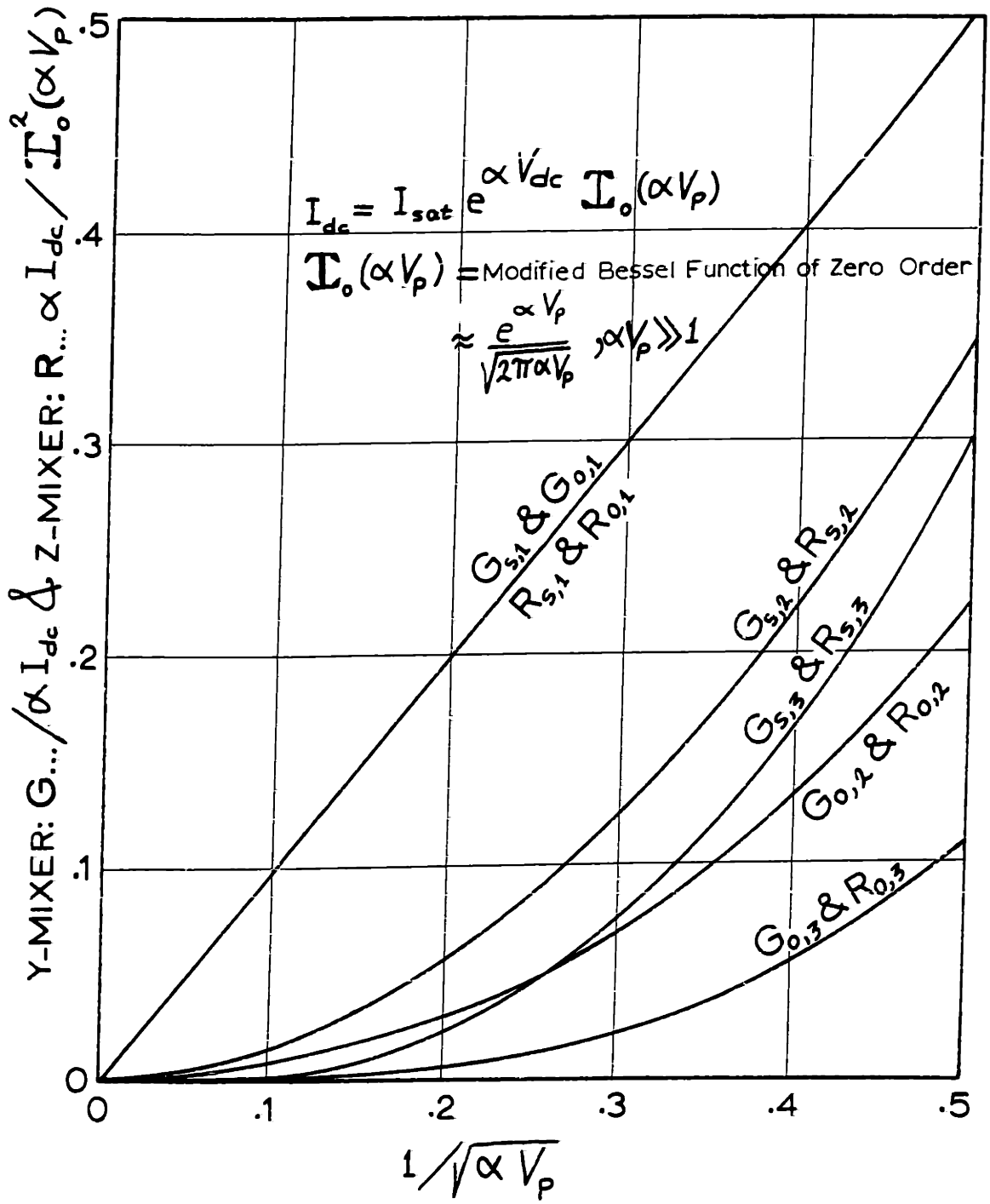

Fig. 4.24. Optimum Source and Output Resistances and Conductances for Ring Z- & Y-Mixers with Sinusoidal Voltage Pumping
Z-Mixer (1. Open Image, 2. Broadband Input, 3. Short Image)
Y-Mixer (1. Short Image, 2. Broadband Input, 3. Open Image)

$$G_{11} = \alpha I_{sat}\, e^{\alpha V_{dc}} \left\langle \operatorname{sech}(\alpha V_p \cos\omega_p t) \right\rangle \quad , \quad (4.139a)$$

$$G_{12} = \left\langle \cos\omega_p t \, \tanh(\alpha V_p \cos\omega_p t) \right\rangle \quad , \quad (4.139b)$$

$$G_{13} = \alpha I_{sat}\, e^{\alpha V_{dc}} \left\langle \cos(2\omega_p t) \, \operatorname{sech}(\alpha V_p \cos\omega_p t) \right\rangle \quad (4.139c)$$

and

$$G_{22} = \frac{e^{-\alpha V_{dc}}}{\alpha I_{sat}} \left\langle \operatorname{sech}(\alpha V_p \cos\omega_p t) \right\rangle \quad , \quad (4.139d)$$

where $\left\langle \ldots \right\rangle = \frac{1}{2\pi} \int_0^{2\pi} \ldots \, d\omega_p t$.

Using the numerical integration of Eqs. (4.139), the performance of the ring G-mixer was calculated for different image terminations with the help of Appendix 2. The results are plotted in Figs. 4.23 and 4.25. The same results also hold for the ring H-mixer because of the duality relation mentioned in the previous section.

If $\alpha V_p \gg 1$, the results of the G-mixer can be approximated by using asymptotic expansions of the integrals The integral required for G_{12} is evaluated in Sec. A7.1 and is given in Eq. (4.56). The remaining integrals are found from Secs. A7.5 and A7.6 to be

$$f_5(A) = \frac{1}{2\pi} \int_0^{2\pi} \operatorname{sech}(A \cos x) \, dx \approx \frac{1}{A} \quad (4.140)$$

and

$$f_6(A) = \frac{1}{2\pi} \int_0^{2\pi} \cos(2x) \operatorname{sech}(A \cos x) \, dx \approx \frac{\pi^2}{2} \frac{1}{A^3} - f_5(A), \quad (4.14$$

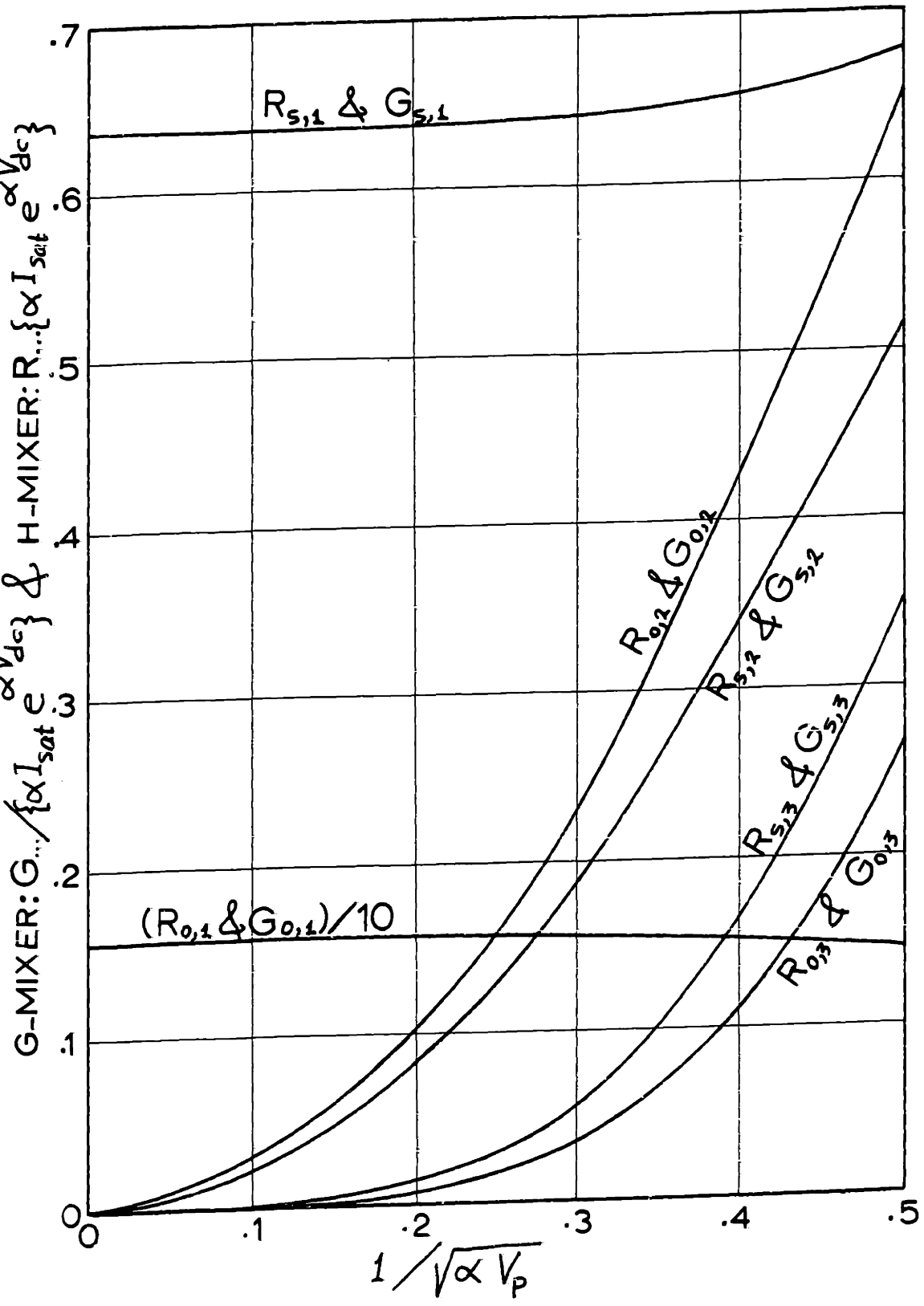

Fig. 4.25. Optimum Source and Output Resistances and Conductances for Ring H- & G-Mixers with Sinusoidal Voltage Pumping
H-Mixer (1. Open Image, 2. Broadband Input, 3. Short Image)
G-Mixer (1. Short Image, 2. Broadband Input, 3. Open Image)

for A >> 1. The G's can now be approximated by

$$G_{11} \approx \alpha I_{sat}\, e^{\alpha V_{dc}} \frac{1}{\alpha\, V_p} \quad , \quad (4.142a)$$

$$G_{12} \approx \frac{2}{\pi} \quad , \quad (4.142b)$$

$$G_{13} \approx \alpha\, I_{sat}\, e^{\alpha V_{dc}} \frac{\pi^2}{2} \frac{1}{(\alpha\, V_p)^3} - G_{11} \quad , \quad (4.142c)$$

and

$$G_{22} \approx \frac{e^{-\alpha V_{dc}}}{\alpha\, I_{sat}} \frac{1}{\alpha\, V_p} \quad . \quad (4.142d)$$

From Appendix 2 we get

$$\epsilon_1 = \frac{-\, G_{12}^2}{G_{11}\, G_{22}} \approx -\, C^2 \quad , \quad (4.143)$$

$$\theta = \frac{G_{13}}{G_{11}} \approx \frac{2}{C^2} - 1 \quad , \quad (4.144)$$

$$\epsilon_2 = \frac{2\,\epsilon_1}{1 + \theta} \approx -\, C^4 \quad , \quad (4.145)$$

and

$$\epsilon_3 = \frac{\epsilon_1}{1 - \epsilon_1} \frac{1 - \theta}{1 + \theta} \approx -\, C^2 \quad , \quad (4.146)$$

where

$$C = \frac{2}{\pi} \alpha V_p \quad . \quad (4.147)$$

The mixer performance becomes:

1. Short Image:

$$L_1 \approx 1 + 2/C \qquad (4.148a)$$

$$\approx 8.686/C \quad \text{db} \qquad (4.148b)$$

$$G_{s,1} \approx \frac{2}{\pi} \alpha I_{sat} e^{\alpha V_{dc}} \qquad (4.149)$$

$$G_{o,1} \approx \frac{\pi^2}{4} G_{s,1} \qquad (4.150)$$

2. Broadband Input:

$$L_2 \approx 2 (1 + 2/C^2) \qquad (4.151a)$$

$$\approx 3 + 8.686/C^2 \quad \text{db} \qquad (4.151b)$$

$$G_{s,2} \approx \frac{4}{\pi} \alpha I_{sat} e^{\alpha V_{dc}/C} \qquad (4.152)$$

$$G_{o,2} \approx \frac{\pi^2}{8} G_{s,2} \qquad (4.153)$$

3. Open Image

$$L_3 \approx 1 + 2/C \approx L_1 \qquad (4.154a)$$

$$\approx 8.686/C \quad \text{db} \qquad (4.154b)$$

$$G_{s,3} \approx \frac{8}{\pi} \alpha I_{sat} e^{\alpha V_{dc}/C^2} \qquad (4.155)$$

$$G_{o,3} \approx \frac{\pi^2}{16} G_{s,3} \qquad (4.156)$$

It can be shown from Appendix 11, where an extensive analysis of square-wave mixers is given, that a square-wave resistance switching between two appropriate levels, say R_f and R_b, can yield the same results as cases 1 (short image) and 2 (broadband input) above. For case 1, $R_f \approx 1/[2\,\alpha V_p\,\alpha I_{sat}\,\exp(\alpha V_{dc})]$ and $R_b \approx 2\alpha V_p/[\alpha I_{sat}\,\exp(\alpha V_{dc})]$, and for case 2, R_f has the same value but $R_b \approx 8(\alpha V_p)^3/[\pi^2 \alpha I_{sat}\,\exp(\alpha V_{dc})]$. On the other hand no square-wave resistance can give the results of case 3 (G-mixer with open image) since in this case the analysis of Appendix 11 predicts that the conversion loss never attains unity while Eq. (4.154) shows that $L_3 \longrightarrow 1$ as $C \longrightarrow \infty$.

The results of this section also apply to the four-diode, single-ended mixer with sinusoidal voltage pumping given in Fig. 4.26. This circuit is called the series mixer (modulator).**

It is clear from Fig. 4.23 that for the same level of sinusoidal voltage pumping, the ring G- and H-mixers are superior to the ring Y- and Z-mixers. In selecting any of the circuits, however, one should take into account the values of the optimum source and output resistances since they vary by several orders of magnitude from one circuit to another. For any given source resistance different from the optimum, Eqs. (4.121) ... (4.125) or

** See for example Caruthers (I) and Tucker (I) and (IV) for the basic circuit of a series modulator.

Sec. A1.5 can be applied to find the corresponding mixer performance.

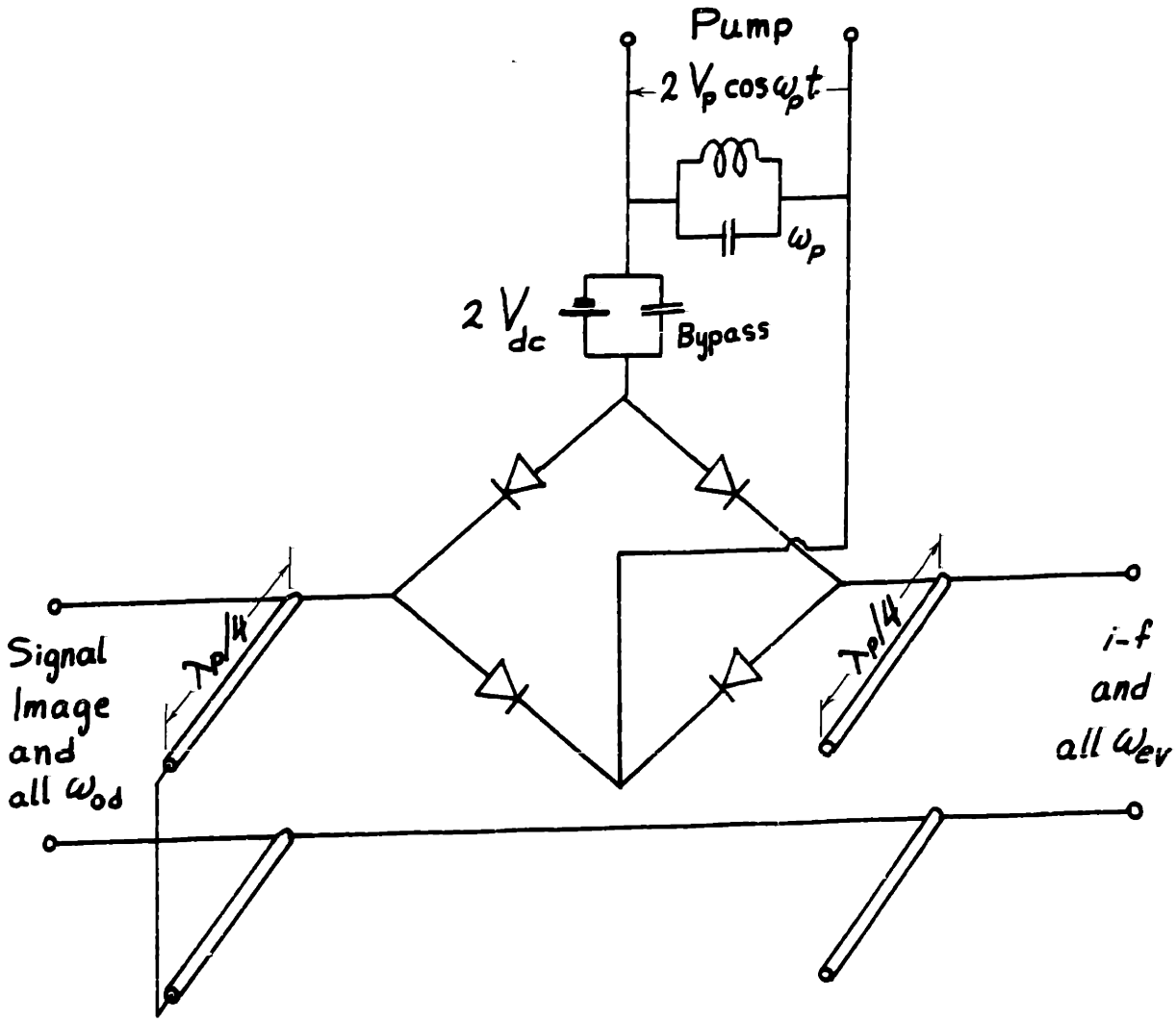

Fig. 4.26. Sinusoidal Voltage Pumping of a Series Mixer (Modulator)

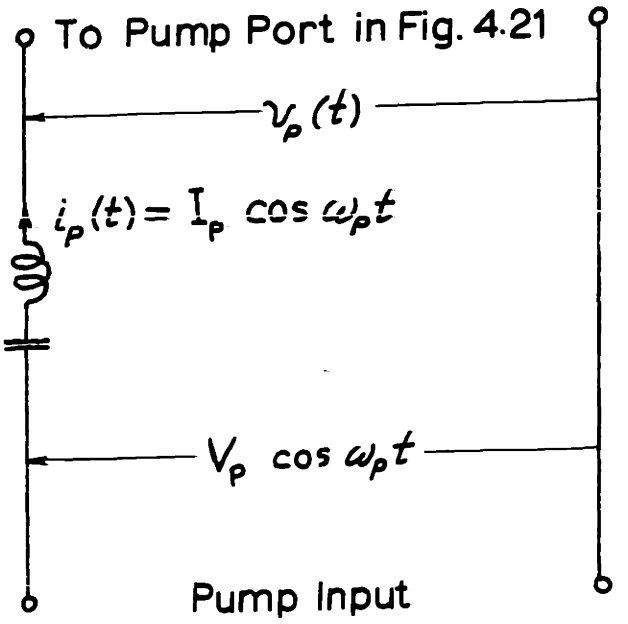

Fig. 4.27. Sinusoidal Current Pumping

4.3.3. Sinusoidal current pumping:

If the ring mixer of Fig. 4.21 is pumped by a sinusoidal current as indicated in Fig. 4.27, it follows that

$$i_p(t) = I_p \cos \omega_p t \quad . \quad (4.157)$$

One should observe that the current waveform, i_d, in each diode is not sinusoidal. To obtain i_d, one should first obtain $v_p(t)$. This is found from Eqs. (4.130) and (4.157) to be

$$\alpha v_p(t) = \sinh^{-1} (A_m \cos \omega_p t) \quad , \quad (4.158)$$

where

$$A_m = \frac{I_p}{4 I_{sat} e^{\alpha V_{dc}}} \quad . \quad (4.159)$$

Substituting Eq. (4.158) in Eq. (4.127), we obtain the diode current

$$i_d = - I_{sat} + I_{sat}\, e^{\alpha V_{dc}} \left\{ A_m \cos\omega_p t + \sqrt{1 + A_m^2 \cos^2(\omega_p t)} \right\} \quad . \quad (4.160)$$

The above equation for the diode current waveform is identical to Eq. (4.86), of the single-diode H-mixer, with A_m replacing A. Thus the results of the large signal analysis for the single-diode H-mixer, Sec. 4.2.4, applies here. However, to obtain identical diode conditions for the single-diode H-mixer and the ring mixer one should pump the latter mixer with four times the current necessary to pump the former.

The small signal conductance waveform for each diode is also identical to that of the single-diode H-mixer, Eq. (4.95). We rewrite it here as

$$g(t) = \alpha\, I_{sat}\, e^{\alpha V_{dc}} \left[A_m \cos\omega_p t + \sqrt{1 + A_m^2 \cos^2\omega_p t} \right] \quad . \quad (4.161)$$

Thus, according to Sec. 2.3, the performance of the ring H-mixer is identical to that of the single-diode H-mixer. Therefore, all the results of Sec. 4.2.4 apply for the ring H-mixer with A_m replacing A.

From the duality relation given in Sec. 4.3.1, it follows that the performance of the ring G-mixer is identically the dual of that of the ring H-mixer. The performance curves for both mixers are plotted in Figs. 4.28 and 4.29 as functions of $1/A_m$. These curves give identical results as those in Figs. 4.15 and 4.16 of the single-diode H-mixer.

The performance of the ring Y- and Z-mixers will also be the dual of one another because of the duality relation of the ring mixer. In the following we find the relations for the Y-mixer.

Expanding g(t) of Eq. (4.161) in terms of its Fourier coefficients, we get

$$g(t) = y_o + 2\, y_1 \cos\omega_p t + 2\, y_2 \cos 2\omega_p t + \text{higher order even harmonics}, \quad (4.162a)$$

where

$$y_o = \alpha\, I_{sat}\, e^{\alpha V_{dc}} \left\langle \sqrt{1 + A_m^2 \cos^2(\omega_p t)} \right\rangle \quad , \quad (4.162b)$$

$$y_1 = \tfrac{1}{2}\, \alpha\, I_{sat}\, e^{\alpha V_{dc}}\, A_m \quad , \quad (4.162c)$$

and

$$y_2 = \alpha I_{sat} e^{\alpha V_{dc}} \left\langle \cos(2\omega_p t)\, \sqrt{1 + A_m^2 \cos^2(\omega_p t)} \right\rangle \quad (4.162d)$$

where $\langle \ldots \rangle = \frac{1}{2\pi} \int_o^{2\pi} \ldots\, d\omega_p y$.

The performance of the Y-mixer can now be calculated from

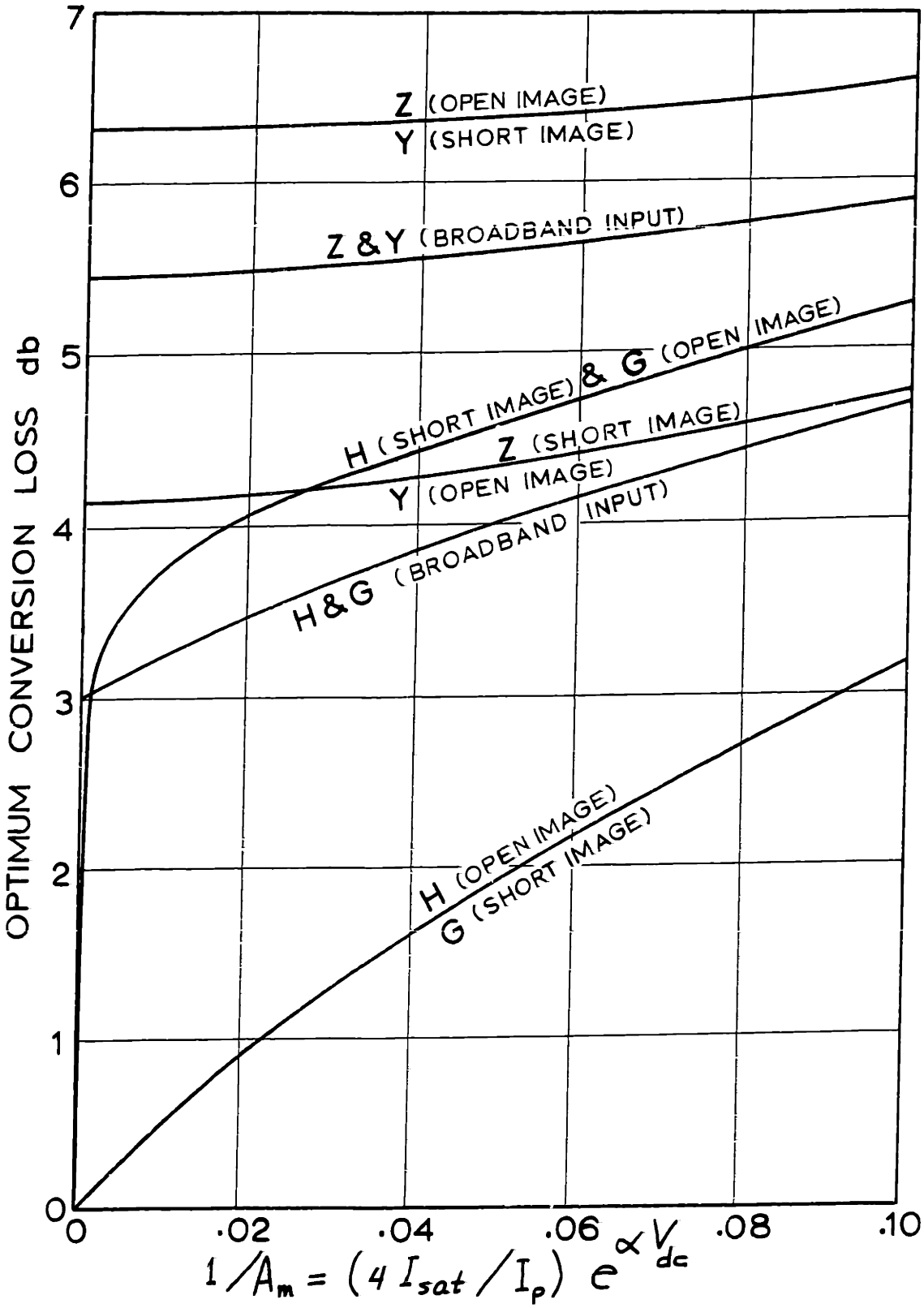

Fig. 4.28. The Optimum Conversion Losses for Different Configurations of Ring Y-, Z-, G- and H-Mixers with Sinusoidal Current Pumping

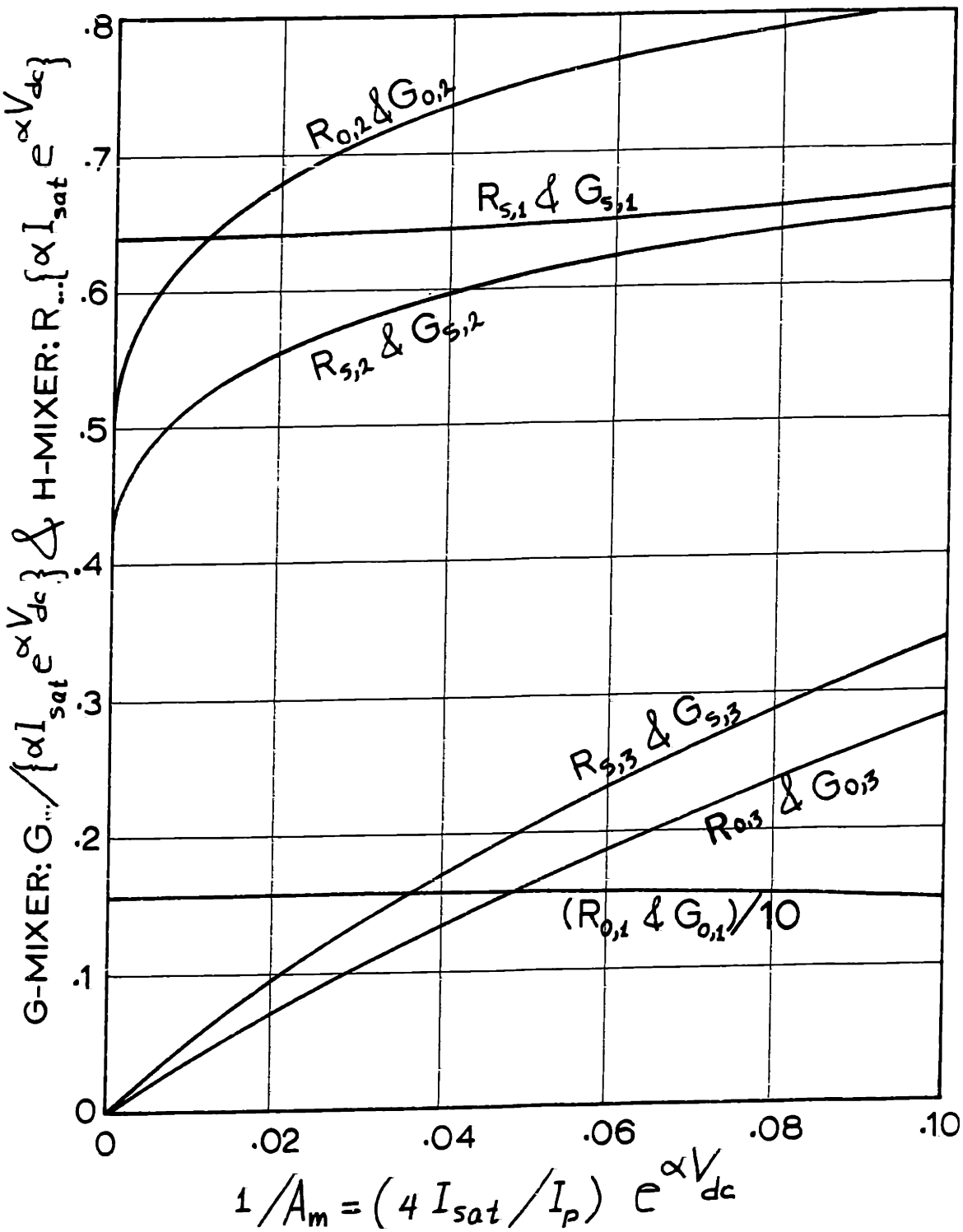

Fig. 4.29. Optimum Source and Output Resistances and Conductances for Ring H- & G-Mixers with Sinusoidal Current Pumping
H-Mixer (1. Open Image, 2. Broadband Input, 3. Short Image)
G-Mixer (1. Short Image, 2. Broadband Input, 3. Open Image)

Appendix 2. The results are given in Fig. 4.28. As mentioned above they also apply for the Z-mixer. One observes that the conversion loss never attains its theoretical minimum of zero db (or 3 db in the case of broadband input). For this reason we did not give the value of the optimum source and output resistances. To calculate the limiting performance we let $A_m \to \infty$. The integrals in Eqs. (4.162b and d) can be approximated by the formulas given in Secs. A7.7 and A7.11. This gives

$$y_o \approx \alpha I_{sat} e^{\alpha V_{dc}} \frac{2}{\pi} A_m \quad , \quad (4.163a)$$

and

$$y_2 \approx \alpha I_{sat} e^{\alpha V_{dc}} \frac{2}{3\pi} A_m \quad . \quad (4.163b)$$

Thus from Appendix 2

$$\epsilon_1 = \left\{\frac{y_1}{y_o}\right\}^2 \approx \frac{\pi^2}{16} \quad , \quad (4.164)$$

$$\theta = \frac{y_2}{y_o} \approx \frac{1}{3} \quad , \quad (4.165)$$

$$\epsilon_2 = \frac{2\epsilon_1}{1+\theta} \approx \frac{3\pi^2}{32} \quad , \quad (4.166)$$

and

$$\epsilon_3 = \frac{\epsilon_1}{1-\epsilon_1} \frac{1-\theta}{1+\theta} \approx \frac{1}{2} \frac{\pi^2}{16-\pi^2} \quad . \quad (4.167)$$

The limiting values of the conversion loss for the different cases of the Y-mixer (and hence for the Z-mixer) become

$$\lim_{A_m \to \infty} L_1 = 4.25 \qquad (4.168a)$$

$$= 6.28 \text{ db} \quad , \qquad (4.168b)$$

$$\lim_{A_m \to \infty} L_2 = 3.50 \qquad (4.169a)$$

$$= 5.45 \text{ db} \quad , \qquad (4.169b)$$

and

$$\lim_{A_m \to \infty} L_3 = 2.58 \qquad (4.170a)$$

$$= 4.12 \text{ db} \quad . \qquad (4.170b)$$

It is clear from Fig. 4.27 that an H-mixer with open-image or a G-mixer with short-image are superior to all other configurations of all ring mixers with sinusoidal current pumping. It can also be shown, using analysis similar to those in Sec. 4.2.5, that these two mixers are superior to all other ring mixers with sinusoidal voltage or current pumping. In chosing any mixer, however, one should consider the value of the optimum source resistance which differs by several orders of magnitude from one mixer to another. If, due to practical limitations, the value of the optimum source resistance could not be supplied in practice, Eqs. (4.121) ... (4.125) or Sec. A1.5 can be applied to find the corresponding mixer performance.

4.4. Comments on the Noise Figure

So far we only considered the conversion loss of a mixer. The noise figure is perhaps a more important factor. Here we touch briefly the problem of noise in mixers, in particular those employing ideal exponential diodes. Also we give reference to several important papers avaliable in the literature which deal directly or indirectly with the general problem of mixer noise.**

In an ideal junction diode, if the series (spreading) resistance is neglected as we have done throughout this chapter, the only relevant source of noise is shot noise. In p-n junction diodes at low frequencies; or in metal-semiconductor junction diodes, such as Schottky-barrier and point-contact diodes, even at microwave frequencies; the shot noise can be accurately described by an "emmission model".*** This model produces a full shot noise effect which is identical to that of a temperature-limited vacuum diode carrying the same current and neglecting the transit time.****

** See also Dragone (I) for an excellent presentation of noise theory in pumped resistive diode mixers, and for extensive references.

*** See for example Anderson and van der Ziel (I); van der Ziel (II and III) and Uhlir (II and III) for a treatment of this problem for p-n junctions. Also see van der Ziel (III, p. 332) for a brief discussion on point contact diodes.

**** See for example Davenport and Root (I, Chapter 7) or van der Ziel (I, Chapter 5) for an analysis of shot noise in vacuum diodes.

With the above conditions in mind, let the instantaneous value of the pumped diode current, $i_p(t)$, be given by its exponential Fourier series

$$i_p(t) = \sum_{m=-\infty}^{\infty} I_{p,m}\, e^{jm\omega_p t} \quad , \quad (4.171)$$

where ω_p is the pump frequency. Note that this equation includes the diode d-c current for m = 0, i.e. $I_{p,o}$. Now, in a mixer we are interested in the shot noise current at all the frequencies which assume the form $m\omega_p + \omega_o$; $m = -\infty, \ldots, +\infty$; where ω_o is the i-f frequency. Let $I_{n,m}$ represent a complex random variable such that** $\overline{I_{n,m}\, I^*_{n,m}}$ represents the mean square noise current in a band Δf around the frequency $m\omega_p + \omega_o$. Thus the total noise current, $i_n(t)$, at all the frequencies involved is given by

$$i_n(t) = \sum_{m=-\infty}^{\infty} I_{n,m}\, e^{j(m\omega_p+\omega_o)t} \quad . \quad (4.172)$$

It was shown by Kim (I) and Dragone (I, Sec. V) that the cross correlation between the noise currents $I_{n,m}$ and $I_{n,k}$, at the frequencies $m\omega_p + \omega_o$ and $k\omega_p + \omega_o$, is given by

$$\overline{I_{n,m}\, I^*_{n,k}} = 2q\,\Delta f\, I_{p,(m-k)} \quad , \quad (4.173)$$

** The overbar indicates ensemble average and the asterisk indicates the complex conjugate.

where q is the electron charge and $I_{p,(m-k)}$ is the complex pump current at frequency $(m-k)\omega_p$ as given in Eq. (4.171). Note that Eq. (4.173) reduces to the well known Schottky's shot noise formula for m = k since $I_{p,o}$ is the diode d-c current.

Let the infinite vector $\underline{I}_n$ represent the noise currents $\{ \ldots, I_{n,-2}, I_{n,-1}, I_{n,o}, I_{n,+1}, I_{n,+2}, \ldots \}$, and the infinite square matrix $\underline{C}_p$ represent the pump current of Eq. (4.171) in much the same way as a time-varying resistance or conductance is represented by an infinite matrix.** Thus the i,j entry of $\underline{C}_p$ is $I_{p,(i-j)}$; note that $\underline{C}_p$ is Hermitian since $I_{p,-m} = I^*_{p,m}$. With this terminology Eq. (4.173) can be put in the matrix form*** Eq. (4.174)

$$\overline{\underline{I}_n^{\dagger}\,\underline{I}_n} = 2\,q\,\Delta f\,\underline{C}_p \qquad , \quad (4.174)$$

For an exponential diode pumped with $i_p(t)$ of Eq. (4.171) the small signal conductance waveform is given from Eq. (4.2) as

$$g(t) = \frac{q}{kT}\, i_p(t) \qquad , \quad (4.175)$$

where q is the electron charge, k is Boltzman's constant and T is the temperature in degrees Kelvin. If g(t) is represented by its infinite admittance matrix, $\underline{Y}$, as given

** See Appendix 3.

*** The dagger † represents the complex conjugate transpose and the overbar indicates ensemble average of each term in the matrix.

in Appendix 3, Eqs. (A3.13) and (A3.14), then Eq. (4.175) can be written in the matrix form

$$\underline{Y} = \frac{q}{kT} \underline{C}_p \quad , \quad (4.176)$$

where $\underline{C}_p$ is the same matrix used in Eq. (4.174). From Eqs. (4.176) and (4.174) it is clear that

$$\overline{\underline{I}_n^+ \underline{I}_n} = 4 k \frac{T}{2} \Delta f \underline{Y} \quad . \quad (4.177)$$

From the work of Twiss (I) & Haus and Adler (I, Chapters 2 and 3) concerning the thermal noise of a passive network at a constant temperature T_n and represented by its admittance matrix $\underline{Y}$, the correlation of the equivalent thermal noise current generators in the different ports is represented by the matrix equation**

$$\overline{\underline{I}_n^+ \underline{I}_n} = 2 k T_n \Delta f (\underline{Y} + \underline{Y}^+) \quad . \quad (4.178)$$

Comparing Eqs. (4.177) and (4.178) and noting that $\underline{Y} = \underline{Y}^+$ for a time-varying conductance, it follows that the noise model of an exponential diode under pumping conditions can be represented by a passive network with an equivalent temperature***

$$T_n = \tfrac{1}{2} T \quad . \quad (4.179)$$

** See also Lenkowski (I) and Dragone (I, Sec. II).

*** Having the equivalent noise temperature as half the room temperature does not violate the second law of thermodynamics since the local oscillator is supplying power to the diode.

In fact Eq. (4.179) has been known and used in the mixer literature for a long time.** However, many still look to it with skepticism since it was proven for exponential diodes with constant d-c bias. However, the above discussion shows clearly that it is valid under pumping conditions and thus applicable for mixers employing exponential diodes.

The problem of the noise figure in an exponential diode mixer becomes trivial by using Eq. (4.179). If all the out-of-band frequencies in the mixer are terminated reactively, then Fig. 4.30 represents the equivalent noisy

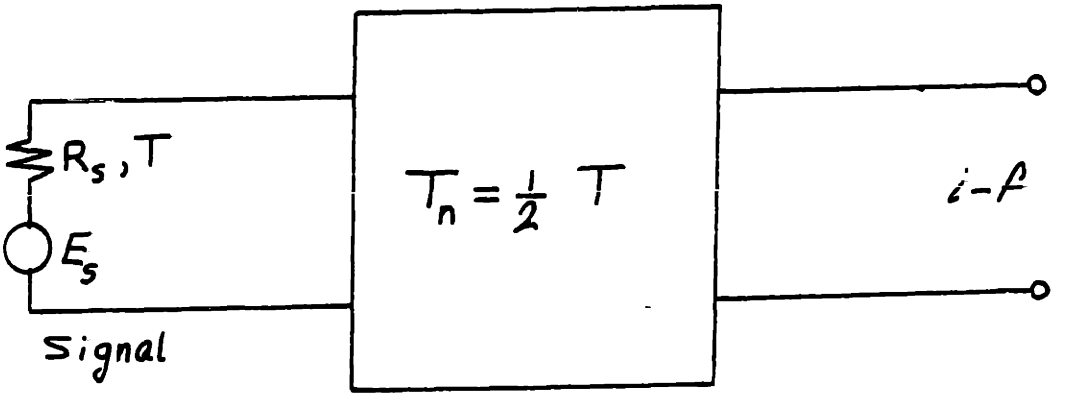

Fig. 4.30. Noisy Two-Port Representation of the Mixer

** This was first shown by Rack (I) in 1938 for vacuum diodes with space charge effect and later by Anderson and van der Ziel (I) in 1952 for p-n junction diodes. Its first application in mixer noise theory was given by Strutt (II) in 1946 and its most recent application by Barber (I) in 1967. See also Torrey and Whitmer (I, Chapter 6).

two-port network. This includes all the mixers discussed in this chapter where the image was short- or open-circuited. If L is the available conversion loss of the mixer in Fig. 4.30 then its noise figure can be easily calculated from the basic definition to be**

$$F = \frac{T_n}{T} L + 1 - \frac{T_n}{T} \quad , \quad (4.180)$$

$$= \frac{1}{2} L + \frac{1}{2} \quad . \quad (4.181)$$

If all the out-of-band frequencies are terminated reactively except the image frequency which has an impedance identical to that of the signal, then Fig. 4.31 represents the equivalent noisy three-port network. This includes all the mixers discussed in this chapter with

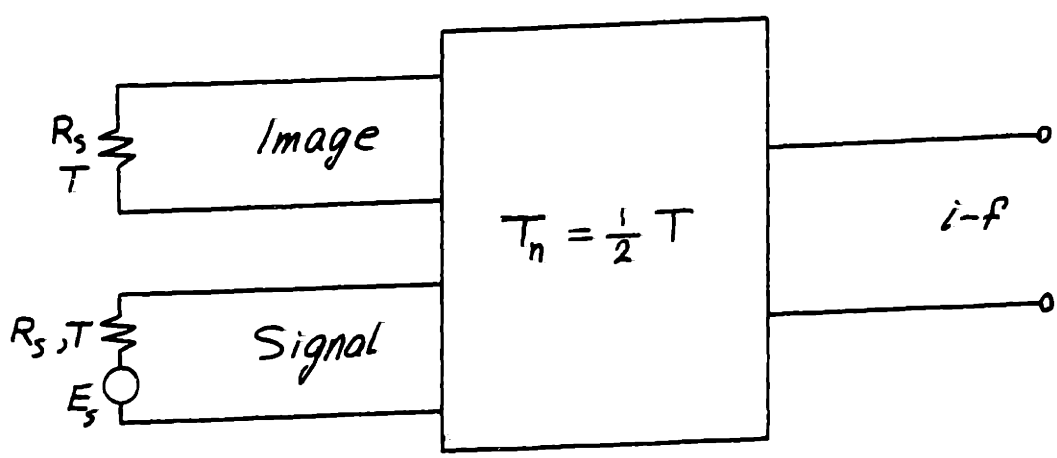

Fig. 4.31. Noisy Three-Port Representation of the Mixer

** See Pritchard (I), Messenger and McCoy (I), and Strum (II) for a proof of (4.180). Also, Docherty (I) and Barber (I) used Eq. (4.181).

broadband input terminations. Let L_s represent the available conversion loss from signal to i-f and L_i represents that from image to i-f. The noise figure of the mixer in Fig. 4.31 can be shown to be**

$$F = \frac{T_n}{T} L_s + \left[1 + \frac{L_s}{L_i}\right]\left[1 - \frac{T_n}{T}\right] \quad , \quad (4.182)$$

If $L_s = L_i = L$, and $T_n = \frac{1}{2} T$, Eq. (4.182) reduces to***

$$F = \frac{1}{2} L + 1 \quad . \quad (4.183)$$

Note that Eqs. (4.181) and (4.183) imply that

Eqs. (4.181) and (4.183) imply that minimizing the conversion loss corresponds to minimizing the noise figure.

The above equations are, of course, simplified expressions for the noise figures of mixers employing exponential diodes. In actual diodes the series resistance also generates thermal noise. In fact if the diode is strongly pumped with a square-wave voltage, the thermal noise generated in the series resistance will be the only considerable noise source in the mixer.**** In this case the mixer acts as a passive network at room temperature and the noise figure should be equal to the conversion loss

** See for example Pritchard (I) and Messenger and McCoy (I) for a proof of Eq. (4.182). See also Strum (II) for a more general analysis.

*** Docherty (I) and Barber (I) used Eq. (4.183).

**** This is true since in the forward direction where the shot noise is large, the junction is nearly short circuited, and in the reverse direction the shot noise is negligible.

[$T_n = T$ in Eqs. (4.180) or (4.182) with $L_i = L_s$]. For arbitrary pumping, both thermal and shot noises should be included.

4.5. Conclusions and Topics for Further Research

In this chapter we treated the pumping problems and found the performances of single- and multi-diode realizations of the Y-, Z-, G- and H-mixers which were introduced in Chapter 2. The diodes employed were assumed to have ideal exponential characteristics. The effects of the diode series resistance and junction capacitance were completely neglected. The analysis given for each mixer consisted of two main parts: large-signal and small-signal analysis. In the first part we calculated the pumped resistance waveform, the pump power, the resistance offered to the pump and the d-c bias conditions. In the second part of the analysis we found the optimum values of conversion loss and source and output resistances for three different image frequency terminations: short image, broadband input (i.e. identical signal and image terminations) and open image. For each case asymptotic approximations were used to obtain simple formulas which are accurate for strongly driven mixers.

Single-diode mixers were compared in Sec. 4.2.5 for the same pump power and d-c bias conditions. It was found that while some mixers give much lower conversion loss than others, their required optimum source resistance is too high to be achievable in practice. Hence another comparison was made in the same section based on supplying

the different mixers with the same source resistance. In most of the cases, mixers that were superior in the first comparison were inferior in the second and vice versa. Thus no general conclusion could be made as to which is the best mixer.

The same problem seems to exist in multi-diode ring mixers, Sec. 4.3. However, these mixers have the advantage that the pumping waveform is independent of the terminations offered to the out-of-band frequencies. This, of course, is not true for single-diode mixers, or in multi-diode mixers where each diode is individually terminated. However, for microwave mixers the latter types of mixers are prefered since it is desirable to terminate the out-of-band frequencies right next to each diode to minimize circuit loss.

The conversion losses of all mixers considered were found to decrease monotonically by increasing any of the three dimensionless parameters $X_1 = I_{dc}/[I_{sat} \exp(\alpha V_{dc})]$, $X_2 = \alpha P_p/[I_{sat} \exp(\alpha V_{dc})]$ or $X_3 = \alpha P_p/I_{dc}$ where P_p is the pump power, I_{dc} and V_{dc} are the d-c bias current and voltage under pumping conditions, I_{sat} is the diode saturation current and $\alpha = q/kT \approx 40$ volt^{-1} at room temperature. Thus it seems that by biasing the diode further in the negative direction one can improve the conversion loss without increasing the pump power. However, the optimum source resistance in this case becomes impractically high. This

in turn deteriorates the mixer performance. Thus to improve the mixer performance one must pump the mixer as strongly as possible without biasing it far in the reverse region. This is the only way one can gain the full capabilities of the mixer for a reasonable source resistance.

In all the analyses given in this chapter, the out-of-band frequencies were assumed to be completely terminated. In practice however, this might not be possible. Thus a study of the effects of incomplete terminations of the out-of-band frequencies on the performance of several mixers was given in Appendices 10 and 11. Simple switch diode models were employed to make the analysis possible. The performance of the mixer so far was based on its conversion loss. In Sec. 4.4 we comment on the noise figure for mixers employing ideal exponential diodes. The results confirm the known fact that the shot noise in a pumped exponential diode can be represented by thermal noise generated by the pumped resistance at half the room temperature. This simplifies the mixer noise analysis considerably. Since this is still a controversial point many important references were given to help further investigations.

The theory of mixers employing exponential diodes given in this chapter can be extended with a minimum amount of work to investigate the following

topics:

1). Harmonics Mixers:

In these mixers the difference between the signal and i-f frequencies is a harmonic of the pump frequency. One of the problems** of interest in this area is whether to use individually biased back-to-back diodes in parallel or in series to achieve the best conversion loss in second-harmonic Z- and Y-mixers. The resistance waveforms and their Fourier coefficients for the necessary analysis of this problem are identical to some of those appearing in this chapter.

2). Image Separation Mixers:***

The reactive termination of the image frequency was found to improve the mixer performance considerably. In microwave mixers this might not be easily achieved by simple filtering since the signal and image frequencies are very close. In this case the signal and image frequencies can be separated by dividing the input signal between two mixers pumped 90° out-of-phase and combining their i-f ports after including a 90° phase shift to one of them. This procedure is identical to that of single sideband receivers. There are four basic methods of combining the

** This was suggested by Steinbrecher (I).

*** The word "separation" is often replaced by "rejection", "cancellation" or "enhancement".

input and output ports of the two mixers; series-series, series-parallel, parallel-series and parallel-parallel. Some of these methods are better than the others depending on type of mixer. The results given in this chapter can be used to provide the basis for this analysis. Another point that can also be considered is the effects of imperfect 90^{o} phase shifting networks in the pump and/or i-f ports.

Other topics for further research which are related to the mixers analyzed in this chapter are given below. They seem to be harder than the ones given above.

1). Diode Parasitics:

In practice, the mixing diode contains parasitics such as the series resistance and junction capacitance. As mentioned in Sec. 2.6, an exact analysis of this problem does not seem possible except if the parasitics were elements in shunt with the time-varying resistance in a Y-mixer or in series with it in a Z-mixer. For diodes with both shunt and series parasitics and for all the mixers discussed, an approximate analysis based on the method suggested in Sec. 2.6 and on the literature work referred to there is needed. To deal with this problem correctly one must consider the effects of the parasitics on the shape of the pump waveform across the diode junction. This last point was not treated for any mixer in the

available literature.

2). Nonlinear distortion:

Nonlinear distortion in mixers forms one of the important bases for judging their quality. Thus an analysis of this problem for the different mixer circuits used in this chapter is desirable. One of the questions that needs an immediate answer is whether or not a single-diode Z-mixer has higher nonlinear distortion than other mixers as mentioned in Sec. 4.2.5. This was argued since the amount of pump power that can be supplied to this mixer without driving the diode to its breakdown region was of the order of a few microwatts for a typical d-c current bias of a few milliamperes. The other mixers did not seem to have this property. Most of the work available in the literature on nonlinear distortion in mixers either deals with mixers with no selective networks** or with mixers where a finite number of sinusoidal voltages or currents exists.*** The last case is applicable for the Y- and Z-mixers. For a G- or an H-mixer however, a new technique is needed since none of the above situations apply.

** Agrowal and Hanson (I), Belevitch (I and II), Gardiner (I), Rafuse (II), Snyder (I) and Tucker (I, II and IV).

*** Gretsch (I), Lepoff and Cowley (I) and Orloff (I).

APPENDIX 1

CONVERSION LOSS, PASSIVITY AND STABILITY OF TWO-PORT NETWORKS

A1.1. Generalized Matrix Representation

Four basic two-port network matrices will be used; namely, the impedance matrix $\underline{Z}$, the admittance matrix $\underline{Y}$ ($= \underline{Z}^{-1}$) and the hybrid matrices $\underline{H}$ and $\underline{G}$ ($= \underline{H}^{-1}$).

Fig. A1.1 Sign Convention

Z-matrix:
$$\begin{bmatrix} V_1 \\ V_2 \end{bmatrix} = \begin{bmatrix} z_{11} & z_{12} \\ z_{21} & z_{22} \end{bmatrix} \begin{bmatrix} I_1 \\ I_2 \end{bmatrix}. \qquad \text{(A1.1)}$$

Y-matrix:
$$\begin{bmatrix} I_1 \\ I_2 \end{bmatrix} = \begin{bmatrix} y_{11} & y_{12} \\ y_{21} & y_{22} \end{bmatrix} \begin{bmatrix} V_1 \\ V_2 \end{bmatrix}. \qquad \text{(A1.2)}$$

H-matrix:
$$\begin{bmatrix} V_1 \\ I_2 \end{bmatrix} = \begin{bmatrix} h_{11} & h_{12} \\ h_{21} & h_{22} \end{bmatrix} \begin{bmatrix} I_1 \\ V_2 \end{bmatrix}. \qquad \text{(A1.3)}$$

G-matrix:
$$\begin{bmatrix} I_1 \\ V_2 \end{bmatrix} = \begin{bmatrix} g_{11} & g_{12} \\ g_{21} & g_{22} \end{bmatrix} \begin{bmatrix} V_1 \\ I_2 \end{bmatrix}. \qquad \text{(A1.4)}$$

Table A1.1. - Two-Port Matrix Interrelations

from → / to ↓	Z	Y	H	G
Z	z_{11} z_{12} z_{21} z_{22}	$\frac{y_{22}}{\Delta y}$ $\frac{-y_{12}}{\Delta y}$ $\frac{-y_{21}}{\Delta y}$ $\frac{y_{11}}{\Delta y}$	$\frac{\Delta h}{h_{22}}$ $\frac{h_{12}}{h_{22}}$ $\frac{-h_{21}}{h_{22}}$ $\frac{1}{h_{22}}$	$\frac{1}{g_{11}}$ $\frac{-g_{12}}{g_{11}}$ $\frac{g_{21}}{g_{11}}$ $\frac{\Delta g}{g_{11}}$
Δz	Δz	$1/\Delta y$	h_{11}/h_{22}	g_{22}/g_{11}
Y	$\frac{z_{22}}{\Delta z}$ $\frac{-z_{12}}{\Delta z}$ $\frac{-z_{21}}{\Delta z}$ $\frac{z_{11}}{\Delta z}$	y_{11} y_{12} y_{21} y_{22}	$\frac{1}{h_{11}}$ $\frac{-h_{12}}{h_{11}}$ $\frac{h_{21}}{h_{11}}$ $\frac{\Delta h}{h_{11}}$	$\frac{\Delta g}{g_{22}}$ $\frac{g_{12}}{g_{22}}$ $\frac{-g_{21}}{g_{22}}$ $\frac{1}{g_{22}}$
Δy	$1/\Delta z$	Δy	h_{22}/h_{11}	g_{11}/g_{22}
H	$\frac{\Delta z}{z_{22}}$ $\frac{z_{12}}{z_{22}}$ $\frac{-z_{21}}{z_{22}}$ $\frac{1}{z_{22}}$	$\frac{1}{y_{11}}$ $\frac{-y_{12}}{y_{11}}$ $\frac{y_{21}}{y_{11}}$ $\frac{\Delta y}{y_{11}}$	h_{11} h_{12} h_{21} h_{22}	$\frac{g_{22}}{\Delta g}$ $\frac{-g_{12}}{\Delta g}$ $\frac{-g_{21}}{\Delta g}$ $\frac{g_{11}}{\Delta g}$
Δh	z_{11}/z_{22}	y_{22}/y_{11}	Δh	$1/\Delta g$
G	$\frac{1}{z_{11}}$ $\frac{-z_{12}}{z_{11}}$ $\frac{z_{21}}{z_{11}}$ $\frac{\Delta z}{z_{11}}$	$\frac{\Delta y}{y_{22}}$ $\frac{y_{12}}{y_{22}}$ $\frac{-y_{21}}{y_{22}}$ $\frac{1}{y_{22}}$	$\frac{h_{22}}{\Delta h}$ $\frac{-h_{12}}{\Delta h}$ $\frac{-h_{21}}{\Delta h}$ $\frac{h_{11}}{\Delta h}$	g_{11} g_{12} g_{21} g_{22}
Δg	z_{22}/z_{11}	y_{11}/y_{22}	$1/\Delta h$	Δg

Δm is the determinant of the matrix $\underline{M}$

The duality relations among the four aforementioned matrices suggest the use of a generalized matrix representation.

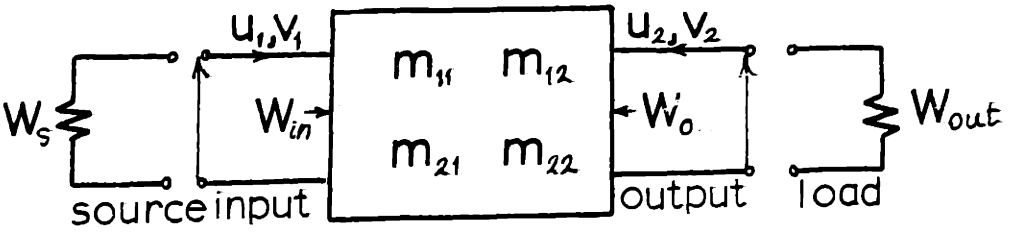

Fig. A1.2. Generalized Representation

M-matrix:
$$\begin{bmatrix} u_1 \\ u_2 \end{bmatrix} = \begin{bmatrix} m_{11} & m_{12} \\ m_{21} & m_{22} \end{bmatrix} \begin{bmatrix} v_1 \\ v_2 \end{bmatrix} . \qquad \text{(A1.5)}$$

or
$$\underline{u} = \underline{M}\,\underline{v} \ . \qquad \text{(A1.6)}$$

The meaning of the u's, v's and W's of the generalized representation depends upon the particular matrix represented by $\underline{M}$. This is given in Table A1.2 and can be found by comparing Eq. (A1.5) by Eqs. (A1.1) . . . (A1.4).

The following notation will be used in conjunction with the generalized representation.

$$m_{ij}^{r} = \text{Re}\,(m_{ij}) \ , \qquad \text{(A1.7a)}$$

$$m_{ij}^{i} = \text{Im}\,(m_{ij}) \ , \qquad \text{(A1.7b)}$$

$$W^{r} = \text{Re}\,(W) \ , \qquad \text{(A1.8a)}$$

and
$$W^{i} = \text{Im}\,(W) \ . \qquad \text{(A1.8b)}$$

Table A1.2. Meaning of Generalized Notation

M	Z	Y	H	G
m_{ij}	z_{ij}	y_{ij}	h_{ij}	g_{ij}
u_1	V_1	I_1	V_1	I_1
v_1	I_1	V_1	I_1	V_1
u_2	V_2	I_2	I_2	V_2
v_2	I_2	V_2	V_2	I_2
W_s	Z_s	Y_s	Z_s	Y_s
W_{in}	Z_{in}	Y_{in}	Z_{in}	Y_{in}
W_o	Z_o	Y_o	Y_o	Z_o
W_L	Z_L	Y_L	Y_L	Z_L

It is important to note that for a reciprocal network $z_{12} = z_{21}$ and $y_{12} = y_{21}$; but, $h_{12} = -h_{21}$ and $g_{12} = -g_{21}$. Thus

$$\text{Reciprocity} \iff m_{12} = \pm m_{21} \quad \begin{cases} + \text{ if } \underline{M} = \underline{Z} \text{ or } \underline{Y} \\ - \text{ if } \underline{M} = \underline{H} \text{ or } \underline{G} \end{cases} \qquad \text{(A1.9)}$$

A1.2. Passivity

A network is passive if and only if the total time-average power P_{net} flowing into the network is nonnegative for all admissible combinations of terminal voltages and currents. A network is active if it is not passive*. Using the generalized representation one can write P_{net} in the matrix form**

$$P_{net} = \tfrac{1}{2} (\underline{v}^{\dagger} \underline{u} + \underline{u}^{\dagger} \underline{v}) \quad . \tag{A1.10}$$

Substituting the network constraint (A1.6) we get

$$P_{net} = \tfrac{1}{2} \underline{v}^{\dagger} (\underline{M} + \underline{M}^{\dagger}) \underline{v} \quad . \tag{A1.11}$$

Passivity implies that the value of the Hermitian form (A1.11) must be nonnegative for any $\underline{v}$. This in turn implies that the Hermitian matrix $\underline{M} + \underline{M}^{\dagger}$ is positive semidefinite***. We write this condition as

$$\text{Passivity} \iff P_{net} \geq 0 \iff \underline{M} + \underline{M}^{\dagger} \geq 0. \tag{A1.12}$$

In fact (A1.12) is true for any matrix representation of an n-port network provided that the exitation vector $\underline{v}$ and the response vector $\underline{u}$ satisfy the power relation (A1.10).

With the notation of (A1.7) the two-port Hermitian

* cf. Kuh and Rohrer (I, Ch. 4 and Ch. 5, Sec. 1).
** The superscript † means the complex conjugate transposed.
*** Hildebrand (I, Sec. 1.19).

matrix $\underline{M} + \underline{M}^{\dagger}$ is given by

$$\underline{M} + \underline{M}^{\dagger} = \begin{bmatrix} 2\, m_{11}^{r} & m_{12} + m_{21}^{*} \\ m_{21} + m_{12}^{*} & 2\, m_{22}^{r} \end{bmatrix} \quad . \qquad (A1.13)$$

It is a necessary and sufficient condition for this matrix to be positive semidefinite that*

$$m_{11}^{r} \geq 0, \qquad m_{22}^{r} \geq 0, \qquad (A1.14a)$$

and

$$\det (\underline{M} + \underline{M}^{\dagger}) \geq 0 \quad . \qquad (A1.14b)$$

Actually (A1.14b) and any one of (A1.14a) conditions imply the other (A1.14a) condition. We can write (A1.14b) in any of the following equivalent forms:

$$4\, m_{11}^{r}\, m_{22}^{r} \geq |m_{12} + m_{21}^{*}|^{2} \qquad (\geq 0) \quad , \qquad (A1.14c)$$

$$4\, m_{11}^{r}\, m_{22}^{r} \geq |m_{12}|^{2} + |m_{21}|^{2} + 2\, \mathrm{Re}(m_{12} m_{21}) \quad , \qquad (A1.14d)$$

$$4\, m_{11}^{r}\, m_{21}^{r} \geq (m_{12}^{r} + m_{21}^{r})^{2} + (m_{12}^{i} - m_{21}^{i})^{2} \quad , \qquad (A1.14e)$$

$$\text{or} \quad 4\, m_{11}^{r}\, m_{22}^{r} \geq 4\, m_{12}^{r}\, m_{21}^{r} + |m_{12} - m_{21}|^{2} \quad . \qquad (A1.14f)$$

If the equalities hold in (A1.14), the matrix $\underline{M} + \underline{M}^{\dagger}$ is identically zero and the network is <u>lossless</u>. Thus

$$\text{Losslessness} \iff m_{11}^{r} = 0,\ m_{22}^{r} = 0 \text{ and } m_{12} = -m_{21}^{*}. \qquad (A1.15)$$

---

* Hildebrand (I, Sec. 1.20)

A1.3. Stability

Stability is the inability of the natural behaviour to grow without limit. Thus, an n-port network terminated with given loads is stable if no oscillations take place. An n-port network is absolutely stable if and only if it is stable when terminated with all possible passive loads. In other words, an n-port network is absolutely stable if and only if the one-port network formed by any of its ports, while terminating the remaining ports with all possible passive loads, is passive. A network is potentially unstable if and only if it is not absolutely stable*.

Thus, for our two-port network of Fig. A1.2, using the generalized representation (A1.5) ... (A1.8), absolute stability is equivalent to

$$W_{in}^r \geq 0 \text{ for any } W_L \text{ with } W_L^r \geq 0, \qquad \text{(A1.16a)}$$

and

$$W_o^r \geq 0 \text{ for any } W_s \text{ with } W_s^r \geq 0, \qquad \text{(A1.16a)}$$

where

$$W_{in} = m_{11} - \frac{m_{12}m_{21}}{m_{22} + W_L}, \qquad \text{(A1.17a)}$$

and

$$W_o = m_{22} - \frac{m_{12}m_{21}}{m_{11} + W_s}. \qquad \text{(A1.17b)}$$

Simple manipulations of (A1.16) and (A1.17) give

---

* This definition of stability considers a lossless network absolutely stable. The bounded input-bounded output definition of stability used by some authors considers a lossless network potentially unstable (Cf. Kuh and Rohrer, I, Ch. 1, Sec. 9 and Ch. 5, Sec. 3).

the necessary and sufficient conditions for absolute stability of two-port networks as

$$m_{11}^r \geq 0, \qquad m_{22}^r \geq 0, \tag{A1.18a}$$

and

$$2\, m_{11}^r\, m_{22}^r \geq |m_{12}m_{21}| + \mathrm{Re}(m_{12}m_{21}) \;(\geq 0)\;. \tag{A1.18b}$$

Actually (A1.18b) and any one of (A1.18a) conditions imply the other (A1.18a) condition. We can write (A1.18b) in the form

$$4\, m_{11}^r\, m_{22}^r \geq |m_{12}|^2 + |m_{21}|^2 - (|m_{12}| - |m_{21}|)^2 + 2\,\mathrm{Re}(m_{12}m_{21}). \tag{A1.18c}$$

Comparing the passivity condition (A1.14a) and (A1.14d) with the stability conditions (A1.18a) and (A1.18c), we deduce that

$$\text{Passivity} \Rightarrow \text{Absolute Stability}\;. \tag{A1.19}$$

Conversely

$$\begin{matrix}\text{Absolute}\\ \text{Stability}\end{matrix} \text{ and } \begin{matrix}\text{Magnitude}\\ \text{Reciprocity}\end{matrix} \Rightarrow \text{Passivity}\;, \tag{A1.20}$$

where magnitude stability means $|m_{12}| = |m_{21}|$.

Regions of passivity and absolute stability constructed from conditions (A1.14) and (A1.18) are given in Fig. A1.3. The figure represents a $\dfrac{\mathrm{Re}(m_{12}m_{21})}{m_{11}^r\, m_{22}^r}$ versus $\dfrac{\mathrm{Im}(m_{12}m_{21})}{m_{11}^r\, m_{22}^r}$ plane. Both m_{11}^r and m_{22}^r are assumed to be

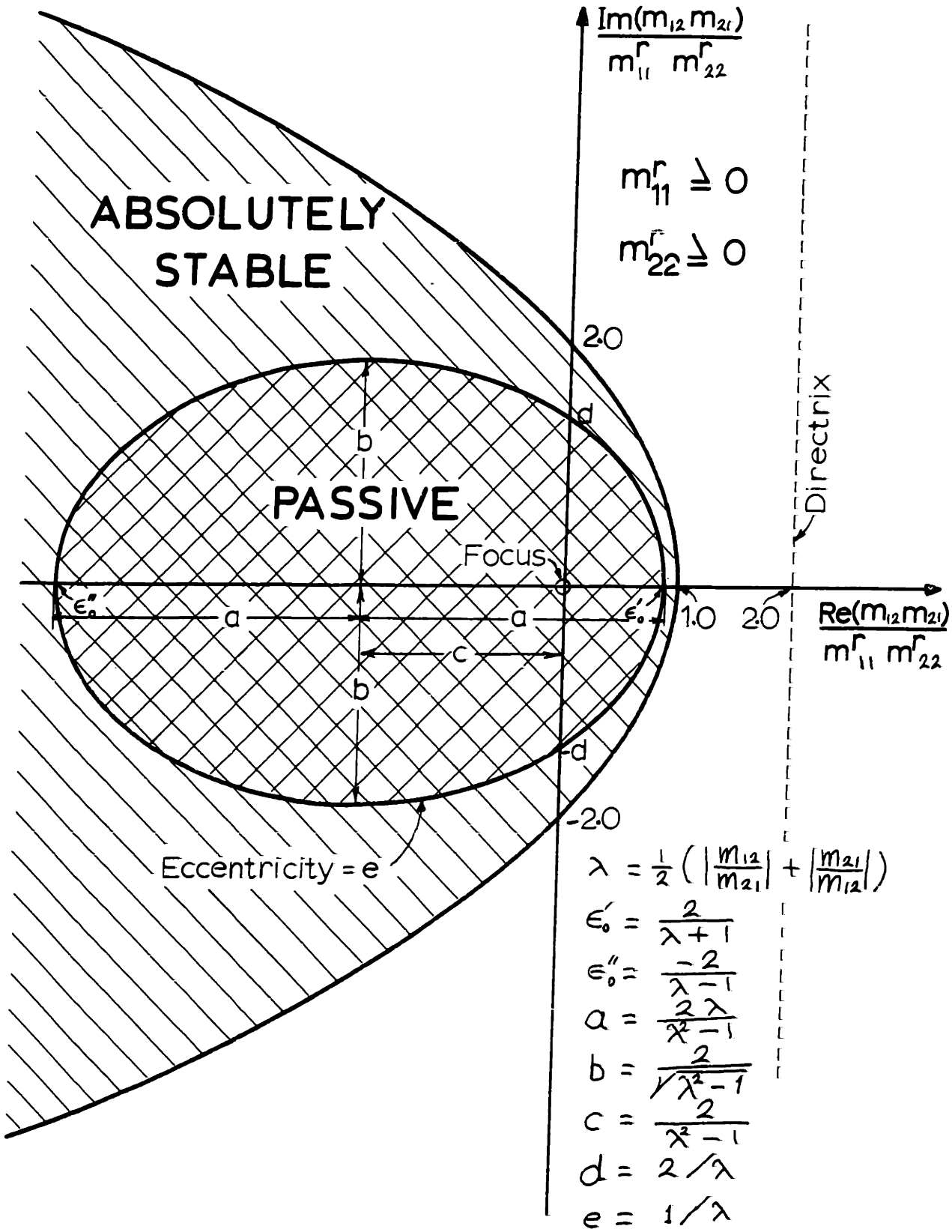

Fig. A1.3. Regions of Passivity and Absolute Stability

nonnegative. The contours are plotted for a given value of $\left|\frac{m_{12}}{m_{21}}\right|$. Actually, the parabola bounding the region of absolute stability is independent of this ratio, while the ellipse bounding the region of passivity depends on it. In the limit when $\left|\frac{m_{12}}{m_{21}}\right|$ approaches unity the ellipse approaches the parabola and the passivity region coincides with the absolute stability region as should be expected from (A1.20).

A1.4. Conversion Loss

In the begining of this section we deal only with absolutely stable, but not necessarily passive networks. At the end we discuss potentially unstable networks briefly. Thus, the conversion loss will be defined here on an <u>available</u> basis as

$$L = \frac{P_{a,s}}{P_{a,o}} \quad , \qquad (A1.21)$$

where $P_{a,s}$ and $P_{a,o}$ are the maximum available powers from the source and output ports respectively. L is a function of the network and the source impedance only.

We now develop general formulas for the conversion loss of the two-port network of Fig. A1.2 using the generalized representation (A1.5) ... (A1.8). If the input exitation function is given by U_s (a voltage generator in series with W_s or a current generator in parallel with W_s, depending upon

the particular matrix represented by $\underline{M}$), we get*

$$P_{a,s} = |U_s|^2 / 4 W_s^r \quad , \tag{A1.22}$$

and

$$P_{o,s} = \left| \frac{U_s m_{21}}{m_{11} + W_s} \right|^2 / 4 W_o^r \quad , \tag{A1.23}$$

where

$$W_o = m_{22} - \frac{m_{12} m_{21}}{m_{11} + W_s} \quad . \tag{A1.24}$$

Substituting in Eq. (A1.21) gives

$$L = \left| \frac{m_{12}}{m_{21}} \right| \frac{m_{11}^r m_{22}^r}{|m_{12} m_{21}|} \frac{m_{11}^r}{W_s^r} \left[\left(1 + \frac{W_s^r}{m_{11}^r}\right)^2 - \frac{\mathrm{Re}(m_{12} m_{21})}{m_{11}^r m_{22}^r} \left(1 + \frac{W_s^r}{m_{11}^r}\right) \right.$$

$$\left. + \left(\frac{m_{11}^i}{m_{11}^r} + \frac{W_s^i}{m_{11}^r}\right)^2 - \frac{\mathrm{Im}(m_{12} m_{21})}{m_{11}^r m_{22}^r} \left(\frac{m_{11}^i}{m_{11}^r} + \frac{W_s^i}{m_{11}^r}\right) \right] \quad . \tag{A1.25}$$

Optimizing L by setting $\frac{\partial L}{\partial W_s^i} = 0$ and $\frac{\partial L}{\partial W_s^r} = 0$, we get

$$L_{opt} = \left| \frac{m_{12}}{m_{21}} \right| \frac{m_{11}^r m_{22}^r}{|m_{12} m_{21}|} \left[(1+S)^2 + \left\{ \frac{\mathrm{Im}(m_{12} m_{21})}{2 m_{11}^r m_{22}^r} \right\}^2 \right] \quad , \tag{A1.26}$$

and

$$W_{s,opt} = m_{11}^r S - j \left[m_{11}^i - m_{11}^r \left\{ \frac{\mathrm{Im}(m_{12} m_{21})}{2 m_{11}^r m_{22}^r} \right\} \right] \quad . \tag{A1.27}$$

* This is a generalization of the usual formulas of conversion loss, Cf. Torrey and Whitmer (I, Sec. 5.8).

for which

$$W_{o,opt} = m_{22}^r S + j\left[m_{22}^i - m_{22}^r \left\{\frac{Im(m_{12}m_{21})}{2\, m_{11}^r\, m_{22}^r}\right\}\right] , \quad (A1.28)$$

where

$$S = \sqrt{1 - \frac{Re(m_{12}m_{21})}{m_{11}^r\, m_{22}^r} - \left\{\frac{Im(m_{12}m_{21})}{2\, m_{11}^r\, m_{22}^r}\right\}^2} . \quad (A1.29)$$

If $W_L = W_{o,opt}^*$ it can be shown that $W_{in} = W_{s,opt}^*$, thus the network is conjugately matched at both ports. In this case maximum power is transfered from the source to the load and the <u>transducer loss</u> is equivalent to the optimum available conversion loss L_{opt}.

L_{opt} can be written in two alternative useful forms as

$$L_{opt} = \left|\frac{m_{12}}{m_{21}}\right| \frac{1 + \sqrt{1 - \epsilon'}}{1 - \sqrt{1 - \epsilon'}} , \quad (A1.30)$$

where

$$\epsilon' = \frac{2\,|m_{12}\, m_{21}|}{2\, m_{11}^r\, m_{22}^r + |m_{12}m_{21}| - Re(m_{12}m_{21})} ; \quad (A1.31)$$

or

$$L_{opt} = \left|\frac{m_{12}}{m_{21}}\right| \frac{\sqrt{1 - \epsilon''} + 1}{\sqrt{1 - \epsilon''} - 1} , \quad (A1.32)$$

where

$$\epsilon'' = \frac{-2\,|m_{12}\, m_{21}|}{2\, m_{11}^r\, m_{22}^r - |m_{12}m_{21}| - Re(m_{12}m_{21})} . \quad (A1.33)$$

Note that

$$(1 - \epsilon')\,(1 - \epsilon'') = 1 \quad . \tag{A1.34}$$

If the $\underline{M}$ matrix is real, the conversion loss equations simplify to

$$L_{opt} = \frac{m_{12}}{m_{21}} \frac{1 + \sqrt{1 - \epsilon}}{1 - \sqrt{1 - \epsilon}} \quad , \tag{A1.35}$$

and

$$W_{s,opt} = m_{11} \sqrt{1 - \epsilon} \quad , \tag{A1.36}$$

for which

$$W_{o,opt} = m_{22} \sqrt{1 - \epsilon} \quad , \tag{A1.37}$$

where

$$\epsilon = \frac{m_{12}\, m_{21}}{m_{11}\, m_{22}} \quad . \tag{A1.38}$$

If $\frac{m_{12}}{m_{21}} \geq 0$, ϵ is equivalent to ϵ' of Eq. (A1.31); otherwise, ϵ is equivalent to ϵ'' of Eq. (A1.33).

Let L_{ij} be defined as the optimum conversion loss from port i to port j ($L_{12} = L_{opt}$ in all the above equations). By interchanging the subscripts 1 and 2 in Eqs. (A1.26), (A1.30) or (A1.32) and comparing them to the original equation, one obtains

$$\frac{L_{12}}{L_{21}} = \left| \frac{m_{12}}{m_{21}} \right|^2 \quad . \tag{A1.39}$$

It is interesting to note the consequences of

absolute stability conditions (A1.18) and passivity conditions (A1.14) on the conversion loss formulas (A1.26)... (A1.39).

Consequences of absolute stability:

$$L_{opt} = L_{12} \geq \left|\frac{m_{12}}{m_{21}}\right| \qquad \text{(A1.40a)}$$

$$L_{21} \geq \left|\frac{m_{21}}{m_{12}}\right| \quad , \qquad \text{(A1.40b)}$$

$$(0 \leq) \quad \epsilon' \leq 1 \quad , \qquad \text{(A1.40c)}$$

and

$$(0 \geq) \quad \epsilon'' \geq -\infty \quad . \qquad \text{(A1.40d)}$$

Consequences of passivity:

$$\min (L_{12}, L_{21}) \geq 1 \quad , \qquad \text{(A1.41a)}$$

$$\max (L_{12}, L_{21}) \geq \max \left(\left|\frac{m_{12}}{m_{21}}\right|^2, \left|\frac{m_{21}}{m_{12}}\right|^2\right) \quad , \qquad \text{(A1.41b)}$$

$$(0 \leq) \quad \epsilon' \leq \frac{4\,|m_{12}m_{21}|}{(|m_{12}| + |m_{21}|)^2} \quad (\leq 1) \quad , \qquad \text{(A1.41c)}$$

$$(0 \geq) \quad \epsilon'' \geq \frac{-4\,|m_{12}m_{21}|}{(|m_{12}| - |m_{21}|)^2} \quad (\geq -\infty) \quad . \qquad \text{(A1.41d)}$$

It is no surprise that the bounds on $L_{12}(= L_{opt})$, L_{21}, ϵ' & ϵ'' set by passivity are tighter than those set by absolute stability since the former is a special case of the latter as given in conditions (A1.19) and (A1.20) and Fig. A1.3.

For a given value of $\left|\frac{m_{12}}{m_{21}}\right|$, the contour representing a constant value of ϵ', ϵ'', L_{12} and L_{21} is an ellipse which shares the focus and directrix with the parabola and the ellipse indicated in Fig. A1.3, and intersects the abscissa at the points ϵ' and ϵ''. The particular contor representing the equalities in conditions (A1.40) is the parabola limiting the absolute stability region and that in conditions (A1.41) is the ellipse limiting the passivity region.

Absolute stability alone, and not necessarily passivity, guarantees the validity of all the conversion loss formulas mentioned in this section. It should be noted that an absolutely stable active network achieves conversion gain in one direction only, i.e. L_{12} or $L_{21} < 1$.

For potentially unstable networks the above formulas do not hold since the minimum available conversion loss in this case is zero, i.e. infinite gain. However, if either

$$2\, m_{11}^r\, m_{22}^r \geq \mathrm{Re}\,(m_{12}\, m_{21}) + |m_{12}\, m_{21}| \quad (\geq 0) \qquad \text{(A1.42a)}$$

or

$$2\, m_{11}^r\, m_{22}^r \leq R_e\,(m_{12}\, m_{21}) - |m_{12}\, m_{21}| \quad (\leq 0) \qquad \text{(A1.42b)}$$

is satisfied, all the square roots involved in the above analysis will be real. Thus, the above formulas will hold and give a stationary point on the conversion loss curve which is not necessarily the minimum. In this case the conversion loss should be defined on an "exchangeable" basis* instead of an "available" basis.

* See Haus and Adler (I, Sec. 2.3).

A1.5. Sensitivity to Source Impedance Variations

If one is given L_{opt} and $W_{s,opt}$ a question arises: Can the conversion loss be determined for any W_s? Examining the general equation for the conversion loss, Eq. (A1.25), we note that we have six unknowns; namely, m_{11}^r, m_{11}^i, m_{22}^r, $Re(m_{12}m_{21})$, $Im(m_{12}m_{21})$ and $\left|\frac{m_{12}}{m_{21}}\right|$. Since we have only three equations, L_{opt}, $W_{s,opt}^r$ and $W_{s,opt}^i$, it looks at first that the answer to the above question is no. However, interestingly enough, the answer is yes <u>if</u> the magnitude reciprocity condition $|m_{12}| = |m_{21}|$ is satisfied.

Algebraic manipulations of Eqs. (A1.25) ... (A1.34) under the assumption that $|m_{12}| = |m_{21}|$ gives

$$\frac{L}{L_{opt}} = \frac{1 + \frac{L_{opt}^2 - 1}{L_{opt}^2 + 1}\left[\frac{1}{2}\left(\frac{W_s^r}{W_{s,opt}^r} + \frac{W_{s,opt}^r}{W_s^r}\right) + \frac{(W_s^i - W_{s,opt}^i)^2}{2\, W_s^r\, W_{s,opt}^r}\right]}{1 + \frac{L_{opt}^2 - 1}{L_{opt}^2 + 1}} \qquad \text{(A1.43)}$$

From the above equation it is clear that the nearer L_{opt} is to unity, the less sensitive the conversion loss is to the source impedance variations. In the limit when $L_{opt} = 1$ for a <u>finite</u> optimum source impedance, it follows that $L = 1$ for any source impedance; this occurs only for a lossless network, condition (A1.15). Actually, examining

Eq. (A1.25), one can deduce that L is independent of W_s if and only if $m_{11}^r = 0$, $m_{22}^r = 0$ and $m_{12} = \mp m_{21}^*$ which yields a value of $L = \pm 1$.

If $W_s^i = W_{s,opt}^i$, Eq. (A1.43) simplifies to

$$\frac{L}{L_{opt}} = \frac{1 + \dfrac{L_{opt}^2 - 1}{L_{opt}^2 + 1} \dfrac{1}{2}\left\{\dfrac{W_s^r}{W_{s,opt}^r} + \dfrac{W_{s,opt}^r}{W_s^r}\right\}}{1 + \dfrac{L_{opt}^2 - 1}{L_{opt}^2 + 1}} \quad . \tag{A1.44}$$

This equation is plotted in Fig. A1.4.

The following useful incremental sensitivity relations can be developed from Eq. (A1.43):

$$\left.\frac{\partial^2 L}{\partial (W_s^r / W_{s,opt}^r)^2}\right|_{W_s = W_{s,opt}} = \left.\frac{\partial^2 L}{\partial (W_s^i / W_{s,opt}^r)^2}\right|_{W_s = W_{s,opt}}$$

$$= \frac{L_{opt}^2 - 1}{2 L_{opt}} \quad . \tag{A1.45}$$

The second derivatives were considered rather than the first derivatives since the latter are zero by definition.

If we are given L_{opt}, $W_{s,opt}$ and $W_{o,opt}$, and if the assumption $|m_{12}| = |m_{21}|$ is still valid, we can add to the above equation the incremental magnitude sensitivity of W_o. This can be found from Eq. (A1.24) to be

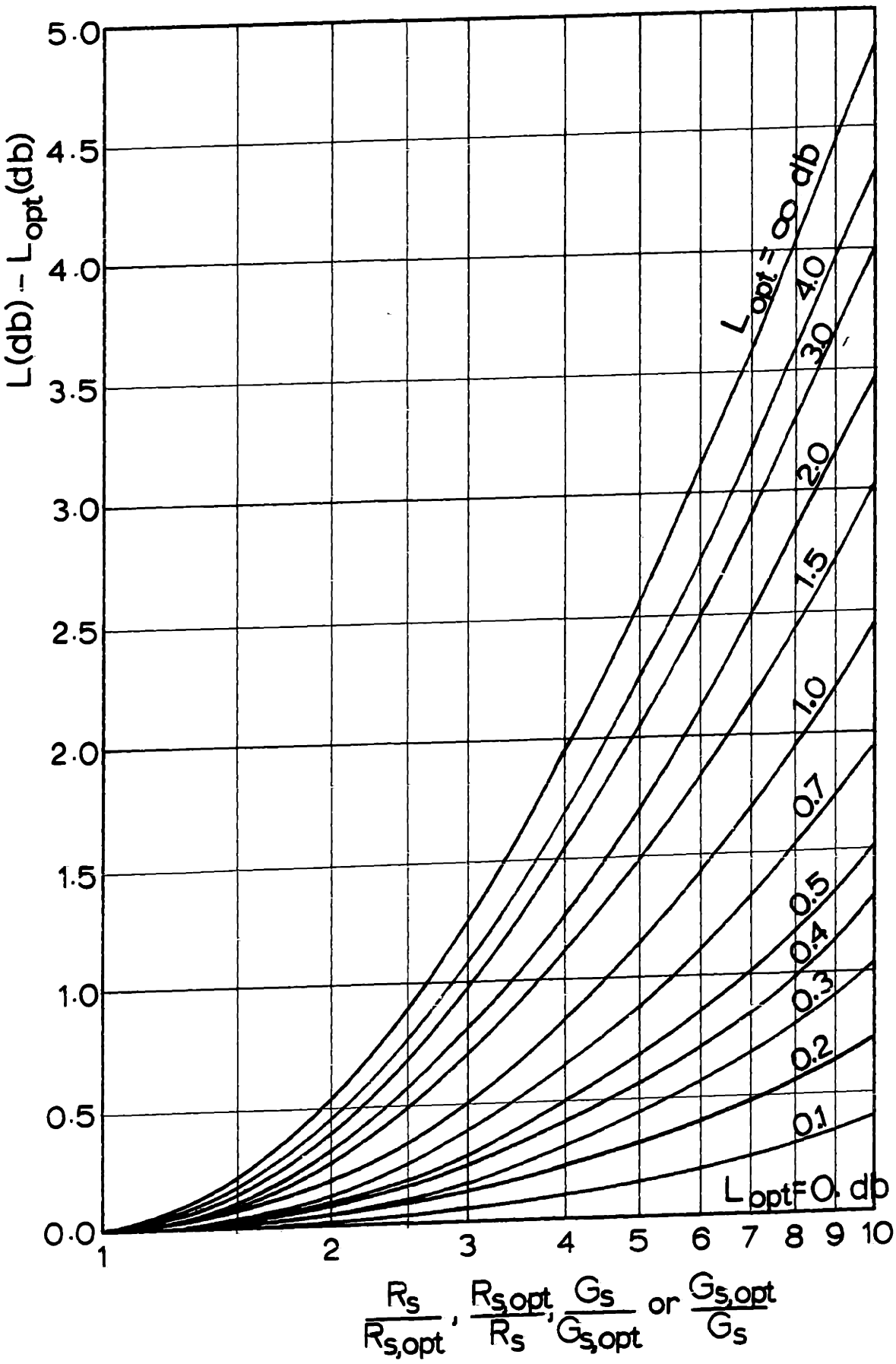

Fig. A1.4. Conversion Loss vs. Normalized Source Resistance

$$\left|\frac{\partial W_o}{\partial W_s}\right| \Bigg|_{W_s=W_{s,opt}} = \frac{W^r_{o,opt}}{W^r_{s,opt}} \frac{1}{L_{opt}} \quad . \qquad \text{(A1.46)}$$

If $|m_{12}| \neq |m_{21}|$ Eqs. (A1.43) . . . (A1.46) must be modified by replacing L_{opt} by $\left|\frac{m_{21}}{m_{12}}\right| L_{opt}$ in their right hand sides.

More useful sensitivity relations can be obtained for W_o if we assume that $m_{12} = \pm m^*_{21}$. This condition implies that the matrix $\underline{M}$ can be real symmetric, real skew symmetric, Hermitian or skew Hermitian. However, there is no restriction on the main diagonal of $\underline{M}$. With this condition Eqs. (A1.24) and (A1.26) . . . (A1.29) gives W_o as a function of W_s, for given values of L_{opt}, $W_{s,opt}$, as

$$W^r_o = W^r_{o,opt} \frac{\left[1+A\frac{W^r_s}{W^r_{s,opt}}\right]\left[A+\frac{W^r_s}{W^r_{s,opt}}\right] + A\left[\frac{W^i_s-W^i_{s,opt}}{W^r_{s,opt}}\right]}{\left[1+A\frac{W^r_s}{W^r_{s,opt}}\right]^2 + A^2\left[\frac{W^i_s-W^i_{s,opt}}{W^r_{s,opt}}\right]^2} \quad , \qquad \text{(A1.47)}$$

$$W^i_o = W^i_{o,opt} + W^r_{o,opt} \frac{\left[\frac{W^i_s-W^i_{s,opt}}{W^r_{s,opt}}\right]\left[1-A^2\right]}{\left[1+A\frac{W^r_s}{W^r_{s,opt}}\right]^2 + A^2\left[\frac{W^i_s-W^i_{s,opt}}{W^r_{s,opt}}\right]^2} \quad , \qquad \text{(A1.48)}$$

where

$$A = \begin{cases} (L_{opt} - 1) / (L_{opt} + 1) & \text{if } m_{12} = m_{21}^* \\ (L_{opt} + 1) / (L_{opt} - 1) & \text{if } m_{12} = -m_{21}^* \end{cases} \quad \text{(A1.49)}$$

If $W_s^i = W_{s,opt}^i$, Eq. (A1.47) simplifies to

$$\frac{W_o^r}{W_{o,opt}^r} = \frac{\frac{W_s^r}{W_{s,opt}^r} + A}{1 + A \frac{W_s^r}{W_{s,opt}^r}} \quad . \quad \text{(A1.50)}$$

This equation is plotted in Figure A1.5.

The incremental sensitivity of W_o can be deduced from Eqs. (A1.47) and (A1.48) to be

$$\left.\frac{\partial W_o}{\partial W_s}\right|_{W_s=W_{s,opt}} = \left.\frac{\partial W_o^r}{\partial W_s^r}\right|_{W_s=Ws,opt}$$

$$= \left.\frac{\partial W_o^i}{\partial W_s^i}\right|_{W_s=W_{s,opt}}$$

$$= \pm \frac{W_{o,opt}^r}{W_{s,opt}^r} \frac{1}{L_{opt}} \quad (\text{for } m_{12}=\pm m_{21}^*), \quad \text{(A1.51)}$$

and

$$\left.\frac{\partial W_o^r}{\partial W_s^i}\right|_{W_s=W_{s,opt}} = \left.\frac{\partial W_o^i}{\partial W_s^r}\right|_{W_s=W_{s,opt}} = 0. \quad \text{(A1.52)}$$

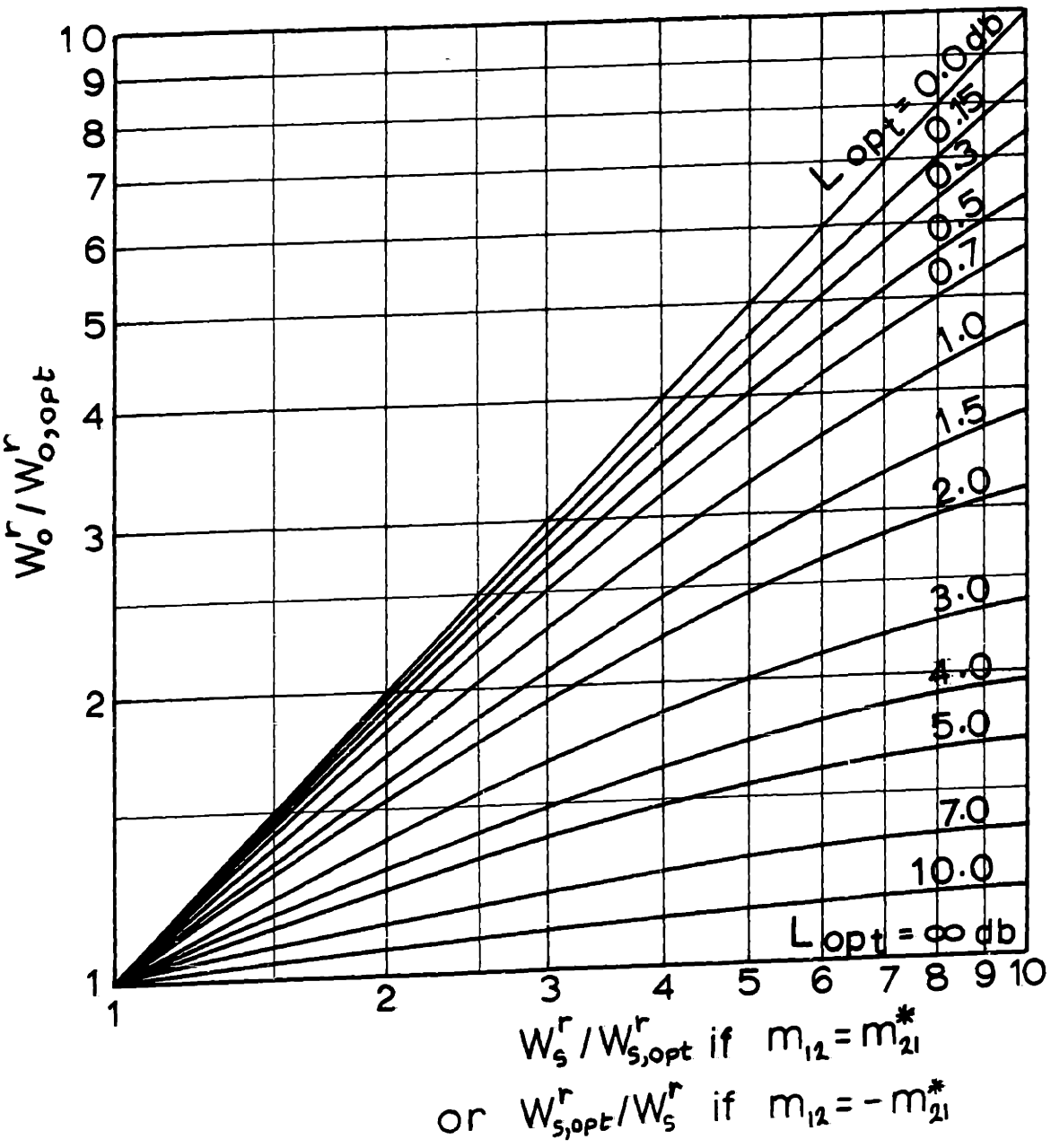

Fig. A1.5. Normalized Output Resistance vs. Normalized Input Resistance

APPENDIX 2

MIXERS WITH IMAGE FREQUENCY TERMINATIONS

A2.1. Generalized Matrix Representation

To study the effects of the image-frequency termination on the performance of a mixer we assume that all the higher order out-of-band frequencies are terminated inside the mixer. Thus we will only consider the signal, image and i-f frequencies. Although the signal and image frequencies appear in the same port, one can conceptually separate them in two different ports. In this case the mixer can be represented as a three-port network as given in Fig. A2.1.

The four basic two-port network matrices discussed in Sec. A1.1 can be extended to represent the three-port network of Fig. A2.1.

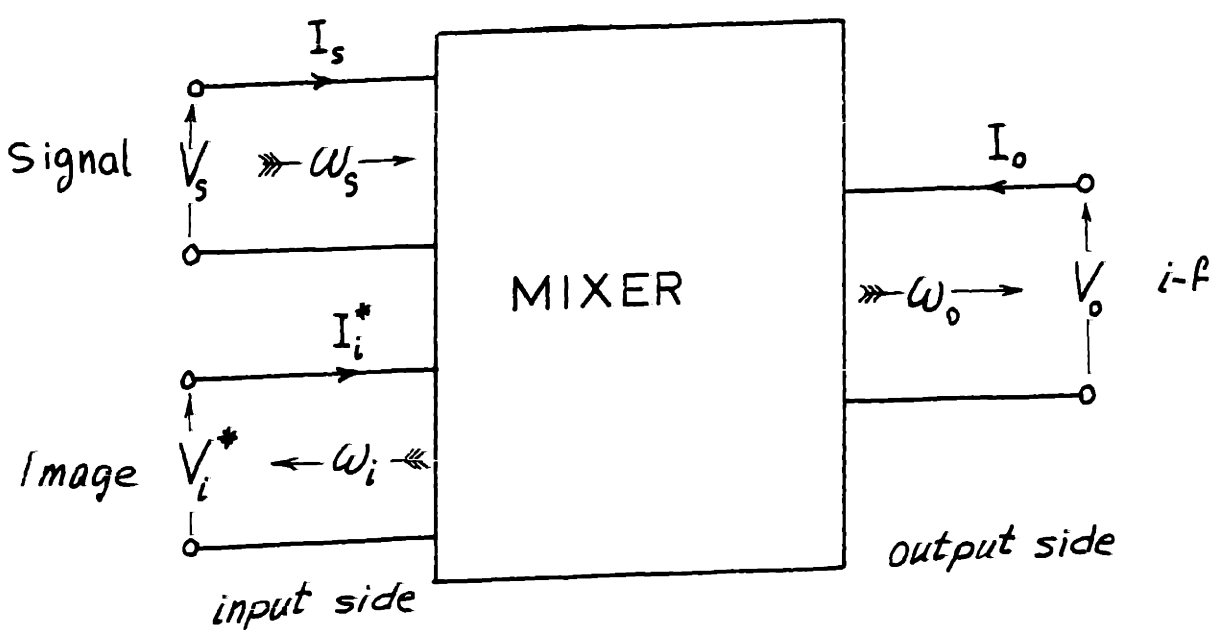

Fig. A2.1. Three-Port Representation of a Mixer

$$\text{Z-matrix} \quad \begin{bmatrix} V_s \\ V_o \\ V_i^* \end{bmatrix} = \begin{bmatrix} z_{11} & z_{12} & z_{13} \\ z_{21} & z_{22} & z_{23} \\ z_{31} & z_{32} & z_{33} \end{bmatrix} \begin{bmatrix} I_s \\ I_o \\ I_i^* \end{bmatrix} \quad . \quad (A2.1)$$

$$\text{Y-matrix} \quad \begin{bmatrix} I_s \\ I_o \\ I_i^* \end{bmatrix} = \begin{bmatrix} y_{11} & y_{12} & y_{13} \\ y_{21} & y_{22} & y_{23} \\ y_{31} & y_{32} & y_{33} \end{bmatrix} \begin{bmatrix} V_s \\ V_o \\ V_i^* \end{bmatrix} \quad . \quad (A2.2)$$

$$\text{H-matrix} \quad \begin{bmatrix} V_s \\ I_o \\ V_i^* \end{bmatrix} = \begin{bmatrix} h_{11} & h_{12} & h_{13} \\ h_{21} & h_{22} & h_{23} \\ h_{31} & h_{32} & h_{33} \end{bmatrix} \begin{bmatrix} I_s \\ V_o \\ I_i^* \end{bmatrix} \quad . \quad (A2.3)$$

$$\text{G-matrix} \quad \begin{bmatrix} I_s \\ V_o \\ I_i^* \end{bmatrix} = \begin{bmatrix} g_{11} & g_{12} & g_{13} \\ g_{21} & g_{22} & g_{23} \\ g_{31} & g_{32} & g_{33} \end{bmatrix} \begin{bmatrix} V_s \\ I_o \\ V_i^* \end{bmatrix} \quad . \quad (A2.4)$$

The duality relation among the above matrices suggest the use of a generalized representation.

$$\text{M-matrix} \quad \begin{bmatrix} u_s \\ u_o \\ u_i^* \end{bmatrix} = \begin{bmatrix} m_{11} & m_{12} & m_{13} \\ m_{21} & m_{22} & m_{23} \\ m_{31} & m_{32} & m_{33} \end{bmatrix} \begin{bmatrix} v_s \\ v_o \\ v_i^* \end{bmatrix} \quad . \quad (A2.5)$$

Table A2.1. Meaning of Generalized Notation

M	Z	Y	H	G
m_{ij}	z_{ij}	y_{ij}	h_{ij}	g_{ij}
u_s	V_s	I_s	V_s	I_s
v_s	I_s	V_s	I_s	V_s
u_o	V_o	I_o	I_o	V_o
v_o	I_o	V_o	V_o	I_o
u_i	V_i	I_i	V_i	I_i
v_i	I_i	V_i	I_i	V_i
W_s	Z_s	Y_s	Z_s	Y_s
W_{in}	Z_{in}	Y_{in}	Z_{in}	Y_{in}
W_o	Z_o	Y_o	Y_o	Z_o
W_L	Z_L	Y_L	Y_L	Z_L
W_i	Z_i	Y_i	Z_i	Y_i

If the image termination is included in the mixer, one obtains the generalized two-port equation

$$\begin{bmatrix} u_s \\ u_o \end{bmatrix} = \begin{bmatrix} M_{11} & M_{12} \\ M_{21} & M_{22} \end{bmatrix} \begin{bmatrix} v_s \\ v_o \end{bmatrix} \quad , \quad \text{(A2.6)}$$

where

$$M_{ij} = m_{ij} - \frac{m_{i3}\, m_{j3}}{m_{33} + W_i^*} \quad i,j = 1,2 \quad . \quad \text{(A2.7)}$$

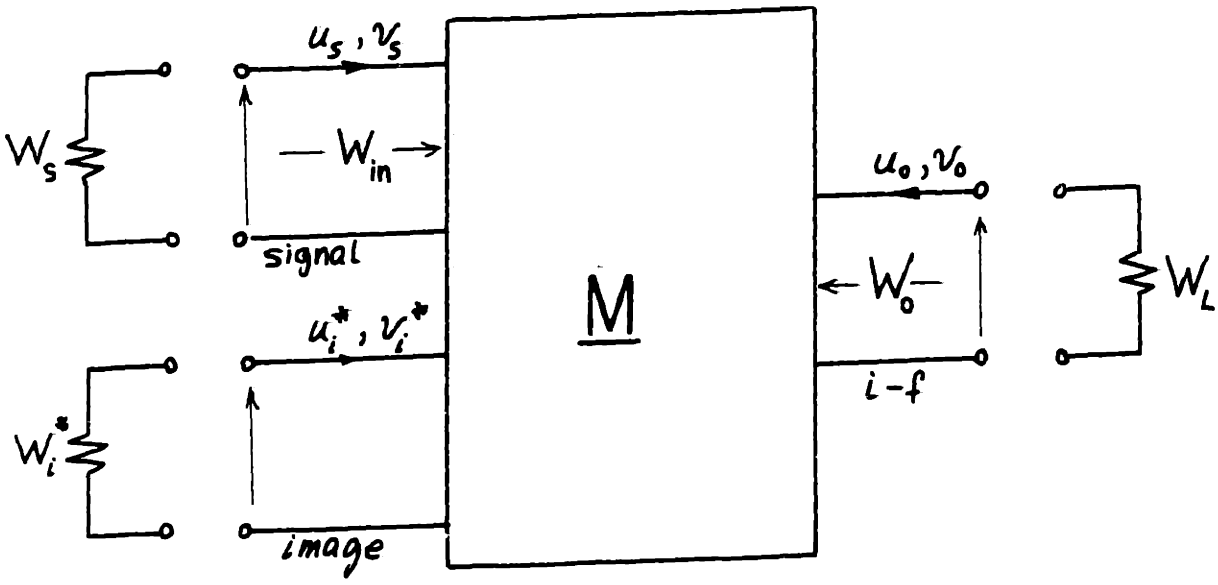

Fig. A2.2. Generalized Representation

The meanings of the u's, v's and W's are given in Table A2.1.

If the i-f frequency is much smaller than the signal frequency such that the signal and image frequencies can not be differentiated from oneanother inside the mixer, it can be shown that the M-matrix assumes the form** it can be shown that the M-matrix assumes the form**

$$\underline{M} = \begin{bmatrix} m_{11} & m_{12} & m_{13} \\ m_{21} & m_{22} & m_{21}^* \\ m_{13}^* & m_{12}^* & m_{11}^* \end{bmatrix} \quad , \quad (A2.8)$$

where m_{22} is real.

** See for example Torrey and Whitmer (I, Sec. 5.2) where the analysis is given for a Y-matrix.

In this case the performance of the mixer can be calculated with the help of Appendix 1.

There are two important questions that need to be answered:

1. What is the optimum image termination?
2. What is the optimum source impedance and conversion loss if the signal and image frequencies are terminated in the same impedance (broad-band input termination)?

The answer to these questions for a general M-matrix is straight forward but is quite involved algebraically. However, if the M-matrix is real, the results are simple. This case is dealt with in Sec. A2.2. The results of Sec. A2.2 can also apply to a complex matrix <u>if</u> it can be transformed to a real matrix by means of a <u>lossless</u> transformation**.

A2.2. Mixers Represented by Real Matrices

If the M-matrix of Eq. (A2.8) is real it assumes the form

$$\underline{M} = \begin{bmatrix} m_{11} & m_{12} & m_{13} \\ m_{21} & m_{22} & m_{21} \\ m_{13} & m_{12} & m_{11} \end{bmatrix} \quad . \quad (A2.9)$$

** See Peterson and Llewellyn (I) or Torrey and Whitmer (I, Sec. 5.12).

In this case it can be shown that the optimum image termination is either an open circuit or a short circuit.** Thus there are three types of image terminations to be considered: short circuit, open circuit and broadband input as given in Table A2.2.

Table A2.2. The Three Important Image Terminations

Case	Condition	Z- or H-Matrix	Y- or G-Matrix
1	$W_i = \infty$	Open Image	Short Image
2	$W_i = W_s$	B R O A D B A N D I N P U T	
3	$W_i = 0$	Short Image	Open Image

The following constants, which are needed later, are only dependent on the mixer and not its terminations.

$$\epsilon_1 = \frac{m_{12}\, m_{21}}{m_{11}\, m_{22}} \qquad (\leq 1) \qquad . \text{(A2.10)}$$

$$\theta = \frac{m_{13}}{m_{11}} \qquad (|\theta| \leq 1) \qquad . \text{(A2.11)}$$

$$\epsilon_2 = \frac{2\,\epsilon_1}{1 + \theta} \qquad (\leq 1) \qquad . \text{(A2.12)}$$

$$\epsilon_3 = \frac{\epsilon_1}{1 - \epsilon_1} \frac{1 - \theta}{1 + \theta} \qquad (\leq 1) \qquad . \text{(A2.13)}$$

$$(1 - \epsilon_1)\,(1 - \epsilon_3) = (1 - \epsilon_2) \qquad . \text{(A2.14)}$$

** See for example Torrey and Whitmer (I, Sec. 5.9). Here we use some of their terminology.

The inequalities hold if the mixer is passive.

We now write the equations for the three types of image terminations.

1. $W_i = \infty$

$$W_o = m_{22} \left[1 - \frac{\epsilon_1}{1 + x_1}\right] \quad . \text{(A2.15)}$$

$$L = \frac{m_{12}}{m_{21}} \frac{(x_1 + 1)(x_1 + 1 - \epsilon_1)}{x_1 \epsilon_1} \quad . \text{(A2.16)}$$

$$x_1 = W_s / m_{11} \quad . \text{(A2.17)}$$

$$L_1 = L_{opt} = \frac{m_{12}}{m_{21}} \frac{1 + \sqrt{1 - \epsilon_1}}{1 - \sqrt{1 - \epsilon_1}} \quad (\geq 1) \quad . \text{(A2.18)}$$

$$W_{s,opt} = m_{11} \sqrt{1 - \epsilon_1} \quad . \text{(A2.19)}$$

$$W_{o,opt} = m_{22} \sqrt{1 - \epsilon_1} \quad . \text{(A2.20)}$$

2. $W_i = W_s$

$$W_o = m_{22} \left[1 - \frac{\epsilon_2}{1 + x_2}\right] \quad . \text{(A2.21)}$$

$$L = 2 \frac{m_{12}}{m_{21}} \frac{(x_2 + 1)(x_2 + 1 - \epsilon_2)}{x_2 \epsilon_2} \quad . \text{(A2.22)}$$

$$x_2 = \frac{W_s / m_{11}}{1 + \theta} \quad . \text{(A2.23)}$$

$$L_2 = L_{opt} = 2 \frac{m_{12}}{m_{21}} \frac{1 + \sqrt{1 - \epsilon_2}}{1 - \sqrt{1 - \epsilon_2}} \quad (\geq 2) \quad . \text{(A2.24)}$$

$$W_{s,opt} = m_{11}\,(1+\theta)\,\sqrt{1-\epsilon_2} \qquad . \text{(A2.25)}$$

$$W_{o,opt} = m_{22}\,\sqrt{1-\epsilon_2} \qquad . \text{(A2.26)}$$

3. $W_i = 0$

$$W_o = m_{22}\,(1-\epsilon_1)\left(1-\frac{\epsilon_3}{1+x_3}\right) \qquad . \text{(A2.27)}$$

$$L = \frac{m_{12}}{m_{21}}\,\frac{(x_3+1)\,(x_3+1-\epsilon_3)}{x_3\,\epsilon_3} \qquad . \text{(A2.28)}$$

$$x_3 = \frac{W_s/m_{11}}{1-\theta^2} \qquad . \text{(A2.29)}$$

$$L_3 = L_{opt} = \frac{m_{12}}{m_{21}}\,\frac{1+\sqrt{1-\epsilon_3}}{1-\sqrt{1-\epsilon_3}} \quad (\geq 1) \qquad . \text{(2.30)}$$

$$W_{s,opt} = m_{11}\,(1-\theta^2)\,\sqrt{1-\epsilon_3} \qquad . \text{(A2.31)}$$

$$W_{o,opt} = m_{22}\,(1-\epsilon_1)\,\sqrt{1-\epsilon_3} \qquad . \text{(A2.32)}$$

The optimum image termination is either $W_i = \infty$ or $W_i = 0$ depending whether $\epsilon_1 > \epsilon_3$ or $\epsilon_3 > \epsilon_1$ respectively.

In cases 1 and 3 the mixer can be considered as a two-port network independent of the source and load terminations, thus the results of Appendix 1 hold. This is not true for case 2 (the broadband input termination). However, the results of Sec. A1.5 concerning the sensitivity of L and W_o to the source impedance variations, can be

applied in this case of L and L_{opt} there are replaced by L/2 and $L_{opt}/2$. An interesting and often overlooked result in the case of broadband input termination is that if the mixer is operating with optimum source impedance and matched i-f port, the signal port is <u>not</u> matched. In fact one can show that if $W_L = W_{o,opt}$ and $W_i = W_{s,opt}$, then

$$\frac{W_{in}}{W_{s,opt}} = \frac{3\,(1-\theta) + (1+\theta)\sqrt{1-\epsilon_2}}{(1-\theta) + 3\,(1+\theta)\sqrt{1-\epsilon_2}} \qquad (A2.33a)$$

$$= \frac{\epsilon_1/\sqrt{1-\epsilon_1} + 3\,\epsilon_3/\sqrt{1-\epsilon_3}}{3\,\epsilon_1/\sqrt{1-\epsilon_1} + \epsilon_3/\sqrt{1-\epsilon_3}} \qquad (A2.33b)$$

The signal port will only be matched if $\epsilon_1 = \epsilon_3$.

APPENDIX 3

THE LINEAR PERIODICALLY TIME-VARYING RESISTANCE

A3.1. Time- and Frequency-Domain Representations

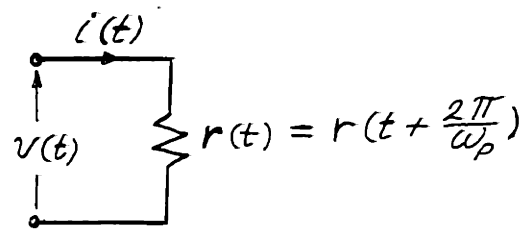

Fig. A3.1 Time-Domain Representations

Let the resistance waveform be

$$r(t) = r_o + 2 \sum_{n=-\infty}^{\infty} r_n \cos(n\omega_p t + \theta_n) \quad , \qquad (A3.1)$$

$$= \sum_{n=-\infty}^{\infty} r_n \, e^{jn\omega_p t} \quad , \qquad (A3.2)$$

where

$$r_n = r_{-n}^{*} = |r_n| \, e^{j\theta_n} \quad , \qquad (A3.3)$$

$$= \langle r(t) \, e^{-jn\omega_p t} \rangle \quad . \qquad (A3.4)$$

If

$$v(t) = \sum_{n=-\infty}^{\infty} V_n \, e^{j(n\omega_p + \omega_o)t} \quad , \qquad (A3.5)$$

and

$$i(t) = \sum_{n=-\infty}^{\infty} I_n \, e^{j(n\omega_p + \omega_o)t} \quad , \qquad (A3.6)$$

then the time domain equation

$$v(t) = r(t) \, i(t) \qquad (A3.7)$$

can be written in the frequency-domain as

$$\begin{bmatrix} \vdots \\ V_{+3} \\ V_{+2} \\ V_{+1} \\ V_0 \\ V_{-1} \\ V_{-2} \\ V_{-3} \\ \vdots \end{bmatrix} = \begin{bmatrix} \ddots & \ddots & \ddots & \ddots & \ddots & \ddots & \ddots & \ddots \\ \ddots & r_0 & r_1 & r_2 & r_3 & r_4 & r_5 & r_6 \\ \ddots & r_1^* & r_0 & r_1 & r_2 & r_3 & r_4 & r_5 \\ \ddots & r_2^* & r_1^* & r_0 & r_1 & r_2 & r_3 & r_4 \\ \ddots & r_3^* & r_2^* & r_1^* & r_0 & r_1 & r_2 & r_3 \\ \ddots & r_4^* & r_3^* & r_2^* & r_1^* & r_0 & r_1 & r_2 \\ \ddots & r_5^* & r_4^* & r_3^* & r_2^* & r_1^* & r_0 & r_1 \\ \ddots & r_6^* & r_5^* & r_4^* & r_3^* & r_2^* & r_1^* & r_0 \\ \ddots & \ddots & \ddots & \ddots & \ddots & \ddots & \ddots & \ddots \end{bmatrix} \begin{bmatrix} \vdots \\ I_{+3} \\ I_{+2} \\ I_{+1} \\ I_0 \\ I_{-1} \\ I_{-2} \\ I_{-3} \\ \vdots \end{bmatrix} \quad .(A3.8)$$

or $$\underline{V} = \underline{Z}\,\underline{I} \qquad (A3.9)$$

where $\underline{V} = \{V_n\}$, $\underline{I} = \{I_n\}$ and $\underline{Z}$ is the $\infty \times \infty$ Hermitian matrix with entries

$$Z_{ij} = Z_{ji}^* = r_{i-j} \qquad i,j = +\infty, \ldots, -\infty. \qquad (A3.10)$$

If the conductance waveform g(t) is given, then

$$i(t) = g(t)\, v(t) \quad , \qquad (A3.11)$$

or $$\underline{I} = \underline{Y}\,\underline{V} \quad , \qquad (A3.12)$$

where $$Y_{ij} = Y_{ji}^* = g_{i-j} \qquad i,j = +\infty, \ldots, -\infty. \qquad (A3.13)$$

with $$g_n = \langle g(t)\, e^{-jn\omega_p t} \rangle \quad . \qquad (A3.14)$$

If $g(t) = 1/r(t)$ then*

$$\underline{Y} = \underline{Z}^{-1} \quad . \qquad (A3.15)$$

* The inverse of an infinite matrix is not necessarily unique; see for example Cooke (I, Sec. 2.2). Thus, $\underline{Y}$ could not be calculated uniquely from Eq. (A3.15).

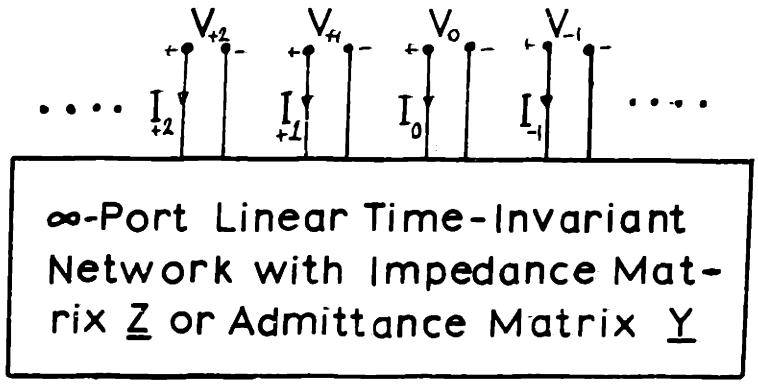

Fig. A3.2. Frequency-Domain Representation

The frequency-domain representation of r(t) is shown in Fig. A3.2. The conceptual separation of signals of different frequencies at different ports is possible because of their mutual orthogonality.

A3.2. Power Relations

If $|V_n|$ and $|I_n|$ of Eqs. (A3.5) and (A3.6) are root-mean-square values then the time-average power in r(t) is given by

$$P = \mathrm{Re} < v(t)\ i^*(t) > \quad . \tag{A3.16}$$

Since $v(t)\ i^*(t) = r(t)\ |i(t)|^2$ is real, then

$$P = < v(t)\ i^*(t) > \tag{A3.17}$$

$$= \sum_{n=-\infty}^{\infty} V_n\ I_n^* \quad . \tag{A3.18}$$

Since P is real it follows that*

* Cf. Manley and Rowe (I, p. 913) and Penfield (I, Frequency Power Formulas Type II).

$$\sum_{n=-\infty}^{\infty} \text{Im}\,(V_n I_n^*) = 0 \quad . \tag{A3.19}$$

Thus
$$P = \sum_{n=-\infty}^{\infty} P_n \quad , \tag{A3.20}$$

where
$$P_n = \text{Re}\,(V_n I_n^*) \tag{A3.21}$$

is the time-average power entering r(t) at frequency $\omega_n = n\omega_p + \omega_o$.

It is to be noted that P_n can be made zero for a given ω_n if: 1. $V_n = 0$, $I_n \neq 0$; 2. $V_n \neq 0$, $I_n = 0$; or 3. $V_n \neq 0$, $I_n \neq 0$ but their phase angle differs by $\pm 90^o$. These three cases correspond respectively to short-circuiting, open-circuiting or reactively terminating the frequency ω_n across the terminals of r(t).

Since $P = \langle r(t) \left|i(t)\right|^2 \rangle$, it follows that if $r(t) \geq 0$ all t, then*

$$P = \sum_{n=-\infty}^{\infty} P_n \geq 0. \tag{A3.22}$$

Thus for a nonnegative r(t), the total power available in all the modulation products is not greater than that supplied by the signal source. In other words, the conversion loss cannot be less than unity.

If $r(t) \geq 0$ then from (A3.22) ∞-port network of Fig. A3.1 is passive and its impedance matrix $\underline{Z}$ is positive

* The frequency power formulas given by Page (I), Pantell (I) and Penfield (I, Formulas Type III) do not have any consequence other than (A3.22) when applied to a nonnegative linear periodically time-varying resistance.

semidefinite*, i.e.

$$r(t) \geq 0 \iff \underline{Z} \geq 0. \qquad \text{(A3.23)}$$

If follows that all the principle minors of $\underline{Z}$ should be nonnegative**, i.e.

$$r_o \geq 0 \quad , \qquad \text{(A3.24a)}$$

$$\begin{vmatrix} r_o & r_n \\ r_n^* & r_o \end{vmatrix} \geq 0 \quad \text{all } n \quad , \qquad \text{(A3.24b)}$$

$$\begin{vmatrix} r_o & r_n & r_{n+m} \\ r_n^* & r_o & r_m \\ r_{n+m}^* & r_m^* & r_o \end{vmatrix} \geq 0 \quad \text{all } n,m \quad , \qquad \text{(A3.24c)}$$

and so on. The dual of the above relations apply if $g(t)$ is known instead of $r(t)$.

* Actually passivity implies that $\underline{Z} + \underline{Z}^+ \geq 0$ (see Sec. A1.2), but since Z is Hermitian then $\underline{Z} \geq \underline{0}$.
** Hildebrand (I, Sec. 1.20)

APPENDIX 4

MATHEMATICAL DERIVATIONS OF OPTIMUM RESISTANCE WAVEFORMS

Here we present the necessary mathematical derivations of the optimum resistance waveforms for the mixer imbedding networks discussed in Sec. 3.2.

A4.1. The Z- and Y-Mixers

The optimum resistance (conductance) waveform for a Z-mixer (Y-mixer) was shown in Sec. 3.2.1, Eq. (3.4), to be the solution of the problem:

Find $y(x)$ to maximize the functional

$$F(y) = \frac{\int_{-\pi}^{\pi} y(x) \cos(x)\, dx}{\int_{-\pi}^{\pi} y(x)\, dx} \qquad \text{(A4.1)}$$

under the constraint $Y_{min} \leq y(x) \leq Y_{max}$.

This problem is equivalent to the problem:

Find $y(x)$ to maximize

$$G(y) = \int_{-\pi}^{\pi} y(x) \cos(x)\, dx \qquad \text{(A4.2)}$$

under the constraints $Y_{min} \leq y(x) \leq Y_{max}$

and $A = \int_{-\pi}^{\pi} y(x)\, dx = \text{constant}$,

where the value of A should be chosen to maximize F(y).

It is clear that for a given area A under the y(x) curve, the value of G(y) can be maximized by concentrating as much area as possible under the y(x) curve around x= 0, i.e., where cos(x) is maximum. This is achieved by making

$$y(x) = Y_{max} \qquad |x| \leq \Delta/2$$

$$= Y_{min} \qquad \Delta/2 < |x| \leq \pi \qquad , \text{(A4.3)}$$

as shown in Fig. A4.1. The value of Δ can be deduced from A.

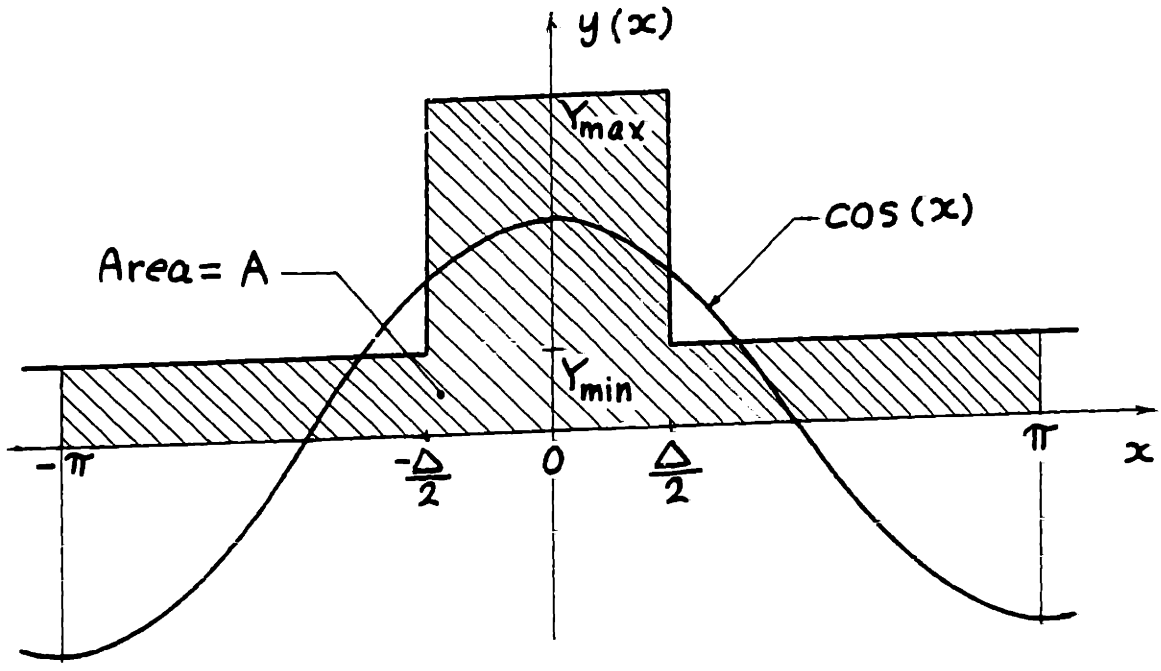

Fig. A4.1. The Optimum y(x)

Now the value of A or Δ , should be chosen to maximize F(y) as mentioned earlier. Substituting the optimum y(x) of Eq. (A4.3) into the expression for F(y) we get

$$F(y) = \frac{2(Y_{max} - Y_{min}) \sin(\Delta/2)}{2\pi Y_{min} + (Y_{max} - Y_{min})\Delta} \qquad . \text{(A4.4)}$$

Differentiating (A4.4) w.r.t. Δ and equating to zero we get the required value of Δ as the solution of the transcendental equation

$$\tan\left(\frac{\Delta}{2}\right) = \frac{\Delta}{2} + \frac{\pi Y_{min}}{Y_{max} - Y_{min}} \quad . \quad (A4.5)$$

A4.2. The H- and G-Mixers

The optimum resistance (conductance) waveform for an H-mixer (G-mixer) was shown in Sec. 3.2.2, Eq. (3.16), to be the solution of the problem:

Find $y(x)$ to maximize the functional

$$F(y) = \left.\frac{\left\{\int_{-\pi/2}^{\pi/2} \frac{y(x) - y(x+\pi)}{y(x) + y(x+\pi)} \cos(x)\, dx\right\}^2}{\int_{-\pi/2}^{\pi/2} \frac{2}{y(x)+y(x+\pi)}\, dx \int_{-\pi/2}^{\pi/2} \frac{2y(x)\, y(x+\pi)}{y(x) + y(x+\pi)}\, dx}\right\} \quad . \quad (A4.6)$$

under the constraint $Y_{min} \leq y(x) \leq Y_{max}$.

Our approach will be to find $y_n(x)$ to maximize the numerator and $y_d(x)$ to minimize the denominator and prove that $y_n(x) = y_d(x)$. This approach is not necessary, but it is certainly sufficient to find the optimum $y(x)$.

Since $\cos(x) \geq 0$, $-\pi/2 \leq x \leq \pi/2$, it follows that the numerator can be maximized by maximizing $\frac{y(x) - y(x+\pi)}{y(x) + y(x+\pi)}$. The latter is maximized by making

$$\left.\begin{aligned} y(x) &= y_n(x) = Y_{max} \\ \text{and} \\ y(x+\pi) &= y_n(x+\pi) = Y_{min} \end{aligned}\right\} \quad -\pi/2 \leq x \leq \pi/2. \quad (A4.7)$$

We now turn to minimizing the denominator, which can be written as

$$D = 4 \int_{-\frac{\pi}{2}}^{\frac{\pi}{2}} \int_{-\frac{\pi}{2}}^{\frac{\pi}{2}} \frac{1}{y(x_1) + y(x_1+\pi)} \frac{y(x_2)\ y(x_2+\pi)}{y(x_2) + y(x_2+\pi)}\ dx_1\ dx_2 \quad . (A4.8)$$

clearly by choosing $y(x_1) = Y_{max}$ and $y(x_2+\pi) = Y_{min}$; D is minimized irrespective of the values of $y(x_1+\pi)$ and $y(x_2)$. Of course, for a consistent choice, if $x_1 = x_2$ it must follow that $y(x_1) = y(x_2)$ and $y(x_1+\pi) = y(x_2+\pi)$; however, we will not use this restriction and later we will deduce that it is obtained. The integral of Eq. (A4.8) becomes

$$D = 4 \int_{-\frac{\pi}{2}}^{\frac{\pi}{2}} \int_{-\frac{\pi}{2}}^{\frac{\pi}{2}} \frac{1}{Y_{max} + y(x_1+\pi)} \frac{y(x_2)\ Y_{min}}{y(x_2) + Y_{min}}\ dx_1\ dx_2 \quad . \quad (A4.9)$$

The above integral can be modified to

$$D = 4 \int_{x_1=-\frac{\pi}{2}}^{\frac{\pi}{2}} \int_{x_2=-\frac{\pi}{2}}^{x_1} f(x_1,x_2)\ dx_1\ dx_2, \qquad (A4.10)$$

where

$$f(x_1,x_2) = \frac{1}{Y_{max} + y(x_1+\pi)} \frac{y(x_2)\ Y_{min}}{y(x_2) + Y_{min}}$$

$$+ \frac{1}{y(x_2) + Y_{min}} \frac{Y_{max}\ y(x_1+\pi)}{Y_{max} + y(x_1+\pi)} \quad . \quad (A4.11)$$

This is shown in Fig. (A4,2).

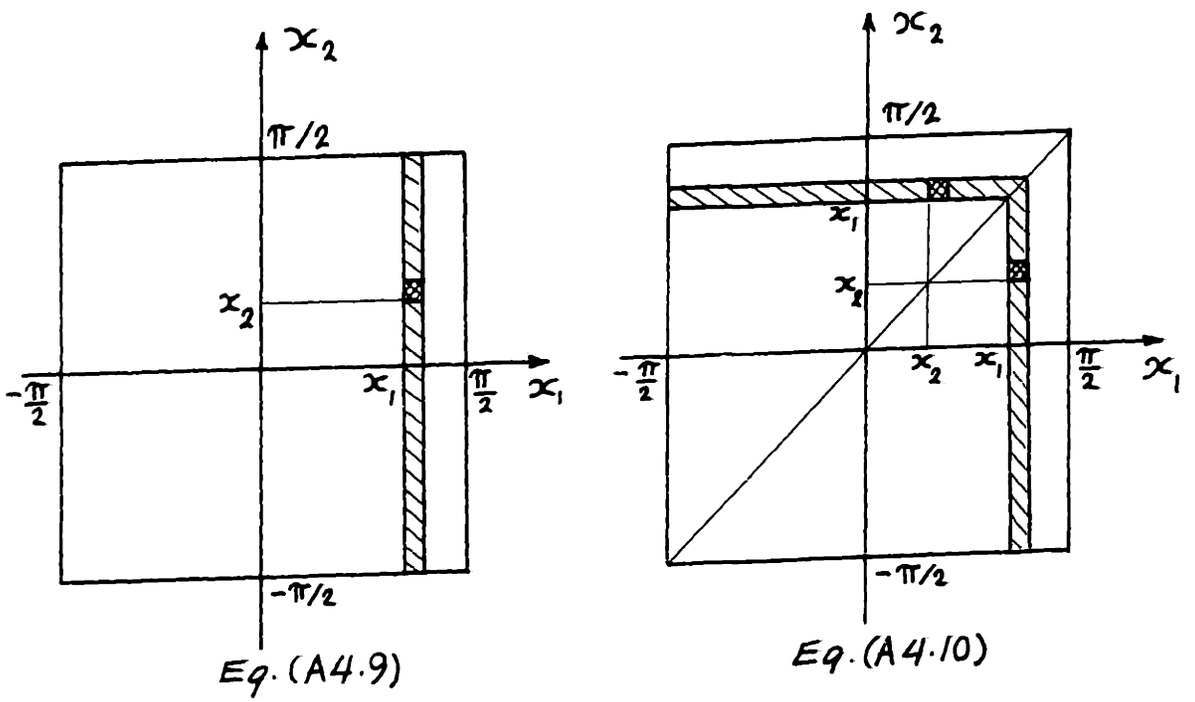

Fig. A4.2. Modifying the Integration

Now

$$\frac{\partial f(x_1,x_2)}{\partial\, y(x_1+\pi)} = \frac{1}{y(x_2) + Y_{min}} \frac{Y_{max}^2 - Y_{min}y(x_2)}{[y(x_1+\pi) + Y_{max}]^2} > 0, \quad (A4.12)$$

and

$$\frac{\partial f(x_1,x_2)}{\partial\, y(x_2)} = \frac{1}{Y_{max} + y(x_1+\pi)} \frac{Y_{min}^2 - Y_{max}y(x_1+\pi)}{[y(x_2) + Y_{min}]^2} < 0 \quad (A4.13)$$

where the inequalities follow because $y(x_2) \leq Y_{max}$ and $y(x_1+\pi) \geq Y_{min}$. From (A4.12) and (A4.13) it follows that $f(x_1,x_2)$ is minimized by setting $y(x_1+\pi) = Y_{min}$ and $y(x_2) = Y_{max}$, which is consistent with the previous choice $y(x_1) = Y_{max}$ and $y(x_2+\pi) = Y_{min}$. Thus we proved that the denom-

inator is minimized by setting

$$\left.\begin{aligned} y(x) &= y_d(x) = R_{max} \\ \text{and} \\ y(x+\pi) &= y_d(x+\pi) = R_{min} \end{aligned}\right\} -\pi/2 \le x \le \pi/2 \quad . \quad (A4.14)$$

Comparing Eqs. (A4.7) and (A4.14) we deduce that $y(x) = y_n(x) = y_d(x)$, $= \pi/2 \le x \le 3\pi/2$, maximized the numerator and minimized the denominator; and hence it maximizes $F(y)$ of (A4.6). This optimum $y(x)$ can be written as

$$\begin{aligned} y(x) &= R_{max} \qquad |x| \le \pi/2 \\ &= R_{min} \qquad \pi/2 \le x \le 3\pi/2 \end{aligned} \quad . \quad (A4.15)$$

A4.3. The H_N- and G_N-Mixers

The optimum resistance waveform for an H_N-mixer was shown in Sec. 3.2.3 to be the solution of the problem

$$\left.\begin{aligned} &\text{Maximize} \quad |\epsilon_N| = \frac{|H_{+1,o}|^2}{H_{+1,+1}\, H_{o,o}} \\ &\text{under the constraint } R_{min} \le r(t) \le R_{max} \end{aligned}\right\} , \quad (A4.16)$$

where the H's are given from Eqs. (2.42) and (2.37).

A detailed analysis of this problem, in the same manner as that used in Sec. A4.2 for the H- and G-mixers,

is quite complex. Without proof we write the primary results of such an analysis in the following:

The optimum r(t) must satisfy

1. $r(t) = r(-t)$
2. $r(t+2k\pi/N\omega_p) =$ Constant $(= R_{max}$ or $R_{min})$ in the range $-\pi/N\omega_p \leq t \leq \pi/N\omega_p$, for $k = 0, 1, \ldots, N-1$.
3. $r(t) = R_{max}$ around the origin and $r(t) = R_{min}$ in the remainder of the cycle.

The optimum r(t) that satisfies the above conditions is shown in Fig. A4.3.

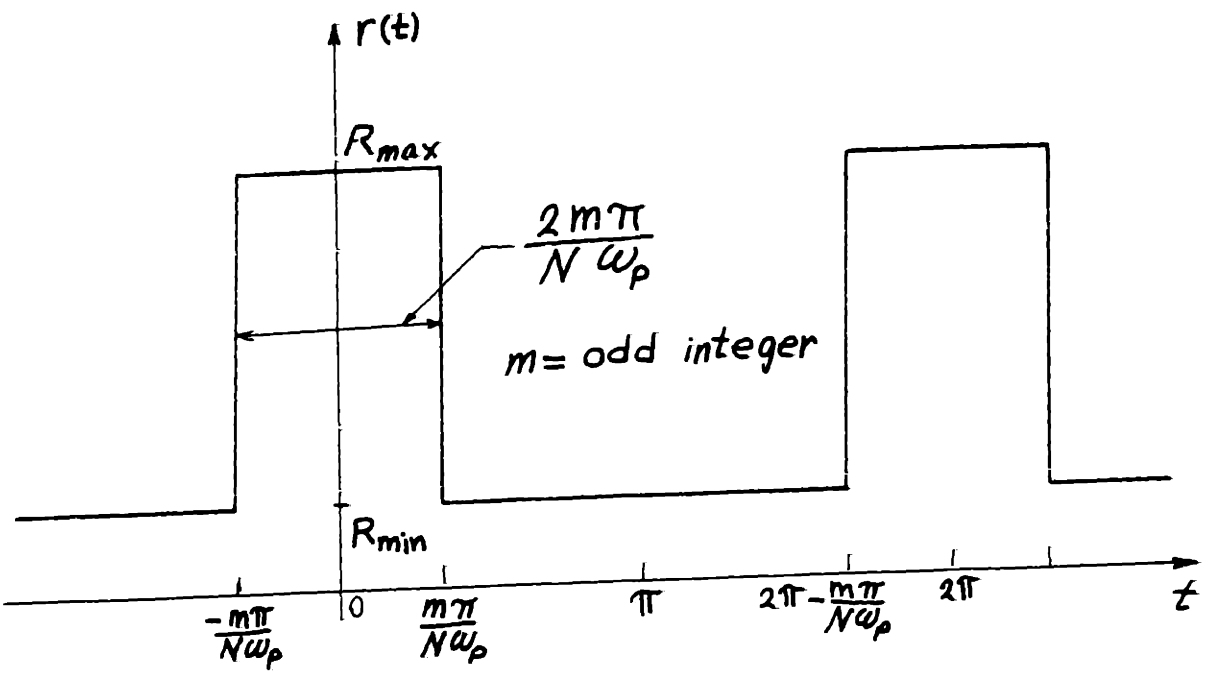

Fig. A4.3. The Suspected Optimum r(t)

We now have to find the optimum value of the odd integer m which produces the maximum value of $|\epsilon_N|$.

Substituting r(t) of Fig. A4.3 in Eq. (2.37) one obtains** for $-\pi/N\omega_p \le t \le \pi/N\omega_p$

$$r_{N\cdot n}(t) = [m R_{max} + (N-m) R_{min}] / N, \qquad (A4.17)$$

and

$$r_{N\cdot n+1}(t) = [R_{max} - R_{min}] / N \qquad . (A4.18)$$

From the above and Eqs. (2.42) we get

$$H_{+1,+1} = \frac{m R_{max} + (N-m) R_{min}}{N} - \frac{(R_{max}-R_{min})^2 / N}{m R_{max} + (N-m) R_{min}} \qquad , (A4.19a)$$

$$H_{o,o} = N / [\, m R_{max} + (N-m) R_{min} \,] \qquad , (A4.19b)$$

$$H_{+1,o} = \frac{\sin (m\pi/N)}{\pi / N} \frac{R_{max} - R_{min}}{m R_{max} + (N-m) R_{min}} \qquad , (A4.19c)$$

and finally

$$\epsilon_N(m) = - \frac{\left[\frac{\sin (m\pi/N)}{\pi / N}\right]^2}{[m + N R_{min}/(R_{max}-R_{min})]^2 - 1} \qquad ,$$

$$m = 1, 3, 5, \ldots ; \; m < N \qquad . (A4.20)$$

For N= 2, i.e. for the H- or G-mixers, or for N= 3 the only possible value for m is m= 1. Thus m= 1

** These formulas are valid for m= odd integer. If m= even integer, the right-hand side of Eq. (A4.18) should be multiplied by cos(π/N). This factor will cause the maximum of $|\epsilon_N|$ to occur for m= odd only.

maximizes $|\epsilon_N|$ for N= 2 or 3 for any value of R_{max}/R_{min}**. For N= 4, there are two possible values for m, m= 1 or 3. It can be shown by setting $|\epsilon_4(1)| \geq |\epsilon_4(3)|$ and solving for R_{max}/R_{min}, that m= 1 maximizes $|\epsilon_4|$ for any value of R_{max}/R_{min}.

For $N \geq 5$ the situation is more complex and the optimum value of m depends on the particular value of R_{max}/R_{min}. However, for a sufficiently large value of R_{max}/R_{min}, such that $N R_{min}/(R_{max}-R_{min}) \ll 1$, $|\epsilon_N|$ attains its maximum value for m= 1. This is true since in this case the denominator of Eq. (A4.20) becomes very small.

From the above we conclude that for any value of R_{max}/R_{min}, N= 2, 3 and 4; or for a sufficiently large value of R_{max}/R_{min}, $N \geq 5$, the optimum r(t) is given by

$$\begin{aligned} r(t) &= R_{max} && |t| \leq \pi/N\omega_p \\ &= R_{min} && \pi/N\omega_p \leq t \leq (2 - 1/N)\pi/\omega_p \end{aligned} \quad , \quad (A4.21)$$

for which

$$\epsilon_N = - \frac{\sin^2(\pi/N) \cdot (R_{max}/R_{min} - 1)/\pi}{2\pi/N + \pi/(R_{max}/R_{min} - 1)} \quad . \quad (A4.22)$$

For $N \geq 5$, it is interesting to find the limit on R_{max}/R_{min} for which the above formulas are valid. This can be calculated by noting that as R_{max}/R_{min} is reduced the optimum value of m shifts from 1 to 3. Thus, the required limit can be obtained by using Eq. (A4.20) and setting

** This was, of course, proven in Sec. A4.2 for N= 2.

$|\epsilon_N(1)| \geq |\epsilon_N(3)|$. This gives the condition for the validity of Eqs. (A4.21) and (A4.22) as

$$R_{max}/R_{min} \geq N\,[\,\cos(2\pi/N) + 1\,]\cos(2\pi/N) + 1 \quad . \text{(A4.23)}$$

The value of the optimum $\Delta/2$ for the Z- or Y-mixers, Eq. (A4.5), can be obtained from the above discussion as $\Delta/2 = m\pi/N$ in the limit as $N \to \infty$. Note that in this case condition (A4.23) is not satisfied except for $R_{max}/R_{min} = \infty$. For a finite value of R_{max}/R_{min}, Eq. (A4.20) gives

$$\lim_{N \to \infty} \epsilon_N(m) = -\left\{ \frac{\sin(m\pi/N)}{m\pi/N + \pi R_{min}/(R_{max}-R_{min})} \right\}^2 \quad . \text{(A4.24)}$$

Differentiating Eq. (A4.24) w.r.t. $m\pi/N$ and setting to zero we obtain the optimum value of $m\pi/N$ as the solution of the transcendental equation

$$\tan(m\pi/N) = m\pi/N + R_{min}/(R_{max}-R_{min}) \quad , \text{(A4.25)}$$

which is the same as Eq. (A4.5) for $\Delta/2$ as was expected.

APPENDIX 5

Proof of Theorems Concerning Optimum Imbedding Networks

Here we prove the theorem given in Sec. 3.3.1 and present an analysis which supports the hypothesis given there. We rewrite them here as

> Theorem: The optimum passive imbedding network for a mixer with a nonnegative time-varying resistance is lossless, i.e., the out-of-band frequencies should be terminated reactively.

> Hypothesis: The optimum passive imbedding network for a mixer with a nonnegative time-varying resistance should offer either an open-circuit or a short-circuit to each of the out-of-band frequencies if the time origin can be chosen to make the resistance waveform an even function of time.

A5.1. Proof of the Theorem

To prove the above theorem we first prove the following more fundamental network theorem.

> Theorem 0: The optimum passive terminations of n ports of a linear, unconditionally stable (n+2)-port network should be reactive to maximize the gain between the remaining two ports.

Note that passivity and reciprocity are not necessary conditions for this theorem. Also note that the theorem does not state that any set of reactive terminations is superior to any set of lossy terminations; in fact this is not generally true. We first prove the theorem for a

three-port network (n+2=3) and then show that it applies for any value of n.

Consider the linear, unconditionally stable three-port network of Fig. A5.1a. The transducer gain from port 1 to port 2 is given by

$$G = \frac{4}{R_1 R_2} \left| \frac{V_2}{I_1} \right|^2 \qquad , \text{(A5.1)}$$

The source and load impedances can be included in the network to form the three-port network of Fig. A5.1b. This network is also unconditionally stable since $R_1 > 0$, $R_2 > 0$ and the original network is unconditionally stable. Further, port 3 can be included in the network to form the reduced two-port network of Fig. A5.1c which is, of course, unconditionally stable. Its Z-matrix parameters can easily be shown to be

$$Z_{ij} = z_{ij} - \frac{z_{i3}\, z_{3j}}{z_{33} + Z_3} \qquad i,j = 1,2 \qquad , \text{(A5.2)}$$

where the z's are the Z-matrix parameters of the three-port network of Fig. A5.1b. Since

$$Z_{21} = \frac{V_2}{I_1} \qquad , \text{(A5.3)}$$

it follows that the gain in Eq. (A5.1) is maximized by maximizing $|Z_{21}|$. Thus we want to prove that $|Z_{21}|$ is maximized, under the constraint $R_3 \geq 0$, when $R_3 = 0$ for

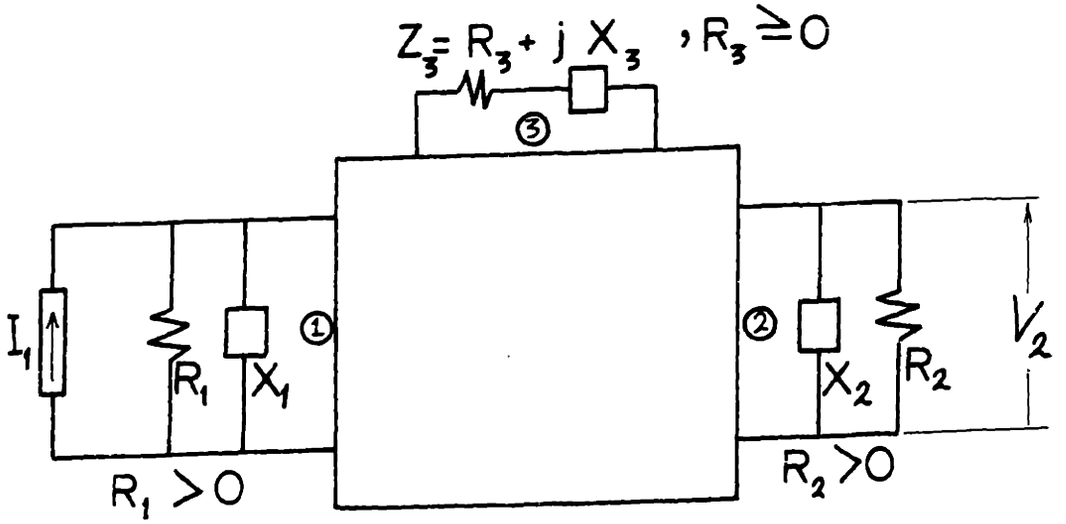

(a) Linear, Unconditionally Stable, Three-Port Network

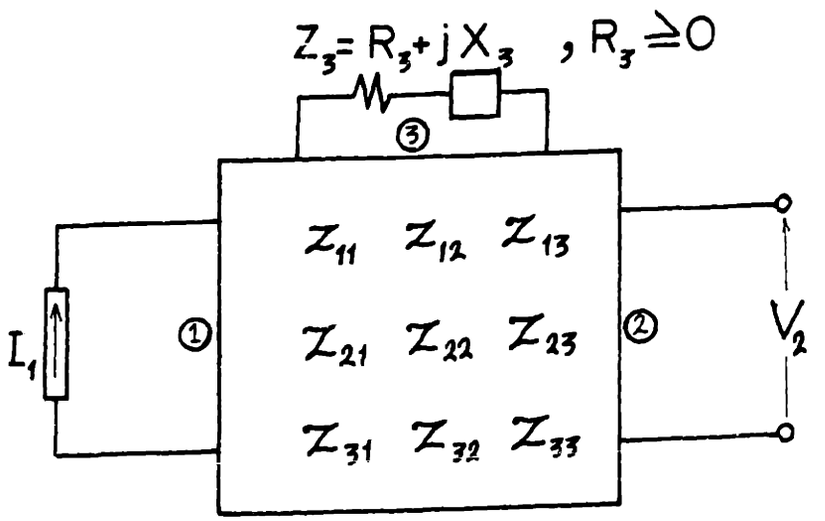

(b) Including the Source and Load Impedances in the Network

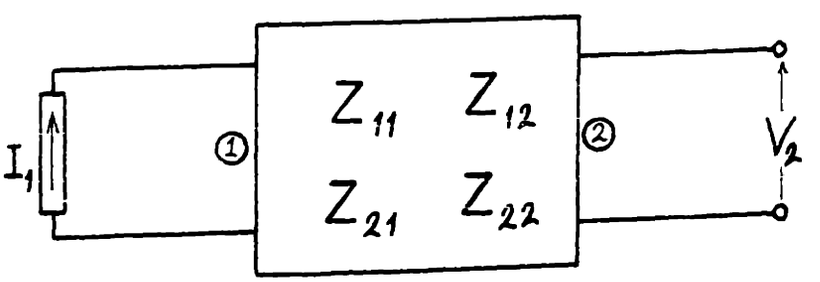

(c) Including Z_3 in the Network

Fig. A5.1. Steps for Proving Theorem 0

some value of X_3.

From Eq. (A5.2) it follows that

$$Z_{21} = z_{21} - \frac{z_{23}\, z_{31}}{z_{33} + Z_3} \qquad . \qquad . \quad (A5.4)$$

The $[1/(z_{33} + Z_3)]$ -plane is given in Fig. A5.2a. The locus of $1/(z_{33} + Z_3)$ for $R_3=0$ as X_3 varies from $-\infty$ to ∞ is clearly the circle shown in the figure. Since the network is unconditionally stable, thus $\mathrm{Re}[z_{33}] > 0$, it follows that the region inside the circle corresponds to $R_3>0$ and that the region outside the circle corresponds to $R_3 < 0$. From Eq. (A5.4) it follows that the locus of Z_{21} for $R_3 = 0$ is still a circle whose interior corresponds to $R_3 > 0$. This is shown in Fig. A5.2b. Clearly if R_3 is constrained to be nonnegative, it follows from this figure that $|Z_{21}|$ is maximized at the point m where $R_3 = 0$. Thus the gain from port 1 to port 2 is maximized when $R_3 = 0$ for some value of X_3. Thus port 3 has to be terminated reactively and hence Theorem 0 is proven for $n+2 = 3$.

If $n > 1$, one can apply the above proof to each of the n ports while considering the terminations of the remaining ports as a part of the network. This is possible since the terminations are restricted to be passive and hence the resulting network which includes the remaining ports is still unconditionally stable. Thus Theorem 0 is fully proven.

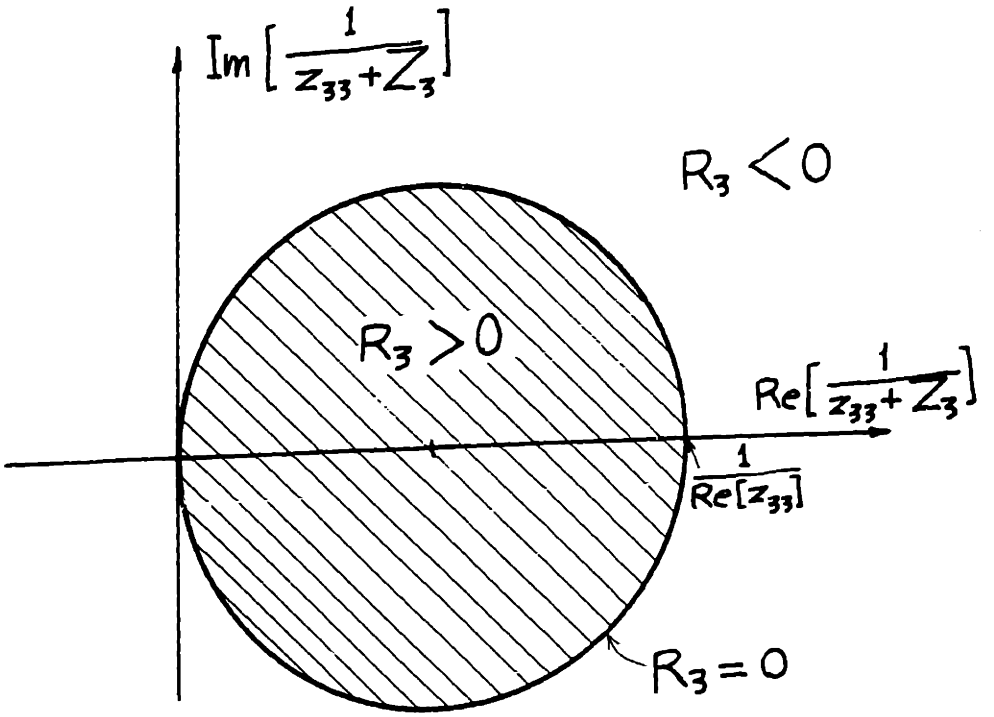

(a) $[1/(z_{33} + Z_3)]$ - Plane

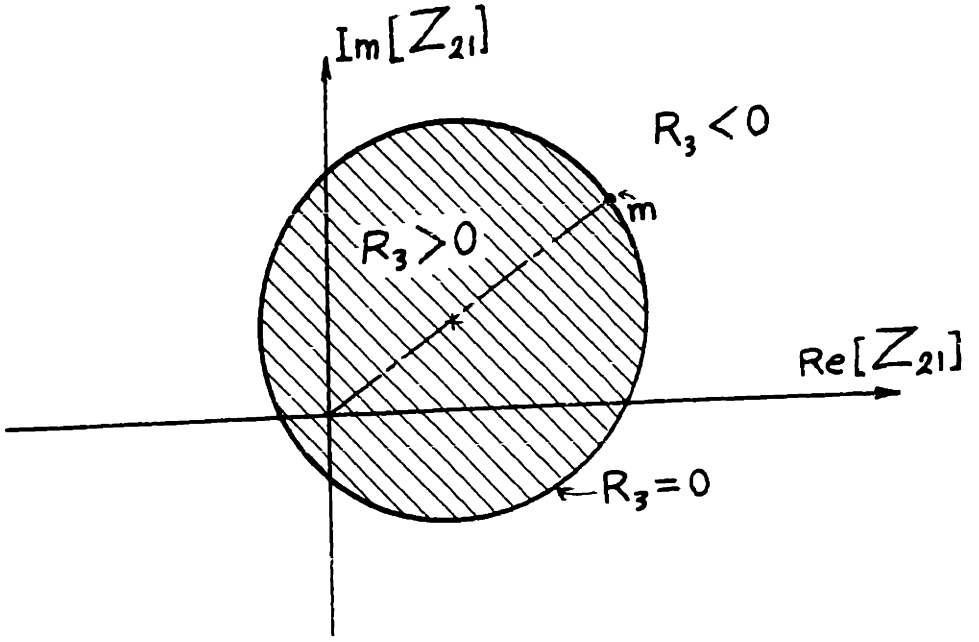

(b) Z_{21} - Plane

Fig. A5.2. Finding the Maximum Value of $|Z_{21}|$ Given $R_3 \geq 0$

Clearly Theorem 0 can be applied to a nonnegative time-varying resistance since this can be represented as a passive, and hence unconditionally stable, infinite-port network as given in Appendix 3. Thus the main theorem is proven.

A5.2. Discussing the Hypothesis

If the resistance waveform, r(t) in a mixer is a nonnegative even function of time it follows from Appendix 3 that the associated $\infty \times \infty$ Z-matrix is real, symmetric, nonnegative definite with equal entries along any line parallel to the main diagonal. From the above theorem and from the fact that r(t) is nonnegative, it follows that the out-of-band frequencies should be terminated reactively for minimum mixer conversion loss. The hypothesis gives a much stronger statement; namely, these reactive terminations should be either zero (short) or infinity (open) if r(t) is an even function of time. The following lemma will certainly support this hypothesis. It is based on the fact that the Z-matrix is real

> Lemma: Let the Z-matrix of an (n+2)-port network be real. Further let n of the ports be terminated in the reactances X_i, i = 1, 2, ... , n. The optimum available loss between the remaining two ports, $L(X_1, X_2, \ldots, X_n)$, will be stationary in the n-dimensional $X_1, X_2, \ldots, X_n$ space at the 2^n points corresponding to $X_i = 0$ or ∞; i =

1, 2, ... , n; excluding the points where L is infinite; i.e., when $L \neq \infty$, then

$$\left.\begin{aligned} &\frac{\partial L}{\partial X_i} = 0 \quad ; \quad i = 1, 2, \ldots, n \\ &\text{at} \quad X_i = 0 \text{ or } \infty \; ; \quad i = 1, 2, \ldots, n \end{aligned}\right\} \quad . \quad (A5.5)$$

This can be proven by noting that by setting all the X's except one, say X_k, to all possible combinations of zeros and infinities, then the optimum available loss, $L(X_k)$, in each case will be a continuous, smooth, even function of X_k, except when $L = \infty$. Thus, it follows that when $L(X_k)$ is finite it is stationary at $X_k = 0$ and ∞. The lemma is proven by letting k assume all the values 1, 2, ... , n.

Of course the above discussion does not prove that there is no other stationary points in the n-dimensional X_1, X_2, ... , X_n space. If this could be proven for any real Z-matrix similar to that of the time-varying resistance of the hypothesis, it would follow that the minimum value of L occurs at one of the points where the X's assume only the values of zero and infinity, and the hypothesis would be true.** If there are other stationary

** This can be proven for any unconditionally stable three-port network (n+2=3) with a general real Z-matrix. See also Torrey and Whitmer (I, Sec. 5.9) where a proof is given for a special three-port real matrix.

points however, one should prove that they do not represent a minima, or at least that if a minima exists it is not the minimum.

At this point a general proof along the above lines is needed, or any counter example should be found; to prove, or disprove, the hypothesis. This remains to be an open question.

Another promising procedure to prove the hypothesis is suggested in Fig. A5.3. It is similar to the procedure given in the previous section to prove the theorem. The network in Fig. A5.3a is a passive reciprocal n-port resistive network. This can represent the nonnegative r(t) which is an even function of time if $n = \infty$. The input and output ports are provided with resistances and reactances (represented in parallel) but the remaining ports are only provided with reactances since this is necessary to guarantee maximum gain between ports 1 and 2 as given in Theorem 0. In Fig. A5.3b, the source and load resistances are included in the network and their reactances are considered as separate ports. The transducer gain of the original network is given in Eq. (A5.1). Also Z_{21} of the modified network is given in Eq. (A5.3). Clearly maximizing the gain corresponds to maximizing $|Z_{21}|$.

The problem now reduces to proving, or perhaps disproving, that the $|Z_{21}|$ of the two-port resistive network with n reactances given in Fig. A5.3b is maximized

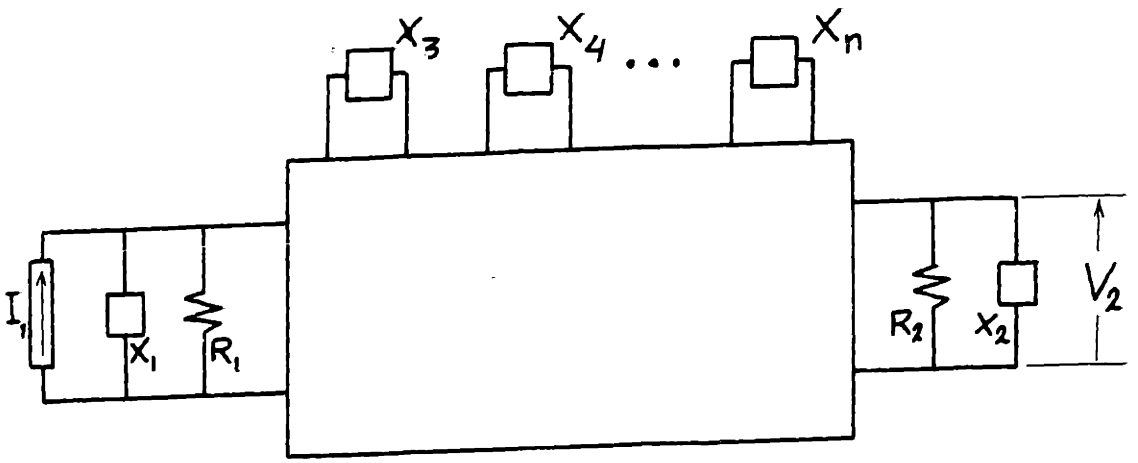

(a) An n-Port Resistive Network

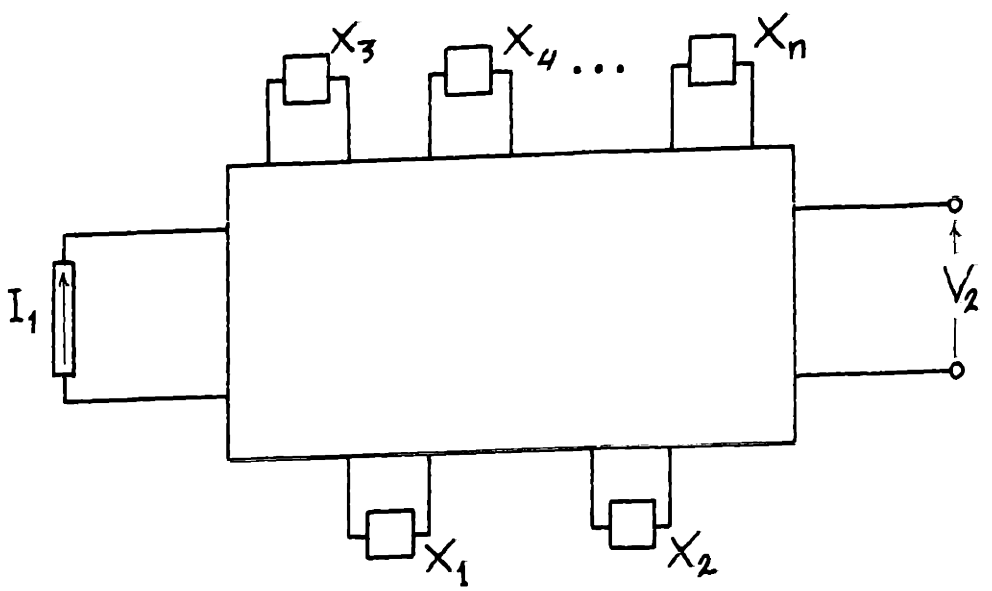

(b) Including R_1 and R_2 in the Network

Fig. A5.3. A Possible Procedure to Prove the Hypothesis

when the X's assume the values of 0 or ∞.

In the literature Huang and Lee (I) gave bounds on the impedance functions Z_{11}, Z_{12} and Z_{22} of any network of the form of Fig. A5.3b when their values are known at the two extremes when <u>all</u> the X's are zero and when <u>all</u> the X's are infinite. Along their line of analysis or employing a different procedure such as that used by Penfield, Spence and Duinker (I) to prove the Huang-Lee theorem, one might be able to obtain a stronger theorem where each of the X's is allowed to assume the value of 0 or ∞ independent of the remaining X's. This may lead to a proof or a disproof of the hypothesis.

APPENDIX 6

MATHEMATICAL DERIVATIONS FOR OPTIMUM IMBEDDING NETWORKS

Here we present the mathematical derivations necessary to determine the optimum imbedding networks for the resistance waveform discussed in Sec. 3.3.

A6.1. The Symmetric Tridiagonal Matrix

Here we find the determinant and inverse of a symmetric tridiagonal matrix of the form

$$\underline{A} = \begin{bmatrix} 1 & x & & & & & \\ x & 1 & x & & & & \\ & x & 1 & x & & & \\ & & x & 1 & \ddots & & \\ & & & \ddots & \ddots & \ddots & \\ & & & & \ddots & \ddots & x \\ & & & & & x & 1 \end{bmatrix} \qquad \text{(A6.1)}$$

This is a principal submatrix of the infinite Z-matrix representation of the normalized sinusoidal resistance waveform $r(t)/r_o = 1 + 2x\cos(\omega_p t)$. The results of this analysis are necessary for the derivation given in the next section.

Let $\Delta_n(x)$ be the determinant of an n x n matrix

of the form given above. It can be easily deduced that $\Delta_n(x)$ satisfies the three term recursion formula

$$\Delta_n(x) = \Delta_{n-1}(x) - x^2 \Delta_{n-2}(x) \quad . \quad (A6.2)$$

This formula is valid for any $n \geq 2$ if we note that

$$\Delta_1(x) = 1 \quad , \quad (A6.3)$$

and define

$$\Delta_o(x) = 1 \quad . \quad (A6.4)$$

A more general recursion formula can be deduced from Eq. (A6.2) as

$$\Delta_{n+m}(x) = \Delta_n(x)\, \Delta_m(x) - x^2 \Delta_{n-1}(x)\, \Delta_{m-1}(x) . \quad (A6.5)$$

Further, one can show that

$$\Delta_n(x) = \sum_{k=0}^{[n/2]} (-1)^k \binom{n-k}{k} x^{2k} \quad , \quad (A6.6)$$

where $[n/2]$ indicates the integer part of $n/2$.

Fortunately, the summation of Eq. (A6.6) can be put in a closed form in terms of the Tschebycheff polynomial of the second kind given by**

** A more common form is $U_n(\cos\theta) = \sin[(n+1)\theta]/\sin\theta$, see for example Abramowitz and Stegun (I, Ch. 22).

$$U_n(z)\begin{cases} = \dfrac{\sin[(n+1)\cos^{-1}z]}{\sqrt{1-z^2}} & , z \leq 1 \quad (A6.7) \\ = \dfrac{\sinh[(n+1)\cosh^{-1}z]}{\sqrt{z^2-1}} & \\ = \dfrac{(z+\sqrt{z^2-1})^{n+1} - (z-\sqrt{z^2-1})^{n+1}}{2\sqrt{z^2-1}} & \end{cases} z \geq 1, (A6.8)$$

which can be written as

$$U_n(z) = \sum_{k=0}^{[n/2]} (-1)^k \binom{n-k}{k} (2z)^{n-2k} \quad . (A6.9)$$

Comparing Eqs. (A6.6) and (A6.9) one obtains

$$\Delta_n(x) = x^n U_n\left[\frac{1}{2x}\right] \quad . (A6.10)$$

It can be shown that

$$\Delta_n(\tfrac{1}{2}) = (n+1)\, 2^{-n} \quad . (A6.11)$$

Now we find the inverse matrix

$$\underline{B} = [b_{ij}] = \underline{A}^{-1} \quad . (A6.12)$$

The entries of $\underline{B}$ can be calculated from**

$$b_{ij} = (-1)^{i-j} M_{ji}/\Delta_n(x) \quad , (A6.13)$$

** See Hildebrand (I, Sec. 1.4 and 1.6).

where M_{ji} is the minor of a_{ji}. It can be verified that

$$M_{ij} = M_{ji} = x^{j-i} \triangle_{i-1}(x) \triangle_{n-j}(x) \quad , \; j \geq i. \quad \text{(A6.14)}$$

Thus

$$b_{ij} = b_{ji} = (-1)^{i+j} \frac{x^{j-i} \triangle_{i-1}(x) \triangle_{n-j}(x)}{\triangle_n(x)} \quad , \; j \geq i. \quad \text{(A6.15)}$$

$$= (-1)^{i+j} \frac{U_{i-1}\left[\frac{1}{2x}\right] U_{n-j}\left[\frac{1}{2x}\right]}{x\, U_n\left[\frac{1}{2x}\right]} \quad , \; j \geq i. \quad \text{(A6.16)}$$

It is interesting to note that as n, i, j, n-i and n-j approach infinity with i-j finite and $x \leq \frac{1}{2}$ then

$$b_{ij} = b_{ji} \approx \frac{1}{\sqrt{1-(2x)^2}} \left[\frac{\sqrt{1-(2x)^2}-1}{2x}\right]^{j-i} \quad . \quad \text{(A6.17)}$$

This relation can be obtained directly from**

$$b_{ij} = b_{|i-j|} = \frac{1}{2\pi} \int_0^{2\pi} \frac{\cos(|i-j|\,\theta)}{1 + 2x\cos\theta}\, d\theta \quad . \quad \text{(A6.18)}$$

A6.2. Analysis of a Mixer with a Sinusoidal Resistance Waveform

Here we derive the two-port equation for the Z-mixer with idlers and a sinusoidal resistance waveform which is discussed in Sec. 3.3.2, Fig. 3.12.

Referring to the figure we note that $I_{\ell+2} = I_{-k-1} = 0$ since the frequencies $\omega_{\ell+2}$ and ω_{-k-1} are not provided with

** This follows by referring to Eqs. (A3.13) ... (A3.15) with the infinite matrices $\underline{Z} = \underline{A}$ and $\underline{Y} = \underline{B}$ for $r(t) = 1 + 2x\cos\omega_p t$.

idlers. It follows that ω_n, $n > \ell+2$ or $n < -k-1$, are decoupled from the remaining frequencies. Hence, the mixer equation can be written in terms of the finite $(\ell+k+2) \times (\ell+k+2)$ Z-matrix as

$$\begin{bmatrix} V_{\ell+1} \\ \vdots \\ V_{+1} \\ V_o \\ \vdots \\ V_{-k} \end{bmatrix} = \begin{bmatrix} r_o & r_1 & & & & \\ r_1 & r_o & r_1 & & \mathbf{0} & \\ & r_1 & r_o & \ddots & & \\ & & \ddots & \ddots & \ddots & r_1 \\ & \mathbf{0} & & \ddots & r_1 & r_o \end{bmatrix} \begin{bmatrix} I_{\ell+1} \\ \vdots \\ I_{+1} \\ I_o \\ \vdots \\ I_{-k} \end{bmatrix} \quad , \quad (A6.19)$$

where both r_o and r_1 are nonnegative.

The short-circuit current idlers make

$$V_n = 0 \quad -k \leq n \leq \ell+1, \; n \neq 1 \text{ or } 0 \quad . \quad (A6.20)$$

The simplest method to write the two-port equation of the mixer is to write Eq. (A6.19) in the Y-matrix representation by inverting the $(\ell+k+2) \times (\ell+k+2)$ Z-matrix. The matrix inversion is given in the previous section with $x = r_1/r_o$ and $n = (\ell+k+2)$. The two-port equation will be the 2 x 2 submatrix relating I_{+1}, I_o, V_{+1} and V_o in the inverted matrix. This is given by

$$\begin{bmatrix} I_{+1} \\ I_0 \end{bmatrix} = \begin{bmatrix} Y_{+1,+1} & Y_{+1,0} \\ Y_{0,+1} & Y_{0,0} \end{bmatrix} \begin{bmatrix} V_{+1} \\ V_0 \end{bmatrix} \quad , \quad (A6.21)$$

where the Y's are deduced from the b's of Eq. (A6.15) as

$$Y_{+1,+1} = \frac{1}{r_o} b_{\ell+1,\ell+1}$$

$$= \frac{1}{r_o} \frac{\Delta_\ell(x)\ \Delta_{k+1}(x)}{\Delta_{\ell+k+2}(x)} \quad , \quad (A6.22)$$

$$Y_{0,0} = \frac{1}{r_o} b_{\ell+2,\ell+2}$$

$$= \frac{1}{r_o} \frac{\Delta_{\ell+1}(x)\ \Delta_k(x)}{\Delta_{\ell+k+2}(x)} \quad , \quad (A6.23)$$

and

$$Y_{+1,0} = Y_{0,+1} = \frac{1}{r_o} b_{\ell+1,\ell+2}$$

$$= -\frac{x}{r_o} \frac{\Delta_\ell(x)\ \Delta_k(x)}{\Delta_{\ell+k+2}(x)} \quad . \quad (A6.24)$$

The Z-parameters turned out to be much simpler than the Y's. To invert the Y-matrix of Eq. (A6.21) we note that by using the recursion formula (A6.5), the determinant of the Y matrix can be written as

$$D_y = \frac{1}{r_o^2} \frac{\Delta_\ell(x)\ \Delta_k(x)}{\Delta_{\ell+k+2}(x)} \quad . \quad (A6.25)$$

Thus

$$Z_{+1,+1} = r_o \frac{\Delta_{\ell+1}(x)}{\Delta_\ell(x)} \quad , \quad (A6.26)$$

$$Z_{0,0} = r_o \frac{\Delta_{k+1}(x)}{\Delta_k(x)} \quad , \quad (A6.27)$$

and

$$z_{+1,0} = z_{0,+1} = r_1 \quad . \quad (A6.28)$$

If $x = r_1/r_o \leq 0.5$, i.e. $r(t) \geq 0$, substituting for the Δ's from Eqs. (A6.8) and (A6.10) gives the required Z-matrix representation as

$$\begin{bmatrix} V_{+1} \\ V_o \end{bmatrix} = r_1 \begin{bmatrix} \dfrac{\sinh[(\ell+2)\alpha]}{\sinh[(\ell+1)\alpha]} & 1 \\ 1 & \dfrac{\sinh[(k+2)\alpha]}{\sinh[(k+1)\alpha]} \end{bmatrix} \begin{bmatrix} I_{+1} \\ I_o \end{bmatrix}, \quad (A6.29)$$

where

$$\cosh \alpha = r_o / 2r_1 . \quad (A6.30)$$

On the other hand if $x = r_1/r_o \geq 0.5$, Eq. (A6.7) gives

$$\begin{bmatrix} V_{+1} \\ V_o \end{bmatrix} = r_1 \begin{bmatrix} \dfrac{\sin[(\ell+2)\theta]}{\sin[(\ell+1)\theta]} & 1 \\ 1 & \dfrac{\sin[(k+2)\theta]}{\sin[(k+1)\theta]} \end{bmatrix} \begin{bmatrix} I_{+1} \\ I_o \end{bmatrix}, \quad (A6.31)$$

where

$$\cos \theta = r_o/2r_1 . \quad (A6.32)$$

A6.3. Analysis of Two Modified H-Mixers with Square-Wave Resistances

Here we analyze the different modified H-mixers discussed in Sec. 3.3.3, Fig. 3.14, driven by a square-wave r(t), Eq. (3.48). Then, we prove that they are inferior to a standard H-mixer.

Referring to Fig. 3.14a, and noting that k is odd ($\neq 1$), we have

$$I_n = 0 \qquad n \text{ odd } (\neq 1 \text{ of } k) \qquad \text{(A6.33)}$$

and

$$V_n = 0 \qquad n = k \text{ or } n \text{ even } (\neq 0) \; . \qquad \text{(A6.34)}$$

The equation relating the voltages and currents at frequencies ω_{+1}, ω_o and ω_k is given from Eq. (2.31) by the H-matrix form

$$\begin{bmatrix} V_{+1} \\ I_o \\ V_k \end{bmatrix} = \begin{bmatrix} H_{+1,+1} & H_{+1,o} & H_{+1,k} \\ H_{o,+1} & H_{o,o} & H_{o,k} \\ H_{k,+1} & H_{k,o} & H_{k,k} \end{bmatrix} \begin{bmatrix} I_{+1} \\ V_o \\ I_k \end{bmatrix} \; . \qquad \text{(A6.35)}$$

To calculate the H's we need to find the odd- and even-harmonic portions of the square-wave r(t) of Eq. (3.48). This can be calculated from Eqs. (2.23b) and (2.24b) and is given in Fig. A6.1. Calculating the

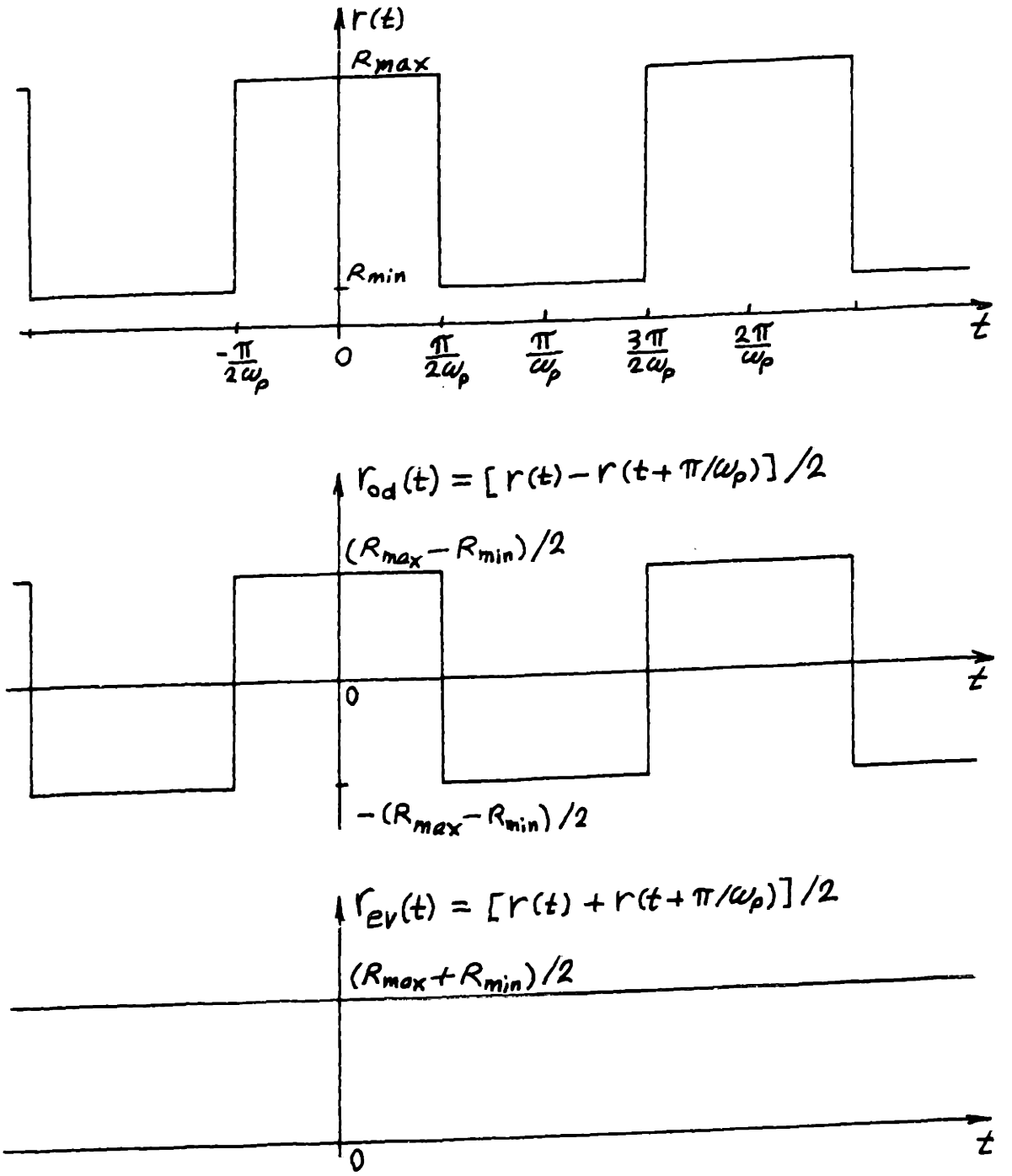

Fig. A6.1. The Square-Wave r(t)
and its Odd- and Even-Harmonic Portions

H's from Eqs. (2.32) and substituting $V_k = 0$, Eq. (A6.35) becomes

$$\begin{bmatrix} V_{+1} \\ I_o \\ 0 \end{bmatrix} = \begin{bmatrix} \alpha & -\gamma & 0 \\ \gamma & \beta & \frac{\gamma}{k} \\ 0 & -\frac{\gamma}{k} & \alpha \end{bmatrix} \begin{bmatrix} I_{+1} \\ V_o \\ I_k \end{bmatrix} \quad , \text{(A6.36)}$$

where

$$\alpha = H_{+1,+1} = \frac{2 R_{max} R_{min}}{R_{max} + R_{min}} \quad , \text{(A6.37)}$$

$$\beta = H_{0,0} = \frac{2}{R_{max} + R_{min}} \quad , \text{(A6.38)}$$

$$\gamma = H_{0,+1} = \frac{2}{\pi} \frac{R_{max} - R_{min}}{R_{max} + R_{min}} \quad . \text{(A6.39)}$$

Eliminating I_k from Eq. (A6.36) we get the two-port equation of the modified H-mixer of Fig. 3.14a as

$$\begin{bmatrix} V_{+1} \\ I_o \end{bmatrix} = \begin{bmatrix} \alpha & -\gamma \\ \gamma & \beta_1 \end{bmatrix} \begin{bmatrix} I_{+1} \\ V_o \end{bmatrix} \quad , \text{(A6.40)}$$

where

$$\beta_1 = \beta \left(1 + \frac{\gamma^2}{\alpha\beta} \frac{1}{k^2}\right) \quad . \text{(A6.41)}$$

Referring to Eqs. (A1.35) and (A1.38) we note that the optimum conversion loss for the above mixer can

be written as

$$L_{opt} = \frac{\sqrt{1 - \epsilon} + 1}{\sqrt{1 - \epsilon} - 1} \quad , \quad (A6.42)$$

where

$$\epsilon = \epsilon_1 = - \frac{\gamma^2}{\alpha\beta_1} \qquad (\leq 0) \quad . \quad (A6.43)$$

For the standard H-mixer, the optimum conversion loss is still given by Eq. (A6.42), however, in this case

$$\epsilon = \epsilon_o = - \frac{\gamma^2}{\alpha\beta} \qquad (\leq 0) \quad . \quad (A6.44)$$

Using Eq. (A6.41) the above two equations give

$$\epsilon_1 = \frac{\epsilon_o}{1 - \epsilon_o/k^2} \quad . \quad (A6.45)$$

Clearly $|\epsilon_1| < |\epsilon_o|$ for any finite value of the odd integer k. Thus, the conversion loss of the standard H-mixer is superior to that of the modified H-mixer of Fig. 3.14a for any values of R_{min} and R_{max}.

It is interesting to note that as $R_{min}/R_{max} \rightarrow 0$, it follows that $\epsilon_o \rightarrow -\infty$ and $\epsilon_1 \rightarrow -k^2$. Thus, the limiting conversion loss of the modified H-mixer is given by

$$L_{1,opt} = \frac{\sqrt{1 + k^2} + 1}{\sqrt{1 + k^2} - 1} \quad (A6.46)$$

while that of the standard H-mixer is unity.

Now we turn to the second modified H-mixer, Fig. 3.14b. In this case, noting that k is odd $\neq 1$ and ℓ is even $\neq 0$, we get

$$I_n = 0 \quad n = \ell \text{ or } n \text{ odd} \neq 1 \text{ or } k \qquad \text{(A6.47)}$$

and

$$V_n = 0 \quad n = k \text{ or } n \text{ even} \neq 0 \text{ or } \ell \qquad \text{(A6.48)}$$

Following the same steps as for the previous mixer, one arrives to the following two-port H-matrix equation for the present mixer:

$$\begin{bmatrix} V_{+1} \\ I_o \end{bmatrix} = \begin{bmatrix} \alpha_2 & -\gamma_2 \\ \gamma_2 & \beta_2 \end{bmatrix} \begin{bmatrix} I_{+1} \\ V_o \end{bmatrix} \qquad \text{(A6.49)}$$

where

$$\alpha_2 = \alpha \left[1 + \frac{\gamma^2}{\Delta \cdot (1-\ell)^2} \right] \qquad \text{(A6.50)}$$

$$\beta_2 = \beta \left[1 + \frac{\gamma^2}{\Delta \cdot k^2} \right] \qquad \text{(A6.51)}$$

and

$$\gamma_2 = \gamma \left[1 - \frac{\gamma^2}{\Delta \cdot k\,(k-\ell)(1-\ell)} \right. \qquad \text{(A6.52)}$$

with

$$\Delta = \alpha\,\beta + \frac{\gamma^2}{(k-\ell)^2} \qquad \text{(A6.53)}$$

where α, β and γ are those given in Eqs. (A6.37)... (A6.39).

The optimum conversion loss of the mixer is obtained from Eq. (A6.42) with

$$\epsilon = \epsilon_2 = -\frac{\gamma_2^2}{\alpha_2 \beta_2} \qquad (\leq 0) \qquad . \text{(A6.54)}$$

Using Eq. (A6.43) for ϵ_o of the standard H-mixer, the above equations give

$$\frac{\epsilon_2}{\epsilon_o} = \frac{\left[1 - \frac{x}{k\,(k-\ell)\,(1-\ell)}\right]^2}{\left[1 + \frac{x}{(1-\ell)^2}\right]\left[1 + \frac{x}{k^2}\right]} \qquad , \text{(A6.55)}$$

where

$$x = \frac{-\epsilon_o}{1 - \epsilon_o/(k-\ell)^2} \qquad (\geq 0) \qquad . \text{(A6.56)}$$

It is an easy matter to prove that the right hand side of Eq. (A6.55) is <u>strictly</u> less than unity for any proper values of the integers k and ℓ (k = odd $\neq$ 1 and ℓ = even $\neq$ 0) and for any possible value of x. Thus, it follows that $|\epsilon_2| < |\epsilon_o|$, and hence, the conversion loss of the standard H-mixer is superior to that of the modified H-mixer of Fig. 3.14b for any values of R_{min} and R_{max}.

It is interesting to note that as $R_{min}/R_{max} \rightarrow 0$, it follows that both ϵ_o and $\epsilon_2 \rightarrow -\infty$. Thus, the limiting conversion loss for both the standard H-mixer and the modified H-mixer of Fig. 3.14b is unity. In fact, it can be shown from the above equations that if $R_{min}/R_{max} \ll 1$,

it follows that for the standard H-mixer

$$L_{o,opt} \approx 1 + 2\pi \sqrt{R_{min}/R_{max}} \quad , \quad (A6.57)$$

and for the modified H-mixer of Fig. 3.14b

$$L_{2,opt} \approx 1 + 2\pi \frac{\left\{[(1-\ell)^2 + (k-\ell)^2][k^2 + (k-\ell)^2]\right\}^{\frac{1}{2}}}{|\ell| \quad |1-k|} \sqrt{R_{max}/R_{min}} \quad , \quad (A6.58)$$

which is greater than $L_{o,opt}$.

APPENDIX 7

SOME ASYMPTOTIC APPROXIMATIONS OF INTEGRALS

Here we develop the asymptotic approximations of the integrals appearing in Chapter 4. In the following, the parameter A is assumed to be much larger than unity. The results have been checked numerically and were found satisfactory for $A \geq 5$ approximately.

A7.0. Definition of the Function $\beta(z)$**

$$\beta(z) = \int_0^\infty \frac{e^{-zt}}{1 + e^{-t}}\, dt, \quad \mathrm{Re}[z] > 0$$

$$= \frac{1}{z} - \beta(z + 1)$$

$$= \sum_{k=0}^{\infty} \frac{(-1)^k}{z + k}$$

A7.1. Integral 1

$$f_1(A) = \frac{1}{2\pi} \int_0^{2\pi} \cos x \tanh(A \cos x)\, dx$$

$$= \frac{2}{\pi} - \frac{2}{\pi} \int_0^{\pi/2} \sin x \left[1 - \tanh(A \sin x)\right] dx$$

$$\approx \frac{2}{\pi} - \frac{2}{\pi} \int_0^\infty \frac{2x\, e^{-Ax}}{e^{Ax} + e^{-Ax}}\, dx, \quad A \gg 1$$

$$= \frac{2}{\pi} - \frac{1}{\pi A^2} \int_0^\infty \frac{t\, e^{-t}}{1 + e^{-t}}\, dt, \quad t = 2Ax$$

$$= \frac{2}{\pi} + \frac{1}{\pi A^2} \frac{d}{dz} \beta(z) \Big|_{z=1}$$

** Gradshteyn and Ryzik (I, Sec. 8.37)

$$= \frac{2}{\pi} - \frac{1}{\pi A^2} \sum_{k=0}^{\infty} \frac{(-1)^k}{(1+k)^2}$$

$$= \frac{2}{\pi} - \frac{\pi}{12} \frac{1}{A^2} \quad **$$

$$\approx \frac{2}{\pi}$$

A7.2. Integral 2

$$f_2(A) = \frac{1}{2\pi} \int_0^{2\pi} \log_e \operatorname{sech}(A \cos x)\, dx$$

$$= \frac{2}{\pi} \int_0^{\pi/2} \left[\log_e 2 - A \sin x + \log_e \frac{e^{A \sin x}}{e^{A \sin x} + e^{-A \sin x}} \right] dx$$

$$= \log_e 2 - \frac{2}{\pi} A + \int_A^{\infty} \left[f_1(A) - \frac{2}{\pi} \right] dA$$

$$\approx \log_e 2 - \frac{2}{\pi} A + \frac{\pi}{12} \frac{1}{A}, \quad A \gg 1$$

$$\approx \log_e 2 - \frac{2}{\pi} A$$

A7.3. Integral 3

$$f_3(A) = \frac{1}{2\pi} \int_0^{2\pi} \operatorname{sech}^2(A \cos x)\, dx$$

$$= \frac{2}{\pi} \int_0^{\pi/2} \operatorname{sech}^2(A \sin x)\, dx$$

$$\approx \frac{2}{\pi} \int_0^{\infty} \operatorname{sech}^2(A x)\, dx \quad , A \gg 1$$

$$= \frac{2}{\pi} \frac{1}{A} \left[\tanh (A x) \right]_0^{\infty}$$

$$= \frac{2}{\pi} \frac{1}{A}$$

** Gradshteyn and Ryzik (I, Formula 0.234, no. 1)

A7.4. Integral 4

$$f_4(A) = \frac{1}{2\pi}\int_0^{2\pi} \cos(2x)\ \mathrm{sech}^2(A\cos x)\,dx$$

$$= \frac{1}{\pi}\int_0^{2\pi} \cos^2 x\ \mathrm{sech}^2(A\cos x)\,dx - f_3(A)$$

$$= 2\frac{d\,f_1(A)}{d\,A} - f_3(A)$$

$$\approx \frac{\pi}{3}\frac{1}{A^3} - f_3(A) \quad , \ A \gg 1$$

A7.5. Integral 5

$$f_5(A) = \frac{1}{2\pi}\int_0^{2\pi} \mathrm{sech}\,(A\cos x)\,dx$$

$$= \frac{2}{\pi}\int_0^{\pi/2} \mathrm{sech}\,(A\sin x)\,dx$$

$$\approx \frac{2}{\pi}\int_0^{\infty} \mathrm{sech}\,(Ax)\,dx, \qquad A \gg 1$$

$$= \frac{2}{\pi}\frac{1}{A}\left[\tan^{-1}\sinh(Ax)\right]_0^{\infty}$$

$$= \frac{1}{A}$$

A7.6. Integral 6

$$f_6(A) = \frac{1}{2\pi}\int_0^{2\pi} \cos(2x)\ \mathrm{sech}(A\cos x)\,dx$$

$$= \frac{4}{\pi}\int_0^{\pi/2} \sin^2 x\ \mathrm{sech}\,(A\sin x)\,dx - f_5(A)$$

$$\approx \frac{4}{\pi}\int_0^{\infty} x^2\ \mathrm{sech}\,(Ax)\,dx - f_5(A), \quad A \gg 1$$

$$= \frac{4}{\pi}\int_0^{\infty} \frac{2\,x^2}{e^{Ax} + e^{-Ax}}\,dx - f_5(A)$$

$$= \frac{1}{\pi} \frac{1}{A^3} \int_0^\infty \frac{t^2 \, e^{-\frac{1}{2}t}}{1 + e^{-t}} \, dt - f_5(A), \quad t = 2Ax$$

$$= \frac{1}{\pi} \frac{1}{A^3} \frac{d^2}{dz^2} \beta(z) \Big|_{z=\frac{1}{2}} - f_5(A)$$

$$= \frac{2}{\pi} \frac{1}{A^3} \sum_{k=0}^{\infty} \frac{(-1)^k}{(\frac{1}{2} + k)^3} - f_5(A)$$

$$= \frac{\pi^2}{2} \frac{1}{A^3} - f_5(A)^{**}$$

A7.7. Integral 7

$$f_7(A) = \frac{1}{2\pi} \int_0^{2\pi} \sqrt{1 + A^2 \cos^2 x} \, dx$$

$$= \frac{2}{\pi} \sqrt{1 + A^2} \int_0^{\pi/2} \sqrt{1 - [A^2/(1+A^2)] \sin^2 x} \, dx$$

$$= \frac{2}{\pi} \sqrt{1 + A^2} \, E\left[A^2/(1 + A^2)\right] ,$$

where E is the complete elliptic integral of the second type. Using the fact that[***]

$$E(m) \approx 1 + \frac{1 - m}{4} \left\{ \log_e \left[\frac{16}{1-m}\right] + 1 \right\} , \quad m \approx 1,$$

we get

$$f_7(A) \approx \frac{2}{\pi} A \left\{ 1 + \frac{1}{4A^2} \left[2 \log_e (4A) + 1\right] \right\} , \quad A >> 1$$

$$\approx \frac{2}{\pi} A .$$

A7.8. Integral 8

$$f_8(A) = \frac{1}{2\pi} \int_0^{2\pi} \cos x \, \sinh^{-1}(A \cos x) \, dx$$

** Gradshteyn and Ryzik (I, Formula 0.234, no. 4)

*** Abramowitz and Stegun (I, Sec. 17.3)

$$= \frac{2}{\pi} \int_0^{\pi/2} \cos x \log_e \left[A \cos x + \sqrt{1 + A^2 \cos^2 x}\right] dx$$

$$= \frac{2}{\pi} \int_0^{\pi/2} \cos x \log_e (2A \cos x)\, dx$$

$$+ \frac{2}{\pi} \int_0^{\pi/2} \cos x \log_e \left[\frac{A \cos x + \sqrt{1 + A^2 \cos^2 x}}{2 A \cos x}\right] dx$$

$$= \frac{2}{\pi} \left[\log(2A) + \log_e 2 - 1\right]$$

$$- \int_A^{\infty} \left[f_{10}(A) - \frac{2}{\pi} \frac{1}{A}\right] dA \,,$$

where $f_{10}(A)$ is given in Sec. A7.10. Thus,

$$f_8(A) \approx \frac{2}{\pi} \left[\log_e(4A) - 1\right] + \frac{1}{2\pi A^2} \log_e(4A), \quad A \gg 1$$

$$\approx \frac{2}{\pi} \left[\log_e(4A) - 1\right] \,.$$

A7.9. Integral 9

$$f_9(A) = \frac{1}{2\pi} \int_0^{2\pi} \frac{1}{\sqrt{1 + A^2 \cos^2 x}}\, dx$$

$$= \frac{2}{\pi} \frac{1}{\sqrt{1 + A^2}} \int_0^{\pi/2} \frac{1}{\sqrt{1 - [A^2/(A^2 + 1)] \sin^2 x}}\, dx$$

$$= \frac{2}{\pi} \frac{1}{\sqrt{1 + A^2}} K\left[A^2/(1 + A^2)\right] \,,$$

where the K is the complete elliptic integral of the first kind. Using the fact that**

$$K(m) \approx \frac{1}{2} \log_e \left[\frac{16}{1-m}\right] \,, \qquad m \approx 1,$$

we get

$$f_9(A) \approx \frac{2}{\pi} \frac{1}{A} \log_e(4A), \quad A \gg 1 \,.$$

** Abramowitz and Stegun (I, Formula 17.3.26)

This result also comes from the relation

$$f_9(A) = \frac{d}{d(1/A)} \left[\frac{1}{A} f_7(A) \right]$$

A7.10. Integral 10

$$f_{10}(A) = \frac{1}{2\pi} \int_0^{2\pi} \frac{\cos^2 x}{\sqrt{1 + A^2 \cos^2 x}} \, dx$$

$$= \frac{1}{A^2} \left[f_7(A) - f_9(A) \right]$$

$$= \frac{2}{\pi} \frac{1}{A^2} \left\{ \sqrt{1 + A^2} \; E\left[A^2/(1 + A^2)\right] - \frac{1}{\sqrt{1 + A^2}} K\left[A^2/(1 + A^2)\right] \right\}$$

$$\approx \frac{2}{\pi} \frac{1}{A} \left\{ 1 - \frac{1}{4A^2} \left[2\log_e(4A) - 1 \right] \right\} \quad , A >> 1$$

$$\approx \frac{2}{\pi} \frac{1}{A} \; .$$

This result can also come from the relation

$$f_{10}(A) = 2 \frac{d}{d(A^2)} f_7(A)$$

$$= \frac{d}{dA} f_8(A).$$

A7.11. Integral 11

$$f_{11}(A) = \frac{1}{2\pi} \int_0^{2\pi} \cos(2x) \sqrt{1 + A^2 \cos^2 x} \; dx$$

$$= \frac{4}{\pi} \int_0^{\pi/2} \cos^2 x \sqrt{1 + A^2 \cos^2 x} \; dx - f_7(A)$$

$$= \frac{4}{\pi} \int_0^{\pi/2} A \cos^3 x \, dx - f_7(A) + \frac{4}{\pi} \int_0^{\pi/2} \cos^2 x \left\{ \sqrt{1 + A^2 \cos^2 x} - A\cos x \right\} dx$$

$$= \frac{8}{3\pi} A - f_7(A) - A \int_A^\infty A\, f_{10}(A)\, d\left(\frac{1}{A^2}\right)$$

$$\approx \frac{2}{3\pi} A - \frac{1}{2\pi} \frac{1}{A} \left[3 - 2 \log_e(4A)\right] , \quad A \gg 1$$

$$\approx \frac{2}{3\pi} A \quad .$$

APPENDIX 8

GENERAL STUDY OF Y-MIXERS WITH PULSED CONDUCTANCE WAVEFORMS

It is well known that the optimum conductance waveform for a Y-mixer is an impulse train**. However, in practice one can only produce pulses with finite width. It was observed by Barber (I) that as long as the pulses of the conductance waveform are narrow, the exact shape of each pulse is not important in the evaluation of the mixer performance. Instead, he suggested the use of an equivalent pulse duty ratio associated with each pulse waveform. This is certainly a powerful idea since it allows us to compare the performances of mixers employing different conductance waveforms by comparing a single number, namely the pulse duty ratio.

In generalizing Barber's results it was observed that he overlooked a small, but important, point. The result of this is that the equivalent pulse duty ratio is not only a function of the conductance waveform as he claimed, but also it depends on the imbedding network (for example on the particular image frequency termination).

In the following we give general approximate analysis for Y-mixers with arbitrary image terminations and pulsed conductance waveforms. It will be shown that

** See Sec. 3.2.1 or Bakanowski (I), Barber(I), Herold (I), Herold, Bush and Ferris (I), Messenger and McCoy (I), Torrey and Whitmer (I), Uhlir (I) and others.

when the pulses are narrow, the optimum conversion losses for the three cases; short image, broadband input and open image; approach their theoretical limits.** Furthermore, the performance of the mixer in the first case is less sensitive to perturbations in the pulse shape than in the last two cases.

Although our analysis is concerned with Y-mixers, the results of the first section can be modified with the appropriate duality relations to include any mixer for which the optimum conversion losses for the three aforementioned image terminations approach their theoretical limits.

A8.1. General Approximations of the Mixer Equations

Consider a passive Y-mixer with arbitrary image termination with a conductance waveform $g(t)$ represented by the Y-matrix***

$$\underline{Y} = \begin{bmatrix} g_o & g_1 & g_2 \\ g_1 & g_o & g_1 \\ g_2 & g_1 & g_o \end{bmatrix} \quad . \quad \text{(A8.1)}$$

From Appendix 2, it is clear that to study the performance of the mixer near the point where the conversion loss

** Zero db for the first and last cases and 3 db for the second case; see for example Appendix 2.
*** See Appendix 3.

for short circuit image approaches unity, one should consider the region where $\epsilon_1 = (g_o / g_1)^2 \approx 1$, and hence** $\theta = g_2 / g_o \approx 1$. Thus, let us approximate ϵ_1 and θ in terms of a second degree polynomial in a small positive parameter "x" as follows***:

$$\epsilon_1 = \left[\frac{g_1}{g_o}\right]^2 \approx 1 - a\,x + b\,x^2 \quad , \quad (A8.2)$$

and

$$\theta = \frac{g_2}{g_o} \approx 1 - c\,x + d\,x^2 \quad . \quad (A8.3)$$

Hence,

$$\epsilon_2 = \frac{2\epsilon_1}{1+\theta} \approx 1 - (a - \tfrac{c}{2})\,x - [\tfrac{c}{2}(a - \tfrac{c}{2}) + \tfrac{d}{2} - b]\,x^2 \quad , \quad (A8.4)$$

and

$$\epsilon_3 = \frac{\epsilon_1}{1-\epsilon_1}\,\frac{1-\theta}{1+\theta} \approx \frac{c}{2a}\,[1 - (a - \tfrac{c}{2} + \tfrac{d}{c} - \tfrac{b}{a})\,x] \quad . \quad (A8.5)$$

The quantity ϵ_3 was not calculated to a second degree in x since this requires the knowledge of ϵ_1 and θ until a third degree in x.

From the above equations and Appendix 2, it follows that as $x \longrightarrow 0$, $\epsilon_1 \longrightarrow 1$ and $\epsilon_2 \longrightarrow 1$, and hence the optimum conversion losses for short-circuit image, L_1, and for broadband input, L_2, approach their theoretical limits of zero and 3 db respectively. However, $\epsilon_3 \longrightarrow c/(2a)$

** $\epsilon_1 \longrightarrow +1$ implies $\theta \longrightarrow +1$ can be proved from passivity.

*** From passivity one can show that:
a, $c \geq 0$ [if $a = 0$ then $b \leq 0$, and if $c = 0$ then $d \leq 0$:] ,
& $a \geq c/2$ [if $a = c/2$ then $b \leq d/2$] .

and hence the optimum conversion loss for open-circuit image, L_3, does not approach its theoretical limit of zero db unless $c = 2a$. Since we are interested in the case where all L_1, L_2 and L_3 approach their theoretical limits we will assume that

$$c = 2a \quad . \quad (A8.6)$$

In the next section we prove that a conductance waveform consisting of a train of narrow pulses with any symmetric shape satisfy Eq. (A8.6). In this case,

$$\epsilon_2 \approx 1 - \left(\frac{d}{2} - b \right) x^2 \quad (A8.7)$$

and

$$\epsilon_3 \approx 1 - \frac{1}{a} \left(\frac{d}{2} - b \right) x \quad . \quad (A8.8)$$

The optimum conversion losses can now be approximated by

$$L_1 \approx 1 + 2 \sqrt{a} \sqrt{x} \quad (A8.9a)$$

$$\approx 8.686 \sqrt{a} \sqrt{x} \quad \text{db} \quad , \quad (A8.9b)$$

$$L_2 \approx 2 \left[1 + 2 \sqrt{\frac{d}{2} - b} \; x \right] \quad (A8.10a)$$

$$\approx 3.01 + 8.686 \sqrt{\frac{d}{2} - b} \; x \quad \text{db} \quad , \quad (A8.10b)$$

and

$$L_3 \approx 1 + 2 \sqrt{\frac{1}{a} \left(\frac{d}{2} - b \right)} \sqrt{x} \quad (A8.11a)$$

$$\approx 8.686 \sqrt{\frac{1}{a} \left(\frac{d}{2} - b \right)} \sqrt{x} \quad \text{db} \quad . \quad (A8.11b)$$

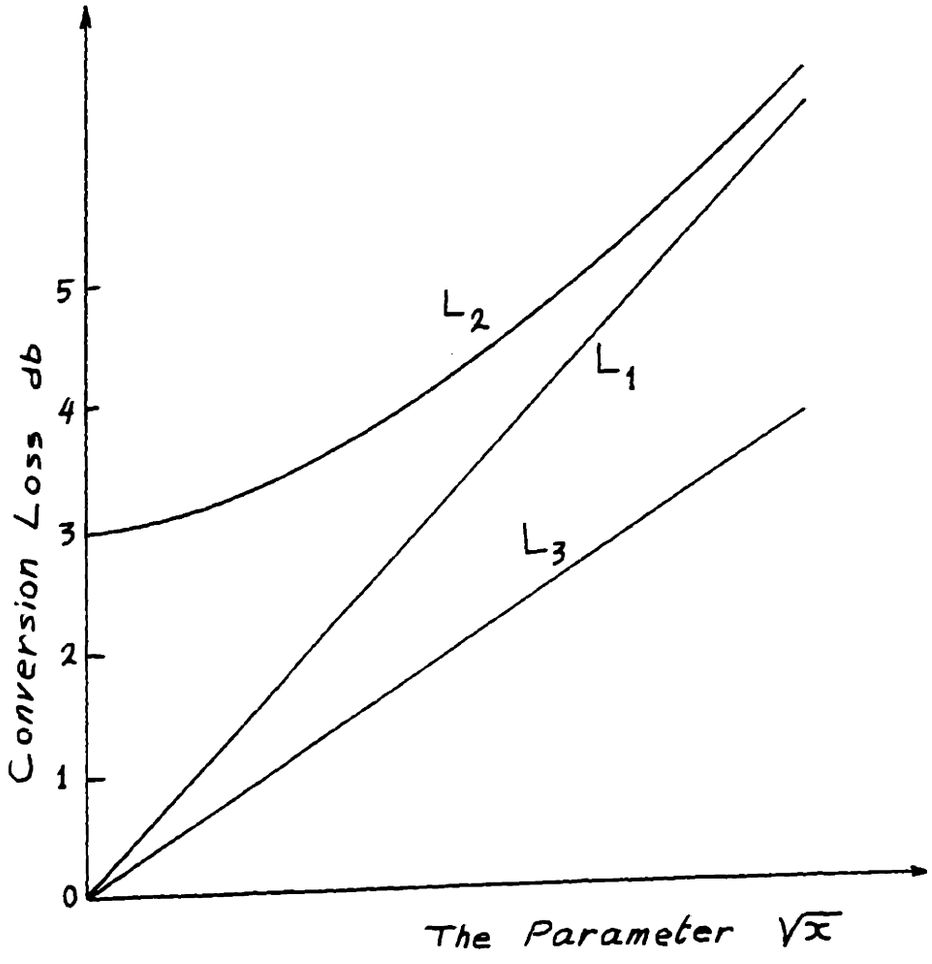

Fig. A8.1. A Typical Plot of the L's

A typical plot of the L's is given in Fig. A8.1.

An important point should be kept in mind in comparing two mixers for which c= 2a. While their L_1's will be approximately equal if their ϵ_1's are equal only up to the linear term in x, their L_2's will be approximately equal and so will their L_3's if their ϵ_1's and θ's agree up to the quadratic term in x. It is this point that was overlooked by Barber (I). Our argument will be made clearer in Sec. A8.3.

It is interesting to note that if in addition to Eq. (A8.6), we also assumed that d = 2b, L_2 and L_3 will depend on a higher order in x, and thus will be smaller in general. Of course, for this case one needs to find ϵ_1 and θ up to cubic terms in x. However, we will not discuss this case here.

A8.2. General Pulsed Conductance Waveforms

Here we want to prove that if the conductance waveform g(t) consists of a train of narrow pulses with any symmetric shape, as indicated in Fig. A8.2, the condition c = 2a assumed in Eq. (A8.6) is satisfied.

If t_o is the width of each pulse in Fig. A8.2,

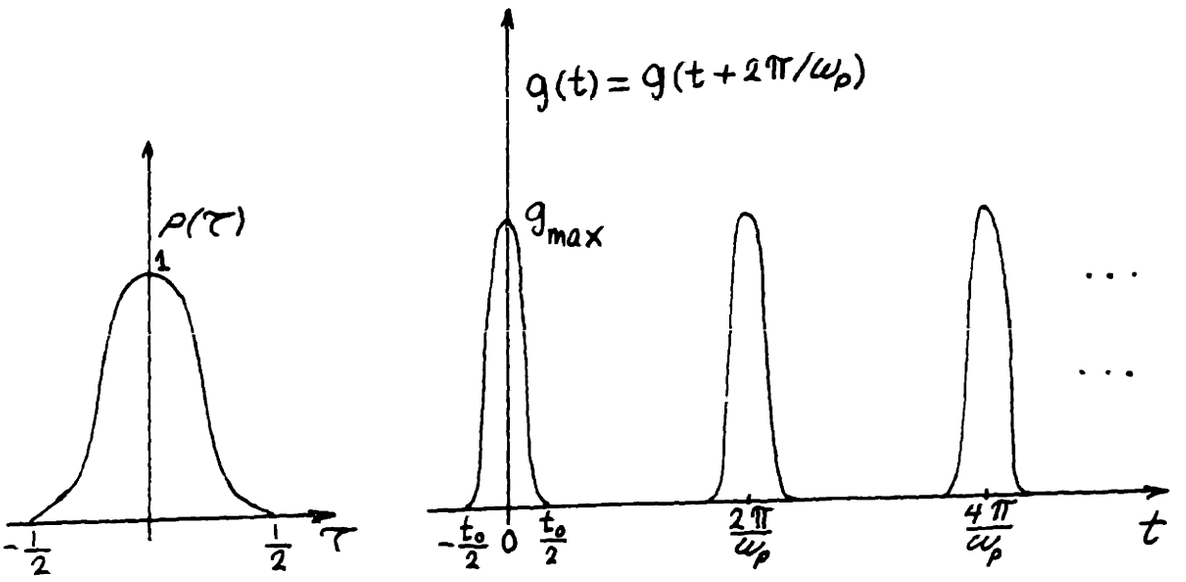

Fig. A8.2. A Pulsed g(t) and its Normalized Prototype Pulse p(t)

i.e.

$$g(t) << g_{max} \text{ for } \quad t_o/2 \leq t \leq 2\pi/\omega_p - t_0/2 \ , \quad \text{(A8.12)}$$

the condition for the pulses to be narrow becomes

$$\delta = \omega_p t_o << 2\pi \quad . \quad \text{(A8.13)}$$

Let us define p(t) as the normalized prototype pulse of g(t) as given in the figure.

Thus,

$$g(t) = \sum_{n=-\infty}^{\infty} g_{max} \ p \left[\frac{t}{t_o} + n \frac{2\pi}{\omega_p}\right] \quad . \quad \text{(A8.14)}$$

From condition (A8.12)

$$p(\tau) \approx 0 \qquad |\tau| > \tfrac{1}{2} \quad . \quad \text{(A8.15)}$$

Also let us define its area and second moment of area as

$$A_o = \int_{-\frac{1}{2}}^{\frac{1}{2}} p(\tau) \, d\tau \quad , \quad \text{(A8.16)}$$

and

$$A_2 = \int_{-\frac{1}{2}}^{\frac{1}{2}} \tau^2 \, p(\tau) \, d\tau \quad . \quad \text{(A8.17)}$$

From the above, one can write the Fourier coefficients of g(t) as

$$g_o = \frac{1}{2\pi} \int_{-\pi}^{\pi} g(t) \, d\,\omega_p t$$

$$= \frac{1}{2\pi} g_{max} \, \delta \, A_o \quad , \quad \text{(A8.18)}$$

$$g_1 = \frac{1}{2\pi} \int_{-\pi}^{\pi} g(t) \cos(\omega_p t)\, d\omega_p t$$

$$= \frac{1}{2\pi} g_{max}\ \delta \int_{-\frac{1}{2}}^{\frac{1}{2}} p(\tau) \cos(\delta\tau)\, d\tau$$

$$\approx \frac{1}{2\pi} g_{max}\ \delta \left[A_o - \frac{1}{2} A_2\ \delta^2 + O(\delta^4)\right] \quad , \text{(A8.19)}$$

and

$$g_2 = \frac{1}{2\pi} \int_{-\pi}^{\pi} g(t) \cos(2\omega_p t)\, d\omega_p t$$

$$= \frac{1}{2\pi} g_{max}\ \delta \int_{-\frac{1}{2}}^{\frac{1}{2}} p(\tau) \cos(2\ \delta\ \tau)\, d\tau$$

$$\approx \frac{1}{2\pi} g_{max}\ \delta \left[A_o - 2\ A_2\ \delta^2 + O(\delta^4)\right] \quad . \text{(A8.20)}$$

Thus,

$$\epsilon_1 = \left[\frac{g_1}{g_o}\right]^2 \approx 1 - \frac{A_2}{A_o}\ \delta^2 + O(\delta^4) \quad , \text{(A8.21)}$$

$$\theta = \frac{g_2}{g_o} \approx 1 - 2\ \frac{A_2}{A_o}\ \delta^2 + O(\delta^4). \quad \text{(A8.22)}$$

Comparing Eqs. (A8.21) and (A8.22) with (A8.2) and (A8.3), if $\delta^2 = x$, It follows that $c = 2a$ which was to be proven.

A8.3. Some Specific Pulsed Conductance Waveforms

1. Rectangular Pulse

If the pulse duty ratio $P \ll 1$ it follows that for g(t) of Fig. A8.3

$$\epsilon_1 = \left[\frac{\sin(\pi p)}{\pi p}\right]^2 \approx 1 - \frac{1}{3}(\pi p)^2 + \frac{2}{45}(\pi p)^4 \quad , \text{(A8.23)}$$

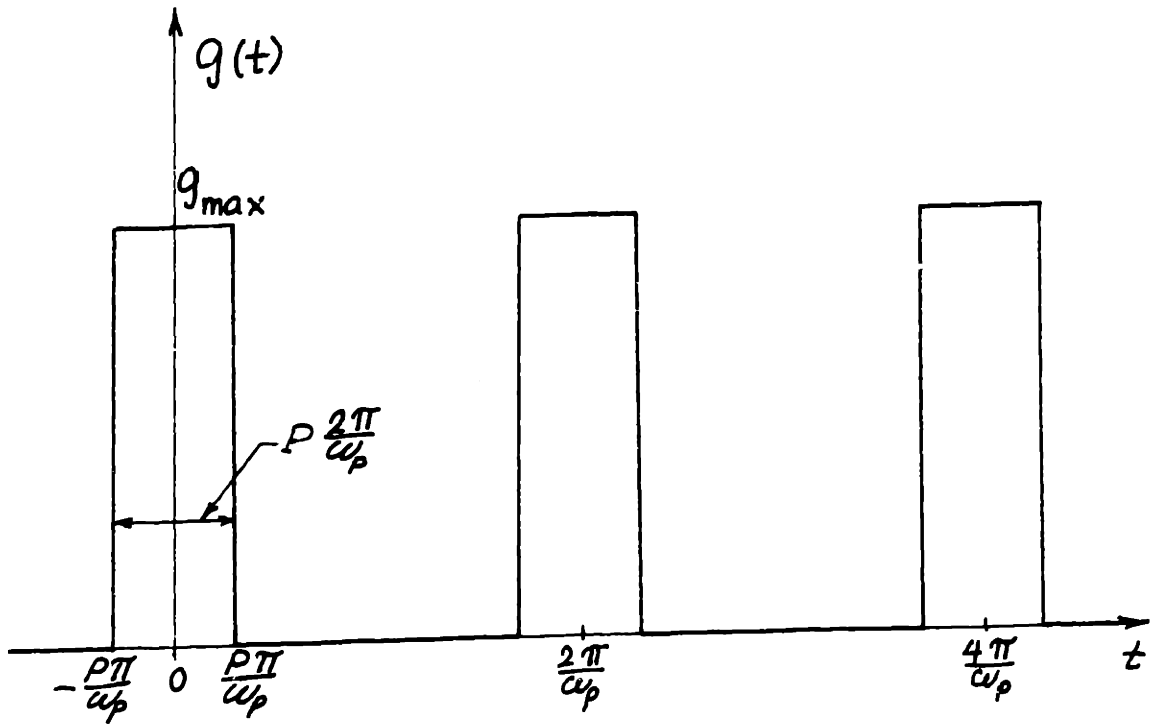

Fig. A8.3. A Rectangular-Pulse g(t)

$$\theta = \frac{\sin(2\pi p)}{2\pi p} \approx 1 - \frac{2}{3}(\pi p)^2 + \frac{2}{15}(\pi p)^4 \quad , \text{(A8.24)}$$

$$\epsilon_2 \approx 1 - \frac{1}{45}(\pi p)^4 \quad , \text{(A8.25)}$$

and

$$\epsilon_3 \approx 1 - \frac{1}{15}(\pi p)^2 \quad . \text{(A8.26)}$$

2. Gaussian Pulse

If $\delta \ll 1$, it follows that for g(t) of Fig. A8.4

$$\epsilon_1 \approx e^{-\frac{1}{2}\delta^2} \approx 1 - \frac{1}{2}\delta^2 + \frac{1}{8}\delta^4 \quad , \text{(A8.27)}$$

$$\theta \approx e^{-\delta^2} \approx 1 - \delta^2 + \frac{1}{2}\delta^4 \quad , \text{(A8.28)}$$

$$\epsilon_2 \approx 1 - \frac{1}{8}\delta^4 \quad , \text{(A8.29)}$$

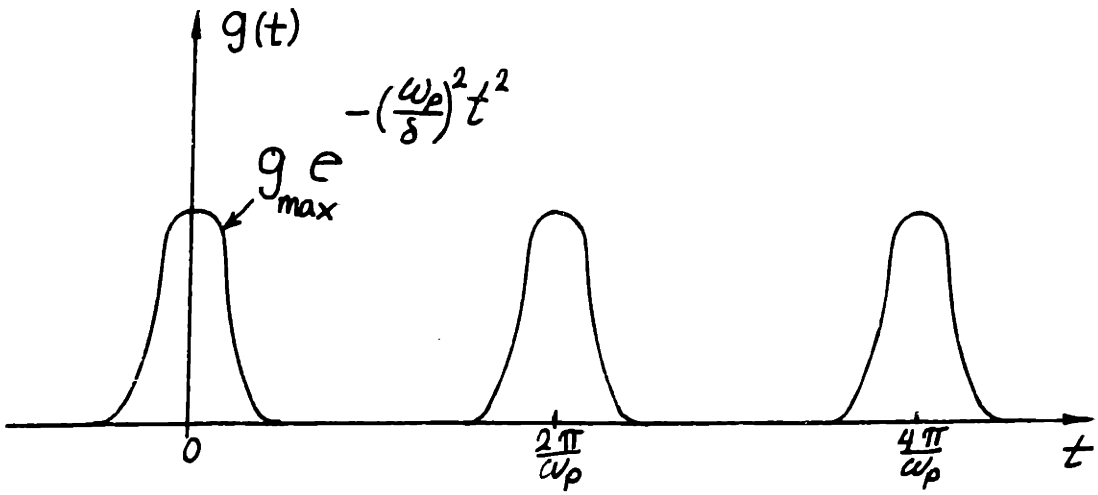

Fig. A8.4. A Gaussian-Pulse g(t)

and $$\epsilon_3 \approx 1 - \frac{1}{4}\,\delta^4 \quad . \quad \text{(A8.30)}$$

3. Exponential Diode Pumped by Sinusoidal Voltage**

If $\alpha V_p >> 1$, it follows that for g(t) of Fig. A8.6***

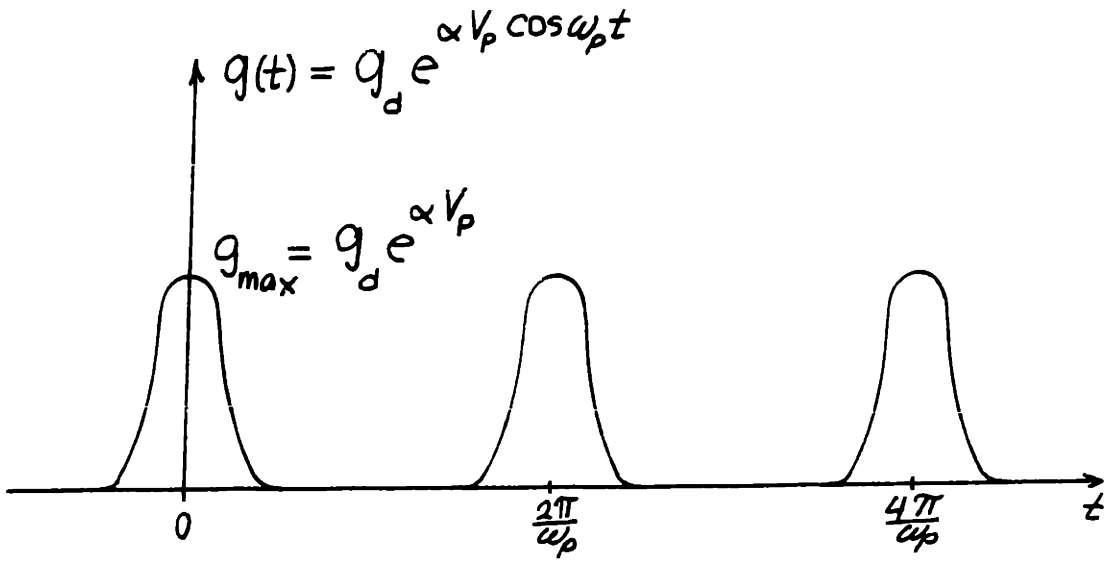

Fig. A8.5. An Exponential-Diode-Pumped-by-a-Sinusoidal-Voltage g(t)

** Compare to Eqs. (4.13) ... (4.16) of Sec. 4.2.1.

*** The $\mathfrak{I}_n$'s are the modified Bessel functions. For their asymptotic expansions see for example Abramowitz and Stegun (I, Eq. 9.7.1).

$$\epsilon_1 = \left[\frac{\mathbb{I}_1(\alpha V_p)}{\mathbb{I}_o(\alpha V_p)}\right]^2 \approx 1 - \frac{1}{\alpha V_p} + 0\left[\frac{1}{(\alpha V_p)^3}\right] \quad , \text{(A8.31)}$$

$$\theta = \frac{\mathbb{I}_2(\alpha V_p)}{\mathbb{I}_o(\alpha V_p)} \approx 1 - \frac{2}{\alpha V_p} + \frac{1}{(\alpha V_p)^2} \quad , \text{(A8.32)}$$

$$\epsilon_2 \approx 1 - \frac{1}{2}\frac{1}{(\alpha V_p)^2} \quad , \text{(A8.33)}$$

and

$$\epsilon_3 \approx 1 - \frac{1}{2}\frac{1}{\alpha V_p} \quad . \text{(A8.34)}$$

A8.4. Comparison and Conclusions

If "x" of Eqs. (A8.2) and (A8.3) is equated to $(\pi P)^2$, δ^2 and $\frac{1}{\alpha V_p}$ for the three aforementioned g(t)'s respectively, one notices that the relation c = 2a applies for all of them. This, of course, was expected from the general analysis given in the previous section.

Now, let us specifically compare the first and third g(t)'s. If we want their L_1's and hence their ϵ_1's to be equal near $L_1 \approx$ zero db, we must have from Eqs. (A8.23) and (A8.31)

$$P = P_1 \approx \frac{\sqrt{3}}{\pi}\frac{1}{\sqrt{\alpha V_p}} \quad . \text{(A8.35)}$$

On the other hand, for their L_2's to be equal

$$P = P_2 \approx \frac{(22.5)^{\frac{1}{4}}}{\pi} \frac{1}{\sqrt{\alpha V_p}} \quad , \quad (A8.36)$$

and for their L_3's to be equal

$$P = P_3 \approx \frac{\sqrt{7.5}}{\pi} \frac{1}{\sqrt{\alpha V_p}} \quad . \quad (A8.37)$$

Since P_1, P_2 and P_3 are not equal, clearly no single equivalent pulse duty ratio could be used to make L_1, L_2 and L_3 for one g(t) to simultaneously track their counterparts for the other g(t)**. Thus in general we conclude that an equivalent pulse duty ratio is a function of both the conductance waveform and the image termination (the imbedding network), and not solely a function of the conductance waveform.

** In Barber's analysis, P_1 of Eq. (A8.35) was assumed to be the equivalent pulse duty ratio for L_1, L_2 and L_3 (see Fig. 3 in his paper). The way his figures are plotted makes his results correct for an exponential diode pumped by a sinusoidal voltage, but incorrect for a rectangular-pulse waveform.

APPENDIX 9

STUDY OF AN EXPONENTIAL-DIODE Y-MIXER WITH AN OPEN-CIRCUIT SECOND HARMONIC

A9.1. Purpose of the Study

For high frequency mixers, the diode junction capacitance tends to short-circuit the higher order out-of-band frequencies. Thus, the realization of a Z-, G- or H-mixer will not be possible since, in each, one needs to open-circuit an infinite sequence of frequencies. On the other hand, if the diode series resistance is neglected, the Y-mixer can be realized easily.

In Sec. 4.2.5, it was shown that the Z-mixer, for example, gives much better conversion loss than that of a Y-mixer for identical d-c bias and pump power. Now if the frequency is high enough such that the frequencies ω_n $(= n\omega_p + \omega_o)$ are short-circuited by the junction capacitance for $n \geq 3$, a question arises: Should we also short-circuit the frequencies $\omega_{\pm 2}$ and thus form a standard Y-mixer, or open-circuit them to obtain a modified Y-mixer as a first approximation for the realization of a G- or Z-mixer? Here we answer the above question by analyzing an exponential-diode Y-mixer with open-circuit second harmonic and comparing it to the standard Y-mixer analyzed in Sec. 4.2.1. The result of the analysis

showed that the standard Y-mixer is superior to the modified one.

At this point it is not clear how many other frequencies should be open-circuited to improve the performance of the Y-mixer. It is hoped that the analysis given here will provide guidelines along which further studies can be conducted.

A9.2. Large Signal Analysis

Consider the single-diode Y-mixer given in Fig. A9.1 where the second harmonic of the pump, $2\omega_p$,

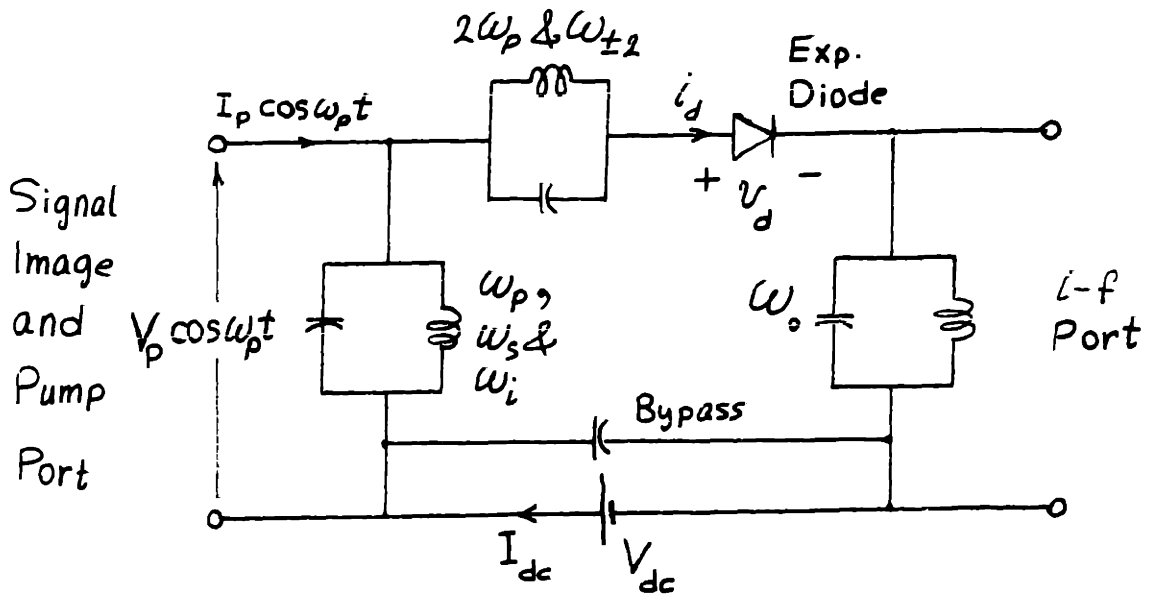

Fig. A9.1. A Y-Mixer with an Open-Circuit Second Harmonic

and its sidebands, ω_{+2} and ω_{-2}, are open-circuited, Clearly the pumping voltage across the diode is constrained to have fundamental and second harmonic (in-phase) components, Thus, let

$$v_d = V_{dc} + V_p \cos \omega_p t + V_{2p} \cos (2\omega_p t) \quad . \text{(A9.1)}$$

The current in the exponential diode is given by

$$i_d = I_{sat}\, e^{\alpha[V_{dc} + V_p \cos \omega_p t + V_{2p} \cos(2\omega_p t)]} - I_{sat} \, . \text{(A9.2)}$$

Again, because of the imbedding network, it must follow that i_d should not contain a second harmonic component, thus

$$\int_0^{2\pi} i_d \cos(2\omega_p t)\, d\,\omega_p t = 0 \quad , \text{(A9.3)}$$

which results in

$$\int_0^{2\pi} e^{\alpha V_p \cos\omega_p t + \alpha V_{2p} \cos(2\omega_p t)} \cos(2\omega_p t)\, d\omega_p t = 0 . \text{(A9.4)}$$

The last equation gives an implicit relation between αV_p and αV_{2p}. This, together with Eq. (A9.2), should give the Fourier coefficients of i_d in terms of αV_p enabling us to find the pump and bias parameters as well as the small signal conductance waveform as functions of αV_p.

There are several numeric methods to solve Eq. (A9.4).** However, since we are interested in finding

** See for example Torrey and Whitmer (I, Sec. 5.14) where they used iterations on a double Fourier series expansion of the integrand of Eq. (A9.4)

the performance of the mixer for large pump signal, we present here a solution based on asymptotic methods which are valid when $\alpha V_p \gg 1$. Our solution starts by assuming that

$$\alpha V_{2p} = a\ \alpha V_p + f(\alpha V_p) \quad , \quad \text{(A9.5)}$$

where

$$\lim_{\alpha V_p \to \infty} f(\alpha V_p) = \text{finite quantity} \quad . \quad \text{(A9.6)}$$

First, neglecting $f(\alpha V_p)$ compared to "a αV_p", a first order asymptotic expansion** of Eq. (A9.4) when $\alpha V_p \gg 1$ gives

$$a \approx -\frac{1}{2\sqrt{2}} \quad . \quad \text{(A9.7)}$$

Thus Eq. (A9.4) assumes the form

$$\int_0^{2\pi} e^{\alpha V_p\left[\cos\omega_p t - \frac{1}{2\sqrt{2}}\cos(2\omega_p t)\right]} \times$$

$$e^{f(\alpha V_p)\cos(2\omega_p t)} \cos(2\omega_p t)\, d\omega_p t = 0. \quad \text{(A9.8)}$$

If we set***

$$f(\alpha V_p) \approx b_o + b_1/(\alpha V_p) + b_2/(\alpha V_p)^2 \quad , \quad \text{(A9.10)}$$

make the substitution $\cos(\omega_p t) = (1-t)/\sqrt{2}$, and obtain higher order asymptotic expansion for Eq. (A9.8) for

** We used the method of Laplace. See for example Copson (I, Chapter 5) or Carrier, Krook and Pearson (I, Sec. 6-2).

*** It was found necessary to expand $f(\alpha V_p)$ up to $(\alpha V_p)^2$ to calculate the mixer performance.

$\alpha V_p >> 1$, we get, after lengthy algebraic manipulations, the values of the b's as

$$b_o = -\frac{3}{4} \quad , \text{(A9.11a)}$$

$$b_1 = -\frac{57}{16}\sqrt{2} \quad , \text{(A9.11b)}$$

and

$$b_2 = -122 \quad . \text{(A9.11c)}$$

Thus the final solution for Eq. (A9.4) is

$$\alpha V_{2p} = -\frac{1}{2}A - \frac{3}{4} - \frac{57}{16}\frac{1}{A} - 66\frac{1}{A^2} \quad , \text{(A9.12)}$$

where

$$A = \alpha V_p/\sqrt{2} \quad >>1 \quad . \text{(A9.13)}$$

Substituting Eq. (A9.12) in Eq. (A9.2) and applying the same asymptotic method used to evaluate Eq. (A9.8), one obtains the diode current in the Fourier series form

$$i_d = I_{dc} + I_p \cos(\omega_p t) + I_{3p} \cos(3\omega_p t) + I_{4p} \cos(4\omega_p t) + \text{higher harmonics} \quad , \text{(A9.14)}$$

where

$$I_{dc} \approx I_d \left[1 + \frac{7}{8}\frac{1}{A} + \frac{1329}{128}\frac{1}{A^2} + \frac{250869}{1024}\frac{1}{A^3} \right] \quad \text{(A9.15)}$$

$$I_p \approx \sqrt{2}\, I_d \left[1 + \frac{3}{8}\frac{1}{A} + \frac{1161}{128}\frac{1}{A^2} + \frac{224289}{1024}\frac{1}{A^3} \right] \quad \text{(A9.16)}$$

$$I_{3p} \approx -\sqrt{2}\, I_d \left[1 - \frac{29}{8}\frac{1}{A} + \frac{201}{128}\frac{1}{A^2} - \frac{4095}{1024}\frac{1}{A^3} \right] \quad \text{(A9.17)}$$

$$I_{4p} \approx - I_d \left[1 - \frac{57}{8}\frac{1}{A} - \frac{591}{128}\frac{1}{A^2} - \frac{264267}{1024}\frac{1}{A^3} \right] \qquad \text{(A9.18)}$$

where

$$I_d = \sqrt{\frac{2}{\pi}}\ I_{sat}\ e^{\alpha V_{dc}}\ \frac{e^{\alpha V_p/\sqrt{2}}}{\sqrt{\alpha V_p/\sqrt{2}}} \qquad \text{(A9.19)}$$

The diode d-c current can be approximated by Eq. (A9.19). The pump power and conductance are given by

$$P_p = \frac{1}{2} I_p V_p \approx I_d\ \ V_p/\sqrt{2} \qquad \text{(A9.20)}$$

and

$$G_p = I_p/V_p \approx \sqrt{2}\ I_d/V_p \qquad \text{(A9.21)}$$

A9.3. Small Signal Analysis

The diode small signal conductance waveform can be put in the form

$$g(t) = y_o + 2y_1\cos\omega_p t + 2y_2\cos(2\omega_p t) + 2y_3\cos(3\omega_p t) + 2y_4\cos(4\omega_p t) + \text{higher order terms} \qquad \text{(A9.22)}$$

where, the y_n's can be calculated from the relation $g(t) = \alpha i_d$ and Eqs. (A9.14) ... (A9.19), as

$$y_o = \alpha I_{dc} , \quad y_1 = \frac{1}{2} \alpha I_p , \quad y_2 = 0,$$

$$y_3 = \frac{1}{2} \alpha I_{3p}, \quad y_4 = \frac{1}{2} \alpha I_{4p} \text{ and so on} \qquad . \text{(A9.23)}$$

The 5 x 5 small signal Y-matrix equation of the mixer becomes

$$\begin{bmatrix} I_{+2} \\ I_s \\ I_o \\ I_i^* \\ I_{-2} \end{bmatrix} = \begin{bmatrix} y_o & y_1 & 0 & y_3 & y_4 \\ y_1 & y_o & y_1 & 0 & y_3 \\ 0 & y_1 & y_o & y_1 & 0 \\ y_3 & 0 & y_1 & y_o & y_1 \\ y_4 & y_3 & 0 & y_1 & y_o \end{bmatrix} \begin{bmatrix} V_{+2} \\ V_s \\ V_o \\ V_i^* \\ V_{-2} \end{bmatrix} \qquad , \text{(A9.24)}$$

where we used the terminology of Sec. 2.1 for the second harmonic sidebands. Now, from the constraints of the circuit given in Fig. A9.1, it follows that

$$I_{+2} = I_{-2} = 0 \qquad . \text{(A9.25)}$$

In this case Eq. (A9.24) is reduced to

$$\begin{bmatrix} I_s \\ I_o \\ I_i^* \end{bmatrix} = \begin{bmatrix} Y_{11} & Y_{12} & Y_{13} \\ Y_{12} & Y_{22} & Y_{12} \\ Y_{13} & Y_{12} & Y_{11} \end{bmatrix} \begin{bmatrix} V_s \\ V_o \\ V_i^* \end{bmatrix} \qquad , \text{(A9.26)}$$

where

$$Y_{11} = y_o - \frac{y_o(y_1^2 + y_3^2) - 2y_1y_3y_4}{y_o^2 - y_4^2}$$

$$\approx y_o \left[\frac{1}{2} - \frac{3}{4} \frac{1}{A^2} \right] \qquad \text{(A9.27a)}$$

$$Y_{12} = y_1$$

$$\approx y_o \left[1 - \frac{1}{2} \frac{1}{A} - \frac{7}{8} \frac{1}{A^2} \right] \qquad \text{(A9.27b)}$$

$$Y_{13} = \frac{y_4(y_1^2 + y_3^2) - 2y_oy_1y_3}{y_o^2 - y_4^2}$$

$$\approx y_o \left[\frac{1}{2} - \frac{1}{A} - \frac{1}{4} \frac{1}{A^2} \right] \qquad \text{(A9.27c)}$$

and

$$Y_{22} = y_o \qquad \text{, (A9.27d)}$$

where we retained terms up to $\frac{1}{A^2}$. Substituting the above equations in Appendix 2, we get

$$\epsilon_1 = \frac{Y_{12}^2}{Y_{11} Y_{22}} \approx 1 - \frac{1}{A} + 0\left(\frac{1}{A^3}\right) \qquad \text{, (A9.28)}$$

$$\theta = \frac{Y_{13}}{Y_{11}} \approx 1 - \frac{2}{A} + \frac{1}{A^2} \qquad \text{, (A9.29)}$$

$$\epsilon_2 = \frac{2\epsilon_1}{1 + \theta} \approx 1 - \frac{1}{2} \frac{1}{A^2} \qquad \text{, (A9.30)}$$

and

$$\epsilon_3 = \frac{\epsilon_1}{1 - \epsilon_1} \frac{1 - \theta}{1 + \theta} \approx 1 - \frac{1}{2} \frac{1}{A} \qquad \text{. (A9.31)}$$

The performance of the mixer for different image terminations becomes:

1. Short Image

$$L_1 \approx 1 + 2/\sqrt{A} \qquad \text{(A9.32a)}$$

$$\approx 8.686/\sqrt{A} \quad \text{db} \qquad \text{(A9.32b)}$$

$$G_{s,1} \approx \tfrac{1}{2}\,\alpha\, I_{dc}/\sqrt{A} \qquad \text{(A9.33)}$$

$$G_{o,1} \approx \alpha\, I_{dc}/\sqrt{A} \qquad \text{(A9.34)}$$

2. Broadband Input

$$L_2 \approx 2\,(\,1 + \sqrt{2}\,/\,A\,) \qquad \text{(A9.35a)}$$

$$\approx 3 + 4.343\,\sqrt{2}\,/\,A \quad \text{db} \qquad \text{(A9.35b)}$$

$$G_{s,2} \approx \alpha\, I_{dc}/(\sqrt{2}\,A) \qquad \text{(A9.36)}$$

$$G_{o,2} \approx \alpha\, I_{dc}/(\sqrt{2}\,A) \qquad \text{(A9.37)}$$

3. Open Image

$$L_3 \approx 1 + \sqrt{2}\,/\,\sqrt{A} \qquad \text{(A9.38a)}$$

$$\approx 4.343\,\sqrt{2}\,/\,\sqrt{A} \quad \text{db} \qquad \text{(A9.38b)}$$

$$G_{s,3} \approx \sqrt{2}\,\alpha\, I_{dc}\,/\,A^{3/2} \qquad \text{(A9.39)}$$

$$G_{o,3} \approx \alpha\, I_{dc}\,/[\,\sqrt{2}\,A^{3/2}\,] \qquad \text{(A9.40)}$$

A9.4. Comparison with a Standard Y-Mixer

Here we compare the performance of the Y-mixer with an open-circuit second harmonic discussed above with the standard Y-mixer discussed in Sec. 4.2.1.

Comparing Eqs. (4.17) ... (4.24) to Eqs. (A9.32) ... (A9.40), and noting that $A = \alpha V_p/\sqrt{2}$, we observe that for any image termination, the conversion loss for both the standard and modified Y-mixers will agree if

$$[\ \alpha V_p/\sqrt{2}\ ]_{\text{modified}} = [\ \alpha V_p]_{\text{standard}} \quad , \quad \text{(A9.41)}$$

In this case the three normalized d-c and bias quantities** In this case the three normalized d-c and bias quantities**

$$x_1 = I_{dc} \ / \ \left[I_{sat}\ e^{\alpha V_{dc}}\right] \quad , \quad \text{(A9.42)}$$

$$x_2 = \alpha P_p \ / \ \left[I_{sat}\ e^{\alpha V_{dc}}\right] \quad , \quad \text{(A9.43)}$$

and

$$x_3 = \alpha P_p \ / \ I_{dc} \quad , \quad \text{(A9.44)}$$

for the two mixers will be related by

$$[x_1]_{\text{modified}} = 2\ [x_1]_{\text{standard}} \quad , \quad \text{(A9.45)}$$

$$[x_2]_{\text{modified}} = 2\ [x_2]_{\text{standard}} \quad , \quad \text{(A9.46)}$$

and

$$[x_3]_{\text{modified}} = [x_3]_{\text{standard}} \quad , \quad \text{(A9.47)}$$

** These are the same quantities used for the comparison of different single-diode mixers in Sec. 4.2.5.

where we used Eqs. (4.7b), (4.9b), (A9.19) and (A9.20). Thus, to obtain the same performance for both mixers with the same d-c voltage bias, the modified mixer needs twice the d-c current bias and twice the pump power of those of the standard mixer. However, for the same d-c current bias, they both need the same pump power.

In conclusion, the standard Y-mixer is superior and less complex than the Y-mixer with an open-circuit second harmonic.

APPENDIX 10

Y-MIXERS WITH INCOMPLETE TERMINATIONS FOR THE UNDESIRED FREQUENCIES

A10.1. Introduction

To build a true Y-mixer, one should short-circuit all the undesired frequencies across the mixer diode. In practice however, this might not be possible. In fact, in the majority of the mixers being built, and assumed to be Y-mixers, no circuit elements are inserted to provide the required short. It is assumed that the diode junction capacitance does this function especially at microwave and millimeter wave frequencies. This assumption is far from being true in many cases since diodes with extremely small junction capacitances are being manufactured today. In this case, the undesired frequencies will be partially dissipated in the signal and/or the i-f terminations. This, of course, will lead to some deterioration in the mixer performance compared to the ideal case.

The purpose of the study given here is to calculate the effect of the incomplete terminations of the undesired frequencies on the conversion loss of a Y-mixer**. The exact analysis of this problem is very

** In Appendix 11 we study this problem for square-wave driven G- and H-mixers.

complex. For this reason we assume that the diode is an ideal on-off switch and that the frequencies which are not provided with a short circuit are terminated in the pure resistive source and/or i-f terminations.

It is clear that if frequencies other than the i-f are terminated in the i-f load resistance, the conversion loss from signal to i-f frequencies will be a function of both the source and i-f resistances. In this case it makes more sense to speak in terms of transducer loss** rather than available conversion loss. Since the diode is assumed to be an ideal on-off switch, the transducer loss will be a function of the ratio of the two above mentioned resistances. Of course, it will also be a function of the diode pulse duty ratio***. Hence, for each mixer circuit, we will be interested in the minimum transducer loss and the corresponding optimum values of the pulse duty ratio and the ratio between the load and source resistances.

A10.2. Incomplete Terminations in the Signal Port Only

The circuit for a Y-mixer with incomplete terminations in the signal port is shown in Fig. A10.1.

** This is defined as the ratio of the maximum available power from the source to the power delivered to the load.
*** This is defined here as the fraction of time where the diode is in its on-state.

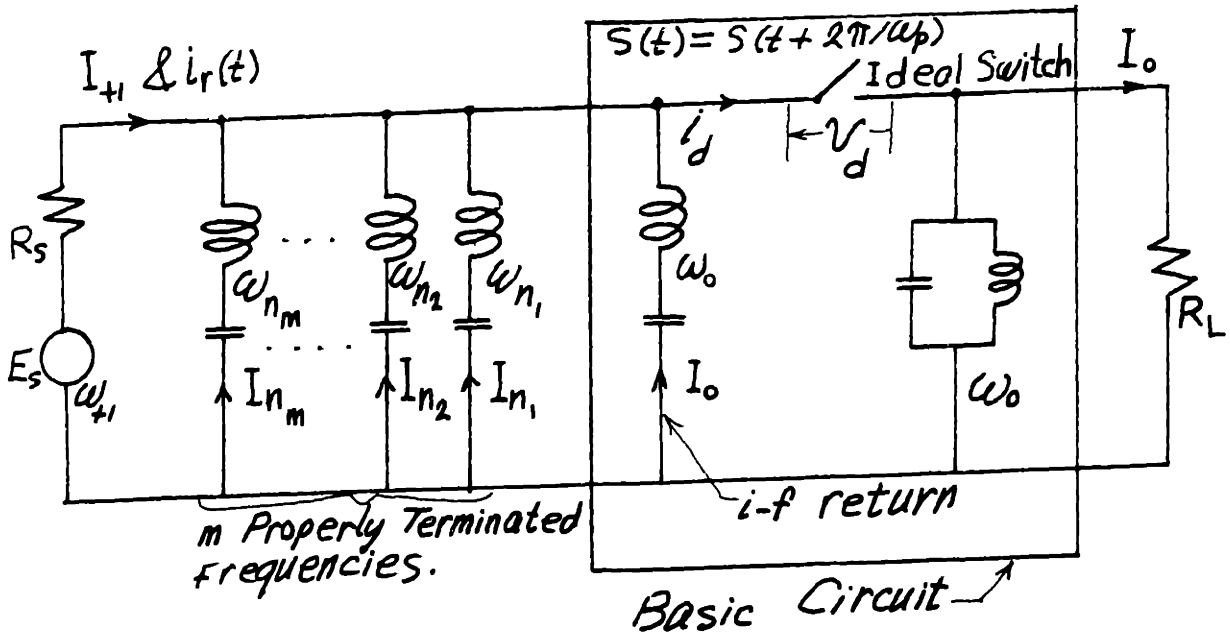

Fig. A10.1. Y-Mixer with Incomplete Terminations in the Signal Port

The m out-of-band frequencies $\omega_{n_1}, \omega_{n_2} \cdots \omega_{n_m}$ are properly terminated, i.e. short-circuited across the diode. The current in the remaining out-of-band frequencies, which will be termed $i_r(t)$, will pass through R_s. Note that the i-f current, I_o, is provided with a return to preventing it from passing through R_s.

Using the frequency notation of Sec. 2.1**, the equations of the mixer of Fig. A10.1 can be written as follows.

** Pump frequency = ω_p, i-f frequency = ω_o, signal frequency = $\omega_{+1} = \omega_p + \omega_o$, image frequency $\omega_{-1} = -\omega_p + \omega_o$ and generally $\omega_n = n\omega_p + \omega_o$.

1. Switch On ($v_d = 0$):

$$E_s e^{j\omega_{+1}t} - R_s[I_{+1}e^{j\omega_{+1}t} + i_r(t)] = R_L I_o e^{j\omega_o t} \quad .(A10.1)$$

2. Switch Off ($i_d = 0$):

$$i_r(t) + I_{+1}e^{j\omega_{+1}t} + I_o e^{j\omega_o t} + \sum_{i=1}^{m} I_{n_i} e^{j\omega_{n_i} t} = 0 \quad .(A10.2)$$

We now introduce the rectangular-pulse switching function

$$\begin{aligned} s(t) &= 1 && \text{Switch On} \\ &= 0 && \text{Switch Off} \end{aligned} \quad . (A10.3)$$

The time origin can be chosen to make the Fourier series of s(t) assume the form

$$s(t) = P \sum_{n=-\infty}^{\infty} \frac{\sin n\theta}{n\theta} e^{jn\omega_p t} \quad , (A10.4)$$

where P is the pulse duty ratio of the on-state and $\theta = \pi P$.

Using s(t), Eqs. (A10.1) and (A10.2) can be combined in one equation which is valid at all "t". This is given by**

** There are several methods of writing this equation. The one given here does not allow s(t) to be multiplied by $i_r(t)$. This is the trick that made the solution possible.

$$R_s \left\{ i_r(t) + I_{+1} e^{j\omega_{+1} t} + I_o e^{j\omega_o t} + \sum_{i=1}^{m} I_{n_i} e^{j\omega_{n_i} t} \right\}$$

$$= s(t) \left[E_s e^{j\omega_{+1} t} + (R_s - R_L) I_o e^{j\omega_{+1} t} + R_s \sum_{i=1}^{m} I_{n_i} e^{j\omega_{n_i} t} \right]$$

. (A10.5)

Presumably, the above equation can be solved for all the currents as functions of E_s. However, since the mixer transducer loss is given by

$$L = \frac{E_s^2}{4 R_s R_L I_o^2} \quad , \text{(A10.6)}$$

we only need to find I_o. Using the Fourier series expansion of s(t), Eq. (A10.4), we note that I_o can be found by solving m + 1 equations in m + 1 unknowns (I_o, I_{n_1}, I_{n_2} . . . I_{n_m}). These equations can be put in the (m+1) x (m+1) matrix form

$$\begin{bmatrix} \frac{1-\rho}{\rho} + \frac{R_L}{R_s} & -\frac{\sin n_1\theta}{n_1\theta} & -\frac{\sin n_2\theta}{n_2\theta} & \cdots \\ \left(\frac{R_L}{R_s} - 1\right)\frac{\sin n_1\theta}{n_1\theta} & \frac{1-\rho}{\rho} & -\frac{\sin(n_2-n_1)\theta}{(n_2-n_1)\theta} & \cdots \\ \left(\frac{R_L}{R_s} - 1\right)\frac{\sin n_2\theta}{n_2\theta} & -\frac{\sin(n_2-n_1)\theta}{(n_2-n_1)\theta} & \frac{1-\rho}{\rho} & \cdots \\ \vdots & \vdots & \vdots & \end{bmatrix} \begin{bmatrix} \frac{I_o R_s}{E_s} \\ \frac{I_{n_1} R_s}{E_s} \\ \frac{I_{n_2} R_s}{E_s} \\ \vdots \end{bmatrix} = \begin{bmatrix} \frac{\sin\theta}{\theta} \\ \frac{\sin(n_1-1)\theta}{(n_1-1)\theta} \\ \frac{\sin(n_2-1)\theta}{(n_2-1)\theta} \\ \vdots \end{bmatrix} .$$

. (A10.7)

Let a_i; i = 1, ... , m + 1; be the elements of the first column in the above square matrix when (R_L/R_s) is set to zero, i.e. $a_1 = (1-P)/P$, $a_2 = - \sin(n_1\theta)/(n_1\theta)$, ... etc. Also, let C_i; i = 1, ... , m + 1; be the cofactors of the same column; and b_i; i= 1, ... , m + 1; be the elements of the column vector in the right hand side of Eq. (A10.7). The solution of the above equation becomes

$$\frac{I_o R_s}{E_s} = \frac{\Sigma C_i b_i}{\frac{R_L}{R_s}\left[\frac{C_1}{P} - \Sigma a_i C_i\right] + \Sigma a_i C_i} \quad , \text{(A10.8)}$$

where the Σ's indicate sums from i = 1 to m + 1. Substituting this in Eq. (A10.6) it can be shown that

$$\left(\frac{R_L}{R_s}\right)_{opt} = \frac{\Sigma a_i C_i}{C_1/P - \Sigma a_i C_i} \quad , \text{(A10.9)}$$

and

$$L_{opt} = \frac{\left[\Sigma a_i C_i\right]\left[C_1/P - \Sigma a_i C_i\right]}{\left[\Sigma C_i b_i\right]^2} \quad . \text{(A10.10)}$$

The above equations give $(R_L/R_s)_{opt}$ and L_{opt} as functions of P. To find P_{opt} analytically, the equations become very complex. Thus, numerical techniques were applied

Table A10.1. The Results for the Circuit of Fig. A10.1 when ω_{+n} and ω_{-n}, any n, can have different terminations

Short Circuited Out-of-Band Frequencies	Their Number m	$\left(\frac{R_L}{R_s}\right)_{opt}$	P_{opt}	L_{opt}	
				Ratio	db
ALL	∞**	1	0	1	0
$\omega_{-5} \cdots \omega_{-1}$ & $\omega_{+2} \cdots \omega_{+5}$	9	0.927	0.190	1.202	0.80
$\omega_{-4} \cdots \omega_{-1}$ & $\omega_{+2} \cdots \omega_{+5}$	8	0.996	0.201	1.222	0.87
$\omega_{-4} \cdots \omega_{-1}$ & $\omega_{+2} \cdots \omega_{+4}$	7	0.902	0.218	1.252	0.98
$\omega_{-3} \cdots \omega_{-1}$ & $\omega_{+2} \cdots \omega_{+4}$	6	0.995	0.233	1.284	1.09
$\omega_{-3} \cdots \omega_{-1}$, ω_{+2} & ω_{+3}	5	0.861	0.258	1.336	1.26
ω_{-2}, ω_{-1}, ω_{+2} & ω_{+3}	4	0.992	0.280	1.391	1.43
ω_{-2}, ω_{-1} & ω_{+2}	3	0.785	0.321	1.501	1.76
ω_{-1} & ω_{+2}	2	0.985	0.356	1.624	2.11
Sum frequency ω_{+2}	1	1.462	0.389	1.978	2.96
Image frequency ω_{-1}	1	0.627	0.440	1.986	2.98
none	0	1	0.5	$\pi^2/4$	3.92
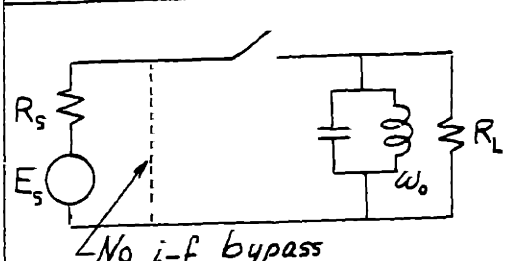	Not** Appli-cable	2.695	0.371	4.336	6.37

** Circuits calculated by methods other than the one given in this section.

Table A10.2. The Results for the Circuit of Fig. A10.1 when ω_{+n} and ω_{-n}, any n, have Identical Terminations

Short Circuited Out-of-Band Frequencies	Their Number m	$\left(\frac{R_L}{R_s}\right)_{opt}$	P_{opt}	L_{opt}	
				Ratio	db
All but ω_{-1}	∞**	2	0	2	3.01
$\omega_{-5} \cdots \omega_{-2}$ & $\omega_{+2} \cdots \omega_{+5}$	8	1.791	0.239	2.033	3.08
$\omega_{-4} \cdots \omega_{-2}$ & $\omega_{+2} \cdots \omega_{+4}$	6	1.721	0.272	2.049	3.12
ω_{-3}, ω_{-2}, ω_{+2} & ω_{+3}	4	1.606	0.317	2.082	3.19
ω_{-2} & ω_{+2}	2	1.401	0.384	2.161	3.35
None	0	1	0.5	$\pi^2/4$	3.92
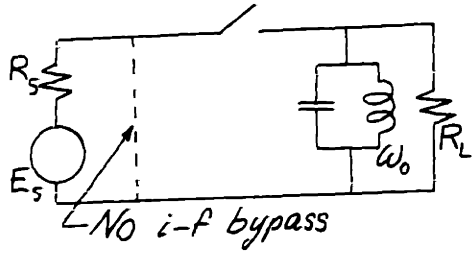	Not** Applicable	2.695	0.371	4.336	6.37
All but ω_{-1}, ω_{-2} & ω_{+2}	∞**	$\frac{36}{17}$	0	$\frac{17}{8}$	3.27
$\omega_{-10} \cdots \omega_{-3}$ & $\omega_{+3} \cdots \omega_{+10}$	16	0.972	0.301	2.165	3.36
$\omega_{-5} \cdots \omega_{-3}$ & $\omega_{+3} \cdots \omega_{+5}$	6	0.848	0.440	2.256	3.53

** Circuits calculated by methods other than the one given in this section.

using a computer. The final results are given in Tables A10.1 and A10.2. The first table considers the cases when ω_{+n} and ω_{-n}, any n, can be terminated differently; and the second table considers the cases when these frequencies are identically terminated.

A10.3. Incomplete Terminations in both Signal and I-F Ports

Here we consider Y-mixers with incomplete terminations in both the signal and i-f ports. For this purpose we assume that current at any frequency which is not shorted across the diode flows through both R_s and R_L. There are two basic kinds of such imperfect mixers. The first kind assumes that ω_{+n} and ω_{-n}, any n, can have different terminations. Such a mixer is shown in Fig. A10.2, where only the signal, ω_{+1}, and <u>not</u> the image, ω_{-1}, is provided with a return in the i-f port. Thus, at least ω_{+1} and ω_{-1} are <u>not</u> identically terminated. Note that this mixer is symmetric and the value of $(R_1/R_s)_{opt}$ is unity independent of the pulse duty ratio.

The second kind of mixer considered is characterized by having identical terminations for ω_{+n} and ω_{-n}, any n, as shown in Fig. A10.3. Note that both the signals and image are provided with returns in the i-f port. Also, the m frequencies shorted across the diode appear in pairs ω_{+n_i} and ω_{-n_i}; i = 1, ... , m/2. Note that m is even.

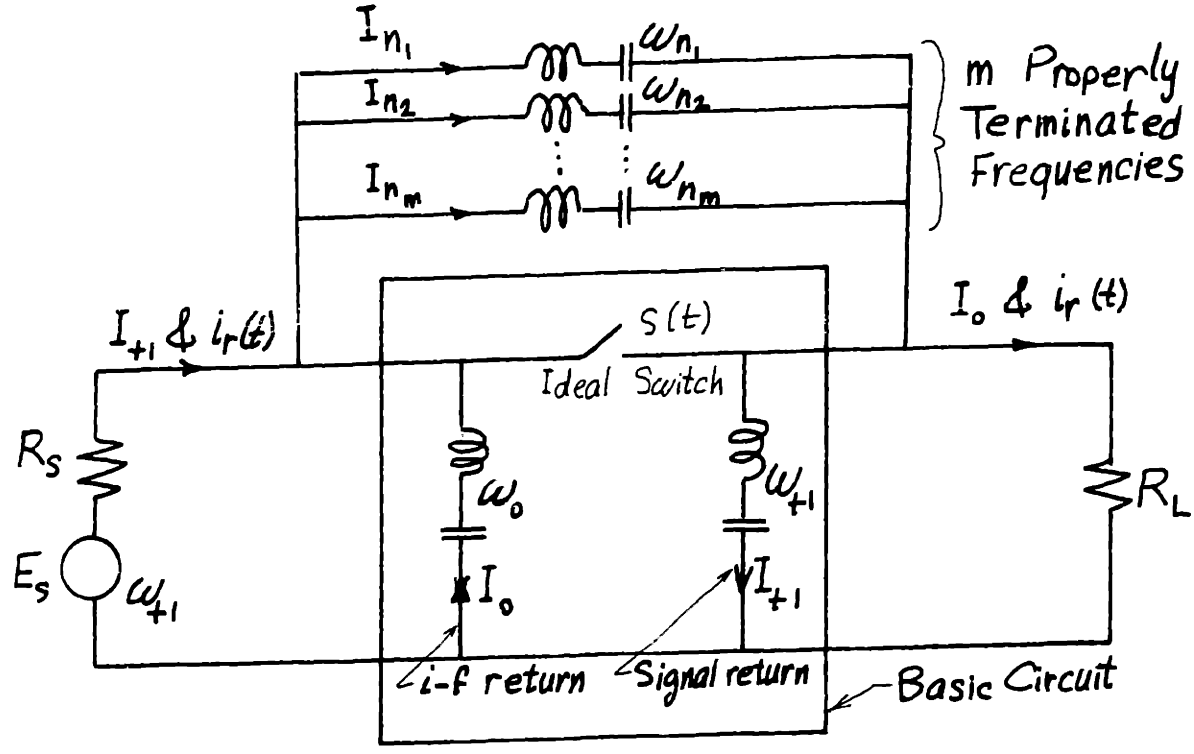

Fig. A10.2. Y-Mixer with Incomplete Terminations in both Ports (ω_{+n} and ω_{-n}, any n, can have different terminations)

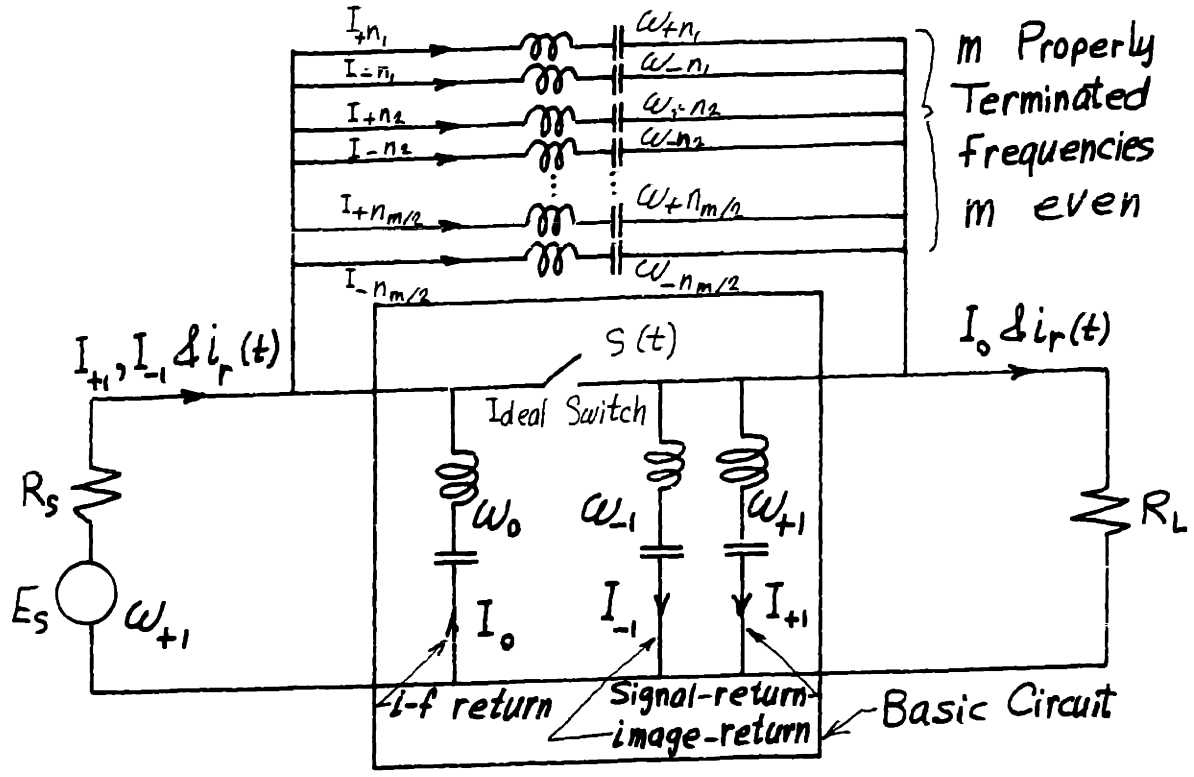

Fig. A10.3. Y-Mixer with Incomplete Terminations in both Ports (ω_{+n} and ω_{-n}, all n, have identical terminations)

Table A10.3. The Results for the Circuit of Fig. A10.2 for which ω_{+n} and ω_{-n}, any n, can have Different Terminations

Short-Circuited Undesired Frequencies	Their Number m	$\left(\frac{R_L}{R_s}\right)_{opt}$	P_{opt}	L_{opt}	
				Ratio	db
ALL	∞**	1	0	1	0
$\omega_{-5} \cdots \omega_{-1}$ & $\omega_{+2} \cdots \omega_{+5}$	9	1	0.209	1.202	0.80
$\omega_{-4} \cdots \omega_{-1}$ & $\omega_{+2} \cdots \omega_{+5}$	8	1	0.223	1.219	0.86
$\omega_{-4} \cdots \omega_{-1}$ & $\omega_{+2} \cdots \omega_{+4}$	7	1	0.240	1.253	0.98
$\omega_{-3} \cdots \omega_{-1}$ & $\omega_{+2} \cdots \omega_{+4}$	6	1	0.261	1.279	1.07
$\omega_{-3} \cdots \omega_{-1}$, ω_{+2} & ω_{+3}	5	1	0.286	1.339	1.27
ω_{-2}, ω_{-1}, ω_{+2} & ω_{+3}	4	1	0.317	1.382	1.41
ω_{-2}, ω_{-1} & ω_{+2}	3	1	0.357	1.515	1.80
ω_{-1} & ω_{+2}	2	1	0.411	1.602	2.05
ω_{-1} or ω_{+2}	1	1	0.482	2.085	3.19
None	0	1	0.633	2.350	3.71
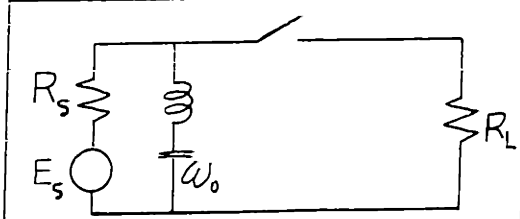	Not** Applicable	0.371	0.629	4.34	6.37
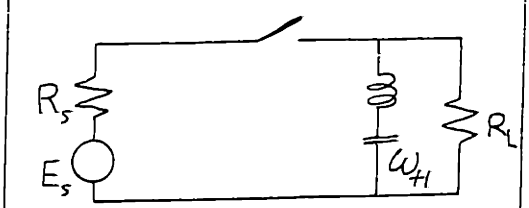	Not** Applicable	2.695	0.629	4.34	6.37
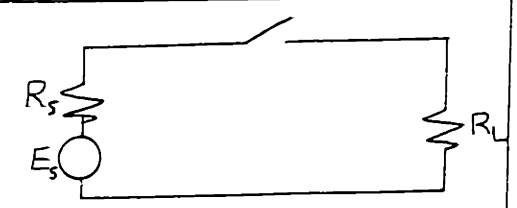	Not** Applicable	1	0.5	π^2	9.94

** Circuits calculated by methods different from that used for the rest of the table.

Table A10.4. The Results for the Circuit of Fig. A10.3 for which ω_{+n} and ω_{-n}, any n, have Identical Terminations

Short-Circuited Undesired Frequencies	Their Number m	$\left(\frac{R_L}{R_s}\right)_{opt}$	P_{opt}	L_{opt}	
				Ratio	db
All but -1	∞**	2	0	2	3.01
$\omega_{-5}, \ldots \omega_{-2}$ & $\omega_{+2} \ldots \omega_{+5}$	8	1.762	0.267	2.032	3.08
$\omega_{-4} \ldots \omega_{-2}$ & $\omega_{+2} \ldots \omega_{+4}$	6	1.682	0.307	2.047	3.11
$\omega_{-3}, \omega_{-2}, \omega_{+2}$ & ω_{+3}	4	1.549	0.360	2.078	3.18
ω_{-2} & ω_{+2}	2	1.314	0.439	2.152	3.33
None	0	0.839	0.579	2.445	3.88
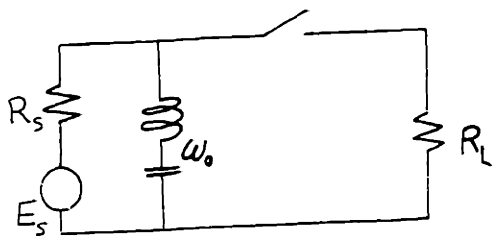	Not** Applicable	0.371	0.629	4.340	4.37
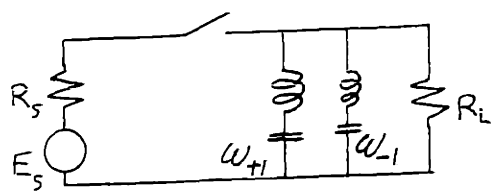	Not** Applicable	2	0.5	$\frac{\pi^2}{2}$	6.93
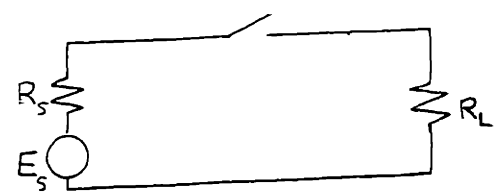	Not** Applicable	1	0.5	π^2	9.94

** Circuits calculated by methods different from that used for the rest of the table.

The results of both the above mentioned mixer circuits are given in Tables A10.3 and A10.4. The methods of analysis used are similar to that given in the previous section and hence, they will not be given here.

A10.4. An Interesting Observation

In this appendix we assumed that the mixer diode is an ideal on-off switch. For each circuit we found the optimum on-state pulse duty ratio to minimize the conversion loss. Some of the circuits we considered where any frequency and its image, ω_{+n} and ω_{-n}, are restricted to have the same termination, were analyzed from a different point of view by Belevitch (II, Chapter V). He assumed that the diode is an ideal rectifier, then he applied pumping voltage from the input port and calculated the resulting diode conduction angle or on-state pulse duty ratio which satisfies the circuit constraints. Interestingly enough this agreed with our optimum on-state pulse duty ratio for all the common circuits considered. The implication of that is that these mixers will be driven by their optimum pulse duty ratio by simply pumping them from the signal port. Whether or not this can be generalized to different mixer circuits is not clear.

APPENDIX 11

A STUDY OF SQUARE-WAVE REVERSING-SWITCH MIXERS

All.1. Introduction

The basic circuit of a square-wave reversing-switch mixer is shown in Fig. All.1. It is often called a ring mixer (modulator) or a doubly-balanced mixer (modulator). The first rigorous analysis of this mixer from a linear point of view was given by Caruthers (I) and later followed by Tucker (I & IV) and Belevitch (II). Recently, Steinbrecher (I), Rafuse (I & III), Mouw (I), Mouw and Fukuchi (I), Bassi (I), and Straca (I) considered high

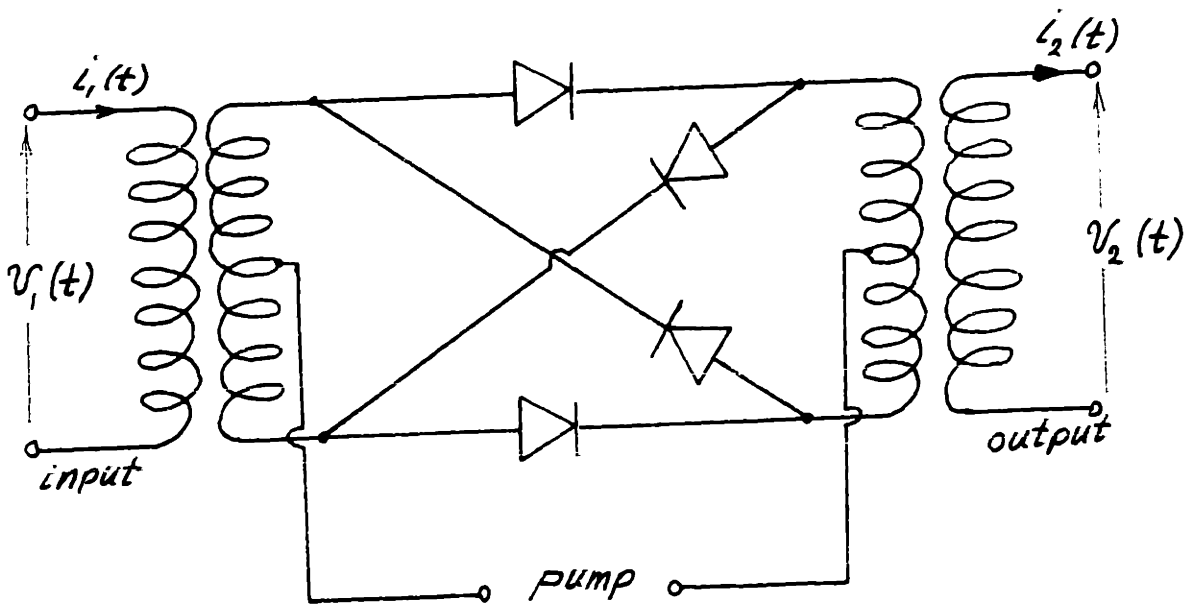

Fig. All.1. A Square-Wave Reversing Switch Mixer

frequency applications.

Nonlinear effects of this mixer due to switching time interference were studied by Belevitch (I & II), Tucker (I, II & IV) and Gardiner (I); and nonlinear effects due to diode nonlinearities were studied by Steinbrecher (I), Rafuse (II & III), Agrowal and Hanson (I), and Snyder (I).

Here we present some new contributions to the linear theory of square-wave reversing switch mixers based on the work of most of the aforementioned authors. Also, we give new interpretations which provide deeper insight to some aspects of the existing theory. In particular, the topics covered in the following five sections are, Fundamental Equations, Single-Ended Realizations at High Frequencies, Complete Selective Terminations, Modified Selective Terminations and Incomplete Selective Terminations.

A11.2. Fundamental Equations

If the diodes in Fig. A11.1 were assumed ideal and if the pump voltage contains only odd harmonics of the pump frequency, ω_p, it follows that the mixer acts as a reversing switch driven in a square-wave fashion. In this case

$$v_2(t) = f(t)\, v_1(t) \quad , \text{(A11.1)}$$

and

$$i_2(t) = f(t)\, i_1(t) \quad , \text{(A11.2)}$$

where f(t) is a zero-mean square-wave function varying between +1 and -1. Since

$$f(t) \cdot f(t) = 1 \quad , \text{(A11.3)}$$

it also follows that

$$v_1(t) = f(t)\, v_2(t) \quad , \text{(A11.4)}$$

and

$$i_1(t) = f(t)\, i_2(t) \quad . \text{(A11.5)}$$

The Fourier series expansion of f(t) is given by

$$f(t) = \frac{2}{\pi} \sum_{n=-\infty}^{\infty} \frac{(-1)^n}{(2n+1)} e^{j(2n+1)\omega_p t} \quad . \text{(A11.6)}$$

Using the frequency terminology of Sec. 2.1.1,** it is clear that if the signal frequency, ω_{+1}, is applied to the input

** Pump frequency $= \omega_p$, i-f frequency $= \omega_o$, signal frequency $= \omega_{+1} = \omega_p + \omega_o$, image frequency $= \omega_{-1} = -\omega_p + \omega_o$ and generally $\omega_n = n\omega_p + \omega_o$.

port, it follows that $v_1(t)$ and $i_1(t)$ contain only odd-order frequencies; ω_n, n odd; and $v_2(t)$ and $i_2(t)$ contain only even-order frequencies; ω_n, n even; since f(t) contains only odd harmonics of ω_p.

The two-port network given in Fig. A11.2 will represent the square-wave reversing-switch mixers satisfying Eqs. (A11.1) ... (A11.5).

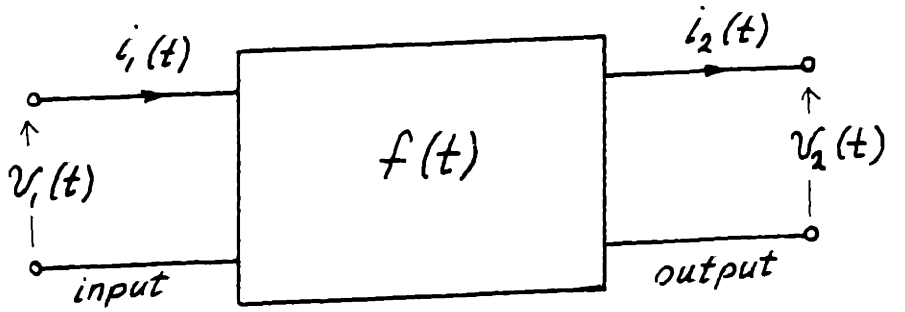

Fig. A11.2. Representation of the Square-Wave Reversing-Switch Mixer

If each diode switches between two resistances** R_f and R_b, the foward and backward resistances of the diode, the mixer in Fig. A11.1 can be represented by the circuit of Fig. A11.3.*** The mixer equations in this case can be

** This can be achieved by using piece-wise linear diodes and applying an odd-harmonic pump waveform, or by using nonlinear diodes and applying a square-wave pump.

*** This circuit can also be represented as a resistive T-network in cascade with an f(t) network since the latter network commutes with resistive networks.

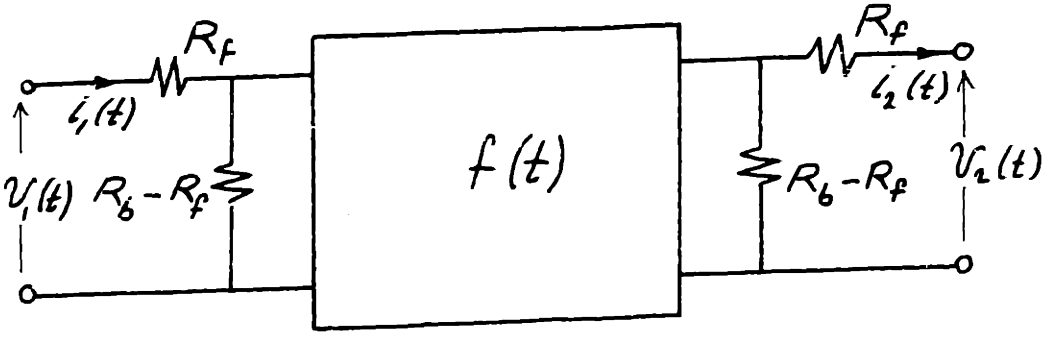

Fig. A11.3. Effect of Diode Forward and Reverse Resistances

put in the ABCD-matrix form

$$\begin{bmatrix} v_1(t) \\ \\ i_1(t) \end{bmatrix} = f(t) \begin{bmatrix} 1+ 2\frac{R_f}{R_b-R_f} & 2R_f\left\{1+ \frac{R_f}{R_b-R_f}\right\} \\ \\ \frac{2}{R_b-R_f} & 1+ 2\frac{R_f}{R_b-R_f} \end{bmatrix} \begin{bmatrix} v_2(t) \\ \\ i_2(t) \end{bmatrix} . \quad \text{(A11.7)}$$

Other useful forms of writing the above equation are the H-matrix form

$$\begin{bmatrix} v_1(t) \\ \\ i_2(t) \end{bmatrix} \approx \begin{bmatrix} 2R_f & f(t) \\ \\ -f(t) & \frac{2}{R_b} \end{bmatrix} \begin{bmatrix} i_1(t) \\ \\ v_2(t) \end{bmatrix} . \quad \text{(A11.8)}$$

and the G-matrix form**

$$\begin{bmatrix} i_1(t) \\ \\ v_2(t) \end{bmatrix} \approx \begin{bmatrix} \frac{2}{R_b} & -f(t) \\ \\ f(t) & 2R_f \end{bmatrix} \begin{bmatrix} v_1(t) \\ \\ -i_2(t) \end{bmatrix} \quad . \quad (A11.9)$$

In deriving the above two equations we assumed that $R_f << R_b$. Note that if $R_f = 0$ and/or $R_b = \infty$, the H- and G-matrices will exist. It can easily be shown that the Z-matrix will be infinite if $R_b = \infty$ and the Y-matrix will be infinite if $R_f = 0$.

** Compare to Eqs. (2.27) and (2.28).

A11.3. Single-Ended Realizations for High Frequencies

The circuit in Fig. A11.1 can be realized at high frequencies by using "magic tee" junctions or transmission line transformers. There also exists some interesting realizations using a star, rather than a ring; connection of the four diodes**. In all these circuits the diodes have to be connected to each other electrically at all harmonic sidebands (theoretically up to infinity) if one wants to isolate the odd- and even-order frequencies in the input and output ports. At microwave and millimeter wave frequencies, however, it is preferable (or perhaps necessary) to terminate each diode separately. For this purpose one needs to realize the doubly-balanced mixer with a single-ended mixer. That is to say, the single-ended mixer should satisfy Eqs. (A11.1) ... (A11.5) if the diode is assumed ideal, and Eqs. (A11.7) ... (A11.9) if the diode switches between R_f and R_b.

From our analysis in Sec. 2.3, it was shown that by using filters for the even- and odd-order frequencies at both ports of the mixer, a single-ended mixer can be made equivalent to a doubly-balanced mixer with the same diode resistance waveform. The required filters are only practical if the i-f frequency, ω_o, is much smaller than the pump frequency, ω_p. In this case quarter-wave transmission

** See for example Mouw (I) and Mouw and Fukuchi (I).

lines can very closely achieve the desired filtering as was given in Fig. 2.7. An open-circuit $\lambda_p/4$ line short-circuits the odd-order frequencies; $\omega_n = n\omega_p + \omega_o$, n odd; and open-circuits the even-order frequencies; $\omega_n = n\omega_p + \omega_o$, n even; and a short-circuited $\lambda_p/4$ line gives the dual effect. Two single-diode realizations of Fig. All.1 are shown in Figs. All.4a and b. Note that $v_1(t)$ and $i_1(t)$ will consist only of odd-order frequencies and $v_2(t)$ and $i_2(t)$ of even-order frequencies. This was done here by the transmission line filters while in Fig. All.1 the same effect was achieved by symetry. The doubly-balanced circuit will, of course, operate satisfactorily over a much wider bandwidth than any of the single-ended circuits.

A natural question arises for the single-ended circuits: How to pump the diode so as to obtain a square-wave resistance? Fortunately it came out that if a strong pump is applied at the input port with the signal, as is usually done in microwave mixers, and if the mixer is terminated as an H- or a G-mixer,** which are the optimum imbedding networks for a square-wave resistance as given in Sec. A3.3.3, then the diode resistance waveform will be a square-wave or very close to a square-wave. This was demonstrated for the single-exponential-diode G- and H-mixer circuits given

** The H-mixer is obtained by open-circuiting all the odd-order out-of-band frequencies (input port) and short-circuiting all the even-order out-of-band frequencies (output port). The G-mixer is the dual case. See Secs. 2.3.2 and 2.4.

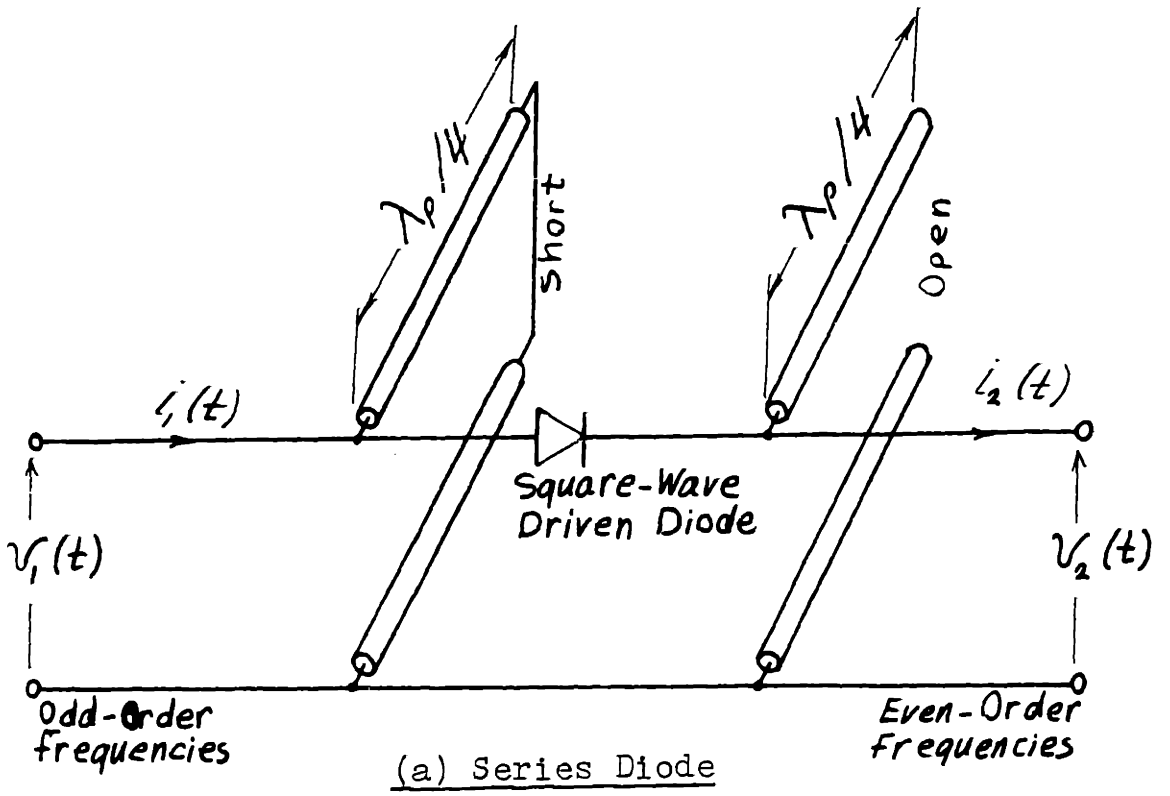

(a) Series Diode

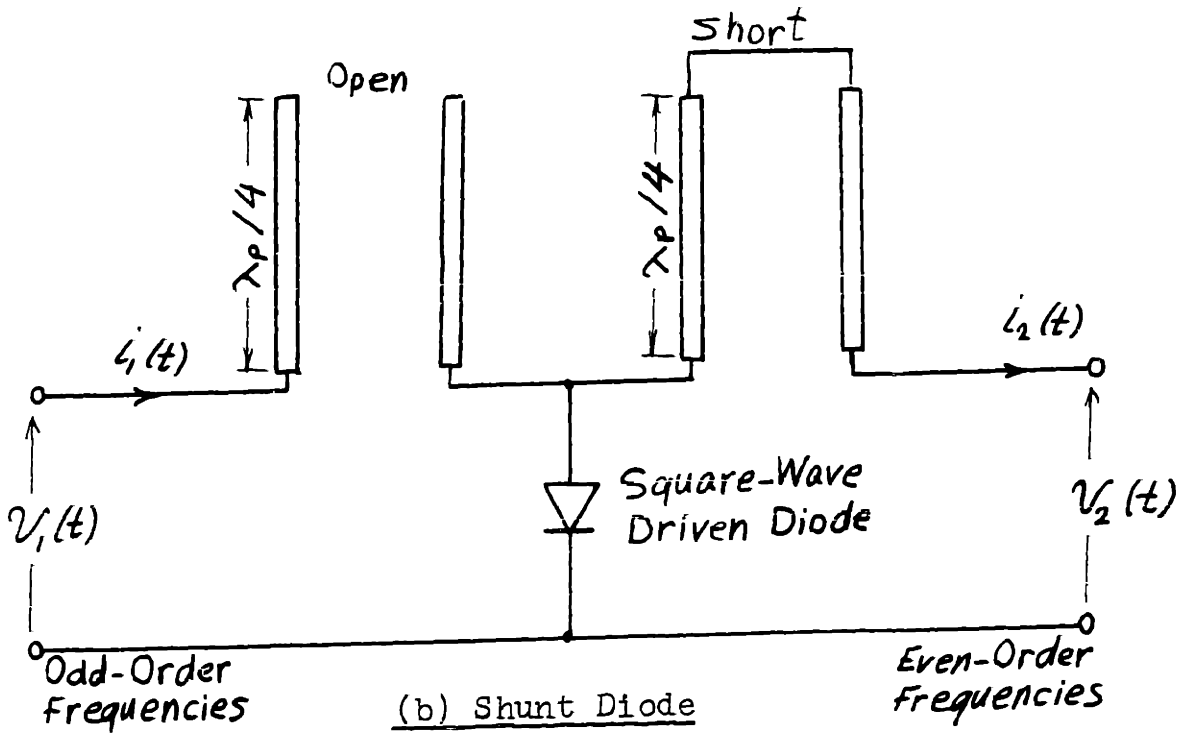

(b) Shunt Diode

Fig. All.4. Two High Frequency Single-Diode Realizations of the Four-Diode Doubly-Balanced Ring Mixer of Fig. All.1, when $\omega_o \ll \omega_p$. (λ_p = the wavelength at the pump frequency ω_p).

in Secs. 4.2.3 and 4.2.4 where the diode resistance waveform was in some sense, a square wave. If the diode is assumed to be piece-wise linear (R_f in the forward direction and R_b in the backward direction) then it can be easily shown that one obtains exactly a square-wave resistance (switching between R_f and R_b) for a single-diode H-mixer with zero d-c voltage bias or for a single-diode G-mixer with zero d-c current bias.

In practice, one needs to connect two single-ended mixers together through a "magic tee" to isolate the signal and local oscillator (pump) ports and to suppress the local oscillator noise.** However, it is clear that the performance of the composite mixer is identical to that of a single-ended mixer driven from a noiseless local oscillator.

For relatively low frequencies, square-wave pumping of a single-ended mixer can be achieved by replacing the diode in any of the mixers in Fig. All.4, by a multiport device, such as a relay, a switching transistor or the four-diode bridge shown in Fig. All.5.

In conclusion, a single-ended mixer can be made equivalent to the doubly-balanced square-wave-reversing switch mixer of Fig. All.1. The results in the next three sections will thus apply to both kinds of mixers.

** See for example Pound (I, Sec. 6.5).

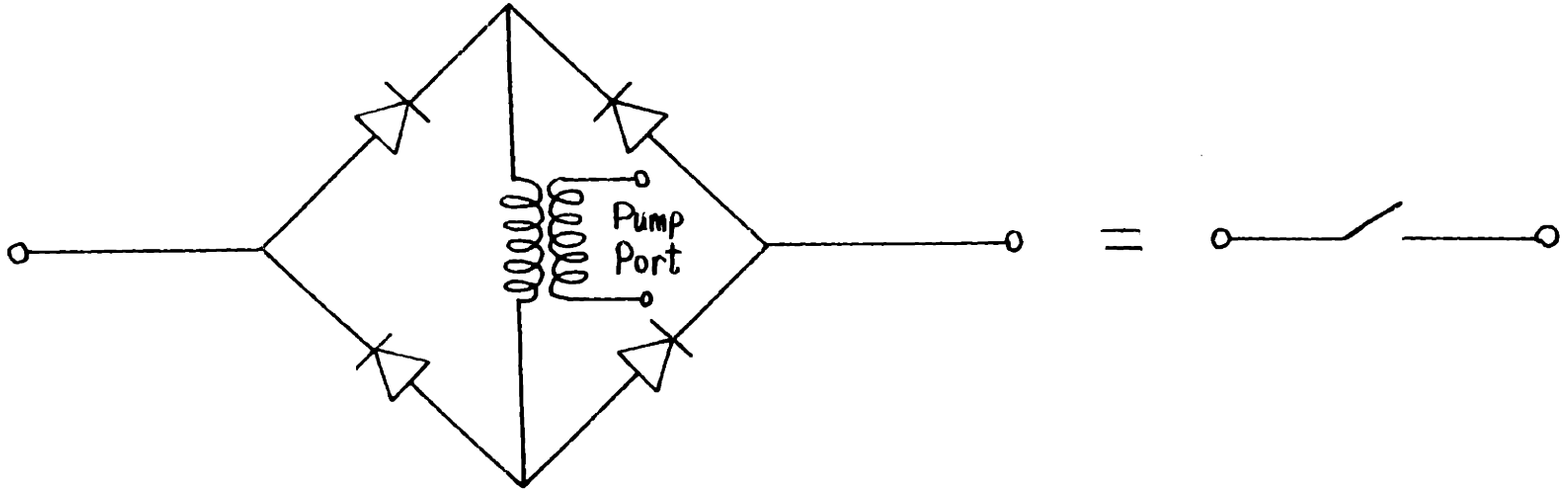

Fig. A11.5. A Possible Method of Pumping the Single-Ended Mixers in Figs. A11.4 at Low Frequencies

All.4. Complete Selective Terminations

The minimum conversion loss of the square-wave reversing switch mixer when no frequency selective terminations are used, as given in Fig. All.6, is known to be $\pi^2/4$ (i.e., 3.92 db)**. To reduce this conversion

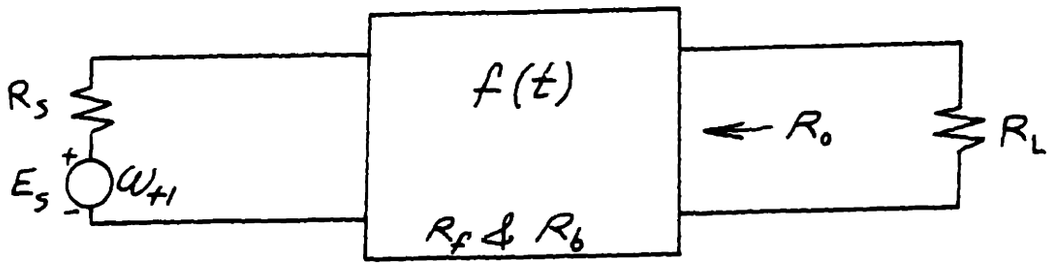

Fig. All.6. Real Broadband Terminations

loss one must use selective terminations to eliminate the loss in R_L and R_s at the undesired frequencies; ω_n, $n \neq 1$ or 0. One can obtain a conversion loss of unity for any source impedance, if $R_f = 0$ and $R_b = \infty$, by short circuiting the undesired frequencies at one port while open-circuiting those at the other port. This forms the H- and G-mixers***,

** This can be shown from the equations in Sec. All.2 by noting that in transforming from ω_{+1} to ω_o there is a factor of $2/\pi$ in the voltage ratio. See also Caruthers (I) and Tucker (I and IV).

*** See the basic definitions in Sec. 2.3.2 and 2.4.

as shown in Figs. All.7 and All.8. The models shown in the figures can be derived from Eqs. (All.8) and (All.9). For example, for the H-mixer, Fig. All.7a, Eq. (All.8) gives

$$\begin{bmatrix} V_{+1} \\ \\ I_o \end{bmatrix} = \begin{bmatrix} 2R_f & \frac{2}{\pi} \\ \\ \frac{-2}{\pi} & \frac{2}{R_b} \end{bmatrix} \begin{bmatrix} I_{+1} \\ \\ V_o \end{bmatrix} \quad , \text{(All.9)}$$

which is valid when $R_f \ll R_b$**. The G-mixer gives the dual equation. If R_f and R_b are finite then the optimum conversion loss for either mixer will be approximately given by $27.3\ \delta$ db, where $\delta = \sqrt{R_f/R_b} \ll 1$, and the optimum source resistance is $\frac{2}{\pi}\sqrt{R_f R_b}$ for the H-mixer and $\frac{\pi}{2}\sqrt{R_f R_b}$ for the G-mixer.

It can easily be shown from Eqs. (All.1) ... (All.5) describing the ideal case, $R_f = 0$ and $R_b = \infty$, that the currents (or the voltages) at <u>both</u> sides of the mixer cannot be constrained to be sinusoidal, otherwise the conversion loss will be infinite. Thus in this case the Z- and Y-mixers given in Figs. All.9 and All.10 give infinite conversion loss. If R_f and R_b are finite then the optimum conversion loss for both mixers is finite

** In this equation and in all the following analysis we used the voltage and current notation of Sec. 2.1.

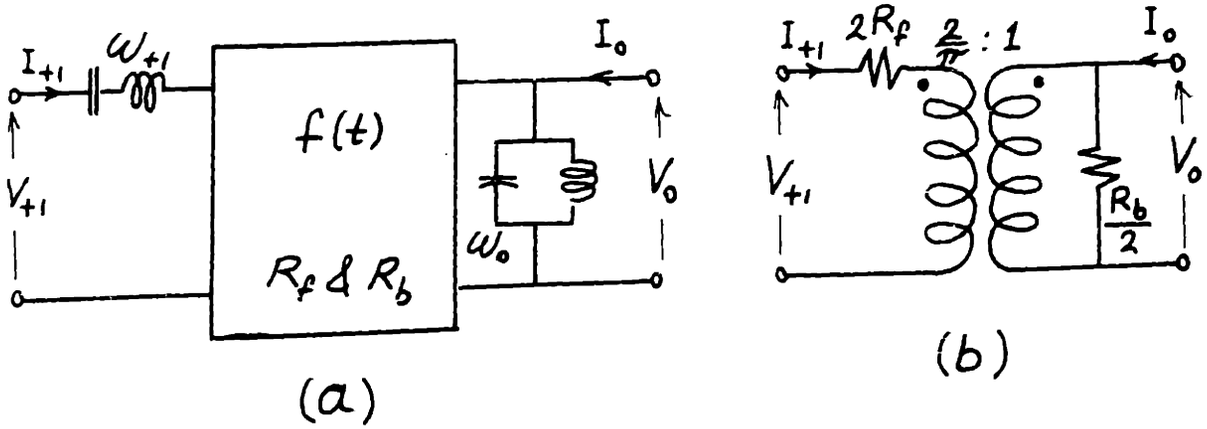

Fig. All.7. The H-Mixer and an Equivalent Model

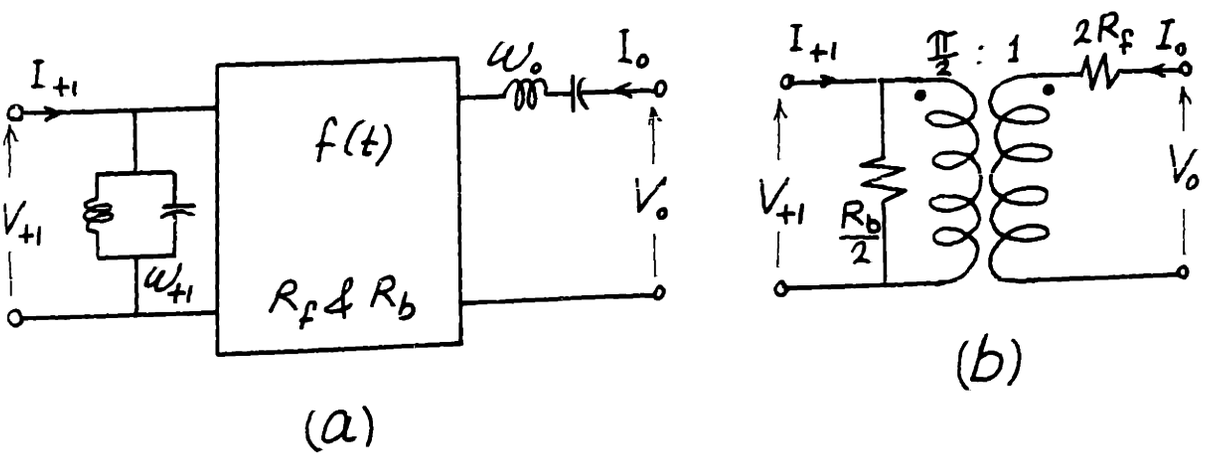

Fig. All.8. The G-Mixer and an Equivalent Model

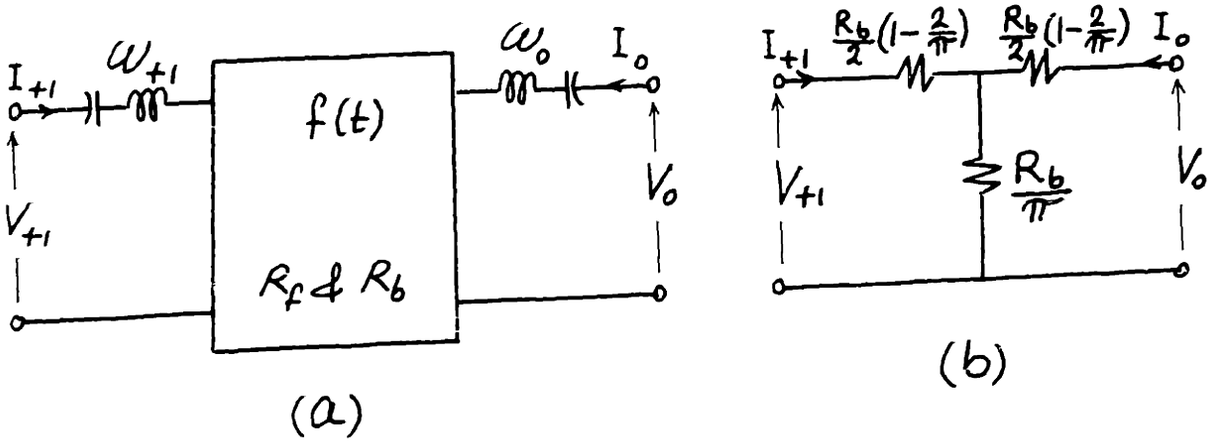

Fig. A11.9. The Z-Mixer and an Equivalent Model

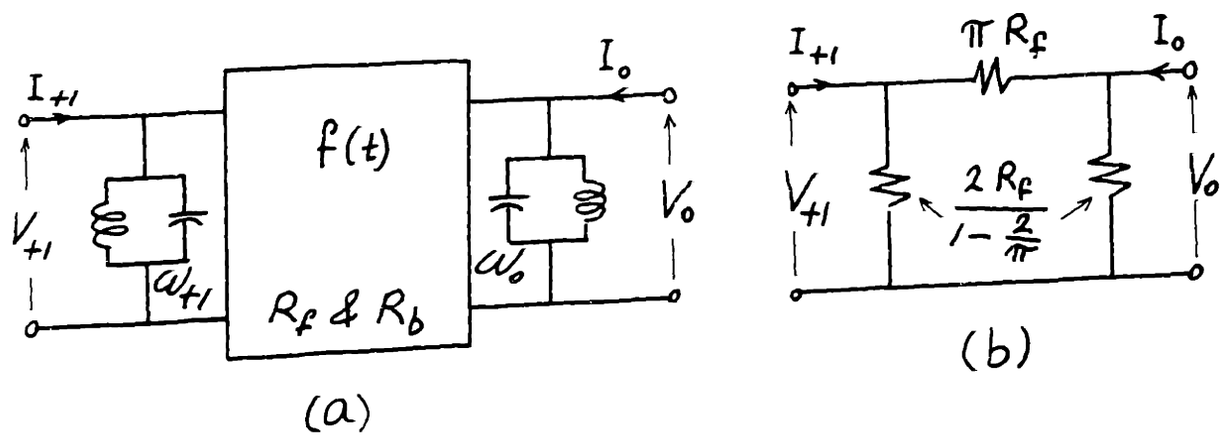

Fig. A11.10. The Y-Mixer and an Equivalent Model

(8.89 db) but the optimum source resistance is either too high, of the order of R_b for the Z-mixer, or too low, of the order of R_f for the Y-mixer .

From the above it seems that the H- and G-mixers are suitable for the square-wave reversing-switch circuit. In fact it was shown in Sec. 3.3.3 that, of all possible mixer imbedding networks, these two mixers give the best possible conversion loss for any given values of R_f and R_b**.

In tables All.1 and All.2 we give the results for the four aforementioned mixers. For each case we considered three image terminations; open image, equal signal and image impedances***, and short image. The first table is for the cases where the conversion loss is less than 4.0 db and the second table for the remaining cases****.

Because of their importance we give the equivalent models for the H- and G-mixers with arbitrary image terminations in Figs. All.11 and All.12. These models can be deduced from Eqs. (All.8) and (All.9). For example, for the H-mixer with arbitrary image terminations,

---

** It is also shown in Sec. 3.2.2 that the square-wave resistance-waveform is the optimum waveform for the H- and G-mixers.

*** In the rest of the thesis, this case is referred to as the "broadband input termination". However, to avoid confusion with pure resistive termination, Fig. All.6, such terminology will not be used here.

**** Compare to Caruthers (I, Table II, p. 21) or Tucker (I, Table opposite p. 200). See also Tables All.3 ... All.6 in Sec. All.6.

Table A11.1. Square-Wave Reversing-Switch Mixers with Complete Selective Terminations for Cases where Conversion Loss is Less than 4.0 db**

MIXER TYPE		L_{opt}, Ratio	L_{opt}, db	$\frac{R_{s,opt}}{\sqrt{R_f R_b}}$	$\left(\frac{R_o}{R_s}\right)_{opt}$	L (Ratio) for $R_s \ll R_{s,opt}$
Real Broadband		$\frac{\pi^2}{4}(1 + 4\delta)$	$3.92 + 17.4\,\delta$	1	1	$\frac{\pi^2}{4}\left(1 + 2\frac{R_f}{R_s}\right)$
H-MIXER	Open Image	$1 + 2\pi\delta$	$27.3\,\delta$	$\frac{2}{\pi}$	$\frac{\pi^2}{4}$	$1 + 2\frac{R_f}{R_s}$
H-MIXER	Equal Signal and Image Impedances	$2(1 + \sqrt{2}\,\pi\,\delta)$	$3.01 + 19.3\,\delta$	$\frac{2\sqrt{2}}{\pi}$	$\frac{\pi^2}{8}$	$2\left(1 + 2\frac{R_f}{R_s}\right)$
G-MIXER	Short Image	$1 + 2\pi\delta$	$27.3\,\delta$	$\frac{\pi}{2}$	$\frac{4}{\pi^2}$	$1 + \frac{\pi^2}{2}\frac{R_f}{R_s}$
G-MIXER	Equal Signal and Image Impedances	$2(1 + \sqrt{2}\,\pi\,\delta)$	$3.01 + 19.3\,\delta$	$\frac{\pi}{2\sqrt{2}}$	$\frac{8}{\pi^2}$	$2\left(1 + \frac{\pi^2}{4}\frac{R_f}{R_s}\right)$

** It is assumed that $\delta = \sqrt{R_f/R_b} \ll 1$; factors of δ^2 are neglected.

Table A11.2. Square-Wave Reversing-Switch Mixers with Complete Selective Terminations for Cases where Conversion Loss is More than 4.0 db**

MIXER TYPE		L_{opt} Ratio	L_{opt} db	$R_{s,opt}$	$R_{o,opt}$	L (Ratio) for $R_b >> R_s >> R_f$
H-Mixer (Short Image)		5.83	7.66	$2.83\ R_f$	$3.49\ R_f$	$3 + \frac{1}{2}\frac{R_s}{R_f}$
G-Mixer (Open Image)		5.83	7.66	$.354\ R_b$	$.287\ R_b$	$3 + \frac{1}{2}\frac{R_b}{R_s}$
Z-MIXER	Open Image	7.74	8.89	$.386\ R_b$	$.386\ R_b$	$3.93 + 0.734\frac{R_b}{R_s}$
	Equal Signal and Image Impedances	5.08	7.06	$.218\ R_b$	$.218\ R_b$	$2.93 + 0.234\frac{R_b}{R_s}$
	Short Image	3.59	5.55	$.282\ R_b$	$.168\ R_b$	$1.93 + 0.234\frac{R_b}{R_s}$
Y-MIXER	Short Image	7.74	8.89	$2.59\ R_f$	$2.59\ R_f$	$3.93 + 0.734\frac{R_s}{R_f}$
	Equal Signal and Image Impedances	5.08	7.06	$4.59\ R_f$	$4.59\ R_f$	$2.93 + 0.234\frac{R_s}{R_f}$
	Open Image	3.59	5.55	$3.54\ R_f$	$5.96\ R_f$	$1.93 + 0.234\frac{R_s}{R_f}$

** Unlike Table A11.1, factors of $\delta^2 = R_f/R_L$, and not δ, appear in the conversion loss formulas; this was neglected since $\delta << 1$.

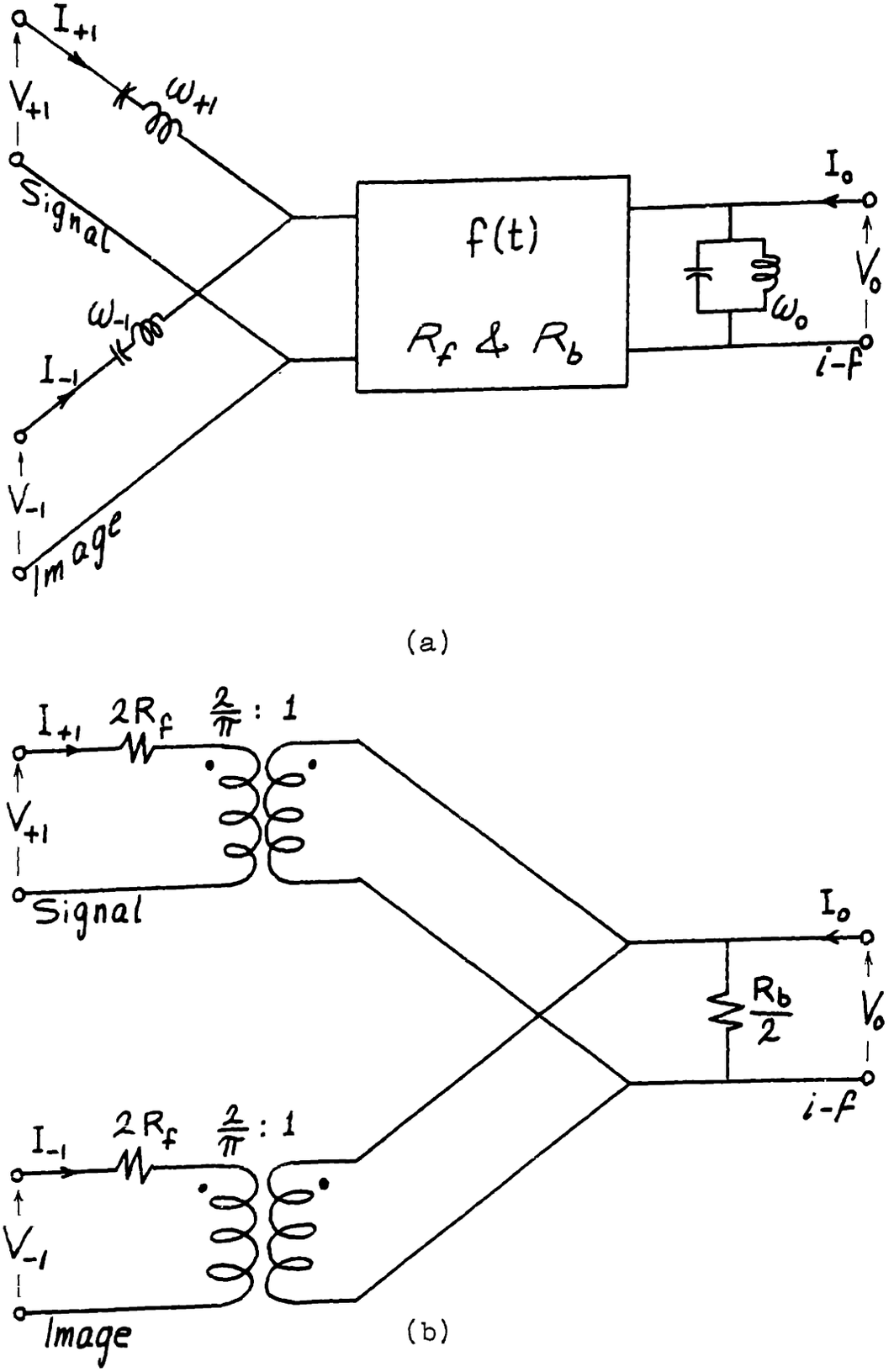

Fig. All.11. An H-Mixer with Arbitrary Image Termination and an Equivalent Model

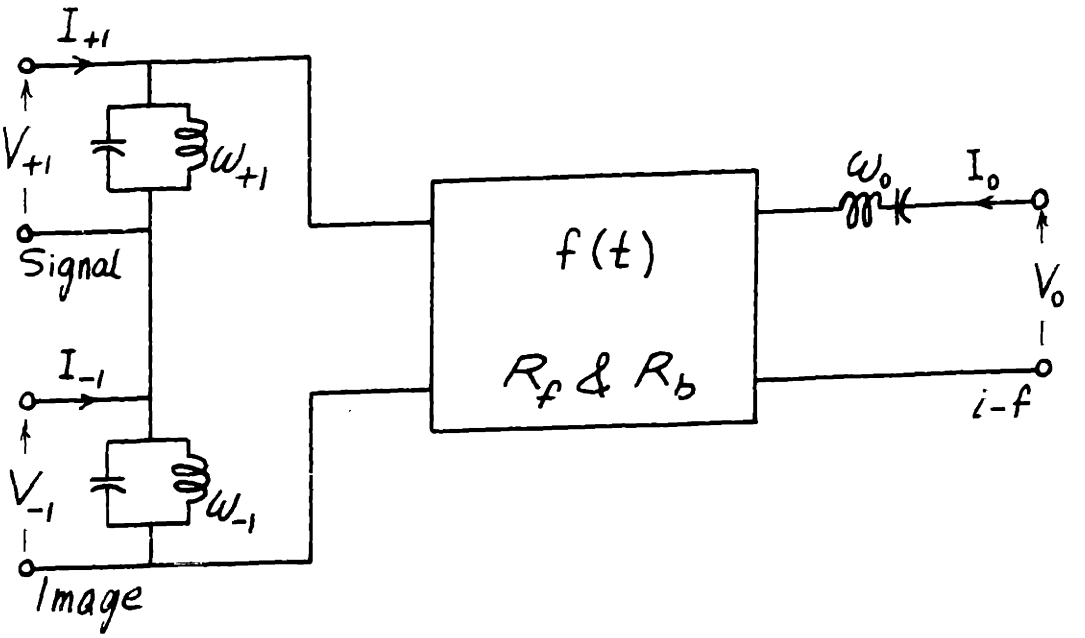

(a)

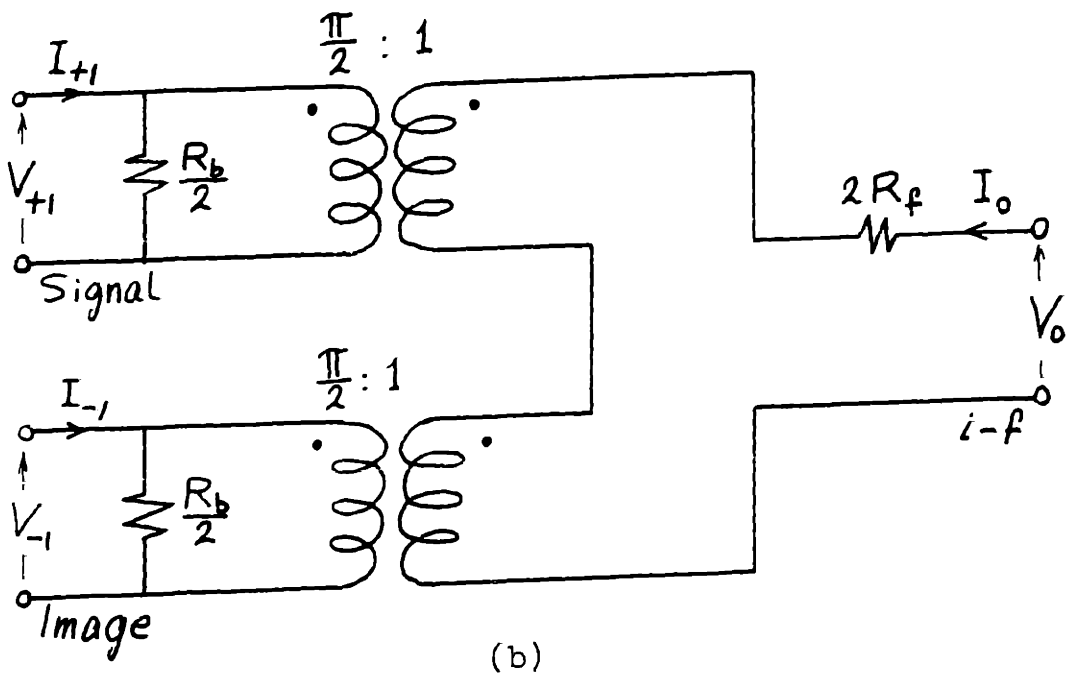

(b)

Fig. A11.12. A G-Mixer with Arbitrary Image Termination and an Equivalent Model

Fig. All.11a, Eq. (All.8) gives

$$\begin{bmatrix} V_{+1} \\ I_o \\ V_{-1} \end{bmatrix} = \begin{bmatrix} 2R_f & \frac{2}{\pi} & 0 \\ \frac{-2}{\pi} & \frac{2}{R_b} & \frac{-2}{\pi} \\ 0 & \frac{2}{\pi} & 2R_f \end{bmatrix} \begin{bmatrix} I_{+1} \\ V_o \\ I_{-1} \end{bmatrix} \quad , \text{(All.10)}$$

which is valid when $R_f << R_b$. It is clear that if the image port of the H-mixer in Fig. All.11a is open circuited, the mixer reduces to the standard H-mixer of Fig. All.7 which gives a small conversion loss as given in Table All.1. On the other hand if the image frequency is short-circuited then the conversion loss is very large, see Table All.2, since the small resistance $2R_f$ in the image port will appear in shunt with the input. In fact if $R_f = 0$ then the conversion loss in this case will be infinite for any finite source impedance. This point will be made clearer in the next section. Of course, the dual of the above discussion holds true for the G-mixer.

If, in addition to the image frequency, ω_{-1}, one likes to consider the sum frequency, ω_{+2}, and its image, ω_{-2}, one can use Eq. (All.8) to show that the H-mixer equation assumes the form

$$\begin{bmatrix} I_{+2} \\ V_{+1} \\ I_0 \\ V_{-1} \\ I_{-2} \end{bmatrix} = \begin{bmatrix} \frac{2}{R_b} & \frac{-2}{\pi} & 0 & \frac{2}{3\pi} & 0 \\ \frac{2}{\pi} & 2R_f & \frac{2}{\pi} & 0 & \frac{-2}{3\pi} \\ 0 & \frac{-2}{\pi} & \frac{2}{R_b} & \frac{-2}{\pi} & 0 \\ \frac{-2}{3\pi} & 0 & \frac{2}{\pi} & 2R_f & \frac{2}{\pi} \\ 0 & \frac{2}{3\pi} & 0 & \frac{-2}{\pi} & \frac{2}{R_b} \end{bmatrix} \begin{bmatrix} V_{+2} \\ I_{+1} \\ V_0 \\ I_{-1} \\ V_{-2} \end{bmatrix} \quad . \quad \text{(A11.11)}$$

This suggests the model shown in Fig. A11.13 which is valid when $R_f << R_b$. Also, the corresponding model for the G-mixer given in Fig. A11.14 can be deduced by duality.**

One should note that the complex conjugate of the impedance offered to ω_{-1} and ω_{-2}, and in general any frequency with negative subscript, rather than the impedances themselves should be used in Eqs. (A11.10) and (A11.11), and in Figs. A11.11 ... A11.14. This point is made clear in Sec. 2.1.2.

** Bassi (I) and Stracca (I) studied the performance of the G-mixer with all possible short and open terminations for ω_{-2}, ω_{-1} and ω_{+2}. Their results, when $R_f << R_b$, can be deduced from the model in Fig. A11.14.

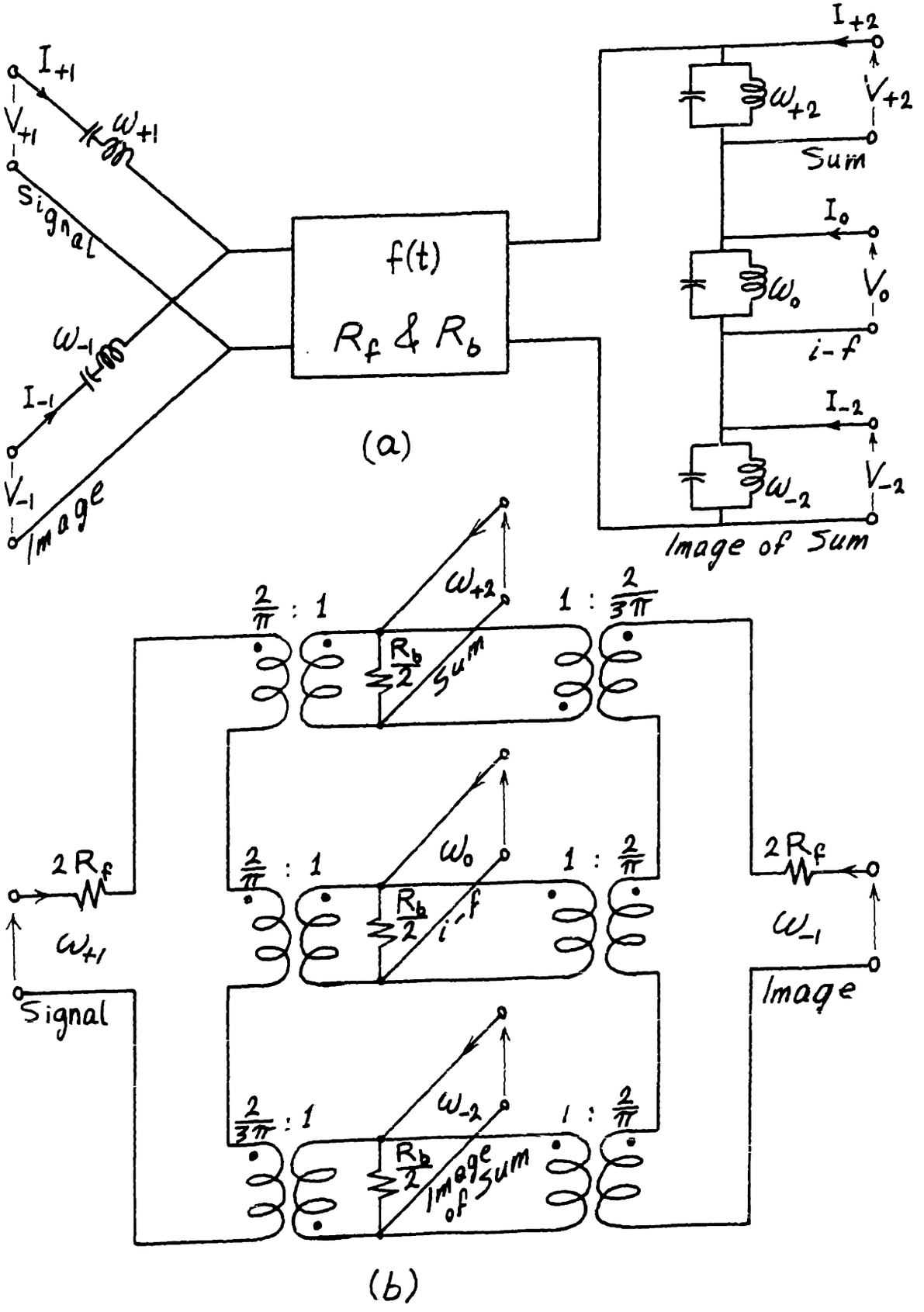

Fig. All.13. An H-Mixer with Arbitrary Terminations for ω_{-2}, ω_{-1} and ω_{+2} and an Equivalent Model

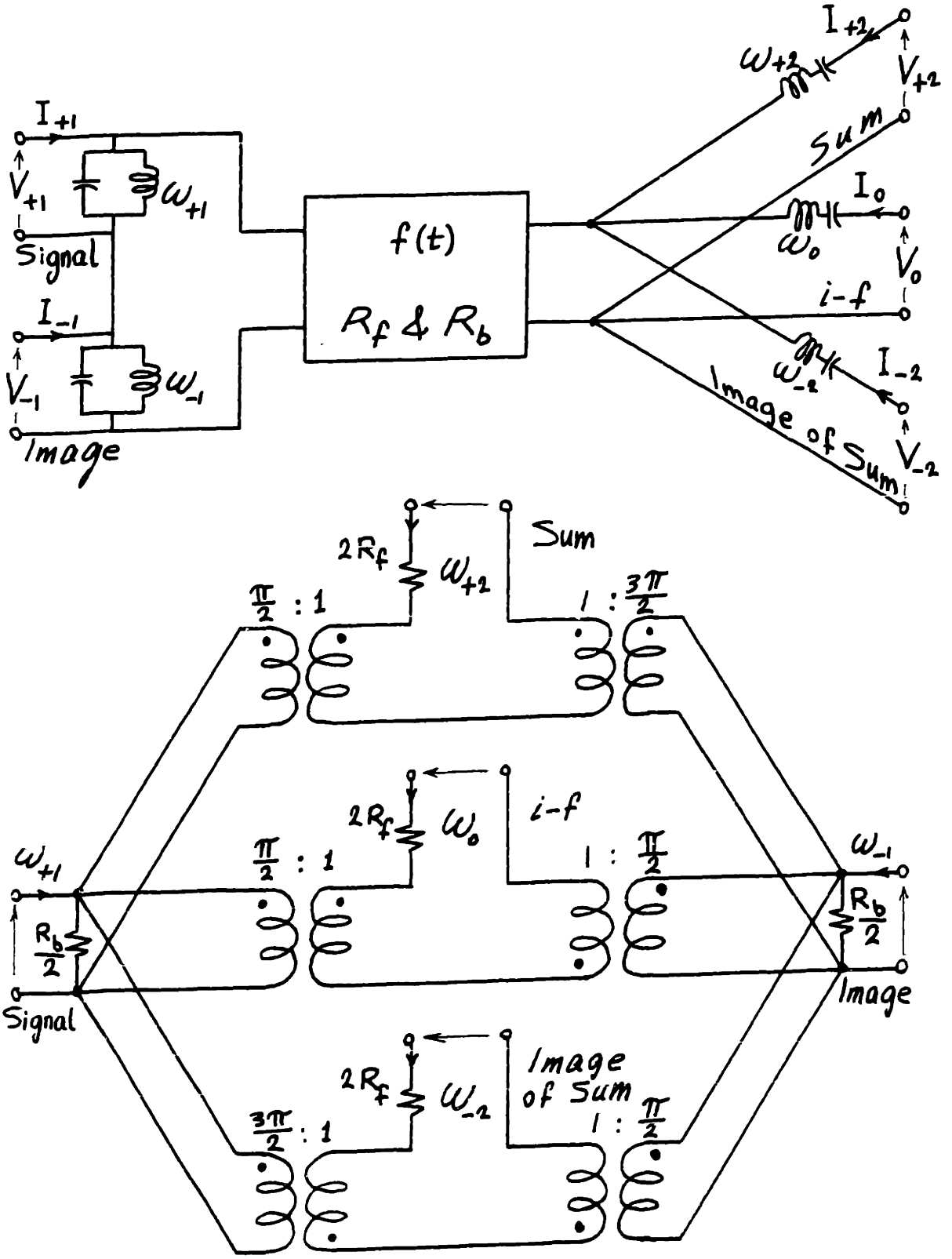

Fig. A11.14. A G-Mixer with Arbitrary Terminations for ω_{-2}, ω_{-1} and ω_{+2} and an Equivalent Model

A11.5. Modified Selective Terminations

It is shown in the previous section that if the image state of an ideal square-wave reversing-switch H-mixer is changed from its standard termination of open circuit to its modified termination of short circu't then the conversion loss changes from unity to infinity. The dual is also true for the G-mixer. Here we generalize this result by proving the following theorem:

> Theorem 1: If the terminations of different numbers of odd-order and even-order frequencies, in an ideal square-wave reversing-switch mixer connected as a standard H- or G-mixer, is changed from open-circuit to short-circuit and vice versa; then the conversion loss will be infinite.

The complementary, and perhaps more surprising theorem is given by:

> Theorem 2: If the terminations of equal numbers of odd-order and even-order frequencies, in an ideal square-wave reversing-switch mixer connected as a standard H- or G-mixer, is changed from open-circuit to short-circuit and vice versa; then the conversion loss will remain unity.

Proof of Theorem 1:

Consider the modified H-mixer of Fig. A11.15 where we changed the terminations of p distinct odd-order

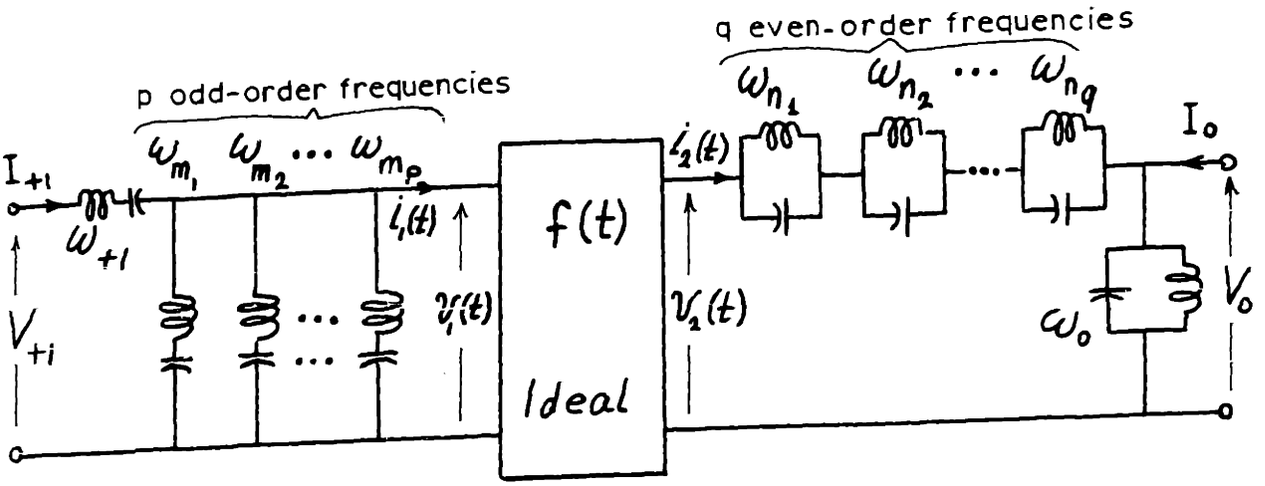

Fig. A11.15. A Modified H-Mixer

frequencies;** ω_{m_i}, i = 1 ... p, (m_i odd); from open to short; and of q distinct even-order frequencies; ω_{n_j}, j = 1 ... q, (n_j even); from short to open. Thus,

$$V_m = 0 \quad , \; m \text{ odd} = m_1 \ldots m_p \qquad , \text{(A11.12)}$$

$$I_m = 0 \quad , \; m \text{ odd} \neq +1 \text{ or } m_1 \ldots m_p \qquad , \text{(A11.13)}$$

$$I_n = 0 \quad , \; n \text{ even} = n_1 \ldots n_q \qquad , \text{(A11.14)}$$

and $$V_n = 0 \quad , \; n \text{ even} \neq 0 \text{ or } n_1 \ldots n_q \qquad . \text{(A11.15)}$$

Now we want to prove that if p ≠ q then the conversion loss of the mixer is infinite. Let us first

** Note the frequency notation in Sec. 2.1.1.

assume that $p > q$. Writing $v_1(t)$ and $v_2(t)$ in terms of their frequency components, it can be shown from Eqs. (A11.4), (A11.6) and (A11.15) that

$$\begin{bmatrix} V_{m_1} \\ V_{m_2} \\ \vdots \\ V_{m_q} \\ V_{m_{q+1}} \end{bmatrix} = \frac{2}{\pi} \left[a_{ij}\right]_{(q+1)\times(q+1)} \begin{bmatrix} V_{n_1} \\ V_{n_2} \\ \vdots \\ V_{n_q} \\ V_o \end{bmatrix} , \quad \text{(A11.16)}$$

where

$$a_{ij} = \frac{(-1)^{\frac{m_i - n_j - 1}{2}}}{m_i - n_j} \qquad i, j = 1, \ldots, q+1 , \quad \text{(A11.17)}$$

where the m's and n's are the same odd and even integers defined above and n_{q+1} is defined to be zero.

It can be shown that the determinant of the above $[a_{ij}]$ matrix is given by

$$\Delta_{q+1} = (-1)^{\left\{\frac{q(q+1)}{2} + \sum_{i=1}^{q+1} \frac{m_i - n_i - 1}{2}\right\}} \frac{\prod_{i=1}^{q} \prod_{j=i+1}^{q+1} (m_i - m_j)(n_i - n_j)}{\prod_{i=1}^{q+1} \prod_{j=1}^{q+1} (m_i - n_j)} ,$$

(A11.18)

Since the m's and n's are distinct, it follows that Δ_{q+1} is nonzero, and hence, the matrix $[a_{ij}]$ is nonsingular.

Since it was assumed that $p > q$, it follows from Eq. (A11.12) that all the entries of the column vector in the left-hand side of Eq. (A11.16) are identically zero. But, since $[a_{ij}]$ is nonsingular, then all the entries of the column vector in the right-hand side of Eq. (A11.16) are also zero. In particular, the output voltage V_o is zero. Thus the conversion loss of the mixer is infinite.

If it is assumed that $p < q$ the above proof obviously does not hold. However, in this case one can proceed in a parallel manner by using Eqs. (A11.12), (A11.6) and (A11.13) to deduce an equation similar to Eq. (A11.16) but relating $\{I_{n_1}, I_{n_2}, \ldots I_{n_{p+1}}\}$ with $\{I_{m_1}, I_{m_2}, \ldots, I_{m_p}, I_{+1}\}$. Then from Eq. (A11.14) and the fact that $[a_{ij}]$ is nonsingular, it can be shown that the input signal current, I_{+1}, is zero. Thus the conversion

loss of the mixer is infinite.

This completes the proof of Theorem 1 for the H-mixer. Obviously, the dual analysis will prove the theorem for the G-mixer.

Proof of Theorem 2:

If in Fig. A11.15, p = q, then by defining m_{q+1} to be +1, Eq. (A11.16) assumes the form

$$\begin{bmatrix} 0 \\ 0 \\ \cdot \\ \cdot \\ \cdot \\ 0 \\ V_{+1} \end{bmatrix} = \frac{2}{\pi} \left[a_{ij} \right]_{(q+1)\times(q+1)} \begin{bmatrix} V_{n_1} \\ V_{n_2} \\ \cdot \\ \cdot \\ \cdot \\ V_{n_q} \\ V_o \end{bmatrix} , \quad \text{(A11.19)}$$

where we made use of Eq. (A11.12). Solving for V_o in terms of V_{+1}, it is easy to show that

$$V_o = \frac{\pi}{2} \frac{\Delta_q}{\Delta_{q+1}} V_{+1} \quad \text{(A11.20)}$$

where Δ_{q+1} is the determinant of $[a_{ij}]$ given in Eq. (A11.18), with $m_{q+1} = +1$ and $n_{q+1} = 0$; and Δ_q is the determinant of

$[a_{ij}]$ with its last row and column deleted; its value can be deduced from Eq. (A11.18) by substituting q for q+1. If this is done, Eq. (A11.20) gives

$$V_o = \frac{\pi}{2} V_{+1} \prod_{i=1}^{q} \frac{m_i(n_i-1)}{n_i(m_i-1)} \quad . \quad (A11.21)$$

In a similar manner it can be shown that

$$I_{+1} = -\frac{\pi}{2} I_o \prod_{i=1}^{q} \frac{m_i(n_i-1)}{n_i(m_i-1)} \quad . \quad (A11.22)$$

Thus the modified H-mixer of Fig. A11.15, when p = q, can be represented by the transformer model shown in Fig. A11.16. The conversion loss of the mixer in this

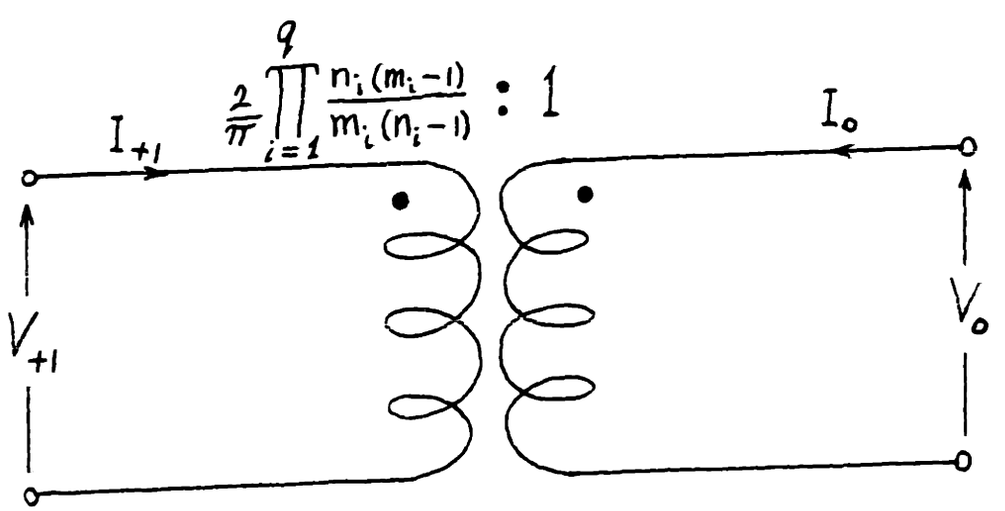

Fig. A11.16. Equivalent Model for the Modified H-Mixer of Fig. A11.15 with p = q

case is obviously unity. This proves Theorem 2 for the H-mixer. For the G-mixer, the theorem is proven by duality.

If the frequencies ω_m's and ω_n's are chosen in consecutive pairs in both sides of ω_{+1} and ω_o up to infinity; i.e., ω_{-1} and ω_{+2}, ω_{-2} and ω_{+3}, ω_{-3} and ω_{+4}, $\ldots\omega_{-\infty}$ and $\omega_{+\infty}$; then the turns ratio of the transformer in Fig. All.16 becomes

$$N = \frac{2}{\pi}\frac{2\times2}{1\times1}\times\left[\frac{2\times4}{3\times3}\right]^2\times\left[\frac{4\times6}{5\times5}\right]^2\times\left[\frac{6\times8}{7\times7}\right]^2\times\ldots$$

$$= \frac{2}{\pi}\left\{\lim_{k\to\infty}\frac{[2\times4\times6\times\ldots\times2k]}{[1\times3\times5\times\ldots\times(2k-1)]\sqrt{2k}}\right\}^4$$

$$= \frac{2}{\pi}\left\{\sqrt{\frac{\pi}{2}}\lim_{k\to\infty}\frac{\Gamma(k+1)}{\sqrt{k}\,\Gamma(k+\frac{1}{2})}\right\}^4 \qquad \text{(All.23a)}$$

It can be shown that the limit inside the parenthesis in the above equation is unity. Thus we get

$$N = \frac{\pi}{2} \qquad \text{(All.23b)}$$

which is recognized, from Fig. All.8, to be the turns ratio of the transformer model for the G-mixer. This, of course, should be expected since we started with an H-mixer and changed the status of all frequencies from short to open and vice versa which gives a G-mixer.

If the diode switches between R_f and R_b instead of zero and infinity, the analysis of general modified H- and G-mixers becomes very complex. However, it is clear that if $R_f \ll R_b$ then Theorem 1 still applies with the word infinite replaced by large, and Theorem 2 applies with the word unity replaced by near unity. Presumably, according to the discussion given in Sec. 3.3.3, the standard H- and G-mixers give better performance, for any R_f and R_b, than any other mixer.**

** Bassi (I) and Stracca (I) considered a G-mixer with all possible short and open terminations for ω_{-2}, ω_{-1} and ω_{+2}. Their results agree with our analysis. For example, referring to Stracca (I, Figs. 26 and 27, p. 328) it is clear that Cases 6 and 7, where the status of one even- and one odd-order frequency has been changed, give low conversion losses, but not as low as the standard G-mixer of Case 1. On the other hand the remaining cases, where the status of different numbers of even- and odd-order frequencies has been changed, give high conversion losses.

A11.6. Incomplete Selective Terminations

It is shown in Sec. A11.4 that an ideal square-wave reversing-switch H- or G-mixer with complete selective terminations, Fig. A11.7 or A11.8, gives a conversion loss of unity (zero db). Further, it was shown that if no selective terminations were used, Fig. A11.6, the conversion loss is $\pi^2/4$ (3.92 db). In this section we study the performance of H- and G-mixers with incomplete selective terminations. In this case, some of the undesired frequencies will be dissipated in the source and/or load terminations while the rest will be properly terminated (i.e. short or open). To simplify the analysis the diodes will be assumed as ideal on-off switches, i.e. $R_f = 0$ and $R_b = \infty$.

It is clear that if frequencies other than the i-f are terminated in the i-f load resistance, the conversion loss from signal to i-f will be a function of both source and i-f resistances. Thus it makes more sense to speak in terms of <u>transducer loss</u>** rather than available conversion loss. Since the diodes are assumed ideal, the transducer loss will be a function of the <u>ratio</u> of the two aforementioned resistances. Hence, for each mixer circuit, we will be interested in the optimum value of the transducer loss and the corresponding resistance ratio.

** This is defined as the ratio of the maximum available power from the source to the power delivered to the load.

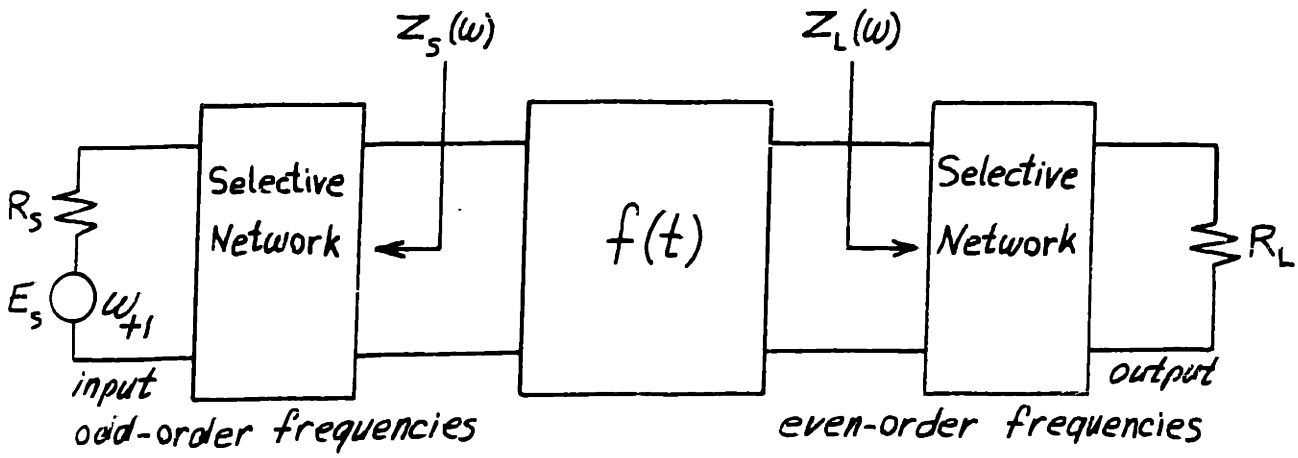

Fig. A11.17. Generalized Mixer Considered in Tables A11.3 ... A11.6

The general mixer circuit considered is shown in Fig. A11.17. The selective networks are such that for the signal and i-f frequencies** $Z_s(\omega_{+1}) = R_s$ and $Z_L(\omega_o) = R_s$. Further, for an H-mixer, with incomplete terminations, $Z_s(\omega) = \infty$ for some odd-order out-of-band frequencies and $Z_s(\omega) = R_s$ for the rest; and $Z_L(\omega) = 0$ for some even-order out-of-band frequencies and $Z_L(\omega) = R_L$ for the rest. The dual situation, of course, exists for a G-mixer with incomplete terminations.

One well known,*** but still very interesting,

** Note the frequency terminology of Sec. 2.1.1.

*** See for example Caruthers (I, Table II, second case, p. 21) or Tucker (I, Table opposite p. 200, cases 2 and 3 of ring mixer).

result is that if $Z_s(\omega) = R_s$ for all ω and <u>any</u> $Z_L(\omega)$ with $Z_L(\omega_o) = R_L$; or if $Z_L(\omega) = R_L$ for all ω and <u>any</u> $Z_s(\omega)$ with $Z_s(\omega_{+1}) = R_s$; the conversion loss is $\pi^2/4$ (i.e. 3.92 db) which is equivalent to the case of the real broadband mixer given in Fig. All.6 for which $Z_s(\omega) = R_s$ and $Z_L(\omega) = R_L$ for all ω. Thus to improve the conversion loss from 3.92 db, selective terminations have to be used at <u>both</u> sides of the mixer.

Expressions for the optimum values of the mixer transducer loss and the ratio R_L/R_s are given in Tables All.3 ... All.5 for different values of $Z_s(\omega)$ and $Z_L(\omega)$. The first table considered the cases where at least one side is completely terminated except for some cases; where any ω_{+k} and ω_{-k}, all k, are identically terminated; the input port can be completely terminated with the exception of the image frequency ω_{-1} which will have the same resistive termination as ω_{+1}. In Table All.4 we consider the cases where <u>one</u> frequency is properly terminated at one side with different terminations at the other side. Further, Table All.5 gives the cases where any <u>two</u> even-order frequencies ω_{+n} and ω_{-n}, n even, are properly terminated at the ouput port with different terminations at the input port such that $Z_s(\omega_{+m}) = Z_s(\omega_{-m})$ all m odd.

For Tables All.4 and All.5 the transducer loss can be calculated from the formula

Table A11.3. Square-Wave Reversing-Switch Mixers with One Port Completely Terminated*

Input Port $Z_s(\omega)$		Output Port $Z_L(\omega)$		L_{opt} (Ratio)
R_s	∞ for H 0 for G	R_L	0 for H ∞ for G	
None	All	None	All	1
$\omega_{m_1}, \ldots, \omega_{m_p}$	Rest	None	All	$1 + \sum_{i=1}^{p} \frac{1}{m_i^2}$
None	All	$\omega_{n_1}, \ldots, \omega_{n_p}$	Rest	$1 + \sum_{i=1}^{p} \frac{1}{(n_i-1)^2}$
ω_{-1}	Rest	None	All	2
ω_{-1}	Rest	$\omega_{\pm n_1}, \ldots, \omega_{\pm n_p}$	Rest	$2\left[1 + \sum_{i=1}^{p} \frac{1}{(n_i^2-1)^2}\right]$
Rest	$\omega_{m_1}, \ldots, \omega_{m_p}$	None	All	$\frac{\pi^2}{4} - \sum_{i=1}^{p} \frac{1}{m_i^2}$
None	All	Rest	$\omega_{n_1}, \ldots, \omega_{n_p}$	$\frac{\pi^2}{4} - \sum_{i=1}^{p} \frac{1}{(n_i-1)^2}$
ω_{-1}	Rest	Rest	$\omega_{\pm n_1}, \ldots, \omega_{\pm n_p}$	$\frac{\pi^2}{4} - 4 \sum_{i=1}^{p} \frac{1}{(n_i^2-1)^2}$
All	None	None	All	$\pi^2/4$
None	All	All	None	$\pi^2/4$

* For H-mixers $(R_s/R_L)_{opt} = 4/\pi^2 \, L_{opt}$ and for G-mixers $(R_L/R_s)_{opt} = 4/\pi^2 \, L_{opt}$. Throughout the Table m = odd $\neq +1$, n = even $\neq 0$, $Z_s(\omega_{+1}) = R_s$ and $Z_L(\omega_o) = R_L$.

Table A11.4. Values of A and B for Eqs. (A11.24) ... (A11.25) for Square-Wave Reversing Switch Mixers with One of the Ports Having only One properly Terminated Frequency*

Input Port $Z_s(\omega)$		Output Port $Z_L(\omega)$		$\frac{\pi^2}{4}$ A	$\frac{\pi^2}{4}$ (B-A)
R_s	∞ for H, 0 for G	R_L	0 for H, ∞ for G		
None	All	Rest	ω_n	$\frac{\pi^2}{4} - \frac{1}{(1-n)^2}$	$\frac{1}{(1-n)^2}$
Rest	ω_m	None	All	$\frac{\pi^2}{4} - \frac{1}{m^2}$	$\frac{1}{m^2}$
$\omega_{m_1} \ldots \omega_{m_p}$	Rest	Rest	ω_n	$\frac{\pi^2}{4} - \frac{1}{(1-n)^2} - \sum_{i=1}^{p} \frac{1}{(m_i-n)^2}$	$\frac{1}{(n-1)^2} + \frac{1}{1-n} \sum_{i=1}^{p} \frac{1}{(m_i-n)m_i}$
Rest	ω_m	$\omega_{n_1} \ldots \omega_{n_p}$	Rest	$\frac{\pi^2}{4} - \frac{1}{m^2} - \sum_{i=1}^{p} \frac{1}{(m-n_i)^2}$	$\frac{1}{m^2} + \frac{1}{m} \sum_{i=1}^{p} \frac{1}{(m-n_i)(1-n_i)}$
Rest	$\omega_{m_1} \ldots \omega_{m_p}$	Rest	ω_n	$\sum_{i=1}^{p} \frac{1}{(m_i-n)^2}$	$-\frac{1}{1-n} \sum_{i=1}^{p} \frac{1}{(m_i-n)m_i}$
Rest	ω_m	Rest	$\omega_{n_1} \ldots \omega_{n_p}$	$\sum_{i=1}^{p} \frac{1}{(m-n_i)^2}$	$-\frac{1}{m} \sum_{i=1}^{p} \frac{1}{(m-n_i)(1-n_i)}$
All	None	Rest	ω_n	0	0
Rest	ω_m	All	None	0	0

* Throughout the Table m= odd $\neq +1$, n= even $\neq 0$, $Z_s(\omega_{+1}) = R_s$ and $Z_L(\omega_0) = R_L$.

Table A11.5. Values of A and B for Eqs. (A11.24) ... (A11.26) for Square-Wave Reversing-Switch Mixers with the Output Port Having Two Properly Terminated Frequencies, ω_{+n} and ω_{-n} **

$Z_s(\omega)$		$Z_L(\omega)$		$\frac{\pi^2}{16}A$	$\frac{\pi^2}{16}(B-A)$
R_s	∞ for H 0 for G	R_L	0 for H ∞ for G		
None	All	Rest	$\omega_{\pm n}$	$\frac{\pi^2}{16} - \frac{1}{(1-n^2)^2}$	$\frac{1}{(1-n^2)^2}$
$\omega_{\pm m_1} \cdots \omega_{\pm m_p}$	Rest	Rest	$\omega_{\pm n}$	$\frac{\pi^2}{16} - \frac{1}{(1-n^2)^2} - \sum_{i=1}^{p} \frac{m_i^2}{(m_i^2-n^2)^2}$	$\frac{1}{(1-n^2)^2} - \sum_{i=1}^{p} \frac{1}{m_i^2-n^2}$
Rest	$\omega_{\pm m_1} \cdots \omega_{\pm m_p}$	Rest	$\omega_{\pm n}$	$\sum_{i=1}^{p} \frac{m_i^2}{(m_i^2-n^2)^2}$	$\frac{1}{(n^2-1)} \sum_{i=1}^{p} \frac{1}{m_i^2-n^2}$
All	None	Rest	$\omega_{\pm n}$	0	0

** Throughout the Table m= odd $\neq \pm 1$, n= even $\neq 0$, $Z_s(\omega_{+1}) = Z_s(\omega_{-1}) = R_s$, $Z_l(\omega_o) = R_L$ and $Z_s(\omega_{+m}) = Z_s(\omega_{-m})$.

$$L = \frac{\pi^2}{4} \frac{(S+1)^2}{S} \left[\frac{S + A}{S + B}\right]^2 \quad , \quad (A11.24)$$

where A and B are given in the tables and

$$S = \frac{R_s}{R_L} \quad \text{for H-mixers} \quad , \quad (A11.25a)$$

$$= \frac{R_L}{R_s} \quad \text{for G-mixers} \quad . \quad (A11.25b)$$

The optimum values of S and hence L can be obtained by solving the cubic equation

$$S_{opt}^3 - (1 + A - 3B) S_{opt}^2 + (B - 3A + AB) S_{opt} - AB = 0. \quad (A11.26)$$

Numerical results for some of the cases of the aforementioned three tables are given in Table A11.6

The derivations of the formulas given are eliminated since they are straight forward, but lengthy, applications of Eqs. (A11.1) ... (A11.6) with the appropriate boundary conditions. However, we mention that once one of the cases is calculated, one can calculate several other cases by using duality and/or reciprocity with the appropriate renumbering of the frequencies. Further, different infinite summations appear in some of the formulas which we give in Table A11.7 for convenience.**

** See for example Jolley (I) for extensive tabulations of infinite summations. Also see Morse and Feshbach (I, p. 413) or Carrier, Krook and Peerson (I, Sec. 3.2) for methods of deriving these infinite summations.

Table A11.6. Numerical Values of Optimum Transducer Losses and Resistance Ratios for Some Square-Wave Reversing-Switch Mixers with Incomplete Selective Terminations as Calculated from Tables A11.3 ... A11.5**

Input Port $Z_s(\omega)$		Output Port $Z_L(\omega)$		$\left(\frac{R_s}{R_L}\right)_{opt}$ for H $\left(\frac{R_L}{R_s}\right)_{opt}$ for G	L_{opt}
R_s	∞ for H 0 for G	R_L	0 for H ∞ for G		db
None	All	None	All	0.41	0
Rest	ω_{-1} & $\omega_{\pm 3}$	None	All	0.51	0.96
None	All	Rest	$\omega_{\pm 2}$	0.55	1.32
None	All	Rest	$\omega_{\pm 2}$	0.59	1.67
Rest	ω_{-1}	None	All	0.59	1.67
Rest	ω_{-1}	Rest	ω_{+2}	0.42	2.50
ω_{-1}	Rest	Rest	ω_{+2}	0.67	2.36
ω_{-1}	Rest	None	All	0.81	3.01
ω_{-1}	Rest	Rest	$\omega_{\pm 2}$	0.82	3.06
Rest	$\omega_{\pm 3}$	Rest	$\omega_{\pm 2}$	0.81	3.32
Rest	ω_{-1} & $\omega_{\pm 3(2k+1)}$*	None	All	0.41	0.77
None	All	Rest	$\omega_{\pm 2(2k+1)}$*	0.5	0.92
Rest	$\omega_{\pm 3(2k+1)}$*	None	All	0.84	3.26
Rest	$\omega_{\pm 3(2k+1)}$	Rest	$\omega_{\pm 2}$	0.89	3.41

** Throughout the Table $Z_s(\omega_{+1}) = R_s$ and $Z_L(\omega_o) = R_L$.

* k= 0,1,2, ... , ∞. These selective terminations can be achieved by using transmission lines with proper length.

Table A11.7. Useful Infinite Summations for the Formulas Appearing in the Previous Tables

FORMULA	CONDITION	RESULT
$\sum_{k=-\infty}^{\infty} \frac{1}{(2k+1)^2}$		$\frac{\pi^2}{4}$
$\sum_{k=-\infty}^{\infty} \frac{1}{(2k+1-n)^2}$	n even	$\frac{\pi^2}{4}$
$\sum_{k=-\infty}^{\infty} \frac{1}{(2k+1-n)(2k+1)}$	n even $\neq 0$	0
$\sum_{k=-\infty}^{\infty} \frac{1}{(2k-m)(2k-1)}$	m odd $\neq +1$	0
$\sum_{k=-\infty}^{\infty} \frac{1}{[(2k+1)^2-n^2]}$	n even $\neq 0$	0
$\sum_{k=-\infty}^{\infty} \frac{1}{(4k^2-1)^2}$		$\frac{\pi^2}{8}$
$\sum_{k=-\infty}^{\infty} \frac{(2k+1)^2}{[(2k+1)^2-n^2]^2}$	n even $\neq 0$	$\frac{\pi^2}{8}$

BIBLIOGRAPHY

Abramowitz, M. and I.A. Stegun, eds.:

I. Handbook of Mathematical Functions with Formulas, Graphs, and Mathematical Tables, National Bureau of Standards - Applied Mathematics Series #55, 1964; Dover, New York, 1965.

Agrawal, P.C. and J.V. Hanson:

I. "Cross-Modulation in Ring Diode Modulators", Proc. IEEE (Letters), vol. 56, no. 2, pp. 191-192, Feb. 1968.

Anderson, R.L. and A. van der Ziel:

I. "On the Shot Effect of p-n Junctions", IRE Trans. Electron Devices, vol. Ed-1, pp. 20-24, Nov. 1952.

Bakanowski, A.E.:

I. "Frequency Conversion by a Nonlinear Resistor" in, BTL First Interim Technical Report on Crystal Rectifiers, pp. 11-21, October 1954, AD-61626.

II. "The Nonlinear Resistor with Parasitic Circuit Elements as a Mixer" in, BTL Second Interim Technical Report on Crystal Rectifiers, pp. 4-11, January 1955, AD-71935.

Barber, M.R.:

I. "Noise Figure and Conversion Loss of the Schottky Barrier Mixer Diode", IEEE Trans. Microwave Theory and Technique, vol. MTT-15, no. 11, pp. 629-635, Nov. 1967.

Bassi, C.:

I. Unpublished work and private communication.

Becker, L. and R.L. Ernst:

I. "Nonlinear-Admittance Mixers", RCA Review, vol. 25, pp. 662-691, no. 4, Dec. 1964.

Belevitch, V.:

I. "Non-Linear Effects in Rectifier Modulators", Wireless Engineer, vol. 27, no. 319, pp. 130-131, April 1950.

II. Theorie des Circuits Non-Lineaires en Regime Alternatif, Librairie Universitaire, Louvain, 1959.

Carrier, G.F., M. Krook and C.E. Pearson:

I. Functions of a Complex Variable, Theory and Technique, McGraw-Hill, New York, 1966.

Caruthers, R.S.:

I. "Copper-Oxide Modulators in Carrier Telephone Systems", B.S.T.J., vol. 18, no. 2, pp. 305-337, April 1939.

Chang, K.K.N., G.H. Heilmeier and H.J. Prager:

I. "Low-Noise Tunnel-Diode Down Converter having Conversion Gain", Proc. IRE, vol. 48, no. 5, pp. 854-858, May 1960.

Cooke, R.G.:

I. Infinite Matrices and Sequence Spaces, Macmillan, London, 1950; Dover, New York, 1955.

Copson, E.T.:

I. Asymptotic Expansions, (Cambridge Tracts in Mathematics and Mathematical Physics, Vol. 55), Cambridge University Press, London, 1967.

Davenport, W.B. and W.L. Root:

I. Random Signals and Noise, McGraw-Hill, New York, 1958.

Docherty, I.S.:

I. "Some Solid State Devices for Frequency Converters", Proc. I.R.E.E. Australia, vol. 25, no. 12, pp. 856-866, Dec. 1964.

Dragone, C.:

I. "Analysis of Thermal and Shot Noise in Pumped Resistive Diodes", B.S.T.J., vol. 47, no. 9, pp. 1883-1902, Nov. 1968.

II. "Amplitude and Phase Modulations in Resistive Diode Mixers", B.S.T.J., vol. 48, no. 6, pp. 1967-1998, July-August 1969.

Edwards, C.F.:

I. "Frequency Conversion by Means of a Nonlinear Admittance", B.S.T.J., vol. 35, no. 6, pp. 1403-1416, Nov. 1956.

Gardiner, J.G.:

I. "The Relationship between Cross-Modulation and Intermodulation Distortion in the Double-Balanced Modulator", Proc. IEEE, vol. 56, no. 11, pp. 2069-2071, Nov. 1968.

Gradshteyn, I.S. and I.M. Ryzhik:

I. Table of Integrals, Series, and Products, 4th ed., Academic, New York, 1965.

Gretsch, W.R.:

I. "The Spectrum of Intermodulation Generated in a Semiconductor Diode Junction", Proc. IEEE, vol. 54, no. 11, pp. 1528-1535, Nov. 1966.

Haus, H.A. and R.B. Adler:

I. Circuit Theory of Linear Noisy Networks, Technology Press and Wiley, Cambridge, 1959.

Herold, E.W.:

I. "Frequency Mixing in Diodes", Part V of "Some Aspects of Radio Reception at Ultra-High Frequencies", Proc. IRE, vol. 31, no. 10, pp. 575-582, Oct. 1943.

———, R.R. Bush and W.R. Ferris:

I. "Conversion Loss of Diode Mixers having Image Frequency Impedance", Proc. IRE, vol. 33, no. 9, pp. 603-609, Sept. 1945.

Hildebrand, F.B.:

I. Methods of Applied Mathematics, 2nd ed., Prentice-Hall, New York, 1965.

Huang, T.S. and H.B. Lee:

I. "Bounds on Impedance Functions of R, ±L, ±C, T Networks", Journal of the Franklin Institute, vol. 279, no. 2, pp. 83-94, Feb. 1965.

Jolley, L.B.W:

I. Summation of Series, 2nd rev. ed., Chapman & Hall, London, 1925; Dover, New York, 1961.

Kim, C.S.:

I. "Tunnel-Diode Converter Analysis", IRE Trans. Electron Devices, vol. ED-8, no. 5, pp. 384-405, Sept. 1961.

Kuh, E.S. and R.A. Rohrer:

I. Theory of Linear Active Networks, Holden-Day, San Francisco, 1967.

Lenkowski, J.:

I. "Noise Relations in Periodically Time Variable Networks," Bulletin de L'Academie Polonaise des Sciences, Serie des Sciences Techniques, vol. XIII, no. 11-12, pp. 975-978, Sept. 1965.

Lepoff, J.H. and A.M. Cowley:

I. "Improved Intermodulation Rejection in Mixers", IEEE Trans. Microwave Theory and Technique, vol. MTT-14, no. 12, pp. 618-623, Dec. 1966.

Macpherson, A.C.:

I. "An Analysis of the Diode Mixer Consisting of Nonlinear Capacitance and Conductance and Ohmic Spreading Resistance", IRE Trans. Microwave Theory and Technique, vol. MTT-5, no. 1, pp. 43-51, Jan. 1957.

Manley, J.M. and H.E. Rowe:

I. "Some General Properties of Nonlinear Elements: Part I- General Energy Relations", Proc. IRE, vol. 44, no. 7, pp. 904-913, July 1956.

Messenger, G.C. and C.T. McCoy:

I. "Theory and Operation of Crystal Diodes as Mixers", Proc. IRE, vol. 45, no. 9, pp. 1269-1283, Sept. 1957.

Morse, P.M. and H. Feshbach:

I. Methods of Theoretical Physics, Part I, McGraw-Hill, New York, 1953.

Mouw, R.B.:

I. "A Broad-Band Hybrid Junction and Application to the Star Modulator", IEEE Transactions on Microwave Theory and Techniques, vol. MTT-16, no. 11, pp. 911-918, Nov. 1968.

———— and S.M. Fukuchi:

I. "Broadband Double Balanced Mixer/Modulators, Part I", Microwave Journal, vol. 12, no. 3, pp. 131-134, March 1969.

O'Neill, H.J.:

I. "Image Frequency Effects in a Microwave Crystal Mixer", Proc. IEE, vol. 112, no. 11, pp. 2019-2024, Nov. 1965.

Orloff, L.M.:

I. "Intermodulation Analysis of Crystal Mixer", Proc. IEEE, vol. 52, no. 2, pp. 173-179, Feb. 1964.

Page, C.H.:

I. "Frequency Conversion with Positive Nonlinear Resistors", J. Nat. Bur. Std., vol. 56, no. 4, pp. 179-182, April 1956.

Pantell, R.H.:

I. "General Power Relationships for Positive and Negative Nonlinear Resistive Elements", Proc. IRE, vol. 46, no. 12, pp. 1910-1913, Dec. 1958.

Penfield, P.:

I. Power-Frequency Formulas, Wiley-M.I.T. Press, New York, 1960.

———— and R.P. Rafuse:

I. Varactor Applications, M.I.T. Press, Cambridge, 1962.

————, R. Spence and S. Duinker:

I. Telegan's Theorem and Electric Networks, M.I.T. Press, to be published.

Peterson, L.C. and F.B. Llewellyn:

I. "The Performance and Measurement of Mixers in Terms of Linear-Network Theory", Proc. IRE, vol. 33, no. 7, pp. 458-476, July 1945.

Pound, R.V.:

I. Microwave Mixers, (M.I.T. Radiation Laboratory Series, Vol. 16), Mc-Graw-Hill, New York, 1948.

Pritchard, W.L.:

I. "Notes on a Crystal Mixer Performance", IRE Trans. Microwave Theory and Technique, vol. MTT-3, no. 11, pp. 37-39, Jan. 1955.

Pucel, R.A.:

I. "Theory of the Esaky Diode Frequency Converter", Solid State Electronics, vol. 3, no. 3, pp. 167-207, Nov. 1961.

Rack, A.J.:

I. "Effect of Space Charge and Transit Time on the Shot Noise in Diodes", B.S.T.J., vol. 17, no. 4, pp. 592-619, Oct. 1938.

Rafuse, R.P.:

I. "Low Noise and dynamic Range in Symmetric Mixer Circuits", in High Frequency Generation and Amplification, Proc. of the 1st Biennial Cornell Conf., Engineering Applications of Electronic Phenomena, August 1967, pp. 147-154; Cornell University, Ithaca, 1967.

II. "Symmetric MOSFET Mixers of High Dynamic Range", in Digest of Technical Papers, Int. Solid-State Circuits Conf., U. of Penna., February 1968, pp. 122-123; IEEE, N.Y., 1968.

III. Unpublished work and private communication.

Snyder, R.E.:

I. Intermodulation Distortion in a Broadband Balanced Mixer, S.M. Thesis, M.I.T., March 1969.

Steinbrecher, D.H.:

I. Unpublished work and private communication.

Stoodley, L.G.:

I. "Intermodulation Analysis of Crystal Mixers", Proc. IEEE, vol. 52, p. 984, no. 8, Aug. 1964.

Stracca, G.B.:

I. "On Frequency Converters Using Non-Linear Resistors", Alta Frequenza, vol. 38, no. 5, pp. 318-331, May 1969.

Strum, P.D.:

I. "Some Aspects of Mixer Crystal Performance", Proc. IRE, vol. 41, no. 7, pp. 875-884, July 1953.

II. "A Note on Noise Temperature", IRE Trans. Microwave Theory and Technique, vol. MTT-4, no. 3, pp. 145-151, July 1956.

Strutt, M.J.O.:

I. "Diode Frequency Changers", Wireless Engineer, vol. 13, no. 149, pp. 73-80, Feb. 1936.

II. "Noise-Figure Reduction in Mixer Stages", Proc. IRE, vol. 34, no. 12, pp. 942-950, Dec. 1946.

Sze, S.M.:

I. Physics of Semiconductor Devices, Wiley-Interscience, New York, 1969.

Torrey, C.T. and C.A. Whitmer:

I. Crystal Rectifiers, (M.I.T. Radiation Laboratory Series, Vol. 15), McGraw-Hill, New York, 1948.

Tucker, D.G.:

I. Modulators and Frequency Changers, MacDonald, London, 1953.

II. "Intermodulation Distortion in Rectifier Modulators", Wireless Engineer, vol. 31, no. 6, pp. 145-152, June 1954.

III. "Unbalance Effects in Modulators", J. Brit. Inst. Radio. Engrs., vol. 15, no. 4, pp. 199-207, April 1955.

IV. Circuits with Periodically-Varying Parameters, Van Nostrand, Princeton, 1964.

Twiss, R.Q.:

I. "Nyquist's and Thevenin's Theorems Generalized for Nonreciprocal Linear Networks", J. Appl. Phys., vol. 26, no. 5, pp. 599-602, May 1955.

Uhlir, A., Jr.:

I. "Frequency Conversion in p-n Junction Devices", in, BTL Second Interim Technical Report on Crystal Rectifiers, pp. 21-40, January 1955, AD-71935.

II. "Shot Noise in p-n Junction Frequency Converters", B.S.T.J., vol. 37, no. 4, pp. 951-988, July 1958.

III. "High-Frequency Shot Noise in p-n Junctions", Proc. IRE (Correspondence), vol. 44, no. 4, pp. 557-8, April 1956.

van der Ziel, A.

I. Noise, Prentice-Hall, New York, 1954.

II. "Theory of Shot Noise in Junction Diodes and Junction Transistors", Proc. IRE, vol. 43, no. 11, pp. 1639-1646, Nov. 1955.

van der Ziel, A. (continued)

III. "Semiconductor Noise" in Noise in Electron Devices, edited by L.D. Smullin and H.A. Haus, M.I.T. Press, Cambridge, 1959, pp. 311-343.

BIOGRAPHICAL NOTE

The author was born on July 8, 1942 in Alexandria, Egypt. In June 1963 he received his B.Sc. in Electrical Engineering (Communications) with first class honors from the University of Alexandria (Egypt, U.A.R.). He was appointed as an instructor and demonstrator in the same department for two years. In 1965 he received a scholarship for graduate studies at the Massachusetts Institute of Technology. M.I.T. awarded him his M.S. in Electrical Engineering in January 1967 upon the acceptance of his thesis entitled "Laser Wave Depolarization by Atmospheric Transmission".

Throughout his academic career the author worked at a variety of summer jobs in Europe and the United States; particularly, General Electric Co., Ltd. of England, Bell Telephone Laboratories, and Sylvania Electric Products.

The author is a member of Sigma Xi.


OF FILM
SE REWIND

[redacted]